



European Research Community On Flow, Turbulence and Combustion

ERCOFTAC is a leading European association of research, education and industry groups in the technology of flow, turbulence and combustion. The main objectives of ERCOFTAC are: To promote joint efforts of European research institutes and industries with the aim of **exchanging technical and scientific information**; to promote **Pilot Centres** for collaboration, stimulation and

application of research across Europe; to stimulate, through the creation of **Special Interest Groups**, well-coordinated European-wide research efforts on specific topics; to stimulate the creation of advanced **training** activities; and to be influential on funding agencies, governments, the European Commission and the European Parliament.

www.ercoftac.org

Honorary Presidents

Mathieu, J. Spalding, D.B. Zienkiewicz, O.

Executive Committee

Chairman Hutton, A.G.
Airbus UK
Building 09B
Bristol BS99 7AR
United Kingdom
Tel: +44 117 936 7519
anthony.hutton@airbus.com

Deputy Chairman Oliemans, R.V.A.
Deputy Chairman Hirsch, C.
Treasurer Duursma, R.P.J.
Deputy Treasurer Ooms, G.
SPC Chairman Leschziner, M.
SPC Deputy Chairman Geurts, B.J.
IPC Chairman Lea, C.
Horizon 10 Chairman Jakirlic, S.
Ind. Engagement Officer Seoud, R.E.
Observer Hunt, J.
Observer Jacquin, L.
Secretary Borhani, N.

ERCOFTAC Administration and Development Office

Director Hirsch, C.
ERCOFTAC ADO
Av. Franklin Roosevelt 5
Brussels B-1050
Belgium
Tel: +32 2 643 3572
ado@ercoftac.be

Webmaster Babayan, A.
webmaster@ercoftac.be

Secretary Laurent, A.
anne.laurent@ercoftac.be

Scientific Programme Committee

Chairman Leschziner, M.
Imperial College London
Aeronautics Department
Prince Consort Road
London SW7 2AZ
United Kingdom
Tel: +44 207 594 5061
mike.leschziner@imperial.ac.uk

Deputy Chairman Geurts, B.J.

Industrial Programme Committee

Chairman Lea, C.
Lea CFD Associates Ltd.
12 Sheraton Way
Derbyshire SK17 6FA
United Kingdom
Tel: +44 1298 767 552
chris.leabuxton@btinternet.com

Deputy Chairman Oliemans, R.V.A.

Engagement Officer Seoud, R.E.
21 Ashbourne Terrace
Wimbeldon SW19 1QX
United Kingdom
Tel: +44 208 543 9343
richard.seoud-ieo@ercoftac.org

ERCOFTAC Coordination Centre

Director Thome, J.R.

Secretary Borhani, N.
ERCOFTAC Coordination Centre
EPFL-STI-IGM-ERCOFTAC
ME G1 465, Station 9
CH-1015 Lausanne VD
Switzerland
Tel: +41 21 693 3503
Fax: +41 21 693 5960
ercoftac@epfl.ch

ERCOFTAC Bulletin 80, September 2009

TABLE OF CONTENTS

SPECIAL THEME

'Transition Modelling'

Editorial <i>E. Dick, W. Elsner</i>	3
DNS of transition in turbomachinery <i>J. Wissink</i>	5
Laminar-turbulent transition in boundary layers on axial turbomachine blades <i>G.J. Walker, J.P. Gostelow</i>	11
Turbulent spots detection during boundary layer by-pass transition <i>P. Jonas, W. Elsner, O. Mazur, V. Uruba, M. Wysocki</i>	16
Wavelet analysis of the wake negative and positive jets influence on the laminar-turbulent transition <i>Z. Wiercinski</i>	20
An experimental study of the Reynold number influence on a laminar separation bubble <i>D. Lengani, D. Simoni, M. Ubaldi, P. Zunino, F. Bertini</i>	24
Efforts to model boundary layer separation induced transition using a non-linear eddy viscosity model and a Reynolds stress model <i>Z. Vlahostergios, K. Yakinthos, A. Goulas</i>	29
Application of the zeta-f turbulence model to steady transitional flow <i>M.E. Kelterer, K. Ramadani, R. Pecnik, W. Sanz</i>	35
Steady numerical investigations of the transition process on an axial multistage high pressure compressor <i>J. Marty, G. Cottin, B. Aupoix</i>	41
The LCTM approach to modelling laminar-turbulent transition <i>F.R. Menter, R.B. Langtry</i>	45
Transition modelling with intermittency transport equations <i>W. Elsner, W. Piotrowski, P. Warzecha</i>	49
Calibrating the γ-Re transition model <i>P. Malan, K. Suluksna, E. Juntasaro</i>	53
Overview of wake induced transition modelling for axial compressors <i>A. Beevers, J. Teixeira, R. Wells</i>	58
An intermittency transport model for wake-induced transition <i>E. Dick, S. Kubacki</i>	61
Physical interpretation of transition sensitive RANS models employing the laminar kinetic energy concept <i>K. Walters</i>	67
Modelling bypass and separation-induced transition by reference to pre-transitional fluctuation energy <i>S. Lardeau, A. Fadaï-Ghotbi, M. Leschziner</i>	72
e^n: why it works; when it doesn't; what's next? <i>C. Atkin</i>	77
Comparison between the wall roughness effect and freestream turbulence impact and their joint action on the boundary layer development <i>P. Jonas, O. Mazur, V. Uruba</i>	82
Bypass transition induced by roughness elements: Prediction using a model based on Klebanoff modes amplification <i>O. Vermeersch, D. Arnal</i>	87

EDITOR Borhani, N.

EDITORIAL BOARD Dick, E.
Elsner, W.
Geurts, B.J.

DESIGN & LAYOUT Borhani, N.

SUBSCRIPTIONS AND SUBMISSIONS

ERCOFTAC Bulletin
ERCOFTAC Coordination Centre
EPFL-STI-IGM-ERCOFTAC
ME G1 465, Station 9
CH-1015 Lausanne VD
Switzerland

Tel: +41 21 693 3503
Fax: +41 21 693 5960
Email: ercoftac@epfl.ch

HOSTED, PRINTED & DISTRIBUTED BY



ÉCOLE POLYTECHNIQUE
FÉDÉRALE DE LAUSANNE

The reader should note that the Editorial Board cannot accept responsibility for the accuracy of statements made by any contributing authors

NEXT ERCOFTAC EVENTS

ERCOFTAC Spring Festival

17th May 2010

TU Delft, The Netherlands.

ERCOFTAC SPC, IPC & EC Meetings

18th May 2010

TU Delft, The Netherlands.



Best Practice Guidance Seminar

'CFD of Dispersed Multi-Phase Flows'

16th October 2009

La Sala Strozzi, University of Florence,
Italy.

ERCOFTAC, a world leader in applied fluid mechanics, is proud to announce a seminar on 'CFD for Dispersed Multi-Phase Flows' as part of the **ERCOFTAC Best Practice Guidance Seminar Series**.

The simultaneous presence of several different phases in external or internal flows such as gas, liquid and solid is found in daily life, environment and numerous industrial processes. These types of flows are termed multiphase flows, which may exist in different forms depending on the phase distribution. Examples are gas-liquid transportation, crude oil recovery, circulating fluidized beds, sediment transport in rivers, pollutant transport in the atmosphere, cloud formation, fuel injection in engines, bubble column reactors and spray driers for food processing, to name only a few. As a result of the interaction between the different phases such flows are rather complicated and very difficult to describe theoretically. For the design and optimisation of such multiphase systems a detailed understanding of the interfacial transport phenomena is essential. For single-phase flows Computational Fluid Dynamics (CFD) has already a long history and it is nowadays standard in the development of air-planes and cars using different commercially available CFD-tools.

Due to the complex physics involved in multiphase flow the application of CFD in this area is rather young. These guidelines give a survey of the different methods being used for the numerical calculation of turbulent dispersed multiphase flows. The Best Practice Guideline (BPG) on Computational Dispersed Multiphase Flows is a follow-up of the previous ERCOFTAC BPG for Industrial CFD and can be used in combination with it. The potential users are researchers and engineers involved in projects requiring CFD of (wall-bounded) turbulent dispersed multiphase flows with bubbles, drops or particles.

Invited Speakers

- Prof. Martin Sommerfeld, *University Halle-Wittenberg, Germany.*
- Prof. René Oliemans, *Delft University, The Netherlands.*
- Prof. Berend van Wachem, *Imperial College, UK.*

Proposed Schedule

- 9:30 *Registration and coffee*
- 9:45 'Fundamentals, classification of multi-phase Flows (MPF), integral characterisation of MPF using: volume fraction, dense v. dilute, inter-particle spacing...'
Prof. René Oliemans
- 11:00 *Refreshments*
- 11:20 'Some examples, sources of errors, and BPG checklist'
Prof. René Oliemans
- 12:10 *Lunch*
- 13:10 'Forces acting on particles, droplets and bubbles. Overview of numerical methods for MPF, RANS based methods, Euler-Lagrange approach. Industrial examples for MPF: Pipe flow, particle laden jets.'
Prof. Martin Sommerfeld
- 15:00 *Refreshments*
- 15:20 'Point-particle DNS LES, Euler/Euler approach. Industrial examples for MPF: Fluidised beds. Some experience with commercial codes.'
Prof. Berend van Wachem
- 17:00 *Brief Q&A*
- 17:20 *Seminar closes*

Registration and fees

- €190 *ERCOFTAC members*
€270 *Non-ERCOFTAC members*

This fee includes: seminar registration, lunch and refreshments, and a copy of the BPG book. Please note that accommodation is not included in this fee. Places are limited, so please contact Dr. Richard Seoud at the earliest opportunity to reserve a place:

Dr. Richard E. Seoud
ERCOFTAC Industry Engagement Officer
Tel: +44 (0)208 543 9343
Email: richard.seoud-ieo@ercoftac.org

SPECIAL THEME

TRANSITION MODELLING

Erik Dick & Witold Elsner

The ERCOFTAC Bulletin Theme Issue on Transition Modelling aims to give an overview of recent progress in SIG10 activity. There are 18 papers with topics ranging over DNS, fundamental mechanisms, detailed experiments, modelling with high quality turbulence models, algebraic intermittency models, transport equation intermittency models, laminar kinetic energy models, the e^N method and the effect of wall roughness. This set of papers present the current knowledge on most important aspects of transition physics as well as on recently developed modelling methods. Each of the paper is briefly characterized below:

- *J. Wissink* describes DNS of transition on the suction surface of a turbine blade due to periodically impinging wakes. The effect of velocity deficit and turbulence level in the wakes on transition in separated and attached state are discussed.
- *G.J. Walker* and *J.P. Gostelow* discuss the fundamental mechanisms of transition and give an overview of the modelling strategies, with emphasis on the physical content of proposed correlations.
- *P. Jonas*, *W. Elsner*, *O. Mazur*, *V. Uruba* and *M. Wysocki* present a method to determine turbulent spot production rates in bypass transition based on wavelet analysis of the wall friction time signal. The influences of turbulence level and length scale are discussed.
- *Z. Wiercinski* discusses wavelet analysis of the velocity signal near a flat plate for flow with periodically impacting positive (towards wall) and negative (away from wall) jets. He demonstrates that behind a negative jet impact no calmed region appears.
- *D. Lengani*, *D. Simoni*, *M. Ubaldi*, *P. Zunino* and *F. Bertini* report on a detailed hot wire study of the Reynolds number influence on steady flow separated state transition. They analyse the inviscid Kelvin-Helmholtz instability mechanism.
- *Z. Vlahostergios*, *K. Yakinthos* and *A. Goulas* discuss the performance of a non-linear eddy viscosity model extended with a laminar kinetic energy equation and a Reynolds stress model for transition in separated state. They show the good predictions of the RSM model in the separation zone.
- *M.E. Kelterer*, *K. Ramadani*, *R. Pecnik* and *W. Sanz* analyse a $k-\varepsilon-\zeta-f$ model, which is a further development of the $k-\varepsilon-v^2-f$ model. They show that the model predicts quite well steady state transition on the suction side of a turbine blade in separated and attached state.
- *J. Marty*, *G. Cottin* and *B. Aupoix* demonstrate the use of an algebraic intermittency model on a 3-stage experimental compressor for steady flow calculations. The differences with a full turbulent calculation are demonstrated for separation induced transition on the suction side and attached state transition on the pressure side of the blades.
- *F. Menter* and *R.B. Langtry* describe the main ideas of the two-equation intermittency transport $\gamma-Re_\theta$ model that they have developed a few years ago and that is implemented in ANSYS-CFX. They demonstrate the performance for steady flow flat plate test cases and a turbine blade for transition in attached state and in separated state.
- *W. Elsner*, *W. Piotrowski* and *P. Warzecha* describe the way they have composed the two correlations in the $\gamma-Re_\theta$ model by Menter et al., not disclosed by the originators: one for start of transition and one for length of transition. They illustrate the good performance for steady flow on a flat plate and for wake-induced transition in attached state on the suction surface of a turbine blade.
- *P. Malan*, *K. Suluksna* and *E. Juntasaro* describe a similar effort as in the previous paper, using experimental data for steady flat plate flows.
- *A. Beevers*, *J. Teixeira* and *R. Wells* describe the application of the $\gamma-Re_\theta$ model of ANSYS-CFX to wake-induced transition in a 1.5 stage experimental axial compressor. They discuss the general agreement with experiments and the detailed differences.
- *E. Dick* and *S. Kubacki* describe a two-equation $\gamma-\zeta$ intermittency transport model. They show the qualities of the model for wake-induced transition in attached state on the suction surface of a turbine blade.
- *D.K. Walters* describes a transition model with a laminar kinetic energy equation added to an eddy viscosity $k-\omega$ turbulence model. He shows good performance for steady flat plate flows at zero pressure gradient and for attached state transition on the suction and pressure sides of a wind turbine profile.
- *S. Lardeau*, *A. Fadai-Ghotbi* and *M. Leschziner* describe the development of a laminar kinetic energy equation linked to a non-linear eddy-viscosity $k-\varepsilon$ model, where the production term of the laminar kinetic energy and the eddy viscosity are made dependent on intermittency, with algebraic description of the intermittency. They demonstrate good qualities of the model for attached state transition in flows on a flat plate and for separated state transition on a turbine blade.
- *C. Atkin* describes the theoretical basis of the e^N method, widely in use in the design of laminar flow wings. He discusses the inherent limitations of the concept leading to correlations producing critical N -factors with a tendency to be rather conservative.
- *P. Jonas*, *O. Mazur* and *V. Uruba* describe experiments on the individual and combined effect of surface roughness and free stream turbulence on a zero pressure gradient boundary layer on a flat plate. They demonstrate that roughness causes earlier transition and shorter transition length, but still with non-negligible transition length. Added free stream turbulence further advances and shortens transition.
- *O. Vermeersch* and *D. Armal* propose an algebraic model for the fluctuating velocity normal to the wall due to pretransitional streaks (Klebanoff modes) generated by roughness elements. With this model, the associated Reynolds stress can be calculated and used in a bypass transition criterion.



The ERCOFTAC Best Practice Guidelines for Industrial Computational Fluid Dynamics

The Best Practice Guidelines (BPG) were commissioned by ERCOFTAC following an extensive consultation with European industry which revealed an urgent demand for such a document. The first edition was completed in January 2000 and constitutes generic advice on how to carry out quality CFD calculations. The BPG therefore address mesh design; construction of numerical boundary conditions where problem data is uncertain; mesh and model sensitivity checks; distinction between numerical and turbulence model inadequacy; preliminary information regarding the limitations of turbulence models etc. The aim is to encourage a common best practice by virtue of which separate analyses of the same problem, using the same model physics, should produce consistent results. Input and advice was sought from a wide cross-section of CFD specialists, eminent academics, end-users and, (particularly important) the leading commercial code vendors established in Europe. Thus, the final document can be considered to represent the consensus view of the European CFD community.

Inevitably, the Guidelines cannot cover every aspect of CFD in detail. They are intended to offer roughly those 20% of the most important general rules of advice that cover roughly 80% of the problems likely to be encountered. As such, they constitute essential information for the novice user and provide a basis for quality management and regulation of safety submissions which rely on CFD. Experience has also shown that they can often provide useful advice for the more experienced user. The technical content is limited to single-phase, compressible and incompressible, steady and unsteady, turbulent and laminar flow with and without heat transfer. Versions which are customised to other aspects of CFD (the remaining 20% of problems) are planned for the future.

The seven principle chapters of the document address numerical, convergence and round-off errors; turbulence modelling; application uncertainties; user errors; code errors; validation and sensitivity tests for CFD models and finally examples of the BPG applied in practice. In the first six of these, each of the different sources of error and uncertainty are examined and discussed, including references to important books, articles and reviews. Following the discussion sections, short simple bullet-point statements of advice are listed which provide clear guidance and are easily understandable without elaborate mathematics. As an illustrative example, an extract dealing with the use of turbulent wall functions is given below:

- Check that the correct form of the wall function is being used to take into account the wall roughness. An equivalent roughness height and a modified multiplier in the law of the wall must be used.
- Check the upper limit on y^+ . In the case of moderate Reynolds number, where the boundary layer only extends to y^+ of 300 to 500, there is no chance of accurately resolving the boundary layer if the first integration point is placed at a location with the value of y^+ of 100.

- Check the lower limit of y^+ . In the commonly used applications of wall functions, the meshing should be arranged so that the values of y^+ at all the wall-adjacent integration points is only slightly above the recommended lower limit given by the code developers, typically between 20 and 30 (the form usually assumed for the wall functions is not valid much below these values). This procedure offers the best chances to resolve the turbulent portion of the boundary layer. It should be noted that this criterion is impossible to satisfy close to separation or reattachment zones unless y^+ is based upon y^* .
- Exercise care when calculating the flow using different schemes or different codes with wall functions on the same mesh. Cell centred schemes have their integration points at different locations in a mesh cell than cell vertex schemes. Thus the y^+ value associated with a wall-adjacent cell differs according to which scheme is being used on the mesh.
- Check the resolution of the boundary layer. If boundary layer effects are important, it is recommended that the resolution of the boundary layer is checked after the computation. This can be achieved by a plot of the ratio between the turbulent to the molecular viscosity, which is high inside the boundary layer. Adequate boundary layer resolution requires at least 8-10 points in the layer.

All such statements of advice are gathered together at the end of the document to provide a 'Best Practice Checklist'. The examples chapter provides detailed expositions of eight test cases each one calculated by a code vendor (viz FLUENT, AEA Technology, Computational Dynamics, NUMECA) or code developer (viz Electricité de France, CEA, British Energy) and each of which highlights one or more specific points of advice arising in the BPG. These test cases range from natural convection in a cavity through to flow in a low speed centrifugal compressor and in an internal combustion engine valve.

Copies of the Best Practice Guidelines can be acquired from:

Ms. Anne Laurent,
ADO-Ercoftac,
Avn. Franklin Roosevelt 5
B-1050 Brussels, Belgium.

Tel: +32 2 642 2800, Fax: +32 3 647 9398
Email: anne.laurent@ercoftac.be

The price per copy (not including postage) is:

Non-ERCOFTAC members: 150 Euros
Non-ERCOFTAC academics: 75 Euros

ERCOFTAC members: 100 Euros
ERCOFTAC academic members: 50 Euros

DNS OF TRANSITION IN TURBOMACHINERY

Jan Wissink

School of Engineering and Design, Brunel University, UK.

1 Introduction

Recently, periodic unsteady flow in Low Pressure (LP) turbines has received much attention. Because of the moderate Reynolds number and the availability of powerful high-performance computers to the computational fluid mechanics community, it has become feasible to perform Large-Eddy Simulations (LES) ([7] and [8]) and Direct Numerical Simulations (DNS) ([15], [3], [10], [13] and [14]) of flow around a section at mid-span of a linear turbine cascade. The first DNS were performed by Wu & Durbin [15] who simulated the flow in a T106 cascade with periodically incoming wakes. They discovered that the wakes, which were passively convected by the free-stream, induced bypass transition of the suction-side boundary layer and longitudinal vortical structures along the pressure surface of the blade. Kalitzin *et al* [3] subsequently performed a similar DNS in the T106 cascade in which the periodically incoming wakes were replaced by free-stream turbulence. With a free-stream turbulence level of $Tu = 5\%$ at the inlet, the boundary layer flow in the adverse pressure-gradient region along the suction side was found to undergo bypass transition.

The presence of free-stream fluctuations is usually sufficient to completely suppress boundary-layer separation along a turbine blade. Fundamental studies of the interactions of free stream fluctuations and a laminar (or early transitional) boundary layer have recently appeared in the literature. For instance, Zaki & Durbin [18] studied the influence of a pressure gradient on boundary layer streaks and breakdown in the framework of continuous mode transition [17]. They observed that adverse pressure gradient enhances the amplification of streaks and, as a result, their secondary instability and breakdown to turbulence. The interaction of streaks with Tollmien-Schlichting (TS) waves was studied by Liu *et al.* [6]. They noted that the streaks reduce the amplification of TS waves, but can lead to a secondary instability and breakdown.

In this paper the focus will be on DNS of bypass transition of flow over the suction surface of a turbine blade and the heat transfer from a heated turbine blade to the free-stream. Two examples will be shown of two physical mechanisms that trigger bypass transition:

1. For separation-induced transition to take place in the presence of external fluctuations, a laminar boundary layer needs to be subjected to a strong adverse pressure gradient. By varying the nature (i.e. the spectral contents) of the periodically passing fluctuations a deeper insight in the physical mechanisms that play a role in transition is obtained.
2. A more common type of by-pass transition involves the triggering of streaks by external fluctuations. As they are convected downstream, the streaks eventually become unstable and evolve into turbulent spots. While streaks can be triggered in both the favourable and adverse pressure gradient portions

of the suction-side boundary-layer, further transition to turbulence is unlikely to happen if the pressure gradient is strongly favourable. The fluctuations that manage to penetrate this region are likely to promote laminar heat transfer.

2 Numerical Method

The three-dimensional incompressible Navier-Stokes equations are solved using a second-order cell-centred finite-volume method in space combined with a three-stage Runge-Kutta method for the time-integration. In the spanwise direction a Fourier solver is used for the Poisson equation for the pressure. To save memory, for the phase-averaging the velocity field is averaged in the homogeneous spanwise direction before updating the two-dimensional statistics. For more information on the numerical method used see [1]. To generate the meshes used to discretise the flows in the cascade-passage, the elliptic grid generation algorithm of Hsu and Lee [2] was employed.

3 Influence of passing wakes on laminar separation

From both experiments and numerical simulations it is known that incoming free-stream disturbances are able to reduce separation significantly – or, in some cases, completely suppress it – by triggering by-pass transition. The experiments performed by Stieger and Hodson [9] addressed the interaction of periodically passing wakes with the separating boundary layer on the suction surface of the blade. The experiments clearly showed the presence of a Kelvin-Helmholtz (KH) instability of the separated boundary layer, which resulted in the roll-up of the shear layer into several rolls. The KH instability was found to be triggered by the passing wake. To further investigate the interaction between periodically incoming fluctuations and the separated suction side boundary layer, DNS of the flow in a T106 turbine cascade with periodically incoming free-stream fluctuations have been performed with a set-up that resembles the set-up used in the experiments. The DNS allows differentiating between the mean effect of the wake and the effect of the small scale fluctuations carried by the wakes. In Wissink [10] a DNS study was presented of the interaction of periodically incoming realistic wakes with the separated suction-side boundary-layer. The main results of this DNS were found to be in agreement with the experiments of Stieger and Hodson [9].

In Figure 1, the cascade geometry and the computational domain of the flow problem are displayed. The row of bars at the left-hand-side is added to illustrate the way in which wakes were generated in the experiments. The bars of diameter $d/L = 0.02327$, where L is the axial chord length of the blade, move with speed $u = u_{bar}$ in the negative y -direction. The distance between the

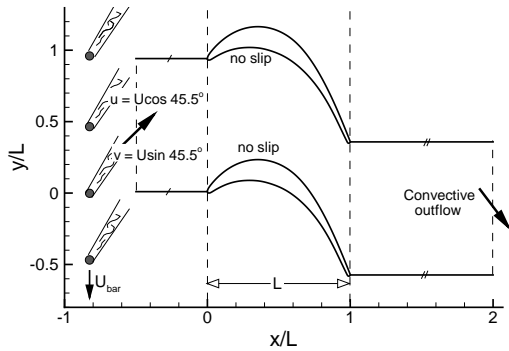


Figure 1: *Spanwise cross-section through the computational domain.*

row of bars and the leading edge of the turbine blades is $0.826L$. In the numerical simulation the wakes are introduced at the inlet plane, using data that have been kindly made available by Xiaohua Wu and Paul Durbin. The statistical properties of these data are described in Wu et al. [16]. At the inlet the free-stream velocity U_0 makes an angle of $\alpha = 45.5^\circ$ with the x-axis. At the outlet a convective boundary condition is applied. Periodic boundary conditions are applied in the spanwise direction and in the y -direction for $x/L < 0$ and $x/L > 1$. Along the blade, for $0 \leq x/L \leq 1$, no-slip boundary conditions are used. The pitch between blades, $P/L = 0.9306$, is precisely twice the distance between bars. Using the fact that the bar speed is $u_{bar}/U = 0.4089$, a dimensionless period of $T = 1.138$ is obtained with which the intersection of a wake with the inflow plane moves from $y/L = 0$ to $y/L = -P/2L$ (see also Figure 1). The Reynolds number, $Re = 51831$, is based on the inflow velocity U and the axial chord length L . The spanwise size was varied between $0.20L \leq l_z \leq 0.25L$. The choice of l_z in the present computation was based on the spanwise size of $l_z = 0.15L$ employed in the simulation of Wu and Durbin [15] as well as on experience gained in the laminar separation bubble computations [12, 11]. The simulations were performed on the Hitachi SR8000-F1 of HLRB in Munich using up to 25×10^6 grid points and up to 120 processors. For the simulations, a computing time of up to 30.7 CPU hours per processor per period was required. To give an impression of the inter-processor communication overhead and hence the scalability of the code: increasing the number of grid points per processor by 42.6%, resulted in a decrease of the computation time per grid point of 13.8%.

Simulation	Structure of the wake	
	velocity deficit	small-scale fluct.
A	30%	yes
B	30%	no
C	0%	yes

Table 1: *Overview of simulations performed.*

Table 1 shows an overview of the performed DNS of flow around a cross-section at midspan of an LPT blade with periodically incoming free-stream fluctuations. The quality of the computational mesh employed in this simulation was assessed earlier in Wissink [10], where the results of a grid refinement study of Simulation A are reported. A detailed comparison of Simulations A and

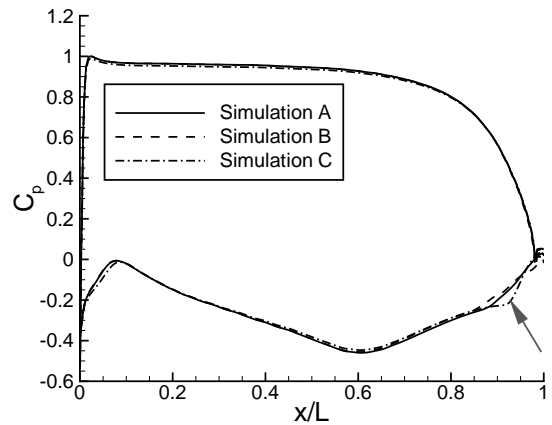


Figure 2: *Simulations A, B, C: Comparison of the mean wall-static pressure coefficient.*

B can be found in Wissink et al. [14].

3.1 Results

Figure 2 shows a comparison of the wall static-pressure coefficients, C_p , from Simulations A, B and C. The arrow points to a distinct kink that indicates boundary layer separation. It can be seen that the kink is most pronounced in Simulation C, in which the mean wake velocity-deficit is absent. Hence, the boundary layer along the downstream half of the suction surface in Simulation C is more likely to be separated than in Simulations A and B. Along the remainder of the blade the wall static-pressure coefficient obtained in the three simulations is found to be in very good agreement. Along the suction surface, moving downstream from the leading edge to the trailing edge, the streamwise pressure gradient is found to be adverse upstream of $x/L \approx 0.15$, favourable between $x/L \approx 0.15$ and $x/L \approx 0.60$, and then adverse again downstream of $x/L \approx 0.60$. Along the pressure surface, the streamwise pressure gradient is mostly favourable. The induced streamwise acceleration of the flow tends to stabilise the boundary layer, thereby inhibiting transition to turbulence and preventing separation.

Phase-averaging is applied by collecting statistics during ten subsequent periods. Each period is divided into 240 equal phases. Before starting the averaging procedure the flow was allowed to develop during at least five periods. Figure 3 shows the suction side mean friction velocity and its phase-averaged envelope for the three simulations. Compared to Simulations A and B, the phase-averaged envelope of the friction velocity in Simulation C is much smaller, indicating that in Simulation C the influence of the periodically impinging fluctuations on the separated boundary layer is smaller than in Simulations A and B. Also, only in Simulation C the boundary layer in the vicinity of $x/L = 0.85$ can be seen to remain separated for all phases. Hence, the absence of a mean velocity deficit in the wake has a significant effect on the dynamics of the phase-averaged separation bubble. The largest variation in the phase-averaged friction velocity is observed in Simulation B where the "wakes" periodically trigger a KH instability leading to the formation of big two-dimensional rolls of re-circulating flow. Owing to the absence of small-scale fluctuations, the re-circulating flow does not undergo further transition to turbulence such that the rolls do not break down. As

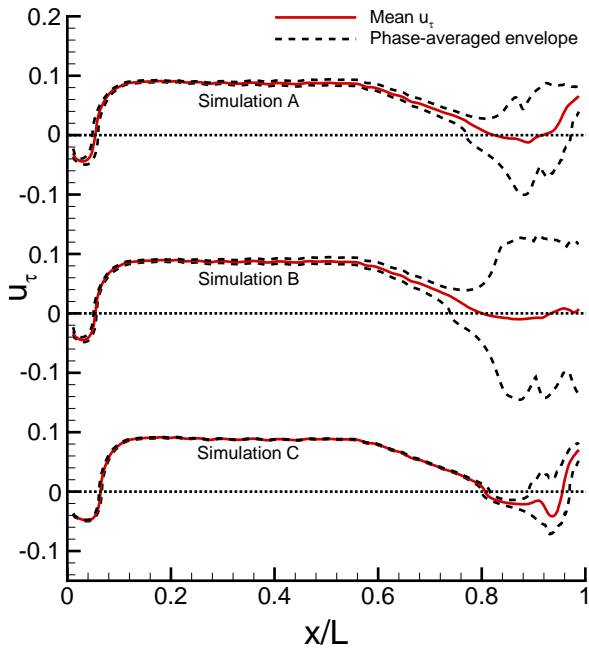


Figure 3: Simulations A, B, C: Mean friction velocity and its phase-averaged envelope along the suction side.

a consequence, the influence on the phase-averaged friction velocity is larger than in Simulations A and C were the rolls do break down due to transition to turbulence.

Figure 4 (upper pane) shows the phase-averaged spanwise vorticity at midspan at $\phi = 0.50$ as obtained in the Simulations A, B and C. While the small-scale fluctuations can be seen to destroy the mean shear in the wake of Simulation A, the shear in the "wake" of Simulation B remains virtually intact. Because of the absence of mean shear in the "wakes" of Simulation C, here no periodically passing fluctuations are visible in the passage between blades. In all simulations the separated boundary layer flow rolls up due to a KH instability, but only in Simulations A and C the rolls are found to undergo further transition to turbulence. Because of the absence of small-scale fluctuations in the free-stream, the rolls in Simulation B remain strictly two-dimensional.

Figure 4 (lower pane) shows the phase-averaged kinetic energy of the fluctuations in the passage between the blades from Simulations A, B and C at $\phi = 0.5$. The absence of small-scale free-stream fluctuations in the wakes of Simulation B is clearly illustrated. Even though the small-scale fluctuations in Simulations A and C were equally strong at the inflow, the fluctuations in Simulation A decrease at a lower rate than in Simulation C. This is explained by the presence of mean shear in the wakes of Simulation A, from which the small-scale fluctuations feed. As a result, the mean shear in Simulation A is slowly destroyed. In contrast to this, in Simulation B - in the absence of small-scale fluctuations - the mean shear remains largely intact. In both Simulations A and C kinetic energy is produced by stretching and straining action by the mean flow on the periodically passing disturbances as they travel through the passage between blades. In Simulation A a significant production of kinetic energy can be seen to occur at the apex of the distorted wake. Similarly, at the same location also a slight production of kinetic energy is observed in Simulation C. The fact that in Simulation B this production of kinetic energy at the apex of the wake is absent indi-

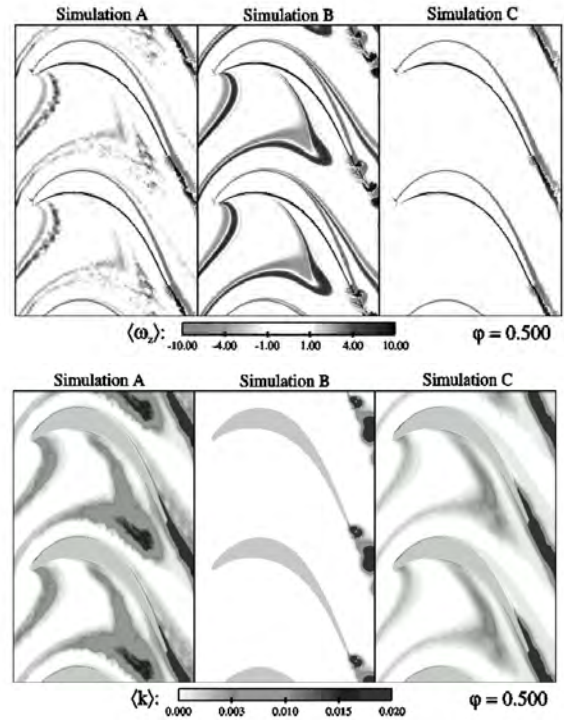


Figure 4: Simulations A, B, C: phase-averaged spanwise vorticity (upper pane) and phase-averaged kinetic energy of the fluctuations (lower pane).

cates that this process needs to be seeded by small-scale fluctuations.

4 Turbulent spots & laminar heat transfer

A second set of simulations to study by-pass transition on non-separated boundary layer flows as well as laminar heat transfer was carried out using a different turbine blade and a higher Reynolds number. The computational setup of these simulations was chosen largely in accordance with the experiments performed by Liu and Rodi [5, 4]. In the experiments the flow around and the heat transfer from a heated MTU turbine was studied. The periodically incoming wakes were generated by bars that were mounted on a squirrel cage. A schematic of the experimental setup is shown in Figure 5. The distance between the leading edge of the middle blade and the squirrel cage was 100mm . The chord-length of the blades was 230mm , while the axial chord-length was $L = 150\text{mm}$. The pitch between blades equals the axial chord length L . The mean inflow velocity in the experiments was $U = 7.5\text{m/s}$, while the speed of the moving cylinders - if present - in the cases for which DNS-s were performed was 10.2m/s . The Reynolds number of the flow problem, based on U and L , was $Re = 72000$.

To simplify the computations, the curvature of the squirrel cage was ignored and a computational domain similar to the one shown in Figure 1 was employed. To account for the wakes that originated from the upstream row of bars in the squirrel cage, free-stream turbulence was added to the inflow plane. In the numerical simulations, the temperature at the surface of the blade was set to $T = T_0$, while the temperature of the oncoming flow was set to $T = 0.7T_0$. The size of the spanwise extent of the computational domain was chosen to be $l_z = 0.20L$. The inflow angle was set to $\alpha = 0^\circ$. The incoming (modelled) wakes and free-stream turbulence were introduced

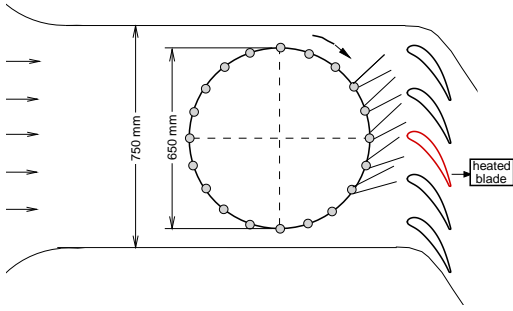


Figure 5: *Schematic of experimental setup.*

at the inflow plane. To model the wakes, data was used that was kindly made available by Xiaohua Wu and Paul Durbin, while for the free-stream turbulence a snapshot of isotropic turbulence in a box was used that was kindly made available by Jochen Fröhlich. See Wissink and Rodi [13] for a more complete description of the computational setup.

Simul.	Wake		D_{cyl}	Tu_{min}
	half-width	vel. def.		
I	-	0%	-	0.0%
II	$0.045L$	30%	$\frac{1}{2}L$	2.8%
III	$0.045L$	30%	$\frac{1}{4}L$	8.4%

Table 2: *Overview of the direct numerical simulations performed. In all simulations a $1254 \times 582 \times 128$ -point grid is employed. Tu_{min} is evaluated at $x/L = -0.2$ and the wake's half-width and velocity-deficit are prescribed at the inlet plane of the computational domain.*

Table 2 shows an overview of the three DNS that were performed. Simulation I was the laminar baseline simulation without any fluctuations in the free-stream. In Simulations II and III, wakes and free-stream turbulence were introduced at the inflow plane. Compared to Simulation II, the frequency of the wakes in Simulation III was twice as high and the free-stream turbulence intensity (identified as the minimum Tu -level in the free-stream at $x/L = -0.2$) was increased from $Tu = 2.8\%$ to $Tu = 8.4\%$. In Simulation I, no wakes were introduced at the inflow plane. In Simulation II, the period of the wakes was $P = \frac{1}{2}L/(1.36U) = 0.3676L/U$, while in Simulation III this period was $P = \frac{1}{4}L/(1.36U) = 0.1838L/U$.

4.1 Results

In this section the focus will be on the flow over and heat transfer from the suction surface of the heated turbine blade. Only a brief overview of some of the key results will be presented. For a more complete description see Wissink and Rodi [13]. (Note that in this section s/s_0 represents the non-dimensional wall-coordinate)

4.1.1 The flow field

Figure 6 shows that the time-averaged wall static-pressure coefficients C_p of Simulations I, II, and III are in good agreement with one another. The absence of any 'kink'-like excursions (see Figure 1) indicates that

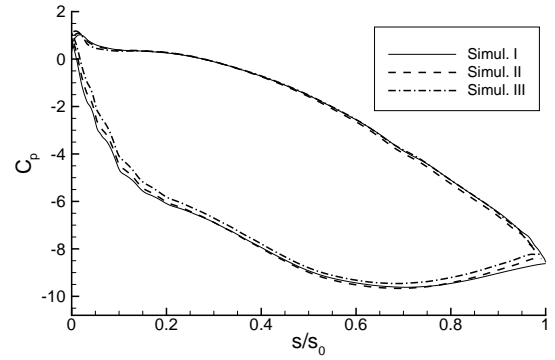


Figure 6: *Simulations I, II, III: wall static-pressure coefficient.*

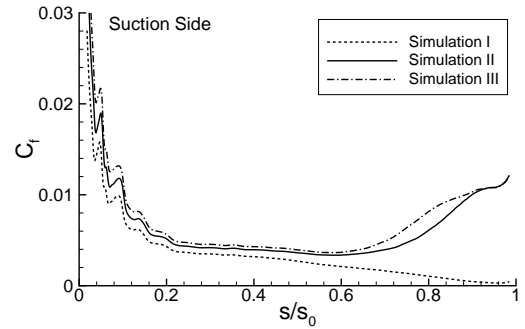


Figure 7: *Simulations I, II, III: time-averaged skin-friction along the suction surface.*

the flow is likely to remain attached in all three simulations. From the C_p distribution it can be seen that the streamwise pressure gradient along the suction surface is favourable between the leading edge and $s/s_0 \approx 0.65$. Farther downstream the pressure gradient is found to be adverse. The accelerating external flow associated with a favourable pressure gradient tends to stabilise the boundary layer, while the decelerating flow induced by an adverse pressure gradient has the opposite effect. Hence, any transition is expected to occur in the region where the pressure gradient is either approximately neutral or adverse.

Figure 7 shows the time-averaged skin-friction C_f along the suction surface of Simulations I-III. Compared to the skin friction in the fully laminar base-line simulation, the slight elevation of C_f upstream of $s/s_0 = 0.6$ in Simulations II and III indicates that external disturbances managed to introduce fluctuations inside the laminar boundary layer. Farther upstream, in both Simulation II and III, the boundary layer undergoes transition in the region around $s/s_0 = 0.75$ – where the pressure gradient is neutral to slightly adverse – as evidenced by the sudden increase in C_f values. Because of the increased level of free-stream fluctuations, in Simulation III transition happens slightly earlier than in Simulation II.

In the phase-averaging procedure, each period was subdivided into 120 equal phases, $\phi = 0, \frac{1}{120}, \dots, \frac{119}{120}$. For each of the phases 15 spanwise-averaged (x, y) -fields containing phase-averaged statistics were stored.

Figure 8 shows the phase-averaged kinetic energy of the fluctuations, $\langle k \rangle$, from Simulation II at phase $\phi = 0$. The location of subsequent wakes can be easily identified

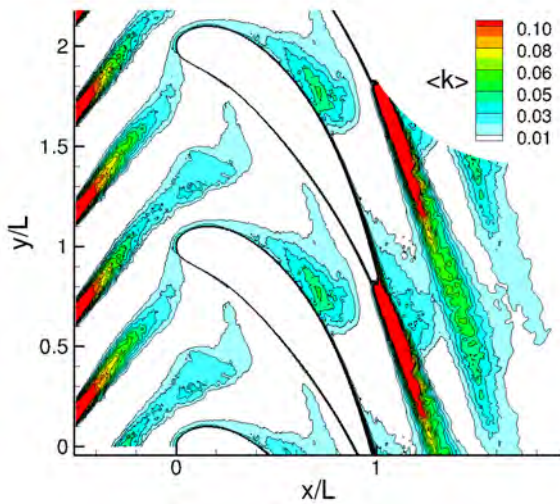


Figure 8: *Simulation II: Contours of the phase-averaged kinetic energy of the fluctuations at $\phi = 0$.*



Figure 9: *Simulation III: contours of the instantaneous velocity in the y-direction in a plane at a distance of $0.0018L$ from the suction side of the blade, showing evidence of a turbulent spot.*

by the increased values of $\langle k \rangle$. The wakes can be seen to deform as they travel through the passage between blades. At the apex of the deformed wake (at $x/L \approx 0.8$) $\langle k \rangle$ reaches a maximum indicating local production of kinetic energy.

As the wakes travel along the suction surface, fluctuations are introduced into the boundary layer. In Simulation III, the disturbances were found to be strong enough to lead to the periodic occurrence of turbulent spots. Evidence of such a spot is shown in Figure 9, where the location of the spot is marked by an ellipse.

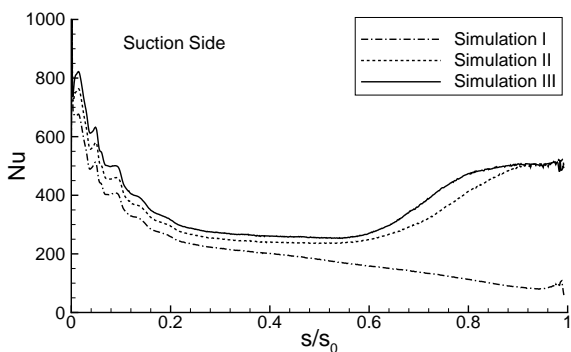


Figure 10: *Simulations I, II, III: time-averaged local Nusselt number along the suction surface.*

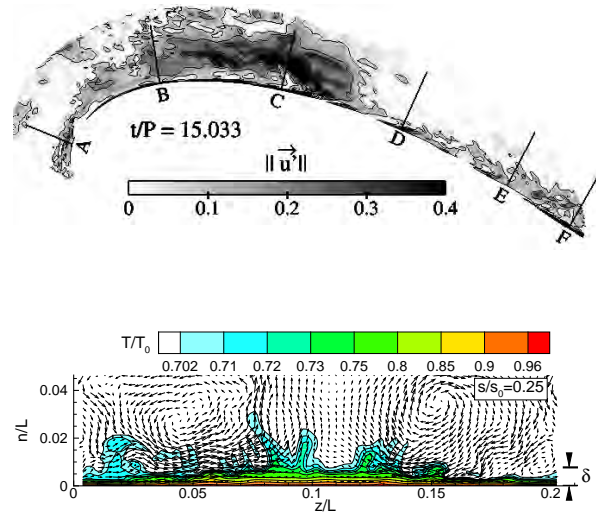


Figure 11: *Simulation II. Upper pane: snapshot showing contours of the magnitude of the fluctuating velocity at midspan; Lower pane: temperature contours T/T_0 and vector field of the fluctuating velocity in a cross section at location "B" (see upper pane) of the suction-side boundary-layer. The vector-field shows vectors in every other grid point and δ identifies the thickness of the viscous boundary layer.*

4.1.1 Heat transfer at the suction surface

The local Nusselt number (using L as length-scale) is defined by

$$Nu = \frac{q_w}{T_0 - \alpha T_0} \frac{L}{k} = \frac{-1}{1 - \beta} \frac{\partial \left(\frac{\bar{T}}{T_0} \right)}{\partial \left(\frac{n}{L} \right)},$$

where q_w is the heat-flux at the wall, k is the thermal conductivity of the fluid, β is the ratio between the temperature of the outer flow and the temperature of the blade and n is the wall-normal distance. In Figure 10 the time-averaged local Nusselt number along the suction surface of Simulations I-III is compared. At the stagnation point Nu can be seen to be maximum. In the laminar simulation (Sim. I) a gradual decrease in Nu almost until the trailing edge of the blade can be seen. In Simulations II and III, Nu initially decreases until $s/s_0 \approx 0.6$ (which approximately corresponds to the onset of transition, see Figure 7). Farther downstream the Nusselt number sharply rises as the boundary layer undergoes transition and becomes fully turbulent. In the laminar portion of the (accelerating) boundary layer (upstream of $s/s_0 \approx 0.6$), the Nusselt number can be seen to increase with the level of free-stream fluctuations (from Simulation I to II to III) as more and more fluctuations manage to penetrate the boundary layer.

Figure 11 (lower pane) shows a cross section through the suction surface boundary layer at $s/s_0 = 0.25$. The location of the cross section is identified by the label "B" in the upper pane, which shows contours of the magnitude of the fluctuating velocity at $t/T = 15.033$ at midspan. The cross section shows contours of the instantaneous temperature T/T_0 and vectors of the fluctuating velocity vector field also at $t/T = 15.033$. The vectors very nicely show the presence of external fluctuations that impinge on the boundary layer and manage to locally transport hot fluid upwards into the free-stream, while cold fluid is transported downwards to the heated blade.

Boundary layer receptivity plays an important role in the selection of the external fluctuations that are effective in the promotion of laminar heat transfer. This fact makes it difficult to design a generally applicable and accurate model for laminar heat transfer that can be used in industrial codes.

5 Future work

The simulations presented above, give only a small example of the work that was performed in collaboration with Wolfgang Rodi, Vittorio Michelassi, Howard Hodson, Tamer Zaki and Paul Durbin. In a continuation of this collaboration, recently a series of DNS of separating flow in a compressor cascade with incoming free-stream turbulence and incoming wakes was carried out. The aim of this work is to perform a detailed study of the interaction of boundary layer separation with streaks and turbulent spots. Separation is found to be very sensitive to the level of external fluctuations and in some cases it is possible to approximately pinpoint the level of external fluctuations needed to obtain intermittent local re-attachment.

Further simulations are performed to study laminar heat transfer in the stagnation region of circular cylinders which is very similar to the stagnation region of turbine blades. It is found that a wake is more effective in triggering laminar heat transfer than isotropic turbulence as the small-scale fluctuations inside the wake tend to survive remarkably well as they feed from the mean shear. Depending on the actual level of external fluctuations and the Reynolds number, the increase in heat transfer in the stagnation region may be quite significant.

Acknowledgements

The author would like to thank the steering committee of the Super Computing Facilities in Bavaria (HLRB) for the computing time granted on the Hitachi SR8000-F1 at LRZ in München and the for funding this project.

References

- [1] M. Breuer and W. Rodi. Large Eddy Simulation for complex turbulent flows of practical interest. In E.H. Hirschel, editor, *Flow simulation with high-performance computers II, Notes in Numerical Fluid Mechanics*, volume 52. Vieweg Verlag, Braunschweig, 1996.
- [2] K. Hsu and L. Lee. A numerical technique for two-dimensional grid generation with grid control at all of the boundaries. *J. Comput. Phys.*, 96, 1991.
- [3] G. Kalitzin, X. Wu, and P.A. Durbin. Dns of a fully turbulent in a lpt passage. *Intl J. Heat Fluid Flow*, 24, 2003.
- [4] X. Liu and W. Rodi. Surface pressure and heat transfer measurements in a turbine cascade with unsteady oncoming wakes. *Exp. in Fluids*, 17, 1994.
- [5] X. Liu and W. Rodi. Velocity measurements in wake-induced unsteady flow in a linear turbine cascade. *Exp. in Fluids*, 17, 1994.
- [6] Y. Liu, T.A. Zaki, and P.A. Durbin. Boundary layer transition by interaction of discrete and continuous modes. *J. Fluid Mech.*, 604, 2008.
- [7] V. Michelassi, J.G. Wissink, J. Froehlich, and W.Rodi. Large-eddy simulation of flow around a low-pressure turbine blade with incoming wakes. *AIAA J.*, 41, 2003.
- [8] B. Raverdy, I. Mary, P. Sagaut, and N. Liamis. High-resolution large-eddy simulation of flow around low-pressure turbine blade. *AIAA J.*, 41, 2003.
- [9] R. Stieger and H.P. Hodson. The transition mechanism of highly loaded LP turbine blades. In *ASME Turbo Expo 2003, paper no GT2003-38304*, 2003.
- [10] J.G. Wissink. Dns of separating, low reynolds number flow in a turbine cascade with incoming wakes. *Intl J. Heat Fluid Flow*, 24, 2003.
- [11] J.G. Wissink and W. Rodi. DNS of a laminar separation bubble in the presence of oscillating flow. In M. Braza, C. Hirsch, and F. Hussain, editors, *Proceedings of the IUTAM Symposium on unsteady separated flows*. Toulouse, 2002.
- [12] J.G. Wissink and W. Rodi. DNS of transition in a laminar separation bubble. In I.P. Castro, P.E. Hancock, and T.G. Thomas, editors, *Advances in Turbulence IX, Proceedings of the ninth european turbulence conference in Southampton*. CIMNE, Barcelona, 2002.
- [13] J.G. Wissink and W. Rodi. Direct numerical simulation of flow and heat transfer in a turbine cascade with incoming wakes. *J. Fluid Mech.*, 569, 2006.
- [14] J.G. Wissink, W. Rodi, and H.P. Hodson. The influence of disturbances carried by periodically incoming wakes on the separating flow around a turbine blade. *Intl. J. Heat Fluid Flow*, 27, 2006.
- [15] X. Wu and P.A. Durbin. Evidence of longitudinal vortices evolved from distorted wakes in a turbine passage. *J. Fluid Mech.*, 446, 2001.
- [16] X. Wu, R.G. Jacobs, J.C.R. Hunt, and P.A. Durbin. Simulation of boundary layer transition induced by periodically passing wakes. *J. Fluid Mech.*, 398, 1999.
- [17] T.A. Zaki and P.A. Durbin. Mode interaction and the bypass route to transition. *J. Fluid Mech.*, 531, 2005.
- [18] T.A. Zaki and P.A. Durbin. Continuous mode transition and the effects of pressure gradient. *J. Fluid Mech.*, 563, 2006.

LAMINAR-TURBULENT TRANSITION IN BOUNDARY LAYERS ON AXIAL TURBOMACHINE BLADES

G.J. Walker¹, J.P. Gostelow^{2,3}

¹ *University of Tasmania, Australia.*

² *University of Leicester, UK.*

³ *National Research Council of Canada, Canada.*

Abstract

The historical development of ideas about the physics of transition processes and of theoretical methods for predicting transitional flow behaviour on axial turbomachine blades is outlined. Enhanced computational resources and experimental techniques have impacted on both prediction methods and experimental observations. There has been a movement from qualitative to quantitative unsteady flow and turbulence observations as data acquisition and processing ability have increased. More detailed turbulence measurements have informed the development of more advanced turbulence models, which in turn have required more computing power. The more sophisticated turbulence models require more detailed unsteady flow observations for validation. This becomes essential as a full account of the operating environment of the machine and its blading is countenanced. The practical importance of transition processes for axial turbomachine blade performance is discussed. An example of this is the optimisation of low pressure turbine blade design to produce improvements in blade lift and weight reduction. The possibility of similar improvements in compressor blade design remains to be demonstrated. Good modelling of the transition region is also essential for predicting other aspects, such as the aeroelastic behaviour of blades.

1 Predicting Transition Onset

Transition onset is generally the outcome of competition between different instability modes. Laminar instability theory describes "natural" transition under low free-stream turbulence. The basis of this was originally confirmed by Schubauer and Klebanoff [1], and led to the e^n prediction method for transition onset [2, 3]. A shortcut method for implementing this technique, in which the envelopes of the maximum disturbance amplification ratio are approximated by empirical relations involving integral boundary layer parameters, was later suggested by Gleyzes et al. [4].

Early methods for predicting transition onset necessarily employed integral boundary layer calculations, due to the rudimentary computation facilities then available. Here, calculation of the laminar layer momentum thickness Reynolds number proceeds from the origin until some previously determined correlation curve for transition commencement is intersected. Crabtree [5] reviewed available data for turbulent breakdown under low free-stream turbulence conditions, and prediction methods proposed by other workers up to that time. He also considered the desirability of allowing for history effects on disturbance amplification over the region of unsta-

ble laminar flow. Crabtree finally opted for a simplified criterion provided by a curve of momentum thickness Reynolds number against the local value of Pohlhausen pressure gradient parameter at breakdown under low free-stream turbulence conditions. He concluded by foreshadowing that a family of similar curves might be required for higher free-stream turbulence conditions.

"Bypass" transition under high free-stream turbulence is a concept originally introduced by Morkovin [6] but never precisely defined. It was erroneously presumed by some workers to imply instantaneous turbulent breakdown with zero length of transitional flow. However this was not the intention: bypass transition does not necessarily exclude instability processes, which are, in fact, essential for transition: only the long region of two-dimensional wave amplification preceding the appearance of three-dimensional disturbances (spanwise periodicity) in low turbulence flow is bypassed.

The approach adopted to bypass transition prediction has built on that of Crabtree [5]. Abu-Ghannam and Shaw [7] observed transition inception on a flat plate over a range of pressure gradients and free-stream turbulence conditions; they further considered the effects of flow history, but were unable to find any simple relation and presented their transition onset criteria for different turbulence levels in the same form as Crabtree, based purely on local conditions at breakdown. Mayle [8] followed a similar approach, but used the acceleration parameter favoured in turbine engineering practice as the pressure gradient parameter: there is no difference in principle, as the latter quantity is a function of both the Pohlhausen pressure gradient parameter and the momentum thickness Reynolds number. Mayle noted that the effects of pressure gradient on transition onset were significantly reduced under the high turbulence levels experienced in a turbomachine; he therefore suggested using the flat plate result, in which the momentum thickness Reynolds number at breakdown was a simple function of the free-stream turbulence level, for predicting transition onset on turbomachine blades.

The method and location of free-stream turbulence measurements is an important issue. Due to the strong accelerations and decelerations experienced in turbomachine blade cascades, the local value of free-stream turbulence at the location of boundary layer transition onset may differ greatly from that at entry to a blade row. Currently used transition onset correlations involve data from several workers, who may have adopted different bases for defining free-stream turbulence values: Abu-Ghannam and Shaw, for example, use neither a local value at breakdown, nor some mean value over the region of unstable flow, but rather an average value of free-stream turbulence taken midway between the lead-

ing edge of their plate and the location in question. The latter point of detail may not be appreciated by many users of their results.

Any blade surface boundary layer must eventually separate if subjected to a strong enough deceleration. Laminar separation bubbles can result from laminar separation followed by sufficiently early transition in the separated shear layer and subsequent turbulent reattachment. Errors in predicting the length of these bubbles has often led to the failure of aerofoil design routines to give stable or accurate solutions. Early attempts at describing separation bubble development and bursting, [9, 10] were based on semi-empirical models assuming a constant pressure over the separated laminar shear layer region, instantaneous transition, and a linear variation of free-stream velocity during turbulent reattachment. An integral boundary layer computation procedure was used, and the transition onset location was predicted using correlations for the length of the separated laminar shear layer in terms of the momentum thickness Reynolds number at separation. The implication here is that separated flow transition represents an entirely different process from that in attached flow. This approach may be fairly reliable for leading edge separation bubbles, but has fundamental problems with the calculation of mid-chord bubbles. The transition onset correlations do not admit the possibility of the bubble length varying continuously to zero as the Reynolds number and/or free-stream turbulence level are increased. This is physically unreasonable, and can lead to bubbles appearing and disappearing in consecutive cycles of iterative calculations with viscous/inviscid interaction procedures. The e^n method of transition onset prediction does not suffer from this problem, and has been employed in the later viscous/inviscid interaction methods [4, 11] it also makes an inherent allowance for history effects by using local values for amplification rate throughout the instability region to compute the amplification factor n .

The MISES code [11] is widely used in the turbomachinery industry for the preliminary design of blade elements in cascade. The viscous layer computation procedure is adapted from the earlier work of Drela & Giles [12] for predicting isolated aerofoil performance. Modifications of the e^n transition onset prediction procedure to allow for elevated free-stream turbulence effects, via the method of Mack [13], are discussed by Drela [14]. The latter publication discusses further modifications adopted in MISES to ensure physically reasonable behaviour and computational stability. It also provides a useful comparison of transition onset predictions from the e^n and Abu-Ghannam & Shaw correlations after first recasting the AG&S correlation by using the shear layer shape factor, instead of the Pohlhausen parameter, as a pressure gradient parameter. This device is necessary to ensure that transition prediction does not fail in a separation bubble, where the pressure gradient falls to zero downstream of separation in the real flow.

Drela's modified e^n transition onset prediction method is also applicable to separated laminar shear layers. Thus the MISES code provides a unified approach to predicting transition onset from the three principal mechanisms (natural, bypass and separated flow transition) that avoids discontinuities introduced by employing different correlations for individual modes. This doubtless contributes to the very creditable performance of the MISES code in capturing both leading edge and mid-chord separation bubbles on compressor and turbine blades.

2 The Physics of Transition Onset

Laminar boundary layers on turbomachine blades only survive until they separate or suffer turbulent breakdown. The viscous instability of a laminar boundary layer was originally investigated by Tollmien. Under low free-stream turbulence conditions instability is initiated when two-dimensional unstable Tollmien-Schlichting (TS) waves are formed; these propagate in the streamwise direction at less than 40% stream velocity. They subsequently develop three-dimensionality and spanwise variations, and a concentration into peaks, valleys and hairpin vortices then occurs. Turbulent spots are formed in the peak regions of vorticity, and eventually coalesce to form continuously turbulent flow. Emmons [15] was the first to propose a turbulent spot model of transitional flow. Schubauer & Klebanoff later observed the growth of an artificial turbulent spot generated on a flat plate without an imposed pressure gradient.

The authors have been working on more accurate transition length predictions, based on measurements of transition length under adverse pressure gradients in natural and by-pass transition [16], and of triggered turbulent spots. It was realised that spot characteristics for adverse pressure gradients could be quite different from those for zero or favourable pressure gradients. The characteristics of turbulent spots under adverse pressure gradients were previously unknown.

Measurements were undertaken of triggered spots under a range of adverse pressure gradients. Under an adverse pressure gradient a spot is formed at the centre of a highly amplified transverse wave packet; it convects at a lower velocity than under a zero pressure gradient. The adverse pressure gradient spot spreads at an included angle as high as sixty degrees, compared with about twenty degrees under zero pressure gradient and even lower under favourable pressure gradients. It has been demonstrated [17] that a triggered spot replicates the development of natural transition; but the behaviour of such a spot additionally seems to represent well the response of the blade boundary layer to an imposed wake disturbance.

Following a turbulent spot is an extensive relaxation trail or "calmed region". The calmed region is effective in delaying the harmonic breakdown to turbulence and in resisting laminar separation [18]. The effect of the calmed region in delaying natural transition after a spot passage is clear: turbulence eventually contaminates the calmed region, but only after the calmed region has had a considerable favourable influence on the downstream flow. Judicious use of this property has resulted in a substantial reduction in the blade count of low pressure (LP) turbines in modern aircraft engines [19].

More recent work has extended the spot-spreading correlations [17] well into the laminar separation region [20, 21]. To reliably predict bubble length, however, it is necessary to gain a better understanding of the dynamics of transition in a separated shear layer and of the differing closure modes of bubbles. This is likely to involve an appreciation of instabilities in the separated shear layer rather than of the TS wave to turbulent spot and by-pass transition routes which have proved useful for attached flows. Kelvin-Helmholtz (KH) instability dominates the separated shear layer at low freestream turbulence levels, but the breakdown mechanism is significantly altered under elevated freestream turbulence, as described by McAuliffe & Yaras [22].

3 Modelling the Transition Region

All models are empirical to some extent. Only direct numerical simulation (DNS) can predict the whole transition process without recourse to empirical data. DNS has shed great light on the detailed physics of transition in boundary layers and separated shear layers under both low and high free-stream turbulence conditions. Because it is so demanding of computer resources, however, it remains impractical for engineering calculations at engine-representative Reynolds numbers.

Large eddy simulation (LES) computations can successfully predict some large scale features of transitional flow, especially in separation bubbles where the KH instability predominates. However they are incapable of predicting the whole transition process and modelling is still needed at the sub-grid scales.

The authors' principal research interest has been modelling of the transition region, or more specifically the transition length. Early correlations of transition length in zero pressure gradient on flat plates predicted excessive lengths for the transition region on aerofoils at low Reynolds numbers. No basis of experimental data had existed which would allow the length of the transition region to be estimated with reasonable accuracy for engineering purposes. An experimental programme was therefore established with the aim of improving transition length correlations for conditions likely to prevail on axial turbomachine blades.

Data for intermittency variation with streamwise distance were obtained over a wide range of turbulence levels and adverse pressure gradients. The objective was to obtain a similarity basis for characterising the transition process. The Narasimha [23] distribution represented the data very well, and proved the key to success in correlating the experimental data. It had not originally been envisaged that this similarity approach would work at high free-stream turbulence levels, or for strong adverse pressure gradients. If properly applied, however, the universal intermittency distribution represents well the observed behaviour over a wide range of those parameters.

In zero pressure gradient flows, and for low free-stream turbulence levels, transition occurs by the stochastic and intermittent appearance of turbulent spots. As the pressure gradient becomes more adverse the amplification of TS waves becomes more pronounced and the flow is dominated by these increasingly periodic effects. This appreciation forms the basis of the Walker [24] model of adverse pressure gradient transition. The qualitative differences in transition between zero and adverse pressure gradients were explained in terms of the influence of pressure gradient on the breakdown mechanism. Whereas the stochastic zero pressure gradient breakdown occurs in sets of TS waves, under an adverse pressure gradient a more continuous breakdown takes place on an equi-spaced spanwise array. These idealised spots, based on each TS wave cycle, eventually coalesce to complete the transition process. Walker developed a simple model for predicting the minimum transition length in an adverse pressure gradient. Measurements of transition length were compared with the predictions of minimum transition length. Improved correlations of spot propagation parameters were later produced and used to give a revised expression for minimum transition length in a limiting adverse pressure gradient.

Gostelow et al. [16] reported comprehensive observations of transitional flow in zero and adverse pressure gradients over a wide range of free-stream turbulence levels.

This led to improved experimental correlations for transition length for surface pressure distributions producing self-similar laminar boundary layer flows. Solomon et al. [25] subsequently developed methods to apply these results for predicting transition length in non-similar flows with arbitrary surface pressure variation in the transition region. This substantially modified the earlier model to allow for variations in spot formation rate and of spot celerities and spreading angles as the pressure gradient is varied. The Chen-Thyson [26] formulation, which only partially allows for pressure gradient effects, was adapted as a framework for the new transition modelling under variable pressure gradients. This theory has been demonstrated successfully in predictions of several ERCOFTAC transition test cases; it also predicts the "subtransition" phenomena in arbitrary surface pressure distributions described by Narasimha [27]. It has been successfully applied to improve predictions for low Reynolds number aerofoils with laminar separation [28, 29].

Although the Solomon et al., [25] model can, in principle, be used for a wide variety of computational approaches the application of a procedure based on integral parameters may be inconvenient in numerical procedures based on differential calculations. Progress is needed toward more efficient procedures for incorporating transition processes into field solutions without compromising the integrity of the physical models. Integral boundary layer calculations, such as the linear combination integral method of Dey and Narasimha [30], which use intermittency to combine laminar and turbulent velocity profiles, have proved to be a robust vehicle for studies of transition region models. Entrainment type integral methods can weight integral shear stress parameter according to turbulent intermittency. In differential boundary layer calculations simple algebraic methods can weight turbulent eddy viscosity according to the intermittency.

The early approach to Reynolds Averaged Navier Stokes (RANS) procedures was to backward extrapolate from the turbulent flow region, and assume that conventional turbulence modelling could also describe transitional flow. This produces transition-like behaviour, which is initiated by diffusion of turbulent energy from the free-stream to the boundary layer; unfortunately, however, it does not model the actual flow physics.

Correlations, such as those described previously, are presented in terms of integral parameters and are not easily applied to differential computations [31]. In order to overcome these difficulties a more recent approach has been to apply intermittency weighting based on local variables [32, 33, 34]. The related intermittency transport methods only claim to provide a sophisticated interpolation method without recourse to a physical basis: "The proposed transport equations do not attempt to model the physics of the transition process ... but form a framework for the implementation of transition correlations into general purpose CFD methods" (Langtry & Menter, [33]).

4 The Operating Environment of Turbomachine Blading and Unsteady Effects

The understanding of transition on axial turbomachine blading was marked by early denial of its existence. Transition was considered irrelevant, as the boundary layer flow was supposed completely turbulent due to the high disturbance levels in a machine. This led to inappropriate distortion of experimental studies by artificially promoting transition. Laminar flow observed on the blading of an undistorted axial compressor was re-

ported quite early by Walker [35], but this result was not generally accepted for a long period.

The extent of transitional flow results from a combination of two processes. These are first, the location of transition onset fluctuations due to unsteady flows and free-stream turbulence, and secondly the distance required for merging of turbulent spots once transition has commenced. The transition region occupies a greater proportion of an aerofoil chord as the Reynolds number is reduced.

Early observations of unsteady transition were made by Fejer [36] in oscillating inviscid flow over a flat plate, and Walker [37] on axial compressor blades subject to upstream wake disturbances. Pfeil and Herbst [38] observed periodic turbulent wake impact on a flat plate boundary layer. Mayle [8] described a multi-mode transition model for axial turbomachine blades. Halstead et al. [39] made definitive observations of transition on both compressor and turbine blades in embedded stages of multi-stage machines. Work at Cambridge on unsteady transition on LP turbine blades, reviewed by Hodson & Howell [19], led to high-lift blade profile development; collaborative work in Cambridge and Tasmania continues on axial compressor blades.

Energy is transferred in a turbomachine by a moving rotor with multiple blades, and the process is inherently unsteady. Pressure disturbances may propagate both upstream and downstream in subsonic flow; this results in periodic disturbances due to the relative blade motion. The convection of wakes from upstream blade rows may subject blade rows further downstream to periodic vortical disturbances and high levels of turbulence.

It has long been recognised that the axial spacing between blade rows and the wake passing frequency affect performance. There may actually be an advantage from minimising the axial spacing. In axial compressors this can amount to an efficiency advantage of 1% or more [40]. Recent investigations have sought to go beyond overall performance measurements to seek explanations of such counter-intuitive effects in more detailed unsteady flow measurements and spatio-temporal representations.

Fundamental work on blade-wake interaction effects is revealing subtle features of unsteady blade boundary layer behaviour which could play a crucial role in determining the critical aerodynamic frequencies. This should facilitate optimisation of blade numbers, resulting in improvements in all aspects of performance including manufacturing cost savings.

Turbomachinery blading is subject to a wide variety of additional flow disturbances. These include wake-wake interactions, shock waves and expansion fields. Rotor blades may experience additional unsteadiness from circumferential inlet flow distortions or from static pressure distortions arising from potential flow interactions with nearby structural features. Acoustic standing and travelling waves may occur in the annulus of a turbomachine.

5 Some Current Issues

It is necessary to appreciate that bypass transition does not exclude instability processes, nor does it imply instantaneous breakdown to turbulent flow. It rather involves a different sequence of instability processes, and only the long region of 2-D wave amplification seen in a low-disturbance environment is effectively excluded.

Under high free-stream turbulence conditions DNS studies show turbulent breakdown originating from KH instability in the outer region of the boundary layer [41] or interactions of TS waves with streamwise struc-

tures having a much smaller spanwise length scale [42]. Narasimha [43] has observed that what makes the turbomachinery problem so interesting is that the Reynolds numbers are low but also the flow is not easy to model. Low pressure turbines are in the feasible Reynolds number range and cannot be easily handled by other models. Turbomachinery is the first major application in which DNS is likely to make an impact.

Transition always requires some form of instability; several forms may occur simultaneously and compete for the initiation of turbulent breakdown. Turbulent spots and instability wave packets may occur in conjunction and interact; the instability of adjacent flow may also play an important role in turbulent spot spreading.

Empirical correlations for transition onset remain the weakest part of engineering calculations:

- There is heavy reliance on the Abu-Ghannam and Shaw experiment, for which free-stream turbulence was not well defined.
- Studies by Mayle et al. [44] indicate that only certain ranges of disturbance scales and frequencies are effective in promoting transition.
- DNS studies by Voke et al. [45] indicate that surface-normal (v') fluctuations are more effective than streamwise (u') fluctuations in promoting turbulent breakdown; hence isotropy of free-stream turbulence is another important issue.
- It may be time to undertake a more detailed experimental study of the influence of free-stream turbulence on turbulent breakdown, informed by recent DNS studies and using modern observation techniques.
- Experimental data for transitional flow under accelerating flow conditions remains poor, as does data on re-laminarisation and its prediction.
- Turbine blade optimisation models currently incorporate the unsteady effects of wake-induced transition, but not the transitional flow effects associated with spot merging.
- Compressor blade optimisation studies have been reported for steady flow conditions, but still lack accurate transitional flow models; true optima may not have been reached, even under steady conditions.
- The presence of streamwise vorticity, on both concave and convex surfaces, and its effects on boundary layers and heat transfer is still not well recognised, understood or predicted.
- Modelling unsteady transition is one of the major problems that need to be pursued. Unsteady transition onset for compressor blades, and the leading edge interaction effects associated with wake passing, are being addressed; the modelling of subsequent transitional flow remains to be incorporated.

References

- [1] Schubauer, G.B. & Klebanoff, P.S., "Contributions on the Mechanics of Boundary Layer Transition," NACA TN3489, 1955.
- [2] van Ingen, J.L. "A Suggested Semi-Empirical Method for the Calculation of the Boundary Layer Transition Region," Rep. VTH-74, TU Delft., 1956.
- [3] Smith, A.M.O. & Gamberoni, N., "Transition, Pressure Gradient and Stability Theory," Proc. 9th Int. Congr. Appl. Mech., Brussels, 1956.
- [4] Gleyzes, C., Cousteix, J.R. & Bonnet, J.L., "Theoretical and Experimental Study of Low Reynolds Number Transitional Separation Bubbles," Conf. on Low Reynolds Number Airfoil Aerodynamics, University of Notre Dame, IN, 1985.

- [5] Crabtree, L.F., "Prediction of Transition in the Boundary Layer on an Aerofoil," *J. Roy. Aero. Soc.*, 62, 1958.
- [6] Morkovin, M.V., "On the Many Faces of Transition," In *Viscous Drag Reduction*, C.S. Wells (ed.) Plenum Press, NY, 1-31, 1969.
- [7] Abu-Ghannam, B.J. & Shaw, R., "Natural Transition of Boundary Layers - The Effects of Turbulence, Pressure Gradient, and Flow History," *J. Mech. Eng. Sci.*, 22, 5, 23-228, 1980.
- [8] Mayle, R. E., "The Role of Laminar-Turbulent Transition in Gas Turbine Engines," *J. Turbomachinery*, 113, 509-537, 1992.
- [9] Horton, H.P., "A Semi-Empirical Theory for the Growth and Bursting of Laminar Separation Bubbles," *ARC CP 1073*, 1969.
- [10] Roberts, W.B., "Calculation of Laminar Separation Bubbles and Their Effect on Airfoil Performance," *AIAA J.*, 18, 25-3, 1980.
- [11] Youngren, H. & Drela, M., "Viscous/Inviscid Method for Preliminary Design of Transonic Cascades," *AIAA-1991-2364*, 27th Joint Propulsion Conference, Sacramento, 1991.
- [12] Drela, M. & Giles, M.B., "Viscous-Inviscid Analysis of Transonic and Low Reynolds Number Airfoils," *AIAA J.*, 25, 1347-1355, 1987.
- [13] Mack, L.M., "Transition Prediction and Linear Stability Theory," in *AGARD-CP-224*, 1.1-1.22, 1977.
- [14] Drela, M., "MISES Implementation of Modified Abu-Ghannam/Shaw Transition Criterion," *MIT Aero-Astro.*, 1998.
- [15] Emmons, H.W., "The Laminar-Turbulent Transition in a Boundary Layer - Part I," *J. Aero. Sci.*, 18, 7, 490-498, 1951.
- [16] Gostelow, J.P., Blunden, A.R. & Walker, G.J., "Effects of Free-Stream Turbulence and Adverse Pressure Gradients on Boundary Layer Transition," *J. Turbomachinery*, 116, 392-404, 1994.
- [17] Gostelow, J.P., Melwani, N. & Walker, G.J., "Effects of Streamwise Pressure Gradient on Turbulent Spot Development," *J. Turbomachinery*, 118, 737-743, 1996.
- [18] Gostelow, J.P., Walker, G.J., Solomon, W.J., Hong, G. & Melwani, N., "Investigation of the Calmed Region behind a Turbulent Spot," *J. Turbomachinery*, 119, 802-809, 1997.
- [19] Hodson, H.P. & Howell, R.J. "The Role of Transition in High-Lift Low-Pressure Turbines for Aeroengines," *Prog. Aerospace Sci.*, 41, 419-454, 2005.
- [20] D'Ovidio, A., Harkins, J.A. & Gostelow, J.P., "Turbulent Spots in Strong Adverse Pressure Gradients, Part 1 - Spot Behavior," *ASME-2001-0194*, 2001a.
- [21] D'Ovidio, A., Harkins, J.A. & Gostelow, J.P., "Turbulent Spots in Strong Adverse Pressure Gradients, Part 2 - Spot Propagation and Spreading Behavior," *ASME-2001-0406*, 2001b.
- [22] McAuliffe, B.R. & Yaras, M.I., "Transition Mechanisms in Separation Bubbles under Low and Elevated Freestream Turbulence." *ASME GT2007-27605*, 2007.
- [23] Narasimha, R., "On the Distribution of Intermittency in the Transition Region of the Boundary Layer," *J. Aero. Sci.*, 24, 711-712, 1957.
- [24] Walker, G.J., "Transitional Flow on Axial Turbomachine Blading", *AIAA Journal*, 27, 5, 595-602, 1989.
- [25] Solomon, W.J., Walker, G.J. & Gostelow, J.P., "Transition Length Prediction for Flows with Rapidly Changing Pressure Gradients," *J. Turbomachinery*, 118, 744-751, 1996.
- [26] Chen, K.K. & Thyson, N.A., "Extension of Emmons' Spot Theory to Flows on Blunt Bodies," *AIAA Journal*, 9, 5, 821-825, 1971.
- [27] Narasimha, R., "The Laminar-Turbulent Transition Zone in the Boundary Layer," *Prog. Aerospace Sci.*, 22, 29-80, 1985.
- [28] Sanz, W. & Platzer, M.F. "On the Navier-Stokes Calculation of Separation Bubbles with a New Transition Model," *J. Turbomachinery*, 120, 36-42, 1998.
- [29] Hobson, G. V., & Weber, S., "Prediction of a Laminar Separation Bubble with Transition over a Controlled-Diffusion Compressor Blade," *ASME 2000-GT-277*, 2000.
- [30] Dey, J. & Narasimha, R., "An Integral Method for the Calculation of 2-D Transitional Boundary Layers," *Report 88 FM 7*, Indian Institute of Science, 1988.
- [31] Di Pasquale, D., Rona, A., & Garrett, S.J. "A Selective Review of CFD Transition Models," *AIAA 2009-3812*, 2009.
- [32] Steelant, J. & Dick, E., "Modeling of Laminar-Turbulent Transition for High Freestream Turbulence", *J. Fluids Engineering*, 123, 22-30, 2001.
- [33] Langtry, R.B. & Menter, F.R., "Transition Modeling for General CFD Applications in Aeronautics," *AIAA 2005-522*, 2005.
- [34] Menter, F.R., Langtry, R.B., Likki, S.R., Suzen, Y.B., Huang, P.G. & Völker, S., "A Correlation-Based Transition Model Using Local Variables-Part I: Model Formulation," *J. Turbomachinery*, 128, 413-422, 2006.
- [35] Walker, G.J., "The Prediction of Boundary Layer Development in Axial-Flow Turbomachine Blades", *Proc. 3rd Australasian Conference on Hydraulics and Fluid Mechanics*, Sydney, pp. 97-104, 1968.
- [36] Obremski, H.J. & Feier, A.A., "Transition in Oscillating Boundary Layer Flows," *J. Fluid Mech.* 29, 1, 93-111, 1967.
- [37] Walker, G.J., "The Unsteady Nature of Boundary-Layer Transition on an Axial Flow Compressor Blade," *ASME 75-GT-135*, 1974.
- [38] Pfeil, H. & Herbst, R., "Transition Procedure of Instationary Boundary Layers," *ASME 79-GT-128*, 1979.
- [39] Halstead, D.E., Wisler, D.C., Okiishi, T.H., Walker, G.J., Hodson, H.P. & Shin, H-W., "Boundary Layer Development in Axial Compressors and Turbines: Parts 1-4." *J. Turbomachinery*, 119, 114-127, 128-139, 225-237, 426-444, 1997.
- [40] Möhle, H., "Untersuchungen über den Einfluss des Abstandes zwischen Lauf- und Leitrad auf das Betriebsverhalten von einstufigen axialen Strömungsmaschinen," *Konstruktion in Maschinen-, Apparate- und Gerätebau*, 13, 213-222, 1961.
- [41] Wissink, J.G. & Rodi, W. "Direct Numerical Simulations of Transitional Flow in Turbomachinery," *J. Turbomachinery*, 128, 668-678, 2006.
- [42] Liu, Y., Zaki, T.A. & Durbin, P.A., "Boundary Layer Transition by Interaction of Discrete and Continuous Modes," *J. Fluid Mech.*, 604, 199-233, 2008.
- [43] Narasimha, R., "Conference Summary," *Proceedings International Workshop on Transition and Unsteady Aspects of Turbomachinery Flows*, Minnowbrook IV, Syracuse, NY. *NASA TM - 2004 212913*, 2003.
- [44] Mayle, R. E., Dullenkopf, K. & Schulz, A. "The Turbulence that Matters," *J. Turbomachinery*, 120, 402-409, 1998.
- [45] Sarkar, S. & Voke, P.R. "Large-Eddy Simulation of Unsteady Surface Pressure Over a Low-Pressure Turbine Blade due to Interactions of Passing Wakes and Inflexional Boundary Layer," *J. Turbomachinery*, 128, 221-231, 2006.

TURBULENT SPOTS DETECTION DURING BOUNDARY LAYER BY-PASS TRANSITION

Pavel Jonas¹, Witold Elsner², Oton Mazur¹, Vaclav Uruba¹, Marian Wysocki²

¹ *Institute of Thermodynamics v.v.i. AS CR, Prague, Czech Republic.*

² *Institute of Thermal Machinery, TU Czestochowa, Poland.*

Abstract

In the present paper, the turbulent spot production rates are evaluated by means of the conditional analysis using wavelets applied on the wall friction time series. The effects of external flow turbulence intensity and length scale are considered.

1 Introduction

The transition from laminar to turbulent flow structure depends on the specific type of flow and on the type of the acting disturbances that influence the process. Regardless to this fact, the final phase of laminar boundary layer transition starts always with the occurrence of first turbulent spots [1]. Spots appear as the building blocks of boundary layer turbulence, they control the length of the transition region etc. The turbulent spots followed by calmed regions are defined structures that dominate the last stage of transition. Spots production affects the length of transition region, e.g. [2]. The turbulent spots creation rate, growth characteristics and their merger lead to fully developed turbulent flow. Since forties, the effect of external flow turbulence intensity Iu on boundary layer laminar turbulent transition is known and systematically investigated, e.g. [3]. Later, the effect of the turbulence length scale L has been also clearly proved, e.g. [4-7]. It has been shown [8] that the same location of by-pass-transition start can be induced by a proper adjustment of turbulence intensity keeping its given length scale and vice versa.

Several attempts were done to find causal connections of the outer stream turbulence length scale effect on by-pass transition, but a clear physical insight into the role of the free stream turbulence (hereinafter FST) scales in transition process has not been achieved yet. The investigation of the spots behaviour during transition at various FST scales can contribute to the problem explanation. The results analysed and discussed in the paper are based on the original experiments [5] made with the aim to collect the data for the COST/ERCOTAC Test Case T3A+ defined e.g. in [9]. The experimental facility, methods and primary procedures have been kept identical to those described in detail in [5].

2 Experimental set up, measurement methods and evaluation procedures

The flat plate boundary layer was investigated experimentally in the close circuit wind tunnel of the Institute of Thermomechanics AS CR. The boundary layer develops itself on the aerodynamically smooth plate 2.75m

long and 0.9m wide in the working section with the cross section (0.5 x 0.9)m².

Free stream turbulence (FST) was controlled by three plane grids/screens of different geometry with cylindrical rods and square mesh holes placed across the incoming flow in a proper distance upstream the plate. All used grids produce homogeneous and close to isotropy FST with equal turbulence level $Tu = 0.03$ but with different values of the dissipation length parameter L , e.g. [10] in the plate leading edge plane, $x = 0$

$$\begin{aligned} Tu &= \sqrt{\overline{u_i u_i}} / 3U_e^2 \cong Iu = \sqrt{\overline{u_1^2}} / U_e; \\ L &= - \left(\overline{u_1^2} \right)^{3/2} / U_e \frac{du_1^2}{dx}; \quad i = 1, 2, 3. \end{aligned} \quad (1)$$

The values of dissipation length parameter $L_e = 3.8\text{mm}$, 5.9mm and 33.4mm respectively were produced in the plane $x = 0$. The subscript "e" denotes quantities in the plane $x = 0$.

Measurements were carried out by means of two single wire probes working in the CTA mode. The first probe, placed in a fixed position in the outer stream, indicated the signal corresponding to the reference velocity $U(t, \vec{x}_r) \approx U_e$ proportional to the external flow mean velocity $U_e \approx 5\text{m/s}$. The second probe, the profile probe, was put into position by a traversing system in the streamwise direction x and in the direction y normal to the surface. The distance y from the wall of the profile probe hot wire was measured with an accurate cathetometer (precision 0.01mm). Digital records of the output signals (25kHz, 750,000 samples, 16 bit) were acquired simultaneously and then records of the relevant instantaneous velocities were evaluated using data from the calibration measurements performed prior to the experiment. Next, the correction [11] of the wall proximity effect on hot-wire cooling has to be applied.

The linear regression of the mean velocity close to the wall

$$U^*(y) = y \left(\frac{\partial \bar{U}}{\partial y} \right)_w \quad (2)$$

was received within this correction.

Evaluation of the instantaneous wall-friction fluctuations τ'_w from the velocity records is apparent from the following relations

$$\begin{aligned} (\tau'_w)_i &= (\tau_w)_i - \bar{\tau}_w; \quad i = 1, 2, \dots, n, \\ (\tau_w)_i &= \left[\mu \left(\frac{\partial U}{\partial y} \right)_w \right]_i \cong \mu K_D \frac{U_i(y_1)}{y_1}, \\ \bar{\tau}_w &= \mu \left(\frac{\partial \bar{U}}{\partial y} \right)_w = \mu K_D \frac{\bar{U}(y_1)}{y_1}; \quad K_D = \frac{\bar{U}^*(y_1)}{\bar{U}(y_1)} \end{aligned} \quad (3)$$

where n denotes the number of averaged samples and the distance y_1 is chosen so that the coefficient K_D would

be as close as possible to 1. The indicated measuring method and evaluation procedures [11] allow determining the instantaneous wall friction time series to be subjected to the relevant statistical analyses.

In this paper, the transitional intermittency analysis uses wall friction time series. The applied method is so called TERA-method (Turbulent Energy Recognition Algorithm-Method), e.g. [12] and the procedure of evaluating the transitional intermittency factor $\gamma(x)$ is very similar to that described in [13 and 14]. The detector function, the threshold and the indicator function $I(t)$ are evaluated successively. The indicator function allows distinguishing the time intervals in those with turbulent structure ($I = 1$) and those with laminar/nonturbulent structure ($I = 0$). The transitional intermittency factor is calculated after the following formulae

$$\gamma(x) = \frac{1}{n} \sum_{j=1}^n I(x, t_j); \quad n = 750,000. \quad (4)$$

The examples of the conditionally averaged distributions of the wall friction during periods with turbulent character or with the laminar one were demonstrated e.g. in [15].

Valuable information on turbulent spots role in transition process can be deduced with regard to Emmons ideas and Narasimha's concept of intermittency as will be shown later.

The application of wavelet transform on the velocity or wall friction digital records represents another approach to the investigation of turbulent spots during boundary layer transition. The advantage of this approach is the clearness of the particular spot passages through the location of observation. The presence of a spot may be confirmed by the time of occurrence, magnitude and shape of the signal and to detect particular frequency components as the spot interior is characterized by much finer turbulence scales than the outer flow. Elsner et al. [16] developed an original detection procedure based on the wavelet analysis. Their procedure employs the Morlet wavelet transform and all calculations are performed with the use of the Wavelet Toolbox of Matlab software [17]. Essentially, this spot detection procedure consists of a few steps. Initially, Morlet wavelet transformation of the rough signal, corresponding to velocity or to wall friction, is applied and then time series for the proper selected value of scale number a , is extracted. Next an absolute value of the time derivative is compared with the defined threshold value, what gives a passing time of individual spots and so their dimensions.

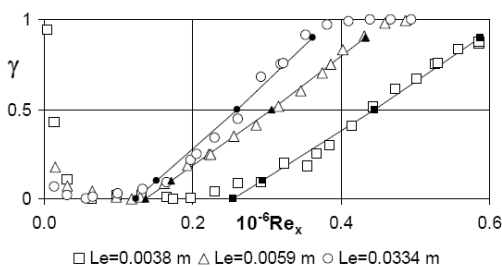


Figure 1: Transitional intermittency factor as function of the local Reynolds number.

3 Results and analysis

The transitional intermittency factor $\gamma(x)$ was evaluated from the wall friction records acquired at different values of the FST length parameter. The distributions $\gamma(x)$ versus Re_x shown in Figure 1 confirm the effect of the length parameter L_e .

Despite of the same intensity $Iu_e = 0.03$ at $x = 0$, the start of transition is moving upstream and the length of transition region is shortening with the increasing FST length scale. In compliance with Narasimha [2] the transitional intermittency factor $\gamma(x)$ can be expressed in form involving the spot production rate n (the number of spots occurring per unit time and space distance) and the Emmons dimensionless propagation parameter σ (including both the stream wise and lateral spot growth, effect of drift)

$$\begin{aligned} \gamma(x) &= 0, \quad x \leq x_t; \\ \gamma(x) &= 1 - \exp \left[- (x - x_t)^2 n \sigma / U_e \right], \quad x \geq x_t \end{aligned} \quad (5)$$

where the term $n\sigma/U_e$ is assumed to be constant. Introducing the local Reynolds number Re_x into the formulae (5) we receive

$$\begin{aligned} \gamma(Re_x) &= 1 - \exp \left[- (Re_x - Re_{tr})^2 n^* \sigma \right], \\ Re_x &= xU_e/\nu, \quad n^* \sigma = n\sigma\nu^2/U_e^3. \end{aligned} \quad (6)$$

Following Narasimha, it is possible introduce a new variable ξ and express the above given formulas in an universal form

$$\begin{aligned} \xi &= (Re_x - Re_{tr})/\Delta Re_{tr}, \\ Re_{tr} &= Re_{x, \gamma=0.5}, \quad \Delta Re_{tr} = Re_{x, \gamma=0.9} - Re_{x, \gamma=0.1}, \\ \gamma(\xi) &\doteq 1 - \exp \left[-a(\xi + b)^2 \right] \doteq 1 - \exp \left[-c(\xi + d)^3 \right]. \end{aligned} \quad (7)$$

The values of empirical parameters a , b , c and d take respectively the values $a = 1.42$ and $b = 0.72$ from the Narasimha's model [2] and $c = 0.6$ and $d = 1.05$ according to the model proposed by Johnson and Fashifar [18]. The comparison of presented results with models proposed in [2] and [18] shown in Figure 2 demonstrates their compatibility with (6) and somewhat better correspondence with the model [18].

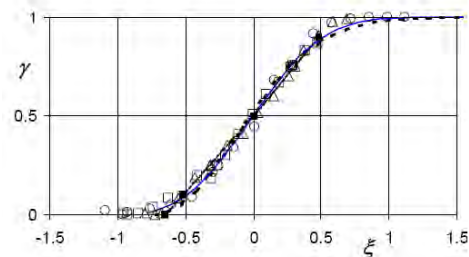


Figure 2: Universal intermittency function (symbols as in figure 1, dotted line model [2], solid line [18]).

The dimensionless spot production rates $n^*\sigma$ were evaluated from the intermittency factor distributions and as well using the wavelet analysis. Results are plotted versus Reynolds number ΔRe_{tr} (6) in Figure 3 together with the dotted line segment interpolating results presented in the paper [18].

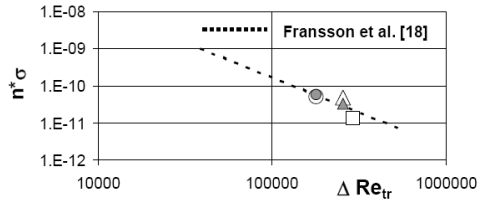


Figure 3: Dimensionless spot production rate versus transition length Re (symbols as in figure 1, filled symbols are calculated from the wavelet analysis).

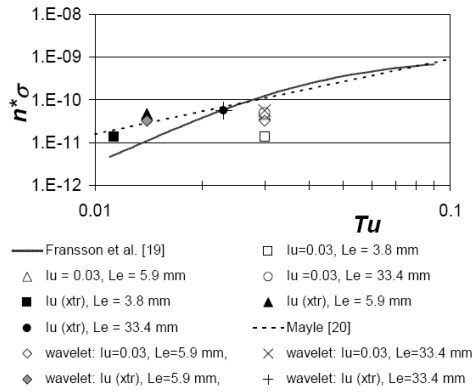


Figure 4: Dimensionless spot production rates versus turbulence level.

Apparently the results obtained from both the intermittency and the wavelet analyses are in accordance not only mutually but also with the results from [18]. An interesting comparison is drawn in Figure 4, where the values $n^*\sigma$ are plotted versus turbulence level either in the leading edge plane $x = 0$, $Iu_e = 0.03$ (empty symbols) or in sections of the transition start $x = x_{tr}$, $Iu_{tr} < 0.03$ (filled symbols). Together with the measurement results are plotted interpolations of results presented in [19] and [20]. It appears that the model proposed by Mayle [20] fits well the dependency $n^*\sigma$ versus turbulence intensity however with the values valid in the section of transition onset Iu_{tr} .

The additional information provided by wavelet analysis is the number of detected spots of the defined length along the transition zone. It was observed the growing number of spots, the increasing average size of spots and the extended scatter of spot dimensions in the course of transition. Figure 5 is presented as an example of results. The behavior is in agreement with the physics of the spot generation process.

Taking into account the growth and the propagation of turbulent spot in time, the normalized - reduced number of spots per metre and per second must be determined for calculations of dimensionless spot production rates $n^*\sigma$. Details on procedure are described in [16]. The distributions of reduced number of spots and the mean length of identified turbulent regions arising from spots are shown as function of the distance x from the leading edge in Figure 6 and as function of the intermittency factor γ in Figure 7.

The distributions suggest that the spot generation starts more intensively at the larger L_e but this difference disappear farther downstream ($\gamma > 0.1$). Maximum of the spot occurrence is near $\gamma = 0.25$ because then the spot production is effectively inhibited due to calming e.g. [21]. The mean length of identified turbulent regions arising from turbulent spots initially slowly grows

regardless the L_e up to the location where $\gamma > 0.7$. A dramatic increase of the mean length of turbulent regions follows farther downstream $\gamma > 0.75$, probably owing to the merging of spots.

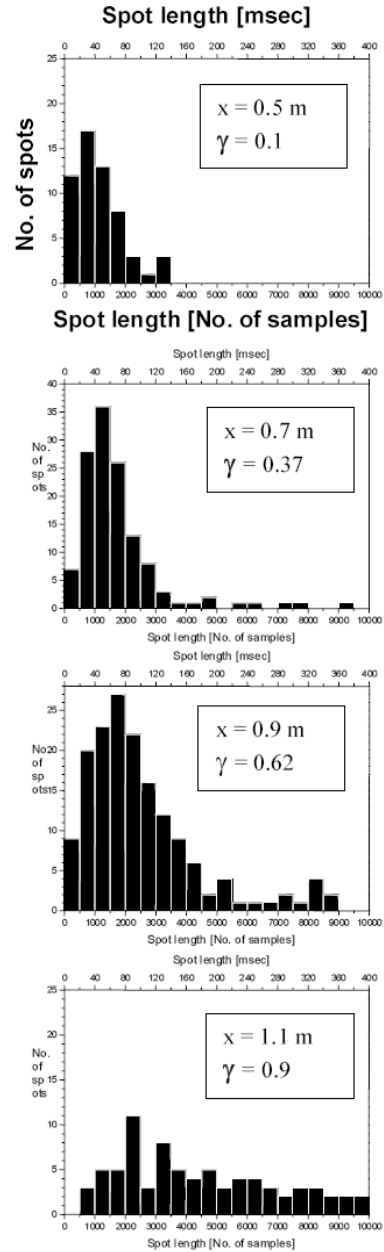


Figure 5: Number of spots as a function of spot length ($Iu_e = 0.03$; $L_e = 33.6\text{mm}$).

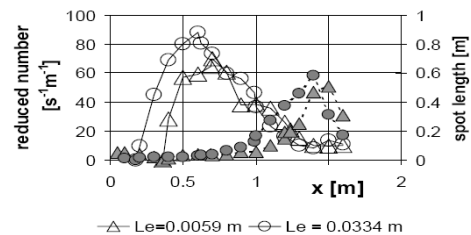


Figure 6: Distribution of reduced number (empty symbols) and mean length of the identified turbulent regions (filled symbols) versus the distance from the onset of boundary.

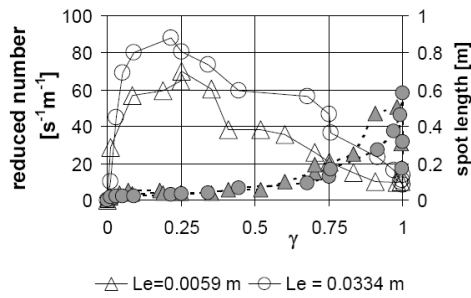


Figure 7: Reduced number (empty symbols) and mean length of the identified turbulent regions (filled symbols) as functions of intermittency factor.

4 Conclusions

Transitional intermittency factor distributions in boundary layer under turbulent flows with different length scales are compatible with the Narasimha [2] universal form but somewhat better correspond with intermittency model proposed by Johnson and Fashifar [18].

The dimensionless spot production rates $n^*\sigma$ evaluated from the applied wavelet analysis and using the Narasimha's intermittency concept are in accordance mutually and also with the published results. The values $n^*\sigma$ depend on Reynolds number, defined with the length of the transition region, regardless on the FST length parameter L_e , like the results received by Fransson et al. [19] at different FST structure (Iu, L) at the onset of boundary layer $x = 0$.

The dependence of the spot production rate on turbulence level compared with models [19] and [20] supports the model proposed by Mayle [20] particularly if the local turbulence level at the transition start would be considered. Possible explanation for this finding follows from the generally known fact that the smaller turbulence length scale L_e , the faster turbulence decay. Owing to this, the local intensity Iu_{tr} in FST with larger L_e exceeds the local intensity in FST with a smaller length scale, despite the same turbulence intensities Iu_e at the onset of boundary layer characterize both flows. Thus probably some spots provoked by large turbulent disturbances upstream from the section of the indifference Reynolds number survive the viscous damping and join those spots generating at the transition start. This explanation support further findings.

The spot occurrence is more numerous at larger length scale namely at the beginning of transition ($\gamma = 0.1$). Difference disappears farther downstream ($\gamma > 0.1$). Maximum of the spot occurrence is near $\gamma = 0.25$ at different length scales because then afterwards the spot production is effectively inhibited due to calming effect.

Mean length of identified turbulent regions arising from turbulent spots initially slowly grows regardless the L_e up to the location where $\gamma \approx 0.7$. This corresponds probably to identification of the individual spots and does not indicate an effect of the L_e . Farther downstream $\gamma > 0.7$ a dramatic increase of the mean length of turbulent regions arises. Obviously the merging of turbulent spots is the reason.

Acknowledgements

This work was supported by the Grant Agency of the Academy of Sciences of the Czech Republic (project A200760614), by Ministry of Education, Youth and

Sports CR (project KONTAKT No. 37) and by the Polish State Committee for Scientific Research under the statutory funds BS-01-103-301/2004/P.

References

- [1] Emmons H.W. (1951), The laminar-turbulent transition in a boundary layer - Part 1. J. Aero. Sci. 18, 490-498.
- [2] Narasimha R. (1985), The laminar-turbulent transition zone in the boundary layer. Prog. Aerospace Sci., 22, 29-80.
- [3] Schubauer G.B. and Skramstad H.K. (1948), Laminar boundary layer oscillations and transition on a flat plate. NACA Rept. 909.
- [4] Jonas P. (1997), On the role of the length scale in the by-pass transition, ZAMM - Z. angew. Math. Mech. 77, S1 S145-S146.
- [5] Jonas P., Mazur O. and Uruba V. (2000), On the receptivity of the by-pass transition to the length scale of the outer stream turbulence. Eur.J.Mech. B 19, 707-722.
- [6] Roach P.E. and Brierley D.H. (2000), Bypass transition modeling: a new method which accounts for free-stream turbulence intensity and length scale. ASME Paper 2000-GT-0278.
- [7] Brandt L., Schlatter P. and Henningson D.S. (2004), Transition in boundary layers subject to free stream turbulence. J. Fluid Mech. 517, 167-198.
- [8] Jonas P., Mazur O. and Uruba V. (2001), By-pass transition experimental study with a control of outer stream turbulence scale. Proc. TSFP-2, KTH, Stockholm, 51-55.[9] Savill A.M. (1995), COST-ERCOFTAC transition SIG COST action workshop IT AS CR Prague, ERCOFTAC Bulletin No. 11, 36-37.
- [10] Hancock P.E. and Bradshaw P. (1989), Turbulence structure of a boundary layer beneath a turbulent free stream. J. Fluid Mech. 205, 45-76.
- [11] Jonas P., Mazur O. and Uruba V. (1999), Statistical characteristics of the wall friction in a flat plate boundary layer through by-pass transition. Z. Angew. Math. Mech. 79, S691-S692.
- [12] Zhang D.H., Chew Y.T. and Winoto S.H. (1996), Investigation of intermittency measurement methods for transitional boundary, Exp. Thermal and Fluid Sci., 12, 433-443.
- [13] Hendley T.B. and Keffer J.F. (1974), Turbulent/non-turbulent decision in an intermittent flow. J. Fluid Mech. 64, 625-644.
- [14] Elsner W. and Kubacki S. (2000), Application of intermittency in boundary layer analysis. ITM TU Czestochowa.
- [15] Jonas P., Mazur O. and Uruba V. (2006), Experimental study of the wall friction development during boundary layer by-pass transition. Proc. Colloquium Fluid Dynamics, Praha, October 25-27, 2006, 67-70.
- [16] Elsner W., Wysocki M. and Drobniak S. (2006), Determination of production rate of turbulent spots using wavelet analysis. Chemical and Process Engng, 27, 935-950.
- [17] Misiti M., Misiti Y., Oppenheim G. and Poggi j. M. (2000), MATLAB. The MathWorks Inc. [18] Johnson M.W. and Fashifar A. (1994), Statistical properties of turbulent burst in transitional boundary layers. Int. J. Heat Fluid Flow 15, 283-290.
- [19] Fransson J.H.M., Matsubara M. and Alfredsson P.H. (2005), Transition induced by free-stream turbulence. J. Fluid Mech. 527, 1-25.
- [20] Mayle R.E. (1991), The role of laminar-turbulent transition in gas turbine engines. ASME Journal of Turbomachinery, 113, pp. 509-537.
- [21] Ramesh N. and Hodson H.P. (1999), A new intermittency model incorporating the calming effect, Proc. 3rd European Conference on Turbomachinery, London, Vol. A, 243-258

WAVELET ANALYSIS OF THE WAKE NEGATIVE AND POSITIVE JETS INFLUENCE ON THE LAMINAR-TURBULENT TRANSITION

Zygmunt Wiercinski

Institute of Fluid-Flow Machinery, PAS, Gdansk, Poland.

Introduction

Investigation of wake - boundary layer interaction on a plate is reported when the harmonic wake is generated by a single rod. This is probably a unique method to produce a series of alternately changing negative and positive jets. In this way it was possible to investigate directly the difference between the influence of negative and positive jet on boundary layer. The existence of serious differences was revealed between them because strong velocity impulses appear behind the negative jet in the place of the local minimum of the velocity, however behind the positive jet strong disturbances appear considerably later and not behind the wake directly. These impulses do not show the signs of chaos and should be rather classified to deterministic structures. Behind the positive jet the calm region was observed also in the area of entirely disturbed flow.

In turbomachinery the blades cut the wake into segments which next flow and deform in the blade passage and interact with flow and especially with boundary layer. Meyer (1958) differentiated between the impinging and suction jet depending on the direction of the flow of wake segment to or from the plate surface. Hodson, 1985, used the notion of "negative jet" to describe the behaviour of wake in the blade passage in turbomachinery, where the wake segment moves towards the trailing edge of a generating blade. But in the paper by Addison and Hodson, 1990, there is a suggestion that the negative jet has a very little effect on the boundary layer which remains either laminar or turbulent. Another phenomenon was also reported in which the relative motion of fluid around the blade was revealed: in compressor Kerrebrock and Mikolajczak (1970) observed the motion from the suction side to the pressure side of blade, whereas in turbine Binder et al., (1984) observed the inverted motion.

So it is well known that depending on the choice of the co-ordinate system: a wake can be treated as a velocity defect in a absolute system of co-ordinates or as a jet in a system of co-ordinates fixed with the mean velocity of flow.

But another meaning of negative and positive jet is also possible. The sign of the jet depends on the sign of the jet velocity relative to the blade surface. The boundary layer on the blade is affected by a positive jet when the speed of the jet is oriented towards the surface of blade so the jet impinges the blade, and affected by a negative jet, if the velocity of the jet is directed from the blade towards the external flow. Probably, Wiercinski, (1995) was the first who used the names negative and positive jets in such a context. It was based on the observation of the earlier inception of transition in a boundary layer on a flat plate behind the negative than behind the positive one. The difference in velocity fluctuations behind the negative and positive jet was measured and

reported in Wiercinski, (1999).

The notion of negative jet was also used in a bypass transition (Hernon et al., 2007) where the first signs of breaks down to turbulence were observed. The lift-up process of a low-speed streaky structure towards the boundary layer edge is called negative jet. Actually, this phenomenon could be described as an internal negative jet, while the jet caused by wakes - as an external negative jet.

Another traces of negative and positive jet can be found in the paper of Jeon et al. (2002) who carried out an investigation of the transition in the boundary layer on a NACA 0012 profile inserted in the squirrel cage. In their investigation they found that for the counter-clockwise rotation of the squirrel cage the wake induced turbulent patches grew more quickly and merged with each other further upstream than those for the clockwise motion of the squirrel cage. It is rather easy to prove that the earlier transition of the boundary layer of NACA0012 profile appears behind the negative jet.

In most experimental research the different impact of negative and positive jet on transition was not noticed probably because they were rather devoted to following the motion of wake segments in the blade-to-blade passage, (e.g. Stieger and Hodson, 2005).

It is also necessary to make an additional distinction of the influence of negative and positive jets relating the side of the blade: on the pressure and suction side of blade. Negative jet (NJ) influence on the suction side (SS) of blades of the rotor in the case of ventilators and compressors, and positive jets (PJ) on pressure ones (PS), Fig. 1a. It is the inverse in turbines, Fig.1b.

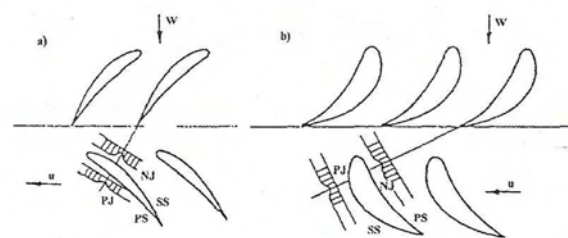


Figure 1: *Positive and negative jets in compressor (a) and turbine stage (b) (Wiercinski, 1999) PJ and NJ - positive and negative jet, PS and SS- pressure and suction side.*

The question of wake influence on flow in the blade-to-blade passage of turbomachinery has already a long history. It will be sufficient here to remember the review on transition by Mayle, (1991). However many questions remain unanswered. Recently new evidence for the strong difference in the influence of the negative and positive jet with the boundary layer were reported in the papers

of Wiercinski and Zabski, 2007, 2008, 2009. Apart the basic importance of the negative and positive jet influence on the LTT, additionally the wake and leading edge interaction for the earlier LTT inception was emphasized in the presentation of Beevers, 2007.

The research reported here is aimed at an investigation of the differences in the influence of positive and negative jets on the boundary layer on a plate at zero pressure gradient and at low intensity of the external stream turbulence. The understanding of the boundary affected by the jets (positive and negative) should give us the tools for the better understanding and modelling of non-stationary phenomena in flow machines and especially the laminar-turbulent transition.

Experimental stand

Measurements were conducted in a low subsonic wind tunnel at the Institute of Fluid-Flow Machinery, Gdansk, with a low level of background turbulence, $Tu \leq 0.08\%$ and a maximum flow speed of $U = 100$ m/s. The measurement chamber with octagonal cross-section has the following dimensions (width, height, length) 600x460x1500 m; see figure 2.. The boundary layer was studied on the upper surface of the flat plate of dimensions 600x700x14 (width, length, thickness). The angle of the attack was zero, so and the gradient of pressure close to zero value was characterized by the coefficient of acceleration $K = 7 \cdot 10^{-8}$. A round rod of diameter 3 mm and length 600 mm served as the wake generator. The upstream distance between the rod and the plate leading edge is equal to $L = 86$ mm, so the ratio $L/d \approx 28.7$. The rod moved up and down with the frequency $f = 4$ Hz, which gives the period 0.25 sec for one negative and one positive jet. The time-phase of the rod motion generating the negative jet was recorded and the moment of time chosen as the phase mark was when the axis of the rod is on the same height as the leading edge of plate. After the phase mark is recorded, the wake produced by the rod moves with a flow speed, so the trace of negative jet is delayed in the relation to the phase mark (on wavelet graphs - perpendicular black interrupted lines). The measurements were carried out by means of the StreamLine hot-wire system with the software StreamWare and the hot-wire sensor 55P15 of DANTEC. The measurements were carried out for the air velocity of $U = 15$ m/s, for eight various Reynolds numbers $Re = 168843, 216979, 257412, 298640, 334414, 374159, 587243, 686918$. The velocity signal recorded for every point took $t = 10$ s and were sampled with the frequency $f = 5$ kHz.

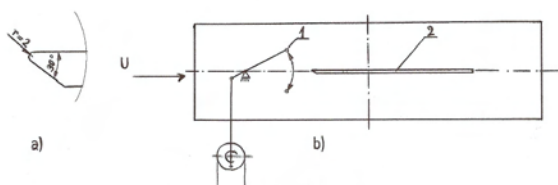


Figure 2: Scheme of the experimental stand, a) leading edge geometry, b) working section, 1) wake generator (rod), 2) plate.

Results of investigations

The wavelet analysis was preceded by the time and phase averaged analysis. The results were presented in Wiercinski and Zabski, 2009. The investigation contained the different velocity profiles and other characteristics of boundary layer such as the thickness of the layer δ , the coefficients of the resistance C_f and so on were derived as well. The investigations of the boundary layer yielded time averaged measurements results comparable with those presented in work Wiercinski, 1999. A diagram of the local friction coefficient C_f distribution is presented below, Fig. 3. It is treated as a reference diagram for the following diagram with the wavelet analysis.

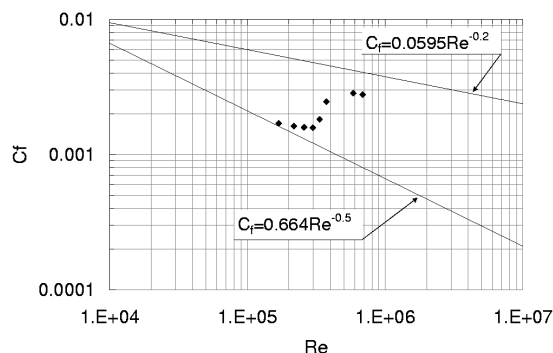


Figure 3: Local drag coefficient C_f distribution along plate.

Results of wavelet analysis

Since its originate the wavelet analysis found many different application, e.g. : detecting discontinuities and breakdown points in observed phenomenon, de-noising signals, identifying frequencies, etc., but it is well known that it is particularly useful for the non-stationary signal analysis, where one has to deal with signals of different frequencies in different time intervals, (MathWorks, 2004, Addison, 2002). And such a case took place in this investigation where one had to do with unsteady signals. This feature of the wavelet analysis is crucially different from the Fourier analysis for which it is necessary to assume that the analysed signal is stationary. In Fourier analysis basically the harmonic functions sine and cosine are used. In wavelet analysis there are many different families of wavelet functions of different features.

In reported experiment the Meyer wavelet was used to analyse the instationary behaviour of flow behind jets. Both the scaling function and wavelet function in the Meyer family wavelet are defined in frequency domain. They are also symmetric and ensures orthogonal analysis. So the wavelet analysis was used as a bandpass filter. The wavelet analysis was made by means of the Wavelet Toolbox of MatLab.

There are many different possibilities to choose the points for the analysis. Usually, the most interesting points were chosen and in this case it was the nearest point to the plate surface, generally, in the range $y^+ = 10 \div 13$. Another four points were: on the other edge of velocity fluctuation distribution and in two maxima and one minimum (not presented). The point at the outside edge of distribution goes beyond conventional borders of layer, that is $U = 0.99U_0$, because the velocity fluctuations are seen outside this border and this point is where

the velocity fluctuations do not get smaller any more and are actually equal to the velocity fluctuation in the outside stream. It is clearly that the points could be chosen in another way.

Beneath, four graphs are presented for varying Reynolds numbers, for the first, third, fourth and last point of the C_f diagram in Fig. 3. Each of these graphs contain the same elements. In the upper graph the velocity time trace is presented, whereas in the central graph the results of wavelet analysis is presented and finally the lower graph shows the section through the second graph for the frequency $f = 192$ Hz. Actually, the central graph is three-dimensional, to visualize it the altitudes of the wavelet coefficient a are shown as isoheights by grey-shades with the grey shadowed bar and scale at the right side. By the vertical lines in the central graph the time for the negative jet is marked, and between them is the positive jet. The black intermittent horizontal line is marking the frequency $f = 192$ Hz mentioned above. The values of wavelet coefficients a for this frequency are introduced in the lowest graph. The time t is marked only once on the horizontal axis of the lowest graph.

Just in the first of these figures, Fig. 4, the considerable velocity difference behind the negative and positive jets are shown. The strong velocity impulses are well seen behind the negative jet, whereas behind the positive they are not disturbances. What is striking here is the local velocity minimum behind the negative jet.

The investigation of Jeon et al. (2002) showed that the averaged static pressure on the profile surface in the case of a counter-clockwise rotating squirrel cage (i.e. negative jets) is considerably smaller than in case of clockwise rotating (i.e. positive jet). Similar pressure differences were reported earlier by Hodson (1985). So the strong velocity disturbances should be connected with both the local pressure and velocity falls caused by the negative jet.

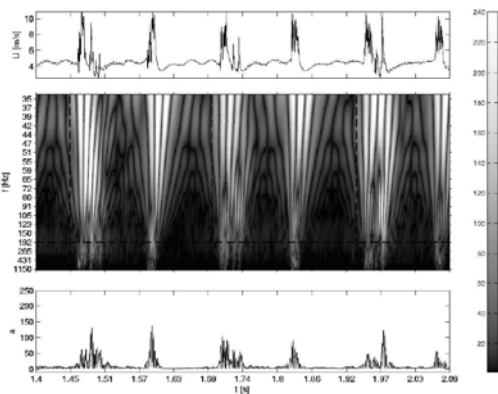


Figure 4: Wavelet chart, $Re = 168843$, $y^+ = 10$.

Two characteristic wave packages of frequencies $f = 42$ Hz and 192 Hz are also seen between the wake jets. Estimating the intensity of the wave package of frequency 192 Hz, it is seen in the lowest graph of Fig. 4 that it is much more present behind the negative jet. The second wave package of frequency 42 Hz basically appears with equal intensity behind both jets. The determined $F = \beta_r \nu / U_o^2 \cdot 10^6$ coefficient of these wave is equal to $F(42)=17$ and $F(192)=80$ and the connected Reynolds number $Re_1 = 660$ places these almost harmonic distortions before the neutral curve of the Tollmien-Schlichting waves. For further Reynolds numbers the phase change and amplification of the amplitude of these waves were not observed so the two principal characteristics of Tollmien-Schlichting waves were

not visible. They can be called only as the waves similar to the Tollmien-Schlichting waves.

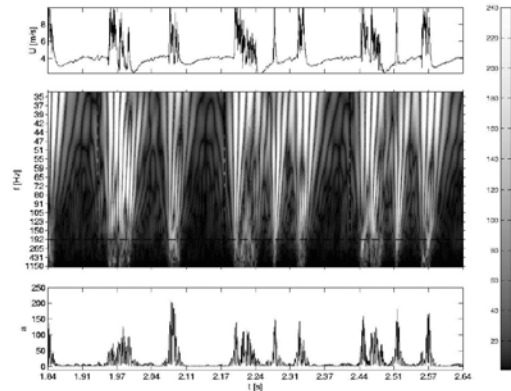


Figure 5: Wavelet chart, $Re = 257412$, $y^+ = 10$.

In Fig. 5, for Reynolds number $Re = 257412$, the third point in Fig. 3, the intensity of the impulses behind negative jets systematically grows, whereas the level of disturbances behind positive jets are furthermore much smaller. It is also striking that behind the negative jet the calm region is rather absent, while it is excellently visible behind the positive jet. Moreover, some additional disturbance disturbances begin to appear behind negative which can be compared to the turbulent spots of natural origin. They appear in the middle behind the negative and positive jets, Fig. 5.

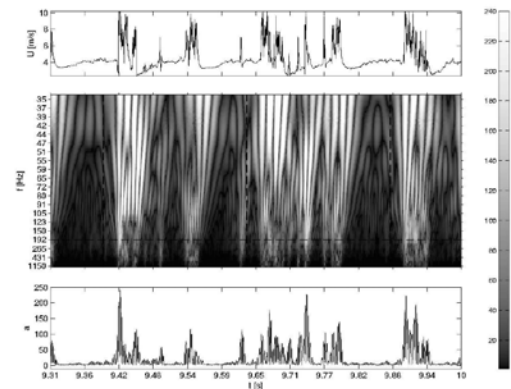


Figure 6: Wavelet chart, $Re = 298640$, $y^+ = 10$.

In Fig. 6 for Reynolds number $Re = 298640$, the fourth point in the C_f graph in Fig. 3, the continued growth of disturbances behind negative jets can be well seen, and even first large impulses of the velocity appear on the background of the increasing level of disturbances in the area before positive jets. Nevertheless there is a further region without disturbances directly behind the positive jet. Thus the zone called calm region behind the positive jet remains. The described symptoms can be well seen in the three diagrams in all figures, where in the upper diagram the time traces show continuously increasing number of impulses, whereas in the central diagram the full wavelet spectrum from 32 to 1050 Hz shows increasing amount of distortion and finally in the third diagram the section for the frequency $f = 192$ Hz also shows increasing level of disturbances.

In Fig. 7 for the Reynolds number $Re = 686918$, the last of the C_f diagram in Fig.3, the area behind the negative jet is entirely filled with strong impulses of the velocity, whereas the calm region behind the positive jet

is maintained. So the flow can not be estimated as full turbulent, which is also to see in Fig. 3, where the C_f value is below the turbulent distribution line.

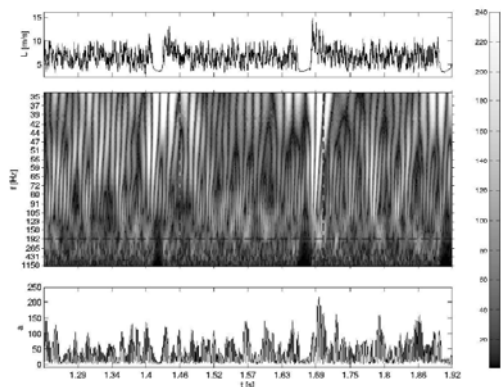


Figure 7: Wavelet chart, $Re_x = 686918$, $y^+ = 13$.

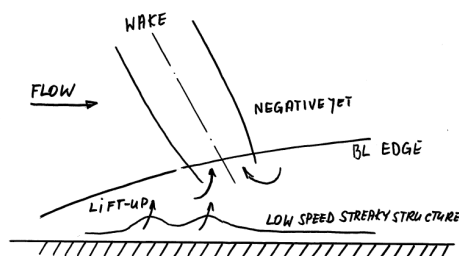


Figure 8: Interaction of wake negative jet with a low speed streaky structure in boundary layer leading to strong velocity disturbances.

Conclusions

It was presented above that the influence of the negative jet on the boundary layer is basically different from the positive jet. Strong velocity distortion were revealed in the area exactly behind the negative jet for the lowest values of the Reynolds number. The experiment was made for the coefficient of acceleration $K = 7 \cdot 10^{-8}$ so for the pressure gradient actually equal to zero. Increased Reynolds number leads to that the quantity of strong impulses grows and they join with larger structures, most probably the turbulent spots or patches. But they clearly still differ from the jet (wake). Additional lonely velocity impulses revealed at the half between the negative and positive jet raising supposition that they are turbulent spot of natural transition. However, what is very striking, the calm region, which is visible behind the positive jet persists for the all investigated Reynolds numbers, whereas such a calm region is very early not visible behind the negative jet.

In Fig. 8 the pictorial picture of proposed explanation for the occurrence of the strong velocity disturbances behind the negative is given. Passing negative jet causes the local pressure and velocity decrease in its neighbourhood. This pressure and velocity falls cause obviously the greater predisposition for destabilization of boundary layer, which could be connected with the earlier growth of the low speed streaky structure and its lift-up. The combining of these two processes could be responsible for the rapid growth of the velocity disturbances only behind the negative jet. Thus, the interaction of the

streaky structures (known from the natural transition) with the wake negative jet should be considered as a cause of appearance of strong disturbance.

Additionally, the harmonic wave packages about frequencies $f = 42$ and 192 Hz in regions between both jets can be recognized probably as - to some extent - similar to Tollmien-Schlichting waves.

Finally, the last conclusion referring the importance of results of this investigation for transition modelling in turbomachinery, it is to emphasize once again that the negative jet is more dangerous for rendering the flow turbulent, because it decreases the static pressure and velocity in its vicinity near the plate surface. In such a way it enhance the predisposition of flow in boundary layer to unstable behaviour. Such a behaviour could be, moreover, connected with regions of local of pressure increase and decrease along the pressure and suction side of the blade.

References

- Addison, P.S., 2002, The Illustrated Wavelet Transform Handbook, IP Publishing Ltd, London.
- Addison, J.S., Hodson H., 1990, unsteady transition in an axial flow turbine: Part 2: cascade measurements and Modelling, ASME J. Turbomachinery, Vol.112, pp. 215-221.
- Beevers, A., 2007, Simulation of wake induced transition on axial compressor stator blade, Workshop on Transition Modelling and Turbulent Combustion, Ghent, November 29-30.
- Binder, A., Forster, W., Kruse, H., Rogge, H., 1984, An Experimental Investigation into the Effect of Wakes on the Unsteady Turbine Rotor Flow, J.Eng.Gas Turb.& Power, Vol. 107, pp.1039-1046.
- Hernon, D., Walsh, E.J., McEligot, D.M., 2007, Experimental investigation into the routes to bypass transition and the shear-sheltering phenomenon, J. Fluid Mech. 2007, Vol. 591, pp. 461-479.
- Hodson, H.P., 1985, Measurements of of wake generated unsteadiness in the rotor passage of axial flow turbines, J. Turbomachinery, Vol. 107, pp. 467-475.
- MathWork, 2004, Manual, MathLab 7.0 + Wavelet Toolbox, v. 3.0.
- Mayle, R.E., 1991, The role of laminar-turbulent transition in gas turbine engines, J. Turbomachinery, vol. 113, pp. 509-537.
- Meyer R.X., (1958), The Effects of Wakes on the Transient Pressure and Velocity Distributions in Turbomachines, Trans. Journal of Basic Engineering, Vol. 80, pp.1544-1552.
- Jeon, W.-P., Park, T.-C., Kang, S.-H. (2002), Experimental study of boundary layer transition on an airfoil induced by periodically passing wake, Experiments in Fluids, vol. 35, 229-241.
- Kerrebrock J.L., Mikolajczak A.A., 1970, Intra-Stator Transport of Rotor Wakes and its Effect on Compressor Performance, ASME Journal of Engineering for Power, Vol. 92, pp. 359-368.
- Stieger, R., Hodson, H.P., 2005, The unsteady development of a turbulent wake trough a downstream low pressure turbine blade passage, J. Turbomachinery, Vol. 127, pp. 388-394.
- Wiercinski, Z., 1995, The Influence of the Periodic Wake behind a Cylinder Pendulating in the Cross-Stream Direction on the Laminar-Turbulent Transition in the Boundary Layer of a Flat Plate, Proc. Conf. Unst.Aerodynamics & Aeroelasticity of Turbomachines, Elsevier, pp. 461-479.
- Wiercinski, Z., Experimental investigation of the influence of the negative and positive jet of Wake with Boundary layer IFFM Transactions, No 98, Gdansk, pp.53-64.
- Wiercinski, Z., 1999, Laminar - turbulent transition in boundary layer induced by wakes, Report IMPPAN, 499/1450/99 (DSc Thesis, in Polish).
- Wiercinski, Z., Zabski, J., 2007, Phase averaged characteristics of boundary layer in the transition induced by wakes, Workshop on Transition Modeling, Ghent, November 29 and 30.
- Wiercinski, Z., Zabski, J., 2008, Investigation of the negative and positive jets in the induced by wakes transition, The 5th. ECCOMAS 2008, June 30 - July 5, 2008, Venice, Italy.
- Wiercinski, Z., Zabski, J., 2009, Influence of the negative and positive jets on the laminar-turbulent transition, 8th European Conference on Turbomachinery Fluid Dynamics and Thermodynamics, 23-27 March 2009, Graz-Austria, Conference Proceedings.

AN EXPERIMENTAL STUDY OF THE REYNOLDS NUMBER INFLUENCE ON A LAMINAR SEPARATION BUBBLE

Davide Lengani¹, Daniele Simoni¹, Marina Ubaldi¹,
Pietro Zunino¹, Francesco Bertini²

¹ DIMSET - University of Genova, Italy.

² AVIO S.p.a., Torino, Italy.

Abstract

The present paper reports the results of a detailed experimental study carried out in a low-speed test facility at the University of Genoa on the separated flow transition process. Laminar boundary layer separation has been studied for different Reynolds numbers over a flat plate installed within a double contoured test section designed to produce the adverse pressure gradient typical of Ultra-High-Lift turbine profiles.

Profile aerodynamic loadings as well as boundary layer velocity profiles have been measured to survey the separation and transition processes. Spectral analysis of hot-wire measurements has been also performed to identify the characteristic frequency of the phenomenon. Sharp peaks, which are the trace of Kelvin-Helmholtz waves generated in the shear layer over the separation bubble, appear in the spectra for the investigated Reynolds numbers at different frequencies.

1 Introduction

During the low Reynolds number operation of aeroengine LP turbines, the boundary layers developing along the blades suction side are mostly laminar, then transitional over a significant length. Therefore, boundary layer separation may occur. This is very detrimental for the performance, especially when the separation bubble is long or, even worse, when the flow massively separates. These phenomena tend to be even more common with the current trend of blade loading increase, lower operating Reynolds number, or just operation at off-design conditions. Therefore the blade design needs particular care in order to avoid the risk of performance reduction. In particular the development of the laminar separation bubble, its transition and consequent reattachment have to be accurately predicted at the different operating conditions, e.g. at different Reynolds numbers. Hence, transition and separation location play a crucial role for the turbine design since they may affect up to the 4% in terms of the engine efficiency [1].

Mayle [2], Walker [3], and Hatman et al. [4] presented critical analyses of transitional phenomena in gas turbine engines. Different prediction models have been proposed, but it has been also stated that there is no complete model to describe the overall separated-flow transition process. Even though empirical data have been obtained by many authors in early stage of the research, [5,6] among others, the physical understanding of laminar separation bubbles has still to be improved.

Recent numerical studies [7-9] showed that a two-dimensional inviscid instability originates from the shear layer flow over the stagnation region of the separation

bubbles via the Kelvin-Helmholtz mechanism. Vortical structures are shed by this instability process and induce fluctuations inside the flow which consequently promote the boundary layer transition. The breakdown to turbulence occurs at around the time-mean reattachment point where the flow starts to develop into the turbulent regime. Similar considerations were pointed out also by recent experimental works [10-12].

The present work, carried out in cooperation between University of Genova and Avio S.p.A., is part of an European research project named 'Turbulence And Transition Modeling for Special Turbomachinery Applications' (TATMo), focused on the experimental and numerical activities, aimed at extending the knowledge on the separated-transition processes especially for Ultra-High-Lift blades. A better physical understanding of the separation bubble behaviour at the different operating conditions may avoid performance deterioration for such highly loaded profiles.

The paper gives an experimental account of the separated flow transition occurring under steady conditions for Reynolds numbers in the range $70,000 < Re < 200,000$, typical of real aeroengine operating points. The boundary layer development has been surveyed along a flat plate installed within a double contoured test section, designed to produce the prescribed adverse pressure gradient typical of Ultra-High-Lift turbine profiles. Measurements have been performed by means of hot-wire instrumentation, within the transition/separation region. In particular, to better explain the transition process and to understand the physics which cause the separation reattachment spectral analysis has been adopted.

2 Experimental apparatus and measuring techniques

Measurements have been performed in the open loop wind tunnel installed in the Laboratory of Aerodynamics and Turbomachinery of Genova University. As shown in Fig. 1, the test section is constituted by a flat plate located between two contoured walls designed to impose an adverse pressure gradient typical of Ultra-High-Lift turbine profiles. The aerodynamic pressure gradient is similar to what analyzed in a single contoured test section by Lou and Hormouziadis [12]. The flat plate is 200 mm long and 300 mm wide.

The flat plate has been instrumented at midspan, along its rear part (downstream of the velocity peak), with a total of 25 pressure taps connected to a Scani-valve. Static pressures were measured by means of high-sensitivity high accuracy low range SETRA differential transducers. The instrument accuracy is better than $\pm 0.075\%$ of the transducer full-scale range (± 620 Pa).

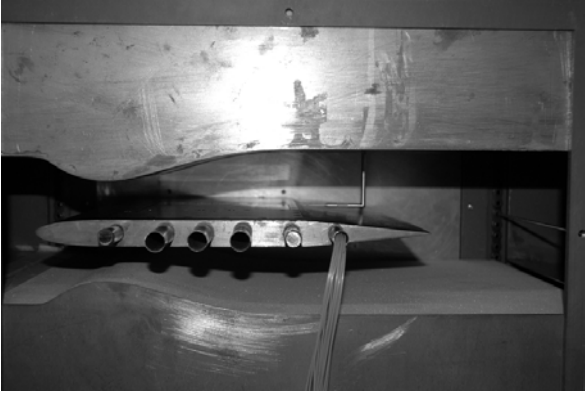


Figure 1: *Double contoured test section.*

The boundary layer developing along the rear part of the plate was surveyed by means of 12 traverses normal to the wall (from $x/L = 0.31$ up to the plate trailing edge). Each traverse was constituted by 31 points along the normal to the wall direction, with smaller spacing close to the wall. A three-axis computer controlled traversing mechanism with a minimum linear translation step of $8\mu\text{m}$ has been employed to allow high movement precision and spatial resolution. The boundary layer development has been investigated within the Reynolds numbers range $70,000 < Re < 200,000$. Measurements have been carried out for steady inflow conditions.

A Dantec single-sensor miniature boundary layer hot-wire probe (type 55P15) has been employed for the measurements. The anemometer output voltages were sampled using a Metrabyte DAS 58 sample and hold AD converter board.

Flow direction in a separation bubble cannot be determined with a single sensor hot-wire, but velocity magnitude can be measured and it was found to be very low and nearly constant within the bubbles investigated in the present study. For what concerns the time mean measurements, in each point, 262,500 samples have been collected with a sampling frequency of 10 kHz. An anti-aliasing low-pass filter set at 5 kHz has been used. Considering a confidence level of 95%, the uncertainty in the velocity measurements has been evaluated to be lower than 2%.

The post processing of the raw signals allows the evaluation of the velocity power density spectra which provides further information for the instability process behaviour. The spectra of the velocity fluctuations have been determined by averaging 32 fast Fourier transforms (FFT) performed on data blocks with a 50% overlapping. With a data sample length of 8192 and a sampling frequency of 10,000 Hz the frequency resolution is 0.61 Hz.

3 Results and discussion

3.1 Static pressure distributions

Blade loadings measured under steady inflow condition in the rear part of the plate are plotted in terms of the static pressure coefficient (C_p) in Fig. 2 for the different Reynolds numbers tested. For the lower Reynolds number, $Re = 70,000$, a large laminar separation bubble can be recognized for the steady case, as suggested by the plateau present in the C_p distribution. Boundary layer separation occurs at x/L equal to about 0.39, while reattachment seems to be completed only at $x/L = 0.69$. Increasing the Reynolds number the laminar separation

bubble appears smaller and smaller as suggested by the plateau length reduction.

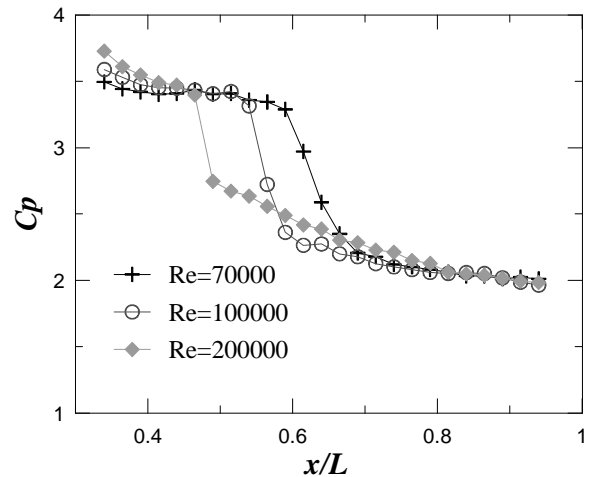


Figure 2: *Pressure coefficient distributions.*

For the highest Reynolds number ($Re = 200,000$), the laminar separation is still present, but it affects a very small portion of the plate. The boundary layer separates at about the same position observed for $Re = 70,000$, but reattaches sensibly upstream, at $x/L = 0.49$. The reduced extension of the separation bubble produces a higher velocity peak (suggested in the figure by the highest C_p value in the first measuring point) and consequently increases the aerodynamic loading.

3.2 Velocity and turbulence intensity fields

The bubble structure can be observed by the velocity and the turbulence intensity distributions reported in Fig. 3, for $Re = 200,000$. Both the velocity and its root mean square contour plots have been made dimensionless by the free-stream velocity measured in the first measuring traverse. The contour plots axes have been set with different scales ratio.

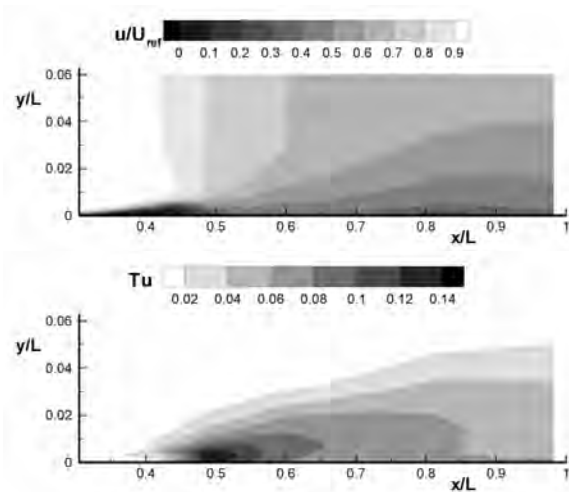


Figure 3: *Velocity and turbulence intensity contour plots: $Re = 200,000$.*

The laminar separation bubble, shown by the black area in the velocity contour plot, appears quite thin and short. Coherently with the C_p distribution, the

maximum thickness of the bubble is located at around $x/L = 0.46$, very close to the recovery point observable in the blade loading. The boundary layer transition process takes place just upstream of $x/L = 0.49$, as shown by the occurrence of a local peak in the turbulence intensity contour plot. The vanishing of the black area close to the wall, observable in the velocity distribution, confirms that the boundary layer has reattached downstream of $x/L = 0.49$.

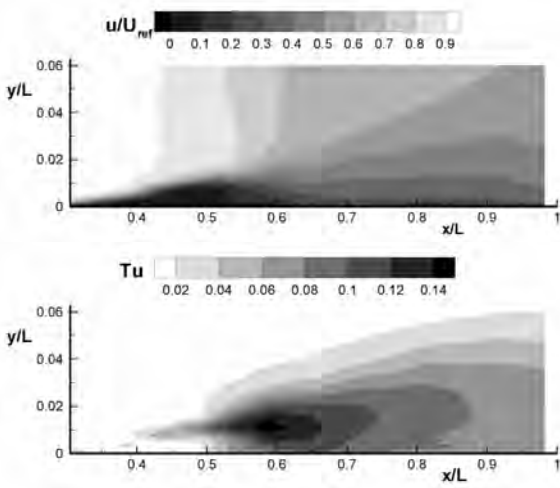


Figure 4: Velocity and turbulence intensity contour plots: $Re = 100,000$.

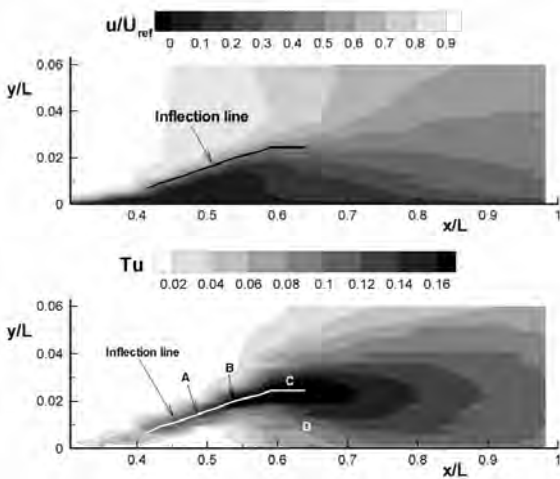


Figure 5: Velocity and turbulence intensity contour plots: $Re = 70,000$.

At the smaller Reynolds numbers the laminar separation bubble became larger and thicker, as shown in Fig. 4 and Fig. 5 for $Re = 100,000$ and $Re = 70,000$ respectively. Also in these cases, the maximum displacement positions of the bubble appear in good agreement with the positions associated with the C_p skew change. The bubble maximum displacement for $Re = 70,000$ is about $y/L = 0.02$. For this Reynolds number the boundary layer begins the transition and consequently the reattachment process downstream of $x/L = 0.59$, as suggested by the high velocity fluctuations occurring in the separated shear layer. However up to $x/L = 0.80$ a high velocity defect is still present close to the wall (dark grey region in the velocity distribution).

Re	f [Hz]	Kl	ω^*
70,000	482	1.2	0.220
100,000	791	0.98	0.215
200,000	2115	0.55	0.217

Table 1: Fundamental instability process parameters.

The boundary layer transition process starts on the separated shear layer just over the bubble, as suggested by the local increase of the turbulence intensity shown by the turbulence intensity contour plots for both the Reynolds numbers. In fact the trace of the velocity profile inflection points coincides with the maxima in the turbulence intensity distributions, as it can be observed in Fig. 5. The inflection line is defined as envelop of the points where $(\partial^2 u / \partial y^2) = 0$ and indicates the region where the boundary layer is intrinsically unstable. The large velocity fluctuations occurring inside the shear layer are due not only to the turbulence activity, but principally to the large scale coherent vortical structures growing in the shear layer due to the boundary layer inviscid instability process [12], as will be confirmed in the following by the spectra analysis.

At around $x/L = 0.5$ and $y/L = 0.018$ (point A reported in Fig. 5), the velocity fluctuations in the shear layer begin to be strongly amplified (point B), due to the shear layer rollup phenomenon that produces vortex shedding. The merging and the mixing out of these vortices introduce oscillations on the flow inducing consequently the boundary layer transition in the surround of the line of the velocity inflection points (point C). Moving downstream the turbulent region propagates towards the wall, promoting the fully turbulent condition of the boundary layer (point D) and the consequent separation bubble reattachment.

3.3 Velocity spectra analysis

The analysis of the velocity power density spectra in the separated shear layer can be useful for a better interpretation of the instability process for the different Reynolds numbers.

The high flow fluctuations observed in the turbulence intensity contour plot are induced by the shear layer instability and occur at a well identified frequency. The frequency range can be deduced from the velocity spectra obtained along the line of inflection points of the velocity profiles (e.g. looking to the black line superimposed on the velocity contour plot for $Re = 70,000$ in Fig. 5).

In Fig. 6 spectra obtained for several points (from A to D) are shown for the case $Re = 70,000$. The presence of a peak at around 480 Hz starts to become visible in the point A. This frequency peak suggests the beginning of the rollup phenomenon of the shear layer and it is in agreement with the theoretical estimation for Kelvin-Helmholtz instability frequency range [13]. For two constant density flows characterized by a continuous variation of the streamwise velocity component along the y direction, as in laminar separation bubble, the Kelvin-Helmholtz instability occurs with the wave number in the range $0 < Kl < 1.2785$, where l is the separated shear layer thickness and the wave number is expressed by $K = 2\pi f / u_{infl}$, as reported in the work of Chandrasekhar [13]. The frequency observed in our tests corresponds to $Kl = 1.21$ for $Re = 70,000$.

The power density spectra also show high energy con-

tent in the low frequency range associated with the bubble fluctuations.

Characteristic parameters for the other Reynolds numbers are provided in Table 1.

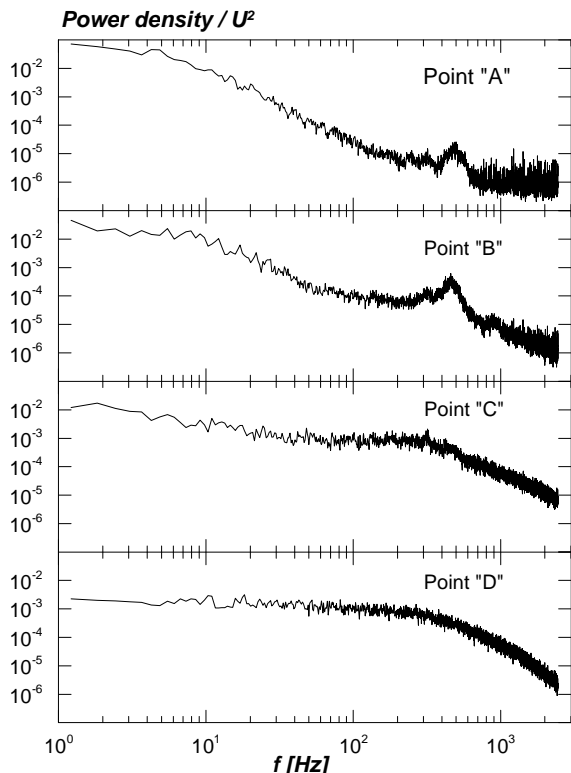


Figure 6: Non-dimensional power density spectra of velocity fluctuations for $Re = 70,000$.

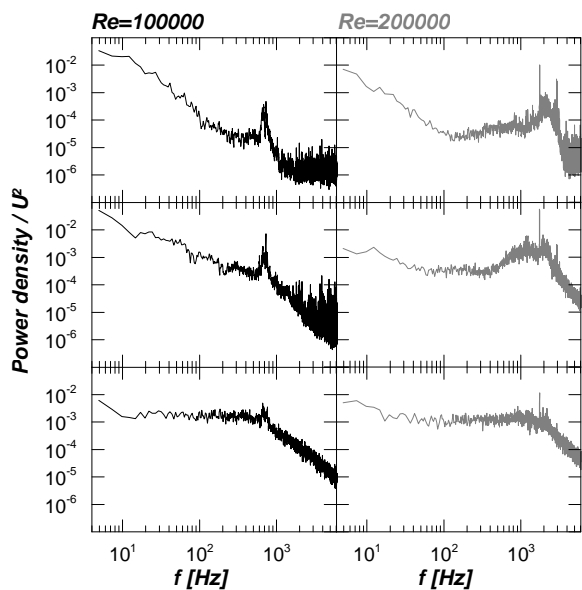


Figure 7: Non-dimensional power density spectra of the velocity fluctuations for $Re = 100,000$ (left column) and $Re = 200,000$ (right column); top, homologous of point A, middle point B, bottom point C.

Going downstream along the separated shear layer (point B), the peak of the power density appears strongly

amplified with respect to the previous point A. This confirms the amplification of the shear layer rollup mechanism. Vortices are then probably shed in correspondence of the top side of the bubble near to the maximum displacement position (at around $x/L = 0.6$) provoking high flow fluctuations inside the boundary layer up to induce its transition process.

Downstream of this position the boundary layer is in an advanced turbulent condition far away from the wall in correspondence of the point C, as confirmed by the power density spectra that assumes almost the typical turbulent distribution (excepted for the low frequency range that still contains large energy). The increasing mixing characterizing the turbulent condition increases the momentum transfer process in proximity of the wall, advecting turbulence towards the wall region (point D) and induces consequently the boundary layer reattachment.

Power density spectra are shown in Fig. 7 also for the other 2 Reynolds numbers tested. Increasing the Reynolds number the frequency peak increases its frequency. Furthermore, for $Re = 200,000$ a sub harmonic seems to appear at around 1000 Hz consistently with the result reported in the work of Malkiel and Mayle [10].

The sharp peak of the power density moves at higher frequency as the Reynolds number increase accordingly with the almost constant value of the dimensionless frequency parameter ω^* . Following the concept that the separated area can be seen as the interface between two distinct layers, characterized by two different velocity u_1 and u_2 separated by the shear layer, the velocity difference and the average velocity can be introduced to characterize the phenomenon $\Delta u = (u_2 - u_1)$ and $\bar{u} = 0.5(u_1 + u_2)$. The separated shear layer can be further characterized by the vorticity thickness $\delta_w = \Delta u / (\partial u / \partial y)_{\max}$. By means of these parameters it is possible to quantify the dimensionless frequency ω^* introduced by Monkewitz and Huerre [14]: $\omega^* = 1/4\delta_w(2\pi f)/\bar{u}$.

The values found for this parameter in the present work are summarized in Table 1 for the different Reynolds numbers and appear in good agreement with the values predicted by Pauley et al. [7] $\omega^* = 0.21$ and Yang and Voke [8] $0.206 < \omega^* < 0.231$.

The inviscid nature of the Kelvin-Helmholtz waves makes the dimensionless frequency almost non dependent on the Reynolds number suggesting a similar mechanism of the shear layer rollup.

4 Conclusions

The structure of laminar separation bubbles developing for a Reynolds numbers in the range $70,000 < Re < 200,000$ was experimentally investigated by a hot wire anemometer on a flat plate with a prescribed adverse pressure gradient typical of Ultra-High-Lift turbine profiles. The high frequency response of the instrumentation allowed analysis of the velocity fluctuations and power density spectra. For the smaller Reynolds number tested, the boundary layer has been found to be affected by a large laminar separation bubble. Aerodynamic loading distributions show that this bubble is strongly reduced increasing the Reynolds number.

Mean velocity and turbulence intensity contour plots for the steady case show that the beginning of boundary layer transition occurs in correspondence of the separated shear layer, where the velocity fluctuations are larger due to the shear layer instability. The maxima in the turbulence intensity contour plots have been found,

for all the Reynolds number conditions, in correspondence of the trace of the velocity profile inflection points.

The velocity spectra show that fluctuations are amplified moving downstream, and proceed into a Kelvin-Helmholtz type of breakdown, involving a rollup of the shear layer shedding a continuous sequence of vortices. The energy peak of the Kelvin-Helmholtz instability frequency is amplified up to the bubble maximum displacement.

The vortical structures generated by the instability introduce fluctuations in the main flow. The boundary layer transition seems consequently be triggered by the breakdown of large scale vortical structures induced by the inviscid instability occurring in the separated shear layer. The turbulent condition following the transition process increases momentum transfer toward the wall forcing the boundary layer reattachment.

The constant value of the dimensionless frequency observed for variable Reynolds numbers indicate the inviscid nature of the instability waves growing within the separated shear layer.

5 Nomenclature

$C_p = \frac{p_{t1} - p}{p_{t1} - p_1}$	pressure coefficient
f	vortex shedding frequency
$K = 2\pi f / u_{infl}$	wave number
l	shear layer thickness
L	plate length
p	static pressure
p_t	total pressure
$Re = U_0 L / \nu$	isentropic inlet Reynolds number
$Tu = rms(u') / U_{ref}$	turbulence intensity
u	streamwise velocity
u'	velocity fluctuation
U	local free-stream velocity
U_0	inlet free-stream velocity
u_{infl}	streamwise velocity at the inflection point
U_{ref}	free-stream velocity at $x/l = 0.3$
y	normal to the wall direction
$\delta_w = \Delta u / (\partial u / \partial y)_{max}$	vorticity thickness
ν	kinematic viscosity
$\omega^* = 1/4\delta_w(2\pi f) / \bar{u}$	instability dimensionless frequency

Acknowledgments

The authors gratefully acknowledge the financial support of the European Commission as part of the research project TATMo, 'Turbulence And Transition Modeling for Special Turbomachinery Applications'.

References

- [1] Hourmouziadis, J., 1989, "Aerodynamic Design of Low Pressure Turbines," AGARD Lecture Series, 167.
- [2] Mayle, R. E., 1991, "The Role of Laminar-Turbulent Transition in Gas Turbine Engines," ASME J. Turbomach., 113, pp. 509-537.
- [3] Walker, G. J., 1993, "The Role of Laminar-Turbulent Transition in Gas Turbine Engine: A Discussion," ASME J. Turbomachinery, 115, pp. 207-217.
- [4] Hatman, A., and Wang, T., 1999, "A Prediction Model for Separated Flow Transition," ASME J. Turbomach., 121, pp. 594-602.
- [5] Gaster, M., 1996, "The Structure and Behaviour of Laminar Separation Bubbles," AGARD CP4 part2, pp. 813-854.

[6] Roberts, W. B., 1975, "The Effect of Reynolds Number and Laminar Separation on Axial Cascade Performances," ASME J. Eng. Power, 97, pp. 261-274.

[7] Pauley, L. L., Moin, P., and Reynolds, W. C., 1990, "The Structure of Two-Dimensional Separation," J. Fluid Mech., 220, pp. 397-411.

[8] Yang, Z., and Voke, P. R., 2001, "Large-Eddy Simulation of Boundary-Layer Separation and Transition at a Change of Surface Curvature," J. Fluid Mech., 439, pp. 305-333.

[9] Spalart, P. R., and Strelets, M. Kh., 2000, "Mechanism of Transition and Heat Transfer in a Separation Bubble," J. Fluid Mech., 403, pp. 329-349.

[10] Malkiel, E., and Mayle, R. E., 1996, "Transition in a Separation Bubble," ASME J. Turbomach., 118, pp.752-759.

[11] Watmuff, J. H., 1999, "Evolution of a Wave Packet into Vortex Loops in a Laminar Separation Bubble," J. Fluid Mech., 397, pp. 119-169.

[12] Lou, W., and Hourmouziadis, J., 2000, "Separation Bubbles Under Steady and Periodic-Unsteady Main Flow Conditions," ASME J. Turbomach., 122, pp. 634-643.

[13] Chandrasekhar, S., 1996, "Hydrodynamic and Hydromagnetic Stability," Clarendon.

[14] Monkewitz, P. A., and Huerre, P., 1982, "The Influence of the Velocity Ratio on the Spatial Instability of Mixing Layers," Phys. Fluids, 25, pp.1137-1143.

EFFORTS TO MODEL BOUNDARY LAYER SEPARATION INDUCED TRANSITION USING A NON-LINEAR EDDY-VISCOSITY MODEL AND A REYNOLDS STRESS MODEL

Z. Vlahostergios, K. Yakinthos, A. Goulas

Laboratory of Fluid Mechanics & Turbomachinery, Aristotle University of Thessaloniki, Greece.

1 Introduction

The physics of the transitional flows is complicated and involves a lot of uncertainties, which make difficult a deterministic modeling approach. The various approaches presented so far are mainly directed in three routes: the use of the e^N method, where the evolution of the first disturbances in a flow are tracked in order to investigate if they grow or diminish, the LES and DNS approaches and the RANS approach. Each of these major approaches has its advantages and deficits. For example, the e^N method can accurately predict the natural transition but it cannot be applied to transitional flows due to boundary layer separation. The LES and DNS approaches, have been proven to have a good potential to model transitional flows but they require a significant amount of computational resources and they are time consuming. Regarding the RANS approach, transition modeling is based on the use of an eddy-viscosity or a Reynolds-stress model (RSM). This approach is quite simple but it has some very critical deficits. For example, the a-priori use of a turbulence model on a theoretically laminar flow (in its early development) has a major drawback. Savill [1, 2] has noticed that the use of a low-Reynolds number variance of a turbulence model is nearly obligatory since it can indirectly take into account the laminar nature of the boundary layer in the near-wall region and this mechanism seems to help significantly the reproduction of the transitional region. A major effort to model accurately the transitional flows using the RANS has been presented by Steelant and Dick [3,4] who developed the conditioned averaged Navier-Stokes equations, together with the intermittency factor concept. Suzen and Huang [5] and Suzen et al. [6] presented also some efforts to model transition using the intermittency transport equation.

Regarding the use of the eddy-viscosity models, it has been recognized that their linear variances for the computation of the Reynolds-stress tensor suffer from an incapability to predict accurately the transitional flows. This behavior has been related to their inability to predict the anisotropic behavior of the normal Reynolds-stresses in the near-wall region. In the past decade, some more sophisticated eddy-viscosity models have been presented, all of them developed on the basis of a non-linear expansion of the Reynolds-stresses tensor explicit equations. This non-linearity leads to an anisotropic representation of the normal Reynolds-stresses close to the wall as shown in the experiments. The non-linear models have been applied mainly in by-pass transitional flows, although there are some published works regarding its application to transitional flows due to boundary layer separation.

On the other hand, when transition is modeled with RSM, excellent results have been presented, for example

by Hadjic and Hanjalic [7] and Vlahostergios et al. [8], for the boundary layer separation-induced transition, although it has been recognized that these models are very difficult to handle since they require a lot of programming effort.

A recently approach is the one presented by Mayle and Schulz [9], who used the laminar kinetic energy k_L , which contributes to the Reynolds-stress tensor and it is present in the pretransitional flow regime inside the laminar boundary layer. In this way, the Reynolds-stresses for the momentum equations are computed using a total turbulent kinetic energy, which is the sum of the laminar kinetic and the turbulent one. Walters and Leylek [10], presented an integrated turbulence model, in the eddy-viscosity framework, where apart from the transport equations of k and ε they introduced a transport equation for the laminar kinetic energy k_L .

In this work, we present computational results for the boundary-layer separation-induced transition using a non-linear eddy-viscosity model, which adopts also one more equation for the laminar kinetic energy. The use of the laminar kinetic energy together with a non-linear constitutive expansion of the Reynolds-stresses has the potential to provide accurate results. The results are compared with the ones obtained with the use of a low-Reynolds number RSM developed by Craft [11].

2 The experimental test cases

The most detailed experimental database, regarding transitional flows, is the ERCOFTAC database for experiments conducted on flat plate flows. These experiments have been carried-out by Coupland and Brierley [12]. The measurements refer to the velocity and u-rms distributions during the flow development on a flat plate having a sharp or semi-circular leading edge leading to by-pass or separation-induced transition respectively. Of course, the most challenging cases, are the ones involving the boundary-layer separation, which are coded as T3L test cases and they refer to various freestream conditions for the inlet velocity and inlet turbulence intensity. The separated boundary layer developed on the flat surface becomes the main transition mechanism. Depending on the inlet conditions, various separation lengths are measured leading to different transition lengths. Table 1 shows the freestream conditions for the six T3L test cases. The experimental setup of the T3L test cases is shown in fig.1

Code	Freestream conditions (turbulence intensity and velocity)
T3L1	$Tu = 0.20\%$, $U_\infty = 5\text{m/s}$
T3L2	$Tu = 0.65\%$, $U_\infty = 5\text{m/s}$
T3L3	$Tu = 2.3\%$, $U_\infty = 5\text{m/s}$
T3L4	$Tu = 5.5\%$, $U_\infty = 5\text{m/s}$
T3L5	$Tu = 2.3\%$, $U_\infty = 2.5\text{m/s}$
T3L6	$Tu = 2.3\%$, $U_\infty = 10\text{m/s}$

Table 1: *T3L test cases: Freestream conditions.*

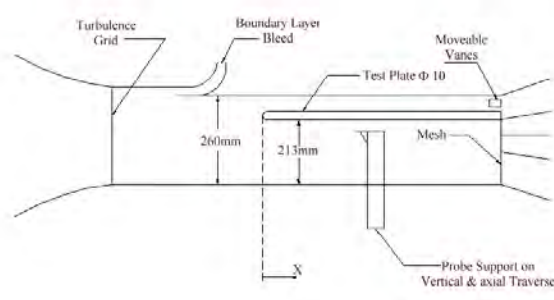


Figure 1: *The experimental setup of the T3L test cases.*

3 Overview of the turbulence models

3.1 The proposed combined model

The model of Walters and Leyelek [10], solves the two typical equations for the turbulent kinetic energy and the turbulence dissipation rate, which are appropriately modified in order to incorporate the transition mechanism. A third transport equation is solved for the laminar kinetic energy k_L :

$$\frac{Dk_L}{Dt} = P_L - R - R_{NAT} - D_L + \frac{\partial}{\partial x_j} \left(\nu \frac{\partial k_L}{\partial x_j} \right) \quad (1)$$

The transport equation for the turbulent kinetic energy has the form:

$$\frac{Dk_T}{Dt} = P_T + R + R_{NAT} - \varepsilon - D_T + \frac{\partial}{\partial x_j} \left[(\nu + \alpha_T / \sigma_k) \frac{\partial k_T}{\partial x_j} \right] \quad (2)$$

while for the turbulence dissipation rate the transport equation is written as:

$$\frac{D\varepsilon}{Dt} = C_{\varepsilon 1} \frac{\varepsilon}{k} (P_T + R_{NAT}) + C_{\varepsilon R} R \frac{\varepsilon}{\sqrt{k_T k_L}} - C_{\varepsilon 2} \frac{\varepsilon^2}{k_T} D_T + \frac{\partial}{\partial x_j} \left[(\nu + a_T / \sigma_\varepsilon) \frac{\partial \varepsilon}{\partial x_j} \right] \quad (3)$$

In these equations, P_L and P_T are the productions of the laminar kinetic energy and turbulent kinetic energy respectively, which are computed using the Boussinesq's linear formulation of the Reynolds-stresses.

$$P_L = \nu_{T,l} S^2 \quad (4)$$

$$P_T = \nu_{T,s} S^2 \quad (5)$$

where, $\nu_{T,l}$ is the large-scale eddy-viscosity and $\nu_{T,s}$ is the small-scale eddy-viscosity. These two viscosities are appropriately computed using various parameters and

coefficients, in the same manner as with a typical eddy-viscosity calculation plus they include an intermittency parameter in order to account for the transitional phenomena. The total eddy-viscosity is the sum of the two eddy-viscosities:

$$\nu_{TOT} = \nu_{T,s} + \nu_{T,l} \quad (6)$$

Additionally, R is a production term modeling the averaged effect of the breakdown of the streamwise fluctuations and R_{NAT} is the production term modeling the natural transition process. The D_L and D_T are the laminar and turbulent near-wall dissipation rates. The transport equation for the laminar kinetic energy has only a laminar diffusion term, while both the equations for the turbulent kinetic energy and the turbulence dissipation rate include the turbulent diffusion term. The latter is computed using the turbulent scalar diffusivity α_T a quantity, which is calculated using a damping function also, in the same way like the computation of an eddy-viscosity.

The expression for the Reynolds-stress tensor, which is used in the momentum transport equations, is given by:

$$-\overline{u_i u_j} = \nu_{TOT} \left(\frac{\partial U_i}{\partial x_j} + \frac{\partial U_j}{\partial x_i} \right) - \frac{2}{3} k_{TOT} \delta_{ij} \quad (7)$$

where,

$$k_{TOT} = k_{T,l} + k_{T,s} + k_L \quad (8)$$

with $k_{T,l}$ and $k_{T,s}$ being the small and the large-scale turbulent kinetic energy, computed by appropriate expressions.

The inclusion of a non-linear Reynolds-stress constitutive expression is straightforward in the framework of the laminar kinetic energy, Vlahostergios et al. [13]. The general form of the cubic expansion of the Reynolds-stresses tensor as presented by Craft et al. [14] is:

$$\begin{aligned} \overline{u_i u_j} = & \frac{2}{3} k \delta_{ij} - \nu_t S_{ij} + c_1 \frac{\nu_t k}{\varepsilon} (S_{ik} S_{jk} - \frac{1}{3} S_{kl} S_{kl} \delta_{ij}) \\ & + c_2 \frac{\nu_t k}{\varepsilon} (\Omega_{ik} S_{jk} + \Omega_{jk} S_{ik}) \\ & + c_3 \frac{\nu_t k}{\varepsilon} (\Omega_{ik} \Omega_{jk} - \frac{1}{3} \Omega_{kl} \Omega_{kl} \delta_{ij}) \\ & + c_4 \frac{\nu_t k^2}{\varepsilon^2} (S_{kl} \Omega_{lj} + S_{kj} \Omega_{li}) S_{kl} \\ & + c_5 \frac{\nu_t k^2}{\varepsilon^2} (\Omega_{il} \Omega_{lm} S_{mj} + S_{il} \Omega_{lm} \Omega_{mj} - \frac{2}{3} S_{lm} \Omega_{mn} \Omega_{ml} \delta_{ij}) \\ & + c_6 \frac{\nu_t k^2}{\varepsilon^2} S_{ij} S_{kl} S_{kl} + c_7 \frac{\nu_t k^2}{\varepsilon^2} S_{ij} \Omega_{kl} \Omega_{kl} \end{aligned} \quad (9)$$

The basic idea in the proposed combined model is to adopt this non-linear formulation in the computation of the turbulence production term: $P_{k,s} = -\overline{u_i u_j} \big|_s \frac{\partial U_i}{\partial x_j}$. This term, replaces the P_T term in equation (2). Correspondingly, the "small-scale" Reynolds-stresses needed for the above turbulent production term are computed by equation (9) and by using now, the small-scale eddy-viscosity $\nu_{T,s}$, the small-scale turbulence kinetic energy $k_{T,s}$ and a new quantity named as "small-scale turbulence dissipation rate" defined by:

$$\tilde{\varepsilon}_s = k_{T,s}^{3/2} / \lambda_{eff} \quad (10)$$

where λ_{eff} is a characteristic turbulence length scale defined by Walters and Leyelek [10].

The final proposed non-linear expression of the Reynolds-stress tensor, needed for the calculation of the momentum transport equations is given by:

$$\overline{u_i u_j} \big|_{TOT} = \overline{u_i u_j} \big|_T + \frac{2}{3} k_L \delta_{ij} \quad (11)$$

where the turbulent part of the total Reynolds-stresses is calculated using the total eddy-viscosity, the turbulent kinetic energy and the so called "isotropic" dissipation rate $\tilde{\varepsilon}$:

$$\tilde{\varepsilon} = \varepsilon - 2\nu \left(\frac{\partial \sqrt{k}}{\partial x_i} \right)^2 \quad (12)$$

The modeling approach is closed with the use of the appropriately adapted transport equation of the "isotropic" dissipation. This equation is based on the original equation of Craft et al. [14] and includes all the terms proposed by Walters and Leylek [10]:

$$\begin{aligned} \frac{D\tilde{\varepsilon}}{Dt} = & C_{\varepsilon 1} \frac{\tilde{\varepsilon}}{k_T} P_{k,\varepsilon} + C'_{\varepsilon 1} \frac{\tilde{\varepsilon}}{k_T} R_{NAT} + \\ & + C_{\varepsilon R} \frac{\tilde{\varepsilon}}{\sqrt{k_T k_L}} - C_{\varepsilon 2} R_{k_T} \frac{\tilde{\varepsilon}^2}{k_T} + \\ & + \frac{\partial}{\partial x_j} \left[\left(\nu + \frac{\alpha_{T,s}}{\sigma_\varepsilon} \right) \frac{\partial \tilde{\varepsilon}}{\partial x_j} + E + Y_c \right] \end{aligned} \quad (13)$$

where, E is a term added to achieve a correct behavior of k near the wall and Y_c is the Yap correction. Details of the model and the definition of the coefficients and parameters can be found in the work of Vlahostergios et al. [13].

3.2 The Reynolds stress model

Craft [11], presented a low-Reynolds number Reynolds-stress model, which was based on the model of Craft and Launder [15]. The general transport equation of the model is given by:

$$\frac{D\overline{u_i u_j}}{Dt} = P_{ij} + \Pi_{ij} - \varepsilon_{ij} + D_{ij} \quad (14)$$

where appropriate expressions are given for the modeling of the pressure term, Π_{ij} , of the dissipation rate ε_{ij} , and of the diffusion D_{ij} . The latter term is split into three parts:

$$D_{ij} = \frac{\partial}{\partial x_k} \left[\nu \frac{\partial \overline{u_i u_j}}{\partial x_k} - \overline{u_i u_j u_k} - \frac{p}{\rho} (u_i \delta_{ij} + u_j \delta_{ik}) \right] \quad (15)$$

The first term into the brackets represents the molecular diffusion and it does not need any modeling, while the two other terms, representing the turbulent diffusion due to the velocity fluctuations and the turbulent diffusion due to the pressure fluctuations need further modeling. In the literature, various expressions have been presented so far for these two terms. Especially for the turbulent diffusion due to the velocity fluctuations, Craft [11], presented a new modeling approach based on the solution of a system of equations for the triple correlation transport equations:

$$\frac{D\overline{u_i u_j u_k}}{Dt} = P_{ijk}^1 + P_{ijk}^2 + \varphi_{ijk} + d_{ijk} - \varepsilon_{ijk} \quad (16)$$

As Craft [11] indicates, this approach is closer to the physics of turbulence but it is more complicated and introduces additional programming effort for a turbulent flow modeling problem. For this reason, we decided to proceed with the use of the GGDH-generalized diffusion hypothesis of Daly and Harlow [16], where the triple correlation term in the turbulent diffusion due to the velocity fluctuations is given by:

$$D_{ij}^t = \frac{\partial}{\partial x_k} (-\overline{u_i u_j u_k}) = \frac{\partial}{\partial x_k} \left(C_s \frac{k}{\varepsilon} \overline{u_k u_l} \frac{\partial \overline{u_i u_j}}{\partial x_k} \right) \quad (17)$$

Details of the model can be found in the work of Craft [11].

4 Results and discussion

The T3L flows have been modeled using an in-house academic flow solver developed from our group. Details for the solver can be found in Vlahostergios et al. [8]. The flow domain has been modeled using an O-type grid having 96,000 computational cells. Fig. 2 shows a part of the grid used for the modeling of the computational domain, at the inlet region.

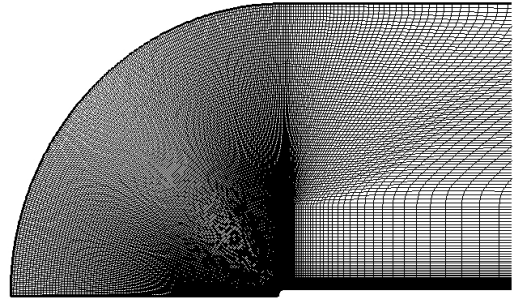


Figure 2: *Detail of the grid at the inlet section. The symmetry condition is applied on the stagnation point line.*

Grid dependency studies have been carried-out in order to investigate whether there are any grid dependencies. The results showed that the final chosen grid provided grid independent results. Special care has been taken also in order to have the correct inlet boundary conditions for the turbulence intensity. Based on our experience, Vlahostergios et al. [8], it has been found that incorrect values for the inlet turbulence intensity could lead to different recirculation zones, thus, to different transition lengths. Figure 3. shows the different separation lengths predicted using the RSM, for the T3L4 test cases, when inappropriate turbulence intensity values are used as inlet boundary conditions.

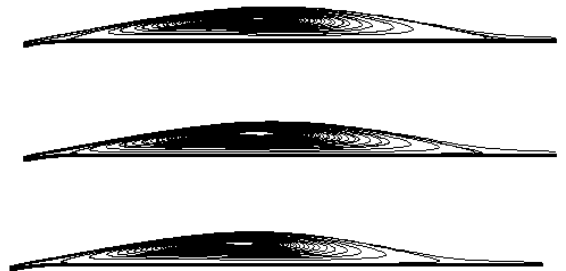


Figure 3: *T3L4 test case: choice of different values for the inlet length scale and their effect in the prediction of the recirculation length.*

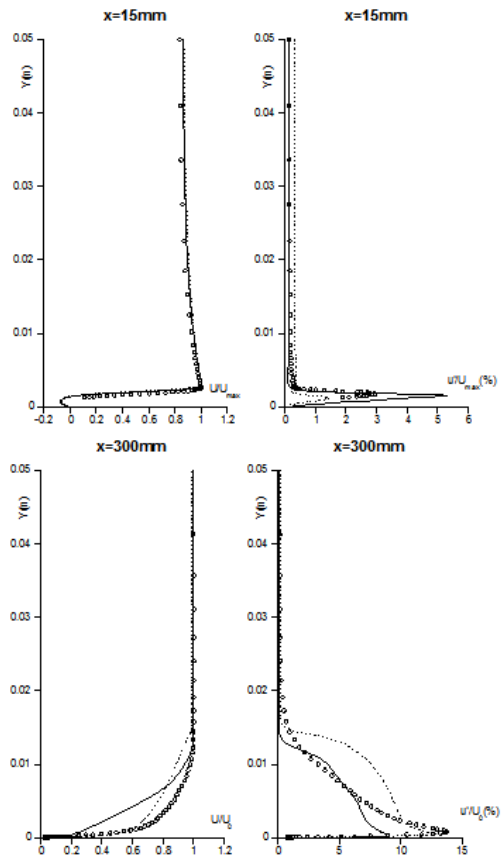


Figure 4: *T3L1*: velocity and *u*-rms distributions. Plain line: RSM model, dotted line: $k-k_L-\epsilon$ non-linear model.

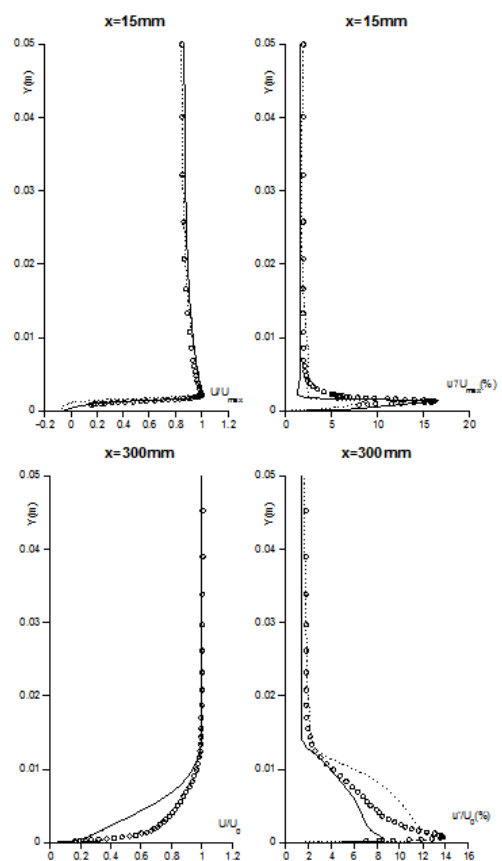


Figure 6: *T3L3*: velocity and *u*-rms distributions. Lines as in fig. 4.

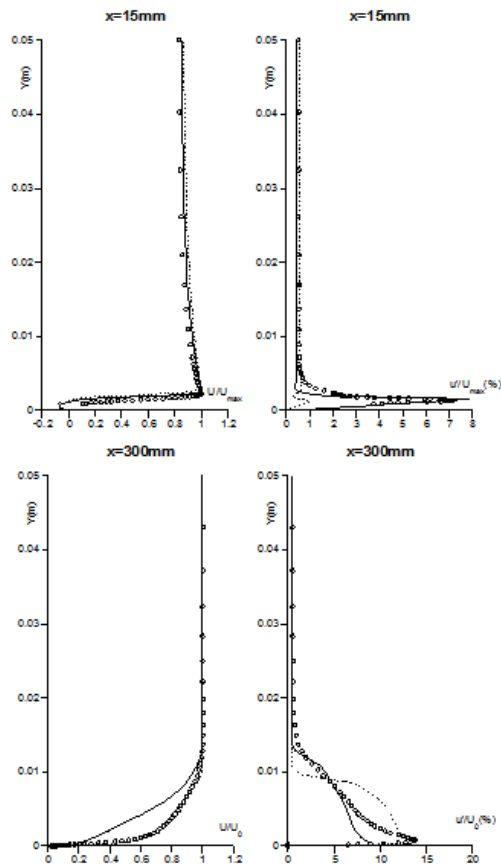


Figure 5: *T3L2*: velocity and *u*-rms distributions. Lines as in fig. 4.

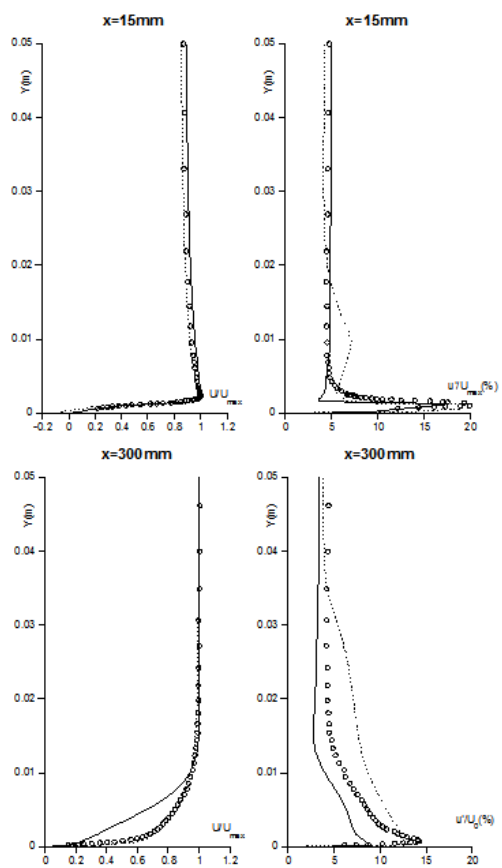


Figure 7: *T3L6*: velocity and *u*-rms distributions. Lines as in fig. 4.

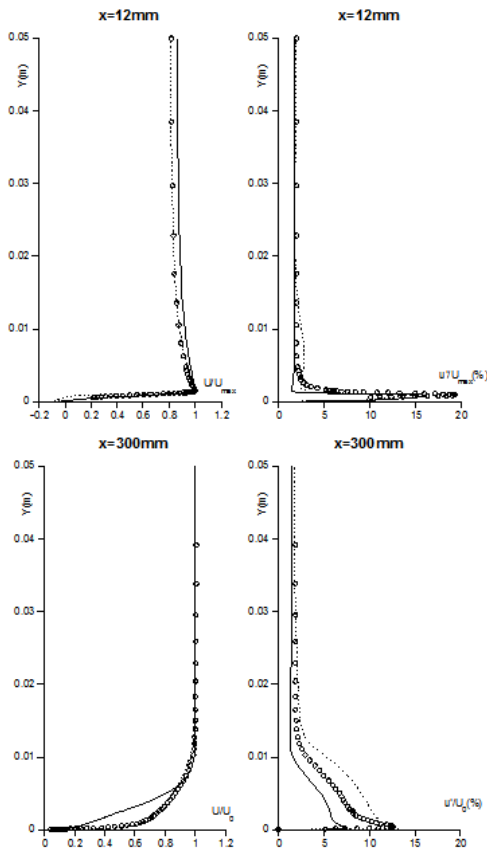


Figure 8: *T3L6: velocity and u -rms distributions. Lines as in fig. 4.*

Depending on the adopted turbulence model, appropriate values were used for the turbulence length scale, when the eddy-viscosity model was used, and for the normal Reynolds-stresses at the inlet, when the RSM was used, assuming always that the turbulence in this domain was isotropic. The check was based on the computed turbulence decay in the freestream flow and in comparison with the experimental measurements.

The convergence criterion has been chosen to be equal to 10^{-5} for the normalized values of the solved flow and turbulence variables. It should be noticed here that the iterations needed to obtain convergence with the RSM were much more than the ones needed when the proposed eddy-viscosity model was adopted (typical values for the RSM were about 10,000 iterations, while for the eddy-viscosity model about 2000 iterations were enough to obtain convergence). It has been also found that additional stability measures should be taken, when the RSM was used, in order to diminish any situation that could lead to divergence.

Figures 4 to 8 show the comparisons between the two models in reference with the experimental data, for both the velocity and u -rms distributions inside the boundary layer. The T3L5 test case is not shown here, since convergence could not be achieved when the RSM was used. For all the test cases, the selected stations refer to the region where the boundary layer is separated and to the region far downstream, where it is fully turbulent.

As a first observation, it is clear that both models are able to provide good results for the velocity and u -rms distributions inside the boundary layer. When the boundary layer is separated, the Reynolds-stress model behaves in a better manner, since it is able to capture the peak values of the u -rms. Here the proposed combined model is not able to predict the maximum val-

ues of the u -rms. On the other hand, the proposed eddy-viscosity model, is able to provide excellent predictions for the velocity distributions in the region located far downstream from the reattachment point, where the boundary layer is turbulent. The RSM predicts velocity profiles, with a distribution, which cannot be characterized as fully turbulent. This behavior can be related with its lower predicted values of the u -rms, compared to the experimental data.

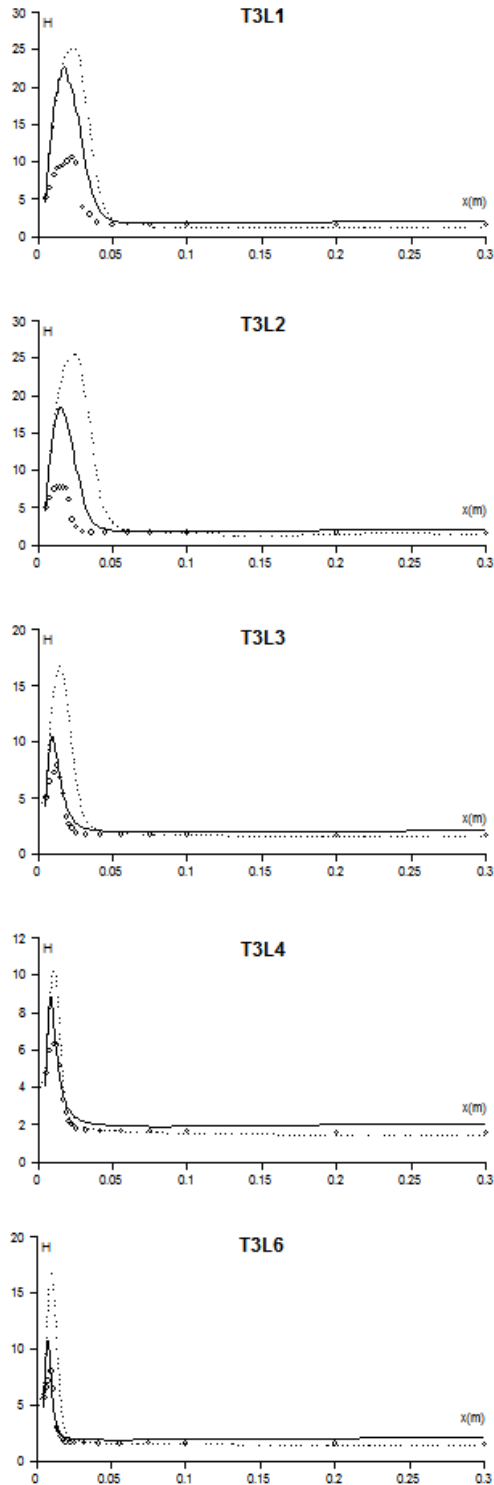


Figure 9: *Shape factor distribution in the streamwise direction. Lines as in fig. 4.*

The capability of the models to predict the transition length can be shown also, in the shape factor distribution in the streamwise direction, fig. 9. Here again, it

is clearly shown that the RSM provides better results for the transition length but it is not able to capture the fully turbulent flow regime, as measured in the experiments, since for all the test cases, in the far downstream region after the reattachment point, the values of the shape factor are larger than the measured ones. On the other hand, the capability of the proposed combined model, to provide excellent velocity distributions in the fully turbulent flow regime is supported by the shape factor distribution, which is an excellent agreement with the experiments, for all the test cases.

5 Conclusions

The modeling of the boundary layer transition from laminar to turbulent is indeed a serious challenge in computational fluid dynamics. So far, various techniques and approaches have been presented in the literature. In this contribution, we presented an effort to model the separation-induced transition using a non-linear eddy-viscosity model, appropriately adapted to include the concept of the laminar kinetic energy. The results have been compared with the ones obtained when a RSM has been used. For all the test cases modeled, it has been shown that the RSM can provide excellent results in the recirculation region for both the velocity and u-rms distributions but it presents not so good results in the region where the boundary layer is fully turbulent. The eddy-viscosity model does not predict in a good manner the distributions of the u-rms in the recirculation region, but it provides excellent results for the velocity distributions in the fully turbulent flow regime.

The answer to the question which model is better, is very difficult. The eddy-viscosity model requires less effort and is more stable but it cannot predict the transition length, while the RSM is more complex, it requires additional measures to obtain convergence but it can predict more accurately the transition length, although it is not able to capture the fully turbulent flow regime, as measured in the experiments. It seems that there is a need for additional investigations, for both models, in order to solve these problematic behaviors.

References

- [1] Savill, A.M. By-pass transition using conventional closures. In: Closure Strategies for Turbulent and Transitional Flows. (B. E. Launder and N. Sandham), Cambridge University Press, Cambridge, UK, 2002.
- [2] Savill, A.M. New strategies in modeling by-pass transition. In: Closure Strategies for Turbulent and Transitional Flows. (B. E. Launder and N. Sandham), Cambridge University Press, Cambridge, UK, 2002.
- [3] Steelant, J. and Dick, E. Modeling of by-pass transition with conditioned Navier-Stokes equations coupled to an intermittency transport equation. *Int. J. Num. Meth. Fluids*, 23, 1996.
- [4] Steelant, J. and Dick, E. Modeling of laminar-turbulent transition for high freestream turbulence. *J. Fluids Eng.*, 23, 2001.
- [5] Suzen, Y.B. and Huang, P.G., Modeling of flow transition using an intermittency transport equation, NASA Report/CR-1999-209313, 1999.
- [6] Suzen, Y.B., Huang, P.G., Hultgren, L.S. and Asphis, D. Predictions of separated and transitional boundary layers under low-pressure turbine airfoil conditions using an intermittency transport equation. *J. Turbomachinery*, 125, 2003.
- [7] Hadzic, I. and Hanjalic, K., Separation-induced transition to turbulence: Second-moment closure modeling. *Flow Turbulence and Combustion*, 63, 1999.
- [8] Vlahostergios, Z., Yakinthos, K. and Goulas, A. Experience Gained Using Second-Moment Closure Modeling for Transitional Flows Due to Boundary Layer Separation. *Flow Turbulence Combustion*, 79, 2007.
- [9] Mayle, R.E. and Schulz, A. The Path to Predicting By-pass Transition. *Journal of Turbomachinery*, 119, 1997.
- [10] Walters, K.D. and Leylek, J.H. A New Model for Boundary Layer Transition Using a Single-Point RANS Approach. *Journal of Turbomachinery*, 126, 2004.
- [11] Craft, T.J. Developments in a Low-Reynolds-number second-moment closure and its application to separating and reattaching flows. *Int. J. Heat Fluid Flow*, 19, 1998.
- [12] Coupland, J. and Brierley, D. Transition in Turbomachinery Flows. Final Report, BRITE/EURAM Project AERO-CT92-0050. Measurements available at the ERCOFTAC site, 1996.
- [13] Vlahostergios, Z., Yakinthos, K. and Goulas, A. Separation-induced transition: Modeling with a non-linear eddy-viscosity model coupled with the laminar kinetic energy equation. *Int. J. Heat Fluid Flow*, 30, 2009.
- [14] Craft, T.J., Launder, B.E., Suga, K. Development and application of a cubic eddy-viscosity model of turbulence. *Int. J. Heat Fluid Flow*, 17, 1996.
- [15] Craft, T.J. and Launder, B.E. A Reynolds stress closure designed for complex geometries. *Int. J. Heat Fluid Flow*, 17, 1996.
- [16] Daly, B.J., and Harlow, F.H. Transport equations of turbulence. *Phys. Fluids*, 13, 1970.

APPLICATION OF THE ZETA-F TURBULENCE MODEL TO STEADY TRANSITIONAL FLOW

M.E. Kelterer, K. Ramadani, R. Pecnik, W. Sanz

Institute for Thermal Turbomachinery and Machine Dynamics, Graz University of Technology, Austria.

Abstract

The accurate numerical simulation of the flow through turbomachinery depends on the correct prediction of boundary-layer transition phenomena. Reynolds stress turbulence models consider more flow physics and model the turbulence redistribution close to the wall which plays an important role within the transition process. Therefore in this paper the $k-\varepsilon-\zeta-f$ turbulence model is applied to turbomachinery flows. The $k-\varepsilon-\zeta-f$ turbulence model is for stability reasons advanced from the $k-\varepsilon-v^2-f$ turbulence model which has already been applied successfully in a commercial code for automotive flows.

The $k-\varepsilon-\zeta-f$ model is validated on the ERCOFTAC test cases T3A and T3C2. Furthermore, it is also applied to the steady flow in a T106A turbine cascade with a compressible code as well as with an incompressible code based on the artificial compressibility concept. It shows very promising results.

1 Introduction

In turbomachines and especially in aircraft engines the Reynolds numbers that determine the evolution of the boundary layers can be relatively low. So a large part of the flow along the blade surfaces is often laminar or transitional. The boundary layer development, losses, efficiency and heat transfer are greatly affected by the laminar-to-turbulent transition. Due to the high turbulence levels by-pass transition is the dominant form of transition in turbomachinery.

The ability to accurately predict the transition process is crucial for the design of efficient and reliable machines. Numerical investigations of transitional flows showed that Reynolds stress models with low-Reynolds-number modifications seem to perform better than two-equation turbulence models (see [1]). Reasons may be that they account for the near wall anisotropy and particularly their ability to reproduce the normal-to-the-wall velocity fluctuations. Another merit is the exact treatment of the turbulence production and of effects of streamline curvature (see [2]). Therefore there is hope that also related Reynolds stress transport models with considerably less computational efforts are also able to predict laminar-to-turbulent transition in satisfying accuracy.

Among these models the $k-\varepsilon-v^2-f$ (V2F) turbulence model of Durbin [3] is very promising and was investigated for turbomachinery applications by Sanz et al. in 2007 [4]. It showed good results for steady flows, but proved to be numerically unstable. Therefore in 2004 Hanjalic et al. [5] suggested modifications to the V2F model in order to improve its numerical stability. Their $k-\varepsilon-\zeta-f$ (ZETA-F) model has already been incorporated in a commercial CFD code for automotive flows (see [6])

and showed very promising results. In order to support the search for more general transition modelling, in this work the ZETA-F model is applied to transitional turbomachinery flows and compared with measurements and V2F calculations. Furthermore this work explores the difference in the solution of the flow around a turbine blade in case an incompressible or a compressible solver is used for low Mach number computations.

2 Numerical Method

The computations were performed using the in-house Navier-Stokes code LINARS, developed at Graz University of Technology (Pecnik et al., 2005 [7]). The compressible Reynolds/Favre-averaged Navier-Stokes (RANS) equations are solved in conservative form by means of a fully-implicit time-marching finite-volume method on structured curvilinear grids in multiblock alignment. The inviscid (Euler) fluxes are discretized with the upwind flux-difference splitting method of Roe (1981) [8]. In order to achieve a high order of spatial accuracy a total variation diminishing (TVD) was used. The viscous flux vector at the cell interfaces is constructed with a second-order accurate central-differencing scheme using Green's theorem. The steady state solution is obtained by iteratively solving (Newton-Raphson procedure) the linearized Navier-Stokes equations using a Line_Gauss-Seidel solver. The main flow equations and the turbulence equations are solved sequentially.

Time-marching algorithms show bad convergence for flows at low Mach numbers due to the ill-conditioned set of equations (stiff equation system) (see [9]). To overcome this problem the Mach number has been increased by retaining the Reynolds number for the herein presented test cases. A second approach to overcome the ill-conditioned equation system is by artificially changing the speed of sound by using the artificial compressibility method (Shin, 2001 [10]). The results obtained for the turbine blade are shown for both solution approaches to point out the differences.

3 Turbulence Model

In this work the $k-\varepsilon-\zeta-f$ turbulence model (ZETA-F) of Hanjalic et al. (2004) [5] is implemented into the LINARS code and applied to steady transitional flows. This model is an advancement of Durbin's $k-\varepsilon-v^2-f$ model (1995) [3]. Both models have been derived from Reynolds stress transport models and can be seen as simplified second moment closures. The near-wall turbulence damping is modeled with an elliptic auxiliary equation. The main difference of these two models is that the V2F model solves the dimensional value of the normal-to-wall Reynolds stress component whereas the ZETA-F model solves a non-dimensional value $-v'^2/k$ (interpretable as

the turbulence anisotropy). LES studies by Yang et al. (1994) [11] showed that the turbulence fluctuation in the wall-normal direction v' plays an important role within the transition process. This motivates to use the aforementioned models to use them to simulate transitional flows without using intermittency functions as they carry some information about the near wall turbulence anisotropy (see also Lien et al., 1998 [12]).

k - ε - ζ - f (ZETA-F) Model

The turbulent scales k and ε are provided by the standard k - ε model for the ZETA-F model.

The V2F suffers from stability problems and often needs many iterations for convergence. To avoid these difficulties, Hanjalic et al [5] proposed a modified V2F model by introducing a dimensionless turbulent velocity scale ratio $\zeta = v'^2/k$ instead of v'^2 . The transport equation for ζ can be directly obtained from the v'^2 - and k -equations of the V2F model. The transformation yields to:

$$\frac{\partial \zeta}{\partial t} + \overline{u}_j \frac{\partial \zeta}{\partial x_j} = \frac{\partial}{\partial x_j} \left(\left(\nu + \frac{\nu_T}{\sigma_\zeta} \right) \frac{\partial \zeta}{\partial x_j} \right) + f - \frac{\zeta}{k} P_k + \frac{2}{k} \left(\nu + \frac{\nu_T}{\sigma_\zeta} \right) \frac{\partial \zeta}{\partial x_j} \frac{\partial k}{\partial x_j} \quad (1)$$

The last term on the right-hand-side, the "cross diffusion", is significant only in the near-wall region. However, in order to simplify the equation into a source-sink diffusion form it is neglected and the constants are retuned for compensation.

The new ζ equation contains the turbulence kinetic energy production P_k instead of the dissipation ε which can be easier reproduced correctly. As a second advantage the boundary condition for the relaxation variable f is $f_w = -(2\nu\zeta)/y^2$, compared to $f_w \sim 1/y^4$ as in the original V2F model. f_w has the same form as ε_w and can be treated together in the numerical procedure. These modifications enhance the stability in the computational procedure.

In the ZETA-F model the rapid component of the pressure-strain term is modelled with the more advanced quasi linear SSG model of Speziale et al. (1991) [13] instead of the simpler assumption of isotropisation of production in the V2F model.

Rearranging the f equation and neglecting some small terms the final form can be written as:

$$L^2 \frac{\partial^2 f}{\partial x_j^2} - f = \frac{1}{T} \left(c_1 + C_2' \frac{P_k}{\varepsilon} \right) \left(\zeta - \frac{2}{3} \right) \quad (2)$$

The eddy viscosity is defined in analogy to the definition in Durbin's V2F model. The ZETA-F model is completed by imposing the Kolmogorov time and length scale as shown below. The following coefficients are used for the ZETA-F model: $C_\mu = 0.22$, $C_{\varepsilon 1} = 1.4(1 + 0.012/\zeta) + 0.4 \exp(-0.1 Re_T)$, $C_{\varepsilon 2} = 1.9$, $c_1 = 0.4$, $C_2' = 0.65$, $C_L = 0.36$, $C_T = 6$, $C_\eta = 85$, $\sigma_k = 1$, $\sigma_\varepsilon = 1.3$, $\sigma_\zeta = 1.2$.

$$\nu_T = C_\mu \zeta k T \quad (3)$$

$$T = \max \left[\min \left[\frac{k}{\varepsilon}, \frac{a}{\sqrt{6} C_\mu |S| \zeta} \right], C_T \sqrt{\frac{\nu}{\varepsilon}} \right] \quad (4)$$

$$L = C_L \max \left[\min \left[\frac{k^{3/2}}{\varepsilon}, \frac{k^{1/2}}{\sqrt{6} C_\mu |S| \zeta} \right], C_\eta \left(\frac{\nu^3}{\varepsilon} \right)^{1/4} \right] \quad (5)$$

The in-house code LINARS solves the k , ε and v'^2/ζ equations implicit in a coupled manner, whereas the elliptic equation for f is solved separately for each time iteration.

4 Results and Discussion

As a first assessment numerical results were compared with the well-documented ERCOFTAC experimental data obtained from transitional flows over adiabatic flat plates with sharp leading edges [14]. These experiments were chosen to test the ability of the models to predict by-pass transition under the effects of free-stream turbulence with zero and varying pressure gradient conditions. The results of this evaluation can be found in Ramadani et al. [15].

Because the calculations of the flat plate test cases showed satisfactory results for both models, as a next validation step the calculation of the steady transitional flow through the low pressure turbine cascade T106A is performed. This flow was experimentally investigated at the Whittle Laboratory from Stieger (2001) [16] for a low free stream turbulent intensity (FSTI) and Opoka and Hodson (2008) [17] for a higher FSTI. This flow is very challenging, because by-pass transition as well as separated-flow transition can occur on the suction side depending on the inlet FSTI. Figure 1 shows the blade geometry and the used computational grid consisting of 5 blocks with an O-block wrapping around the blade. The O-block contains 320 x 88 grid cells with a maximum y_{max}^+ value below 1 along most of the blade surface.

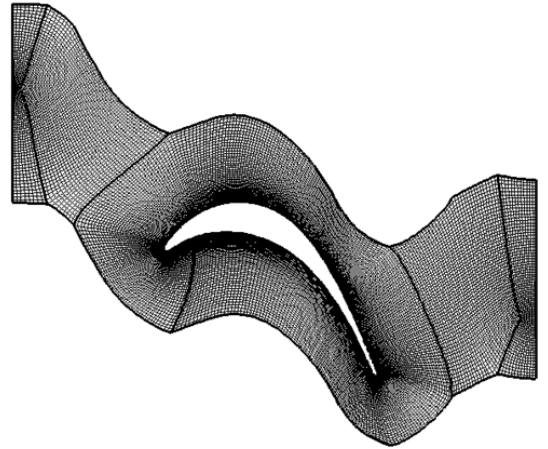


Figure 1: Computational grid for T106A cascade flow (O-block with 320 x 88 cells).

The main goal of the experiments was to study the influence of unsteady inflow conditions on the transitional blade flow. The unsteady inflow is provided by moving bars, located 70 mm upstream of the cascade inlet. In this work only the steady flow without bars is investigated, but further unsteady simulations are envisaged. Table 1 gives the main operating conditions from the experiments used for the numerical investigations. The inlet Mach number is very low, so that the flow can be considered as fully incompressible. Figure 2 and Figure 3 show the measured pressure distribution on blade suction and pressure side for both inlet FSTI. At a surface position of $s/s_{max} = 0.44$ the peak suction occurs. From this point the boundary layer decelerates under the influence of an adverse pressure gradient. In

$Re_{out,c}$	Inlet Mach number	FSTI [%]	Chord length [mm]	l_{ax} [mm]	Pitch [mm]
160000	~ 0.02	0.5 & 4.0	198	85.97	158.2

Table 1: *Main operating conditions of the T106A cascade.*

the case of the lower free-stream turbulence, the suction surface boundary layer separates at a surface position of $s/s_{max} = 0.63$ indicated by the start of a pressure "plateau". It extends up to a $s/s_{max} = 0.83$, where the transition process starts which leads to a recovery of the surface pressure. At a surface distance of $s/s_{max} = 0.9$, the boundary layer is attached again. In the case of the higher free-stream turbulence, the pressure distribution on the suction side lacks the pressure plateau between $s/s_{max} = 0.6$ and $s/s_{max} = 0.8$. This suggests that bypass transition prevents the formation of a separation bubble.

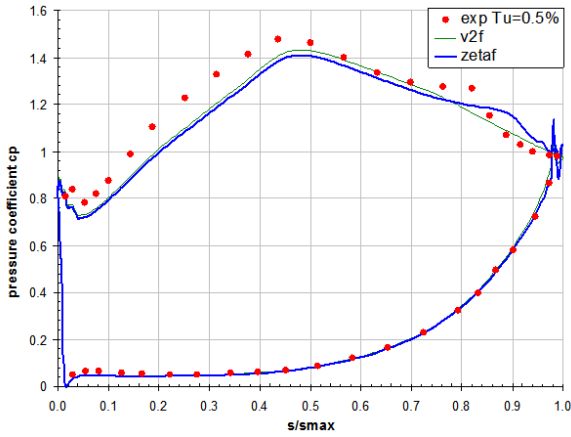


Figure 2: *Pressure coefficient along the T106A cascade with 0.5% FSTI.*

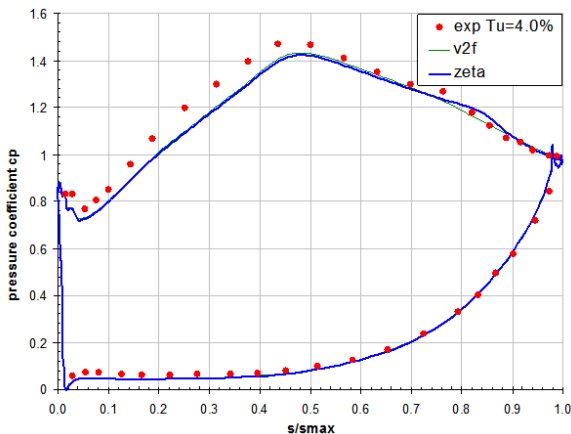


Figure 3: *Pressure coefficient along the T106A cascade with 4% FSTI.*

4.1 Compressible Results

Although the flow is incompressible, the first calculations were done with the time-marching code without

any preconditioning and thus the outlet Mach number is set to 0.4, whereas the Reynolds number matches the experiment. The measurement data does not include the turbulent mixing length or turbulent dissipation at the inflow, so that these values are varied at the inlet. This is done by imposing different turbulence mixing lengths. For an inlet FSTI a relative turbulence mixing length (l_{mix}/l) of 0.015 is used, and for the higher FSTI a relative turbulence mixing length of 0.002 is used.

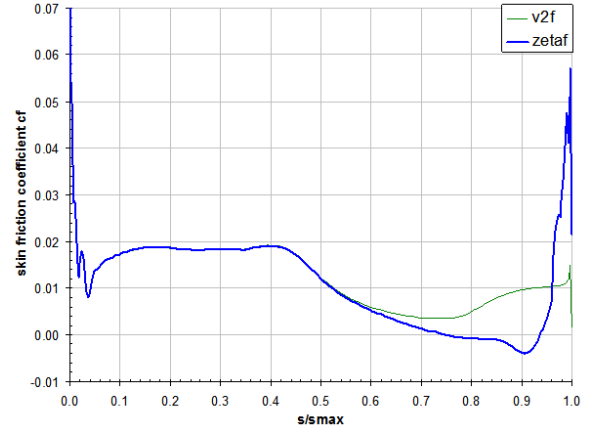


Figure 4: *Skin Friction Coefficient along suction side of the T106A cascade with 0.5% FSTI.*

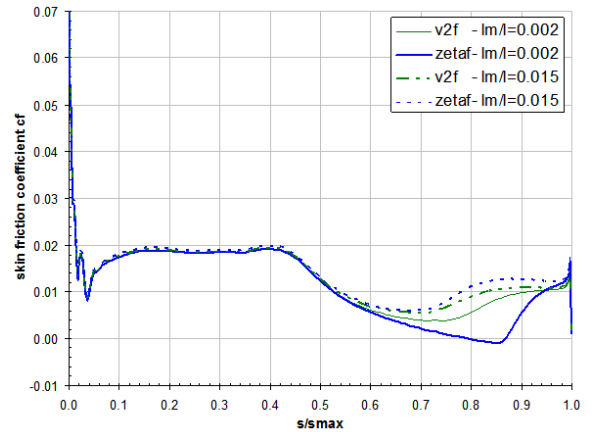


Figure 5: *Skin Friction Coefficient along suction side of the T106A cascade with 4% FSTI.*

Figure 2 shows the measured and computed pressure distribution for an inlet FSTI of 0.5% and Figure 4 shows the resulting skin friction distribution along the blade suction side. The values on the pressure side are in very good agreement with the experimental data, whereas a remarkable deviation can be observed along the whole suction side. The pressure distribution of the V2F model does not indicate any separation for all different turbulence mixing lengths, which is confirmed by the skin friction distribution. On the other hand, the ZETA-F model is able to predict the laminar separation bubble on the suction side. For $l_{mix}/l = 0.015$ the separation onset is predicted at $s/s_{max} = 0.75$ compared to the measured value of 0.63, but the length of the separation zone is very similar (see skin friction distribution). The results for higher l_{mix}/l were also calculated, but they predict a slightly further downstream separation onset and a shorter bubble. Best agreement was found for

$l_{mix}/l = 0.015$ and $l_{mix}/l = 0.002$ for the lower FSTI respectively for the higher FSTI).

The situation is similar for the case with an inlet FSTI=4% (see Figure 3 and Figure 5). Both models give similar results for the pressure distribution besides the small bulge at about $s/s_{max} = 0.8$. This bulge is also predicted by the ZETA-F model, but again too far downstream. The measurements indicate that the boundary layer is close to separation, whereas the skin friction for ZETA-F shows a small separation bubble. This bubble is only predicted by $l_{mix}/l = 0.002$, but not for higher l_{mix}/l values at the inlet. The skin friction distribution shows local minima at about $s/s_{max} = 0.7$. Only the ZETA-F model shows a small separation zone for $l_{mix}/l = 0.002$. The sharp increase at $s/s_{max} > 0.8$ indicates beginning transitional flow. For the same mixing length as used in the lower inlet FSTI case ($l_{mix}/l = 0.015$), no separation is predicted. It is interesting that the ZETA-F model is more sensible to variations of the turbulence mixing length than the V2F model.

The better results of the ZETA-F model could be caused by the improved modelling of the shear stress and of the production of turbulent kinetic energy (see model description above).

4.2 Incompressible Results

Finally the T106A turbine cascade is calculated with the incompressible code version of LINARS using artificial compressibility (Shin, 2001 [10]). For comparing the incompressible calculation with the compressible one, the mixing length is set equal in both calculations.

For both inlet FSTI the agreement with the measured pressure distribution is much better, especially for 4% inlet FSTI (see Figure 6 and Figure 7). The main reason for this disagreement of the compressible calculation is the too high Mach number of 0.4 used for the compressible calculation and the thus resulting compressibility effects.

The V2F model is again not able to predict any separation. For the 0.5% FSTI case the ZETA-F model predicts the separation onset closer to the measured location, the length of the separation zone is slightly too small. The skin friction distribution (see Figure 8 and Figure 9) is similar to the compressible calculations, whereas the V2F model seems to predict a rapid transition to turbulence closely after the peak pressure location.

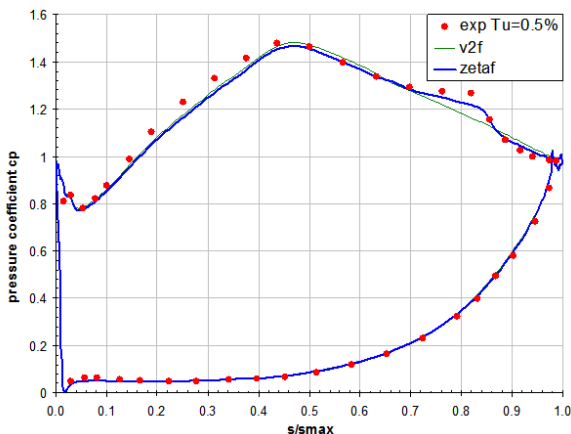


Figure 6: Pressure coefficient along the T106A cascade with 0.5% FSTI.

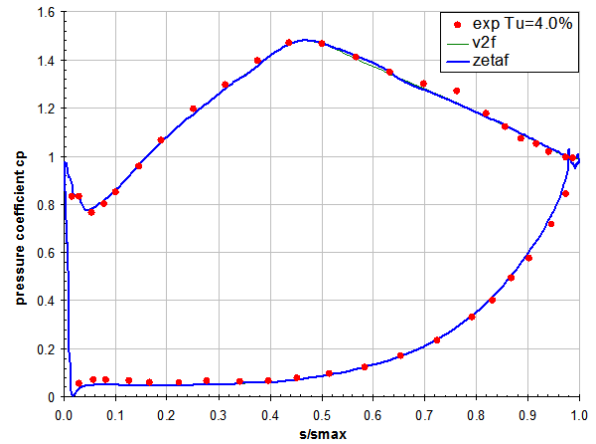


Figure 7: Pressure coefficient along the T106A cascade with 4% FSTI.

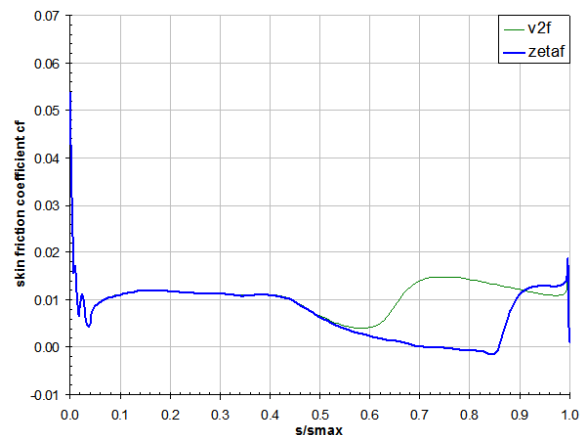


Figure 8: Skin Friction Coefficient along suction side of the T106A cascade with 0.5% FSTI.

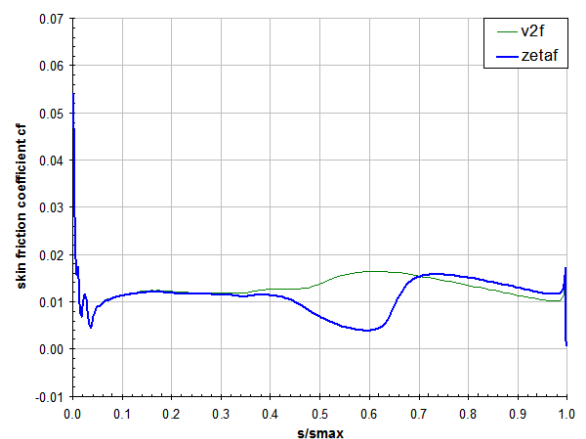


Figure 9: Skin Friction Coefficient along suction side of the T106A cascade with 4% FSTI.

For the 4% inlet FSTI case the incompressible calculation does not predict any separation, although the ZETA-F prediction has a minimum at $s/s_{max} = 0.6$. The V2F model predicts transition even more upstream due to the higher free-stream turbulence.

The comparison of the measured and the computed shape factor along the blade suction side for an inlet

FSTI of 0.5% and 4.0% is shown in Figures 10 and 11. Because of the difficulties in determining the boundary layer thickness, two methods calculating the boundary layer thickness are used, the method of Schobeiri et al. (2009) [18] and a method based on the assumption of a constant pressure in the boundary layer. Both methods lead to similar distributions with a peak at the same location but to different absolute values. According to Schlichting [19] the peak in the shape factor indicates the location of the transition onset. So in Figures 10 and 11 the shape factor starts to decrease when the skin friction increases, indicating laminar-to-turbulent transition. The computed peak in the shape factor is slightly more upstream than in the measurements, although the separation occurs a little bit earlier in the measurements. This leads to the conclusion that in the measurements the separation zone remains longer laminar before the transition occurs than in the calculation, where the separated flow triggers transition much earlier.

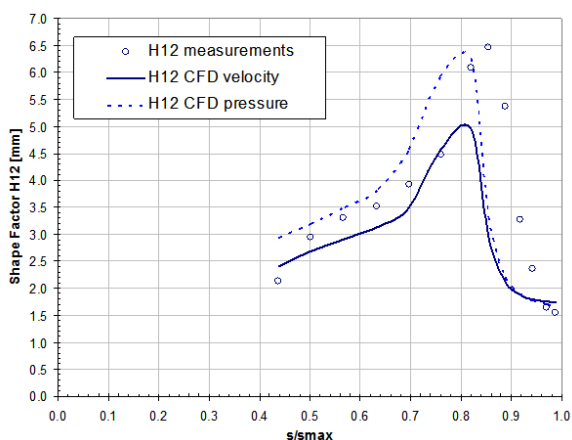


Figure 10: Shape factor along the T106A cascade with 0.5% FSTI.

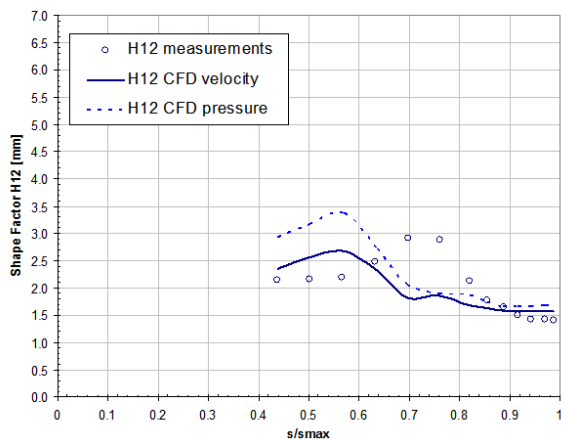


Figure 11: Shape factor along the T106A cascade with 4% FSTI.

5 Conclusion

In order to improve the reliability of numerical transition prediction, the ZETA-F model of Hanjalic et al. (2004) is investigated for turbomachinery flows and compared to the V2F model of Durbin (1995). Both models are derived from the Reynolds stress model and thus

have good chances to satisfactorily predict laminar-to-turbulent transition. The ZETA-F model is an advancement of the V2F model with a better numerical stability. Both models do not need an intermittency function.

The predictions of the steady transitional flow around the T106A low pressure turbine cascade are compared with the measurements and the V2F model. The ZETA-F model is able to predict the separation bubble on the suction side for 0.5% inlet FSTI, although a little bit too far downstream. For the 4% inlet FSTI the agreement with the measurements is excellent, especially for the incompressible calculation. The shape factor shows that the transition takes place much earlier in the separation zone than in the measurements. In general, the incompressible calculations give better results than the compressible code. In our calculations the ZETA-F model shows a great potential to predict transitional flows in turbomachinery applications.

Nomenclature

c_f	skin friction coefficient
c_p	pressure coefficient
C	model parameter
H_{12}	shape Factor
k	turbulent kinetic energy
L	flat plate length or length scale
p	pressure
P_k	turbulence production term
Re	Reynolds number
S	magnitude of strain rate
u, v, U	velocity
y	wall distance
ε	turbulence dissipation rate
ζ	velocity scale ratio
ν	kinematic viscosity
ρ	density

Sub/Superscripts

ax	axial
in	inlet
out	outlet
w	wall
$+$	dimensionless

Acknowledgements

The work was supported by the Austrian Federal Ministry of Transport, Innovation and Technology (BMVIT) within the Austrian Aviation Program "TAKE OFF" (project "CFD-TRANS") as well as by the Austrian Science Foundation (FWF) (project P16761 "Steady and Unsteady Transition Modeling").

References

- [1] Hanjalic K. and Hadzic I. (1996): Modelling the Transition Phenomena With Statistical Turbulence Closure Models, In: Henkes, R.A.W.M. and van Ingen, J.L. (eds.) "Transitional Boundary Layers in Aeronautics". North- Holland, Amsterdam.
- [2] Hadzic I. and Hanjalic K. (1999): Separation-Induced Transition to Turbulence: Second-Moment Closure Modelling, Flow Turbulence and Combustion, 1999, Vol. 63, pp. 153-173.
- [3] Durbin P.A. (1995): Separated Flow Computations with the k - v^2 model; In AIAA J., Vol 33, pp.659-664.
- [4] Sanz W., Pecnik R., Tratnig A. and Heitmeir F. (2007): Application of modern turbulence models to steady transitional flow,

ETC 2007, Athena, Greece.

- [5] Hanjali? K., Popovac M. and Haddiabdi? M (2004): A robust near-wall elliptic-relaxation eddy-viscosity turbulence model for CFD, In International Journal of Heat and Fluid Flows, Vol. 25, pp. 1047-1051.
- [6] Basara B. (2005): Calculation of vortex shedding from a circular cylinder in uniform and shear flows. Proceedings of 2005 ASME Fluids Engineering Division Summer Meeting, FEDSM2005, pp. 2295-2300.
- [7] Pecnik R., Pieringer P. and Sanz W. (2005): Numerical Investigation of the Secondary Flow of a Transonic Turbine Stage Using Various Turbulence Closures. ASME paper GT2005-68754, ASME Turbo Expo 2005, Reno-Tahoe, Nevada, USA.
- [8] Roe P.L. (1981): Approximate Riemann Solver, Parameter Vectors and Differencing Scheme, Journal of Computational Physics Vol 43, pp. 357-372.
- [9] Reed C.L., Anderson D.A.(1997): Application of low speed preconditioning to the compressible Navier-Stokes equations. AIAA Paper 97-0873.
- [10] Shin S. (2001): Reynolds-Averaged Navier-Stokes Computation of Tip Clearance Flow in a Compressor Cascade Using an Unstructured Grid. PhD thesis, Virginia Polytechnic Institute and State University, Blacksburg, Virginia, USA.
- [11] Yang Z., Voke P.R. and Savill A.M. (1994): Mechanism and Models of Boundary Layer Receptivity deduced from Large-Eddy Simulation of Bypass Transition. Direct and Large-Eddy Simulation Vol 1, P. R. Voke, L. Kleiser & J. Chollet (eds.) 225-236, Kluwer Academic Publishers.
- [12] Lien F.S., Kalitzin G. and Durbin P.A. (1998): RANS Modelling for Compressible and Transitional Flows, CTR Proceedings of the Summer Program 1998.
- [13] Speziale C.G., Sarkar S. and Gatski T.B. (1991): Modelling the pressure-strain correlation of turbulence: an invariant dynamical systems approach. J. Fluid Mech., Vol 227, pp. 245-272.
- [14] Savill A M. (1992): A synthesis of T3 Test Case Predictions. Numerical Simulation of Unsteady Flows and Transition to Turbulence, O. P. et al., ed., Cambridge University Press, pp. 404-442.
- [15] Ramdani K., Kelterer M.E., Pecnik R., Sanz W. (2009): Application of the ZETA Application of the ZETA-F-Turbulence Model to Steady Transitional Flow. In the Proceedings of the 8th European Conference on Turbomachinery, Fluid Dynamics and Thermodynamics, 23-27 March 2009, Graz, Austria, pp. 119-130.
- [16] Stieger R. D. (2002): The Effects of Wakes on Separating Boundary Layers in Low Pressure Turbines, PhD thesis, Cambridge University Engineering Department, February 2002.
- [17] Opoka M. M. and Hodson H. H.(2008): An Experimental Investigation of the Unsteady Transition Process on the High Lift T106A Turbine Blade, Journal of Propulsion and Power 24 (3), p. 424-432.
- [18] Schobeiri M.T., and B. Ozturk (2009): Experimental Study of the Effects of Periodic Unsteady Wakes on Flow Separation in Low Pressure Turbines. NASA/CR-2009-214831.
- [19] Schlichting H. and Gerster K. (2005): Grenzschicht-Theorie. Springer, Berlin Heidelberg.

STEADY NUMERICAL INVESTIGATIONS OF THE TRANSITION PROCESS ON AN AXIAL MULTISTAGE HIGH PRESSURE COMPRESSOR

Julien Marty¹, Guillaume Cottin², Bertrand Aupoix²

¹ *Snecma, Aerodynamics Methods Department, France.*

² *ONERA, Aerodynamics and Energetics Department, France.*

1 Introduction

For turbomachinery applications, the laminar-turbulent transition location is a crucial point in the boundary layer development. In turbines it significantly changes the heat transfer distribution which is important in the blade design. Both in compressors and turbines the boundary layer are thinner which modifies the skin friction distribution and the low momentum fluid area location. It influences boundary layer separation and the interaction with other secondary flows as passage vortex and tip leakage vortex. So blockage, losses and performances are affected by transition and may not be correctly predicted by a fully turbulent simulation. Several transition mechanisms can be found in compressor flow [12] : natural transition [7], by-pass transition [18], separation-induced transition [16, 6], wake-induced transition [8, 6] and shock-induced transition [16].

The purpose of this paper is to assess the transition effects on the flow and performance prediction of a 3 stage axial high pressure compressor. The application of a transition criterion allows to take the laminar part of the boundary layer into account. The criterion must be well-suited for the transition mechanism which occurs in the test case. This paper discusses the transition effects on compressor flow predictions and compares results to experimental data and fully turbulent computations.

2 CREATE research compressor

Experimental facility

The experimental facility is the 3 stage experimental compressor CREATE (figure 1) located at Acoustic and Fluid Mechanics Laboratory (LMFA-Lyon). This compressor is representative of median or rear stages of a modern, highly loaded multi-stage one. The table 1 sums up its main characteristics. On the CREATE compressor, the number of blades of each rotor and stator is a multiple of 16. The rotational speed is 11500 rpm and the design massflow 12.7 kg/s. The three stages allow to have flow conditions close to the ones in a realistic compressor.

Experimental data have been obtained through detailed instrumentation of the compressor, using both pneumatic measurements and laser Doppler anemometry techniques at several measurement planes. The measurements are performed in the circumferential direction at different constant radius locations downstream from each row. As the spatial periodicity of the compressor is 22.5 degrees, the azimuth measurements allow aerodynamic phenomena interacting over a complete spatial period to be represented. In order to have traversing

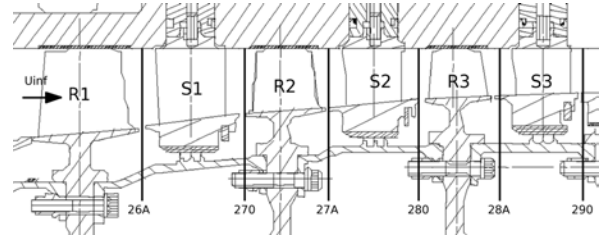


Figure 1: *CREATE high pressure compressor and measurement planes (black thick lines).*

probes between blade and vane rows, the axial gap was slightly increased compared to current compressors. A detailed description of the compressor is provided by Touyeras et al. [17] and Ottavy et al. [13].

Compressor modelling

Steady computations were run on the 3 stages of the compressor and carried out using the *elsA* (Ensemble Logiciel de Simulation en Aérodynamique) software developed by ONERA [2]. The *elsA* code is a versatile CFD tool allowing a wide choice of turbulence models and numerical schemes. *elsA* solves the mass-weighted averaged Navier-Stokes equations on structured meshes with a cell-centered finite-volume technique. The numerical parameters have been tested in a former study [10] and the following were retained: 2nd-order Jameson scheme for spatial discretization, LUSSOR method with the backward Euler time integration scheme. Multistage effects are accounted for with the classic mixing plane approach. The inlet conditions are based upon measurements and the freestream turbulence intensity is 2%. The turbulence model is the k-l Smith one [15] which develops well the turbulence after the transition onset. It has a good numerical behaviour and predicts better the separation than the k- ϵ model. Other compressor modelling details are given by [14, 10].

Disc	Blade count
Rotor 1 (R1)	64
Stator 1 (S1)	96
Rotor 2 (R2)	80
Stator 2 (S2)	112
Rotor 3 (R3)	80
Stator 3 (S3)	128

Table 1: *Characteristics of CREATE compressor.*

Mesh

The meshes used for this compressor are based upon a multi-block strategy and were generated using Numeca's Autogrid 5 meshing tool using a O4H topology (10.2 million points). They are composed of 85 radial grid points with 25 points in the tip-clearance gap. Meshes with different resolutions were generated in order to assure the grid independence of the solution and a sufficient mesh point number in the boundary layer. They were refined along the blade as well as the hub and the casing. In order to well capture the thinner the boundary layer, the meshes were again refined around the blade in comparison to a fully turbulent simulation mesh. Grid quality was checked by looking at the values of y^+ on solid walls which were found to be lower than 0.6.

3 Transition modelling

Transition criterion

Two criteria have been used for the streamwise and the cross-flow instability modes. For the streamwise one, the transition criterion is the AHD criterion (Arnal et al. [1]) combined with the Gleyzes criterion (Gleyzes et al. [5]). The first criterion results from linear stability analysis of the laminar boundary layer and the second one from a theoretical and experimental study of separation bubbles. This combined criterion is well suited for attached boundary layer as well as for separation bubbles. If the shape factor is greater than 2.8, the applied criterion is the Gleyzes one, otherwise it is the AHD criterion. For the cross-flow mode of instability the transition criterion is the C1 criterion. The transition computation strategy is presented by Cliquet et al. [3].

Turbulence development

The turbulence development is based upon the intermittency concept (equation (1)) where μ , μ_t and γ are the molecular viscosity, the eddy viscosity and the intermittency. The factor γ defines the influence of turbulence on the transition process. This factor takes a value between 0 (laminar flows) and 1 (turbulent flows).

$$\mu_{total} = \mu + \gamma\mu_t \quad (1)$$

Cliquet et al. [3] have implemented a simple function of the following form. The intermittency function reaches one as soon as Re_θ has increased by 15%. Since the intermittency factor has reached one, the turbulence development is performed by the turbulence model.

$$\gamma = \frac{1}{0.15^2} \left[\frac{Re_\theta - Re_{\theta T}}{Re_{\theta T}} \right]^2 \quad (2)$$

4 Results

The Reynolds number based upon the first rotor chord is about 300 000, the external turbulence level is nearly 0.6% close to the leading edge of the first rotor. In these conditions a laminar boundary layer exists and the transition must be taken into account.

Separation-induced transition

The figure 2 shows the skin friction distribution and the transition onset obtained on the suction side of the first rotor. The transition onset is depicted by the dotted line. Along the spanwise direction the transition does

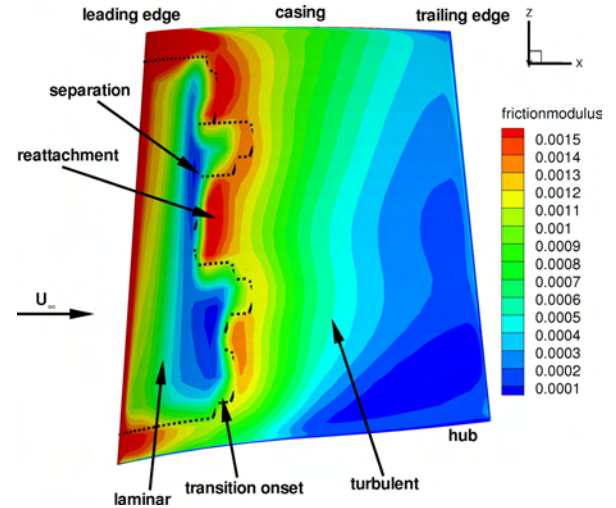


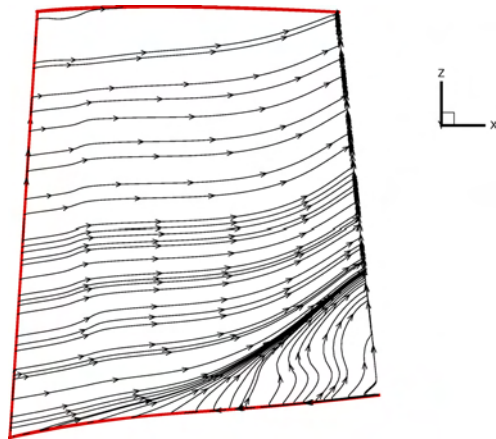
Figure 2: Skin friction distribution on the suction side of the first rotor. The flow comes from the left. The transition onset is depicted by the black dotted line.

not take place at the same axial location. It strongly depends upon the incoming flow properties, notably the incidence. The suction surface boundary layer is initially subjected to a favorable pressure gradient followed by a strong adverse pressure gradient which causes the laminar boundary layer to separate. The laminar separation is followed by turbulent reattachment. This is consistent with the results of Zaki et al. [18] where the laminar shear layer detaches and breaks down to turbulence prior to reattachment. On the pressure side, transition occurs without separation and the transition onset is closer to the leading edge. The laminar part is rather important nearly 30% of the axial chord on the suction side and 20% on the pressure side of the first rotor.

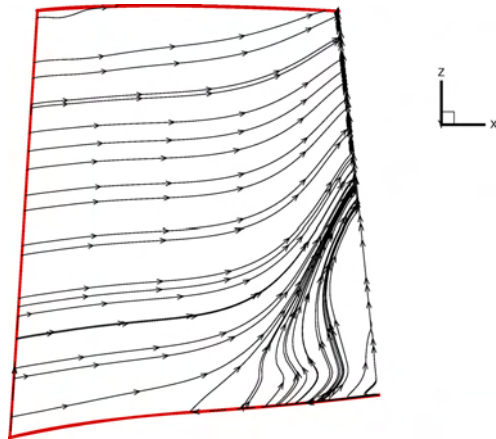
Transition effects on the first rotor flow

Due to the wake of each row, the external turbulence level grows from 0.6% at the leading edge of the first rotor to 2.5% at the leading edge of the third stator. Thus, the transition onset is closer and closer to the leading edge and the transition effects are more intense for the first rotor.

The wall streamlines on the suction side of the rotor 1 are depicted in the figure 3. The figure 3(a) shows the wall streamlines for the transition simulation and the figure 3(b) for the fully turbulent one. The hub corner stall is clearly visible on the suction side. It is a loss mechanism [4] and produces entropy. The transition simulation leads to a separation region which is less spread in the spanwise direction in comparison to the fully turbulent simulation. Nevertheless, the separation region is slightly more spread near the hub in the pitchwise direction due to the low momentum fluid distribution as seen in the figure 4. The figures 4(a) and 4(b) present the entropy distribution in the measurement plane downstream of the rotor 1 for the transition and fully turbulent simulations respectively. The separation area is visible on these figures. In addition the entropy level is slightly smaller for the fully turbulent simulation near the hub.



(a) With transition



(b) Fully turbulent

Figure 3: Wall streamlines on the suction side of the rotor 1. The flow comes from the left.

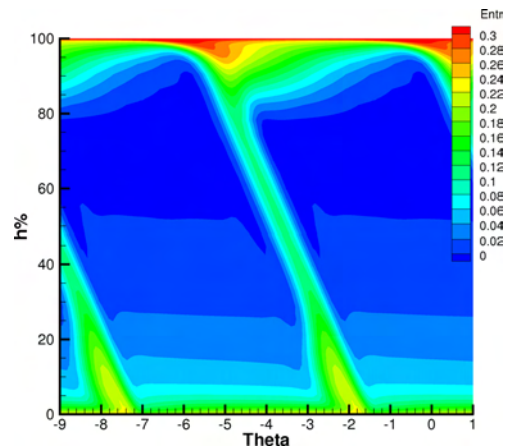
According to a laminar region yields thinner turbulent boundary layer so the separation is delayed and moreover the skin friction loss is smaller. Thus the losses are less important with transition as shown by the figure 4 where the wakes are thinner for the transition computation in comparison to the fully turbulent one far from the hub.

The main consequence of this hub corner stall area modification is shown on the figure 5 on which the pitchwise averaged total pressure profile is depicted in the same measurement plane. The total pressure level is higher for the transition simulation, except near the hub. The total pressure deficit is due to the corner stall which is more intense and less spread near the hub for this simulation. With transition computation, the total pressure level is closer to experimental data, except near the hub. The total pressure gap between the computational and experimental data which is near the hub is due to the leakage flows [14]. Transition effects on other blade rows are given by Marty et al.[11].

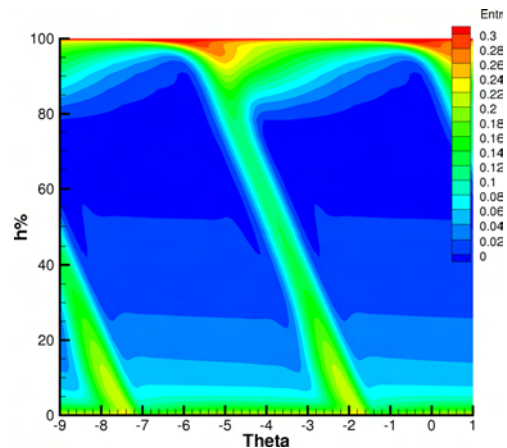
Compressor performances

The compressor map is shown in figure 6. Near design point and near surge line the compression ratio obtained with transition is higher than the fully turbulent one for the above explained reasons. An important discrepancy appears near the choke line. The transition simulation leads to higher separation on the second and third stage. This is probably due to the off-design conditions. The choke massflow is smaller but the gap is less than the measurement uncertainties (1%). The isentropic efficiency is better with transition criterion by nearly 1%

even at choke line.



(a) With transition



(b) Fully turbulent

Figure 4: Entropy distribution in the measurement plane downstream of the first rotor. The abscissa represents the pitchwise direction and the ordinate the spanwise direction from the hub to the casing.

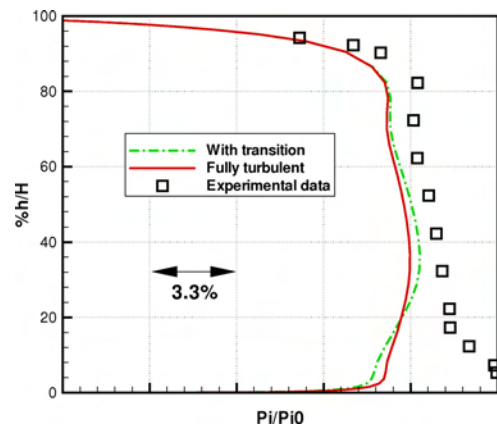
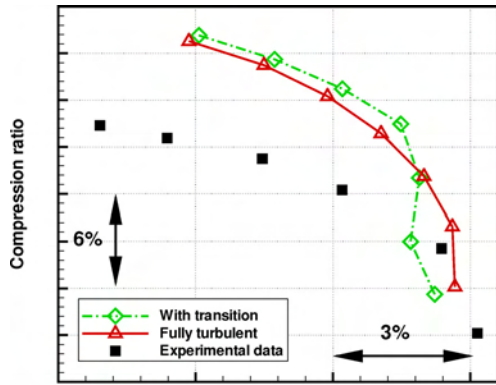


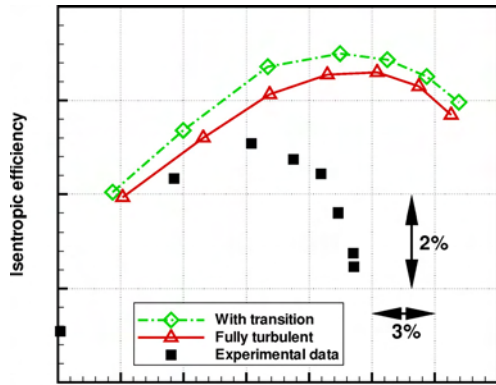
Figure 5: Circumferentially averaged total pressure distribution.

5 Conclusion

Laminar-turbulent transition has been studied on a 3 stage axial high pressure compressor, especially in the first rotor where the transition effects are more pronounced. On the suction side a separation-induced transition occurs. The transition onset is nearly 15-30% of the axial chord according to the studied row. There is no separation bubble on the pressure side.



(a)



(b)

Figure 6: Compressor performances - Compression ratio vs Mass flow rate (left) and isentropic efficiency vs compression ratio (right).

The transition process modifies the boundary layer development. The boundary layers are thinner. So the separation is delayed and moreover the skin friction loss is smaller. The hub corner stall is less spread than the fully turbulent one. It results in higher total pressure level, smaller losses and better performances.

References

- [1] D. Arnal. Special course on stability and transition of laminar flow. *AGARD Special Course at the von Kármán Institute, AGARD Report 709, March 26-30, 1984*
- [2] L. Cambier and J.P. Veillot. Status of the elsA CFD Software for Flow Simulation and Multidisciplinary Applications. *AIAA 2008-664, 46th AIAA Aero-space Sciences Meeting and Exhibit, Reno, NV, Jan. 2008.*
- [3] J. Cliquet, R. Houdeville and D. Arnal. Application of Laminar-Turbulent Transition Criteria in Navier-Stokes Computations. *AIAA Journal Vol. 46(5), pp 1182-1190, May 2008.*
- [4] J.D. Denton. Loss Mechanisms in Turbomachines. *Journal of Turbomachinery Vol. 115 pp 621-656, October 1993.*
- [5] C. Gleyzes, J. Cousteix and J. Bonnet. Theoretical and experimental study of low Reynolds number transitional separation bubbles. *Conference on low Reynolds number airfoil aerodynamics, UNDAS-CP-77B123, 1985.*
- [6] T. Hildebrandt, M. Swoboda and E. Lorrain. Steady and unsteady transitional 3D Navier-Stokes calculation of a 1.5-stage axial low speed compressor. *in: Proceedings of 17th International Symposium on Airbreathing Engines, 4-9 September 2005, Munich, Germany, 2005.*
- [7] J.D. Hughes and G.J. Walker. Natural Transition Phenomena on an Axial Compressor Blade. *Journal of Turbomachinery Vol. 123, pp 392-401, 2001.*
- [8] J. Iseler, L. Hilgenfeld and M. Pfitzner. Investigations of the boundary layer on a highly loaded compressor cascade with wake-induced transition. *ASME Turbo Expo 2006, May 8-11, Barcelona, Spain, ASME Paper GT2006-90665, 2006.*
- [9] R.B. Langtry, F.R. Menter, S.R. Likki, Y.B. Suzen, P.G. Huang and S. Völker. A Correlation-Based Transition Model Using Local Variables - Part 2 : Test Cases and Industrial Applications. *Journal of Turbomachinery Vol. 128, pp 423-434, July 2006.*
- [10] J. Marty, B. Aupoix, M. Schvallinger and V.C. Sharma. Effet de la modélisation de la turbulence en proche pompage dans un compresseur multi-étages. *43ème Colloque d'Aérodynamique Appliquée - AAAF, 2008.*
- [11] J. Marty, G. Cottin and B. Aupoix. Turbulence modelling and transition to turbulence effects for a high pressure multistage compressor. *8th European Turbomachinery Conference, Paper Nr227, Graz, Austria, 23-27 March 2009.*
- [12] R.E. Mayle. The role of laminar-turbulent transition in gas turbine engines. *ASME Journal of Turbomachinery, Vol. 113 pp 509-537, 1991*
- [13] X. Ottavy, I. Trebinjac, A. Vouillarmet and D. Arnaud. Laser Measurements in High Speed Compressors for Rotor-Stator Interaction Analysis. *Proceedings of ISAI 6th, Shanghai, April 2003, International Journal of Thermal and Fluid Sciences, 2003.*
- [14] V.C. Sharma, M. Schvallinger, J. Marty and H. Gaible. Turbulence modelling effects on off-design predictions for a multistage compressor. *ISABE-2007-1183, 2007.*
- [15] B.R. Smith. A Near Wall Model for the $k-l$ Two Equation Turbulence Model. *AIAA Paper 94-2386 25th Fluid Dynamics Conference, Colorado Springs, Colorado, June 20-23 1994.*
- [16] H. Thermann, M. Müller and R. Niehuis. Numerical Simulation of the Boundary Layer Transition in Turbomachinery Flows. *ASME Paper 2001-GT-0475, 2001*
- [17] A. Touyeras and M. Villain. Aerodynamic Design and Test Result Analysis of a Three Stage Research Compressor. *ASME Paper - GT2004-53940, 2004.*
- [18] T. Zaki, P. Durbin, J. Wissink and W. Rodi. Direct numerical simulation of by-pass and separation-induced transition in a linear compressor cascade. *ASME Turbo Expo 2006, May 8-11, Barcelona, Spain, ASME Paper GT2006-90885, 2006.*

THE LCTM APPROACH TO MODELLING LAMINAR-TURBULENT TRANSITION

F. R. Menter¹, R.B. Langtry²

¹ ANSYS Germany GmbH.

² The Boeing Company.

Introduction

Laminar-turbulent transition was for many decades the most prominent white spot on the map of physical models in industrial CFD codes. This is surprising, as most technical flows are in the Reynolds number range of 10^4 - 10^6 , where significant portions of the boundary layers can be laminar. In order to close this gap, the authors proposed a new concept for modelling laminar-turbulent transition in general-purpose CFD codes (e.g. Menter et al. 2006a). The concept is based on the combination of transport equation using only local quantities, with experimental correlations on transition location and transition length. The concept was termed LCTM - Local Correlation-based Transition Modelling. Within this framework, a LCTM model was developed using two transport equations. One equation is for the turbulent intermittency, γ , and the second one for the transition onset Reynolds number, Re_θ . The model was termed γ - Re_θ model and was published in a series of papers (Menter et al. 2002, Menter et al. 2006a, Menter et al. (2006b) Langtry et al. (2006)). It is important to stress, that the model addresses exclusively transition in wall-boundary layers, which is however the main problem in technical flows. Free shear layer transition is not attempted by the formulation.

There are several reasons why transition modelling has posed and still poses a substantial challenge within general purpose CFD codes. The first is that transition occurs through different mechanisms in different applications. In aerodynamic flows, transition is typically the result of a flow instability (Tollmien-Schlichting waves or in the case of highly swept wings cross-flow instability), where the resulting exponential growth of two-dimensional waves eventually results in a non-linear break-down to turbulence. Transition occurring due to Tollmien-Schlichting waves is often referred to as natural transition (Schlichting, 1979). In turbomachinery applications, the main transition mechanism is bypass transition (Morkovin, 1969) imposed on the boundary layer by high levels of turbulence in the freestream. The high freestream turbulence levels are for instance generated by upstream blade rows. Another important transition mechanism is separation-induced transition (Malkiel and Mayle, 1996), where a laminar boundary layer separates under the influence of a pressure gradient and transition develops within the separated shear layer (which may or may not reattach). In addition, a turbulent boundary layer can re-laminarize under the influence of a strong favorable pressure gradient (Mayle, 1991). While the importance of transition phenomena for aerodynamic and heat transfer simulations is widely accepted, it is difficult to include all of these effects in a single model.

The second complication arises from the fact that con-

ventional Reynolds averaged Navier-Stokes (RANS) procedures do not lend themselves easily to the description of transitional flows, where both linear and non-linear effects are relevant. RANS averaging eliminates the effects of linear disturbance growth and is therefore difficult to apply to the transition process. While methods based on the stability equations such as the e^n method of Smith & Gamberoni (1956) and van Ingen (1956) avoid this limitation, they are not compatible with general-purpose CFD methods as typically applied in complex geometries. The reason is that these methods require a priori knowledge of the geometry and the grid topology. In addition, they involve numerous non-local operations (e.g. tracking the disturbance growth along each streamline) that are difficult to implement into today's CFD methods (Stock & Haase, 2000). This is not to argue against the stability approaches, as they are an essential part of the desired "spectrum" of transition models required for the vastly different application areas and accuracy requirements. However, much like in turbulence modeling, it is important to develop engineering models that can be applied in day-to-day operations by design engineers on complicated 3D geometries.

The main requirements for a fully CFD-compatible transition model are:

- Allow the calibrated prediction of the onset and the length of transition
- Allow the inclusion of different transition mechanisms
- Be formulated locally (no search or line-integration operations)
- Avoid multiple solutions (same solution for initially laminar or turbulent boundary layer)
- Do not affect the underlying turbulence model in fully turbulent regimes
- Allow a robust integration down to the wall with similar convergence as the underlying turbulence model
- Applicable to three-dimensional boundary layers

Considering the main classes of engineering transition models (stability analysis, correlation based models, low- Re models) it was that none of these methods could meet all of the above requirements.

The model given in Menter et al. (2006a, 2006b) and Langtry et al. (2006) has been developed in a joint project between GE Global Research, ANSYS-CFX and the University of Kentucky. The model consists of two components. The first is the generic infrastructure provided by two transport equations, which link the CFD code to experimental correlations. The second component is the correlations themselves. These correlations were partly built on internal data and have not been

published at the time. This has caused effort by external groups of re-constructing these correlations (see also current special issue) so that full formulations are now available.

Model Formulation

Space limitations do not allow a full representation of the model formulation. Only the main idea will therefore be sketched.

Instead of using the momentum thickness Reynolds number to trigger the onset of transition, the current model is based on the strain-rate (or vorticity) Reynolds number, Re_v , (Menter et al. 2002):

$$Re_v = \frac{\rho y^2}{\mu} S \quad (1)$$

where y is the distance from the nearest wall, ρ is the density, μ is the dynamic viscosity and S is the absolute value of the strain rate. Since the strain-rate Reynolds number depends only on density, viscosity, wall distance and the strain-rate (some formulations use the vorticity) it is a local property and can be easily computed at each grid point in an unstructured, parallel Navier-Stokes code. A scaled profile of the vorticity Reynolds number is shown in Figure 1 for a Blasius boundary layer. The maximum of the profile is proportional to the momentum thickness Reynolds number, Re_θ , and can therefore be related to the transition correlations (Menter et al., 2002) as follows:

$$Re_\theta = \frac{\max(Re_v)}{2.2} \quad (2)$$

Based on this observation, a general framework can be formulated, which can serve as a local environment for correlation based transition models.

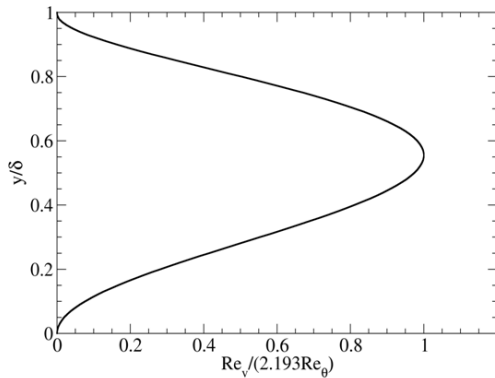


Figure 1: Scaled vorticity Reynolds number (Re_v) profile in a Blasius boundary layer.

The transition model is built on a transport equation for intermittency, which can be used to trigger transition locally. In addition, to the transport equation for the intermittency, a second transport equation is solved for the transition onset momentum-thickness Reynolds number. This is required in order to capture the non-local influence of the turbulence intensity, which changes due to the decay of the turbulence kinetic energy in the free-stream, as well as due to changes in the free-stream velocity outside the boundary layer.

The intermittency function is coupled with the SST $k-\omega$ based turbulence model (Menter, 1994). It is used to turn on the production term of the turbulent kinetic energy downstream of the transition point based

on the relation between transition momentum-thickness and strain-rate Reynolds number. As the strain-rate Reynolds number is a local property, the present formulation avoids another very severe shortcoming of the correlation-based models, namely their limitation to 2D flows. It therefore allows the simulation of transition in 3D flows. It is beyond the scope of the present overview to give all equations in detail. They can be found in Menter et al (2006a). The essential part is an onset function used to trigger the production of intermittency at the transition onset location. It is essentially formulated as:

$$F_{onset} = \max\left(\frac{Re_v}{2.2 Re_{\theta c}} - 1, 0\right) \quad (3)$$

where experimental information enters through $Re_{\theta c}$. As Re_v increased with the running length of the Blasius boundary layer, this function is activated once $Re_v > 2.2 Re_{\theta c}$. This then triggers the transition process in the equations.

The $\gamma-Re_\theta$ model is implemented into both ANSYS codes (ANSYS Fluent and ANSYS CFX) and is used by industrial clients now for almost 5 years. The model has gained popularity in very diverse fields (amongst others) like:

- Turbomachinery
- Wind turbine design
- Racing cars (spoiler and wings)
- Low to mid range Renumber aerodynamic bodies
- Appendages of yachts for the America cup races

Testcases

Flat Plates

The flat plate testcases that were used to calibrate the model are the ERCOFTAC T3 series of flat plate experiments (Savill, 1993 and 1996) and the Schubauer and Klebanof (1955) flat plate experiment, all of which are commonly used as benchmarks for transition models. Also included is a test case where the boundary layer experiences a strong favorable pressure gradient that causes it to re-laminarize (McIlroy and Budwig, 2005).

Figure 2 shows the comparison of the model prediction with experimental data for these cases. It also gives the corresponding FSTI values. In all simulations, the inlet turbulence levels were specified to match the experimental turbulence intensity and its decay rate. As the freestream turbulence increases, the transition location moves to lower Reynolds numbers.

The T3C test cases consist of a flat plate with a favorable and adverse pressure gradient imposed by the opposite converging/diverging wall. The wind tunnel Reynolds number was varied for the four cases (T3C5, T3C3, T3C2, T3C4) thus moving the transition location from the favorable pressure at the beginning of the plate to the adverse pressure gradient at the end. The cases are used to demonstrate the transition models ability to predict transition under the influence of various pressure gradients. Figure 3 details the results for the pressure gradient cases. The effect of the pressure gradient on the transition length is clearly visible with favorable pressure gradients increasing the transition length and adverse pressure gradients reducing it. For the T3C4 case the laminar boundary layer actually separates and undergoes separation induced transition.

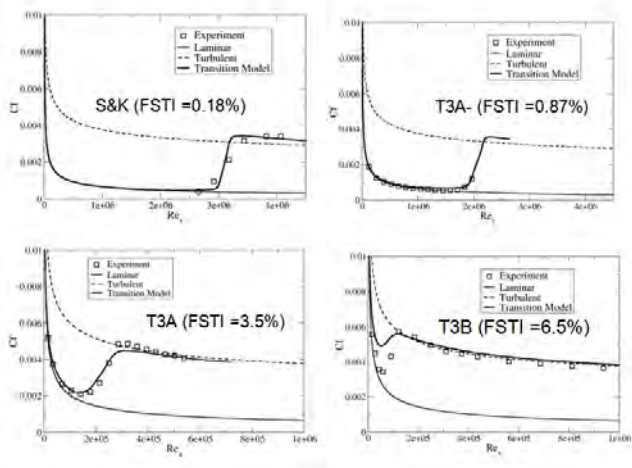


Figure 2: Results for flat plate test cases with different freestream turbulence levels (FSTI - Freestream Turbulence Intensity).

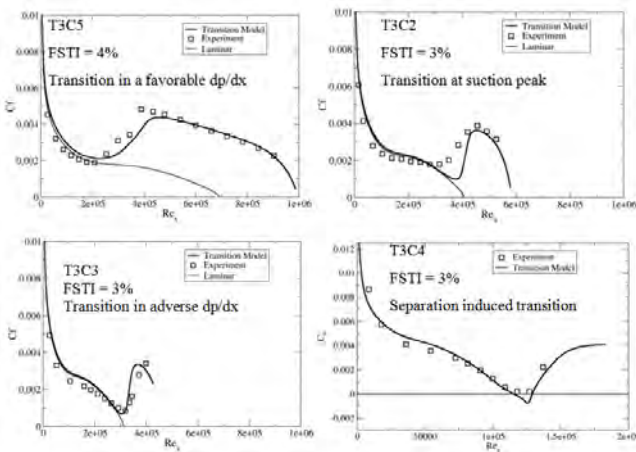


Figure 3: Results for flat plate test cases where variation of the tunnel Reynolds number causes transition to occur in different pressure gradients (dp/dx).

The re-laminarization test case is shown in Figure 4. For this case the opposite converging wall imposes a strong favorable pressure gradient that can re-laminarize a turbulent boundary layer. In both the experiment and in the CFD prediction the boundary layer was tripped near the plate leading edge. In the CFD computation this was accomplished by injecting a small amount of turbulent air into the boundary layer. Downstream of the trip the boundary layer slowly re-laminarizes due to the strong favorable pressure gradient.

For all of the flat plate test cases the agreement with the data is generally good, considering the diverse nature of the physical phenomena computed, ranging from bypass transition to natural transition, separation-induced transition and even re-laminarization.

Pak-B Turbine Blade

Due to space limitations, only one industrial flow will be shown, namely the Pak-B turbine cascade investigated experimentally by Huang et al. (2003) for a range of Reynolds numbers and turbulence intensities. The experiments were performed at the design incidence angle for Reynolds numbers of 50,000, 75,000, and 100,000 based on inlet velocity and axial chord length, with turbulence intensities of 0.08%, 2.35% and 6.0% (which

corresponded to values of 0.08%, 1.6%, and 2.85% at the leading edge of the blade). The computed pressure coefficient distributions for various Reynolds numbers and freestream turbulence intensities compared to experimental data are shown in Figure 5. On the suction side, a pressure plateau due to a laminar separation with turbulent reattachment exists. The fully turbulent computation completely misses this phenomenon because the boundary layer remains attached over the entire length of the suction surface. The transition model can predict the pressure plateau due to the laminar separation and the subsequent turbulent reattachment location. The pressure side was predicted to be fully attached and laminar. In Figure 5, the comparisons are organized such that the horizontal axis denotes the Reynolds number whereas the vertical axis corresponds to the freestream turbulence intensity of the specific case. The size of the separation bubble is actually a complex function of the Reynolds number and the freestream turbulence value. As the Reynolds number or freestream turbulence decrease, the size of the separation and hence the pressure plateau increases. The computations with the transition model compare well with the experimental data for all of the cases considered, illustrating the ability of the model to capture the effects of Reynolds number and turbulence intensity variations on the size of a laminar separation bubble and the subsequent turbulent reattachment.

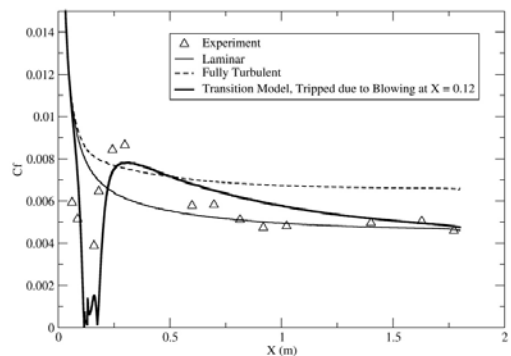


Figure 4: Predicted skin friction (C_f) for a flat plate with a strong acceleration that causes the boundary layer to relaminarize.

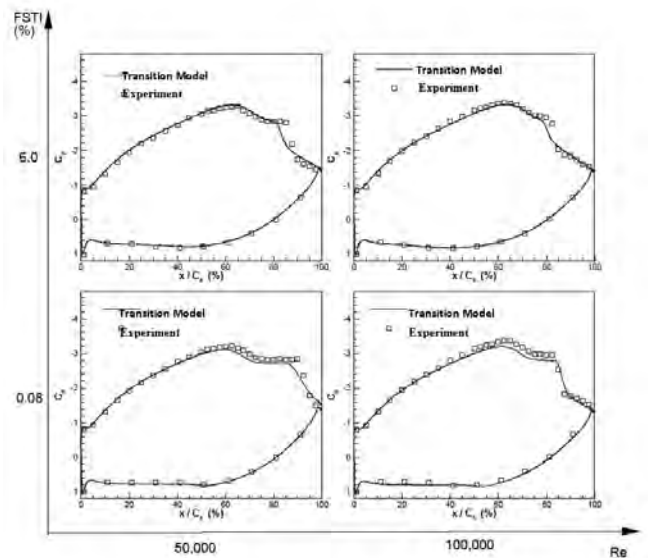


Figure 5: Blade loading for the Pak-B Low-Pressure turbine at various freestream turbulence intensities (FSTI) and Reynolds numbers (Re).

Summary

The concept of LCTM - Local Correlation-based Transition Modelling and its realization in the framework of the γ - Re_{θ} model has sparked widespread attention and interest both in the academic community and by industrial users. The model is now widely used in many diverse fields of applications. In addition numerous correlations compatible with the basic model formulation have been developed. It is expected that the LCTM approach will continue to be an area of intense model development as its potential is not yet fully exploited. Areas of interest are:

- Reduction of number of equations from two to one
- Extension of correlations for cross-flow instability and high speed flows
- Combination with other turbulence models

The authors feel that LCTM offers an attractive framework for including effects of laminar-turbulent transition at least to 1st order in complex CFD simulations.

Acknowledgment

The model development was sponsored by GE Aircraft Engines and GE Global Research.

References

- Gamberoni, N., (1956), "Transition, Pressure Gradient and Stability Theory," Douglas Aircraft Company, Long Beach, Calif. Rep. ES 26388.
- Langtry, R.B., Menter, F.R., Likki, S.R., Suzen, Y.B., Huang, P.G., and Völker, S., (2006), "A Correlation based Transition Model using Local Variables Part 2 - Test Cases and Industrial Applications", ASME Journal of Turbomachinery, Vol. 128, Issue 3, pp. 423 - 434.
- Malkiel, E. and Mayle, R.E., (1996), "Transition in a Separation Bubble," ASME Journal of Turbomachinery, Vol. 118, pp. 752-759.
- Mayle, R.E., (1991), "The Role of Laminar-Turbulent Transition in Gas Turbine Engines," Journal of Turbomachinery, Vol. 113, pp. 509-537.
- McIlroy, H.M. and Budwig, R.S., (2005). The Boundary Layer over Turbine Blade Models with Realistic Rough Surfaces, ASME-GT2005-68342, ASME TURBO EXPO 2005, Reno-Tahoe, Nevada, USA.
- Menter, F.R., (1994), "Two-Equation eddy-viscosity turbulence models for engineering applications", AIAA Journal, Vol. 32, No. 8, pp. 1598-1605.
- Menter, F.R., Esch, T. and Kubacki, S., (2002), "Transition Modelling Based on Local Variables", 5th International Symposium on Engineering Turbulence Modelling and Measurements, Mallorca, Spain.
- Menter, F. R., Langtry, R., Völker, S. (2006a), "Transition Modelling for General Purpose CFD Codes". Flow, Turbulence and Combustion, Volume 77, Numbers 1-4, Springer Netherlands.
- Menter, F.R., Langtry, R.B., Likki, S.R., Suzen, Y.B., Huang, P.G., and Völker, S., (2006b), "A Correlation based Transition Model using Local Variables Part 1- Model Formulation", ASME Journal of Turbomachinery, Vol. 128, Issue 3, pp. 413 - 422.
- Morkovin, M.V., (1969), "On the Many Faces of Transition", Viscous Drag Reduction, C.S. Wells, ed., Plenum Press, New York, pp 1-31.
- Savill, A.M., (1993), Some recent progress in the turbulence modeling of by-pass transition, In: R.M.C. So, C.G. Speziale and B.E. Launder, Eds.: Near-Wall Turbulent Flows, Elsevier, p. 829.
- Savill, A.M., (1996), One-point closures applied to transition, Turbulence and Transition Modeling, M. Hallböck et al., eds., Kluwer, pp. 233-268.
- Schubauer, G.B. and Klebanoff, P.S., (1955), "Contribution on the Mechanics of Boundary Layer Transition," NACA TN 3489.

Smith, A.M.O. and Schlichting, H., (1979), Boundary Layer Theory, McGraw-Hill, 7th edition. Stock, H.W. and Haase, W., (2000), "Navier-Stokes Airfoil Computations with eN Transition Prediction Including Transitional Flow Regions," AIAA Journal, Vol. 38, No. 11, pp. 2059 - 2066.

Van Ingen, J.L., (1956), "A suggested Semi-Empirical Method for the Calculation of the Boundary Layer Transition Region," Univ. of Delft, Dept. Aerospace Engineering, Delft, The Netherlands, Rep. VTH-74.

TRANSITION MODELLING WITH INTERMITTENCY TRANSPORT EQUATIONS

Witold Elsner¹, Wladyslaw Piotrowski², Piotr Warzecha¹

¹ *Institute of Thermal Machinery, TU Czestochowa, Poland.*

² *GE Oil&Gas EDC Warsaw, Poland.*

Abstract

The paper presents validation of $\gamma-Re_\theta$ model proposed by Menter at al (2006), which was extended by in-house correlations on onset location and transition length. The tests performed were based on experimental data on the flat plate test cases where $l-t$ transition, laminar separation and reattachment were present. The model was applied both for steady and unsteady calculations. It was shown that the model was able to reproduce some essential flow features related to the bypass, separated and wake-induced transition and the simulations reveal good agreement with the experimental results.

1 Introduction

The proper prediction of the transition is among the most challenging and most important problems in the design process of turbomachinery stages. The location of the onset and the extension of transition are of major importance since they determine drag and lift forces as well as heat fluxes that are crucial for an overall efficiency and performance of a variety of machinery and devices. Among the most common examples of the machinery, where the laminar-turbulent transition is of particular importance, are the gas and aero-engine compressors and turbines.

The variety of possible transition mechanisms in turbomachinery flows make it difficult to propose the general strategy for numerical simulation. RANS methods and for unsteady calculations URANS with appropriately modelled transitional boundary layer is the only presently applicable engineering tools to study the transitional flows. Transition process, could be described by intermittency parameter γ , which gives information about the fraction of time, when the flow is turbulent. That is why the coupling with intermittency seems to be the best way to take into account the physical mechanism of transitional flow and to model transition in proper way. The general description of intermittency could be obtained from a dynamic intermittency convection-diffusion-source equation. The three most known models, which rely on this approach are models of Suzen and Huang [1], Lodefier and Dick [2] and Menter at al. [3]. The advantage of the last approach ($\gamma-Re_{\theta t}$ model) is that the start of the transition is achieved locally through the use of the vorticity Reynolds number. For this purpose apart from intermittency equation momentum thickness Reynolds number $Re_{\theta t}$ transport equation has been introduced. This transport equation takes a non-local empirical correlation and transforms it into a local quantity, which is then compared to the local vorticity Reynolds number to detect transition onset. On top of this advantage, this model may easily be adapted

for parallel calculations on unstructured grids and that is why this model was considered as a promising perspective. Recently, the extension of the Menter's model has been proposed by Piotrowski at al [4]. It was done by development of two in-house correlations on onset location and transition length, which are confidential in the original Menter's model.

The aim of the paper is to present further modifications of the previous in-house correlations and show their applicability for two flat plate cases i.e. the zero gradient Test Case (T3A) available at ERCOFTAC Data Base [5] and Lou and Hourmouziadis [6] Test Case (denoted as LH04), with pressure profile typically encountered on highly-loaded turbine airfoils. Finally, sample results of unsteady calculations of turbine blade profile which is a stator vane of the high-pressure part of the TK-200 steam turbine, investigated at Czestochowa University of Technology [7]. The experiment was performed on a linear turbine blade cascade with upstream wake generator in the form of the wheel equipped with cylindrical bars. For the analysed test case (N3-60_04) inlet freestream turbulence levels 0.4% and 4 mm bars were applied.

2 Modelling method description

The detailed description of the mathematical formulation of the $\gamma-Re_\theta$ model is given in the paper of Menter at al [3]. Here, all the transport equations for intermittency and momentum thickness Reynolds number as well as SST $k-\omega$ turbulence model were implemented in the commercial package Fluent via of User Defined Functions (UDFs). To limit an excessive level of kinetic energy near the leading edge a time scale bound according to Medic and Durbin [8] was applied.

In the $\gamma-Re_{\theta t}$ transition model two parameters play an important role i.e. F_{onset} , which triggers the intermittency production at the beginning of the transition and the F_{length} , which controls the length of the transition zone. The onset parameter F_{onset} is formulated as a function of critical transition Reynolds number $Re_{\theta c}$ and vorticity Reynolds number Re_V i.e. $F_{onset} = f(Re_V, Re_{\theta c})$. $Re_{\theta c}$ determines location where the intermittency starts to increase in the boundary layer, that occurs upstream of the transition Reynolds number $Re_{\theta t}$. To determine $Re_{\theta c}$ Menter [3] proposed to tie its value with $\widetilde{Re}_{\theta t}$ which comes from the transport equation of the momentum thickness Reynolds number $Re_{\theta t}$ according to the relation:

$$Re_{\theta c} = F_P \widetilde{Re}_{\theta t} \quad (1)$$

where F_P is an unknown function. Estimation of this function together with correlation for F_{length} parameter was the first issue of the paper.

To understand the process it is necessary to remind that outside the boundary layer, $\widetilde{Re}_{\theta t}$ is forced to follow the transition Reynolds number $Re_{\theta t}$ provided by the empirical correlation [3]. The transported scalar is then diffused into the boundary layer by a standard diffusion term. In the wall vicinity $\widetilde{Re}_{\theta t}$ changes along the distance from the leading edge and depends on the local pressure gradient, i.e. increases in the favourable pressure gradient and decreases in the zone of adverse pressure gradient. The initiation of $l-t$ transition depends on boundary layer flow features and that is why it was decided to use $\widetilde{Re}_{\theta t}$ values determined at the wall. It is known that $l-t$ transition in turbomachinery occurs usually in the zone of adverse pressure gradient i.e. in the zone behind the maximum value of $\widetilde{Re}_{\theta t}$. Therefore, it seems reasonable to relate the F_P function with the maximum value of $\widetilde{Re}_{\theta t}$ determined in the wall vicinity i.e. $\widetilde{Re}_{\theta t max}$.

The determination of F_P function was done based on flat plate ERCOFTAC Test Cases denoted as T3A, T3B (zero pressure gradient flow) and T3C1, T3C2, T3C3, T3C (varying pressure gradient flow) [4]. Further on the function was verified with the calculation of N3-60 and LH04 Test Cases.

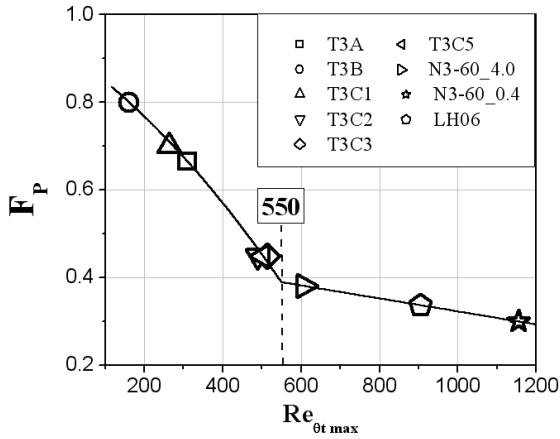


Figure 1: Evolution of F_P parameter versus $\widetilde{Re}_{\theta t max}$.

For all analyzed Test Cases the values of $\widetilde{Re}_{\theta t max}$ and the corresponding values of F_P have been shown in Fig. 1 together with the approximating line. In order to obtain a better fit it was decided to split the analyzed range of $\widetilde{Re}_{\theta t max}$ into two subranges i.e. $\widetilde{Re}_{\theta t max} > 550$ and $\widetilde{Re}_{\theta t max} \leq 550$, where the approximating lines are given by the following functions:

$$\begin{aligned} \widetilde{Re}_{\theta t max} \leq 550 : \\ F_P = -6.23 \cdot 10^{-7} \widetilde{Re}_{\theta t}^2 - 6.12 \cdot 10^{-4} \widetilde{Re}_{\theta t} + 0.915 \\ \widetilde{Re}_{\theta t max} > 550 : \\ F_P = -1.48 \cdot 10^{-4} \widetilde{Re}_{\theta t} + 0.471 \end{aligned} \quad (2)$$

One may notice that the sensitivity of F_P parameter is elevated for $\widetilde{Re}_{\theta t max} \leq 550$ and decreases for higher momentum thickness Reynolds number. It is apparent that the above formulas approximate well the flow cases both for flat plate cases as well as turbine blade that allows to hope for their universal character.

The similar approach has been applied to develop correlation describing the length of the transition i.e. the F_{length} function. Because F_{length} parameter is located

in the production term of intermittency transport equation if influences not only the length of transition zone but also the onset location. This feature was demonstrated during numerical experiment for T3A and T3C1 test cases presented in [4]. It was shown that too small values of this parameter (e.g. $F_{length} = 0.1$) increase the length of transition zone, but at the same time they introduce the non - physical shift of the onset towards the trailing edge. That is why the selection of F_{length} parameter should be accompanied by the analysis of correlation for the onset.

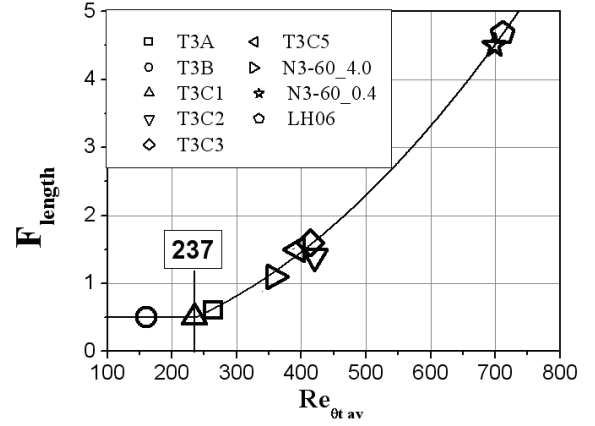


Figure 2: Evolution of F_{length} parameter versus $\widetilde{Re}_{\theta t av}$.

F_{length} parameter is also dependent upon the global properties of the flowfield and in order to account for this fact it was decided to relate F_{length} with $\widetilde{Re}_{\theta t av}$ i.e. to the mean value of $\widetilde{Re}_{\theta t}$ distribution at the wall. This idea differs from the assumption adopted in the previous work [4], where $\widetilde{Re}_{\theta t max}$ was the independent factor. The $\widetilde{Re}_{\theta t av}$ values and the corresponding values of F_{length} have been shown in Fig. 2 for all test cases analyzed and their distribution has been approximated with the following relations:

$$\begin{aligned} \widetilde{Re}_{\theta t av} \leq 237 : \\ F_L = 0.5 \end{aligned} \quad (3)$$

$$\begin{aligned} \widetilde{Re}_{\theta t av} > 237 : \\ F_L = 9.23 \cdot 10^{-6} \widetilde{Re}_{\theta t av}^2 + 2.04 \cdot 10^{-5} \widetilde{Re}_{\theta t av} - 0.021 \end{aligned}$$

The relation proposed above, together with correlations for the onset supplement the transport equations for intermittency γ and Reynolds number $\widetilde{Re}_{\theta t}$ form the complete calculation procedure for $l-t$ transition modelling, which is referred to as ITM in the following part of the paper.

3 Steady flow test cases

For testing the steady flow behaviour of the model, several test cases with various inlet and boundary conditions were considered [4]. In the present investigation it was decided to select well known zero pressure gradient flat plate T3A Test Case available at ERCOFTAC Data Base [5] and Lou and Hourmouziadis Test Case - LH04, with pressure profile typically for suction side of highly-loaded turbine airfoil [6].

T3A Test Case was computed with a structural numerical grid containing 150 150 nodes, while for the LH06 case a grid of 150x340 nodes was used. These grids

Case	$\frac{\partial p}{\partial x}$	U_{in} [m/s]	Tu_{in} [%]	μ_t/μ	k [m ² /s ²]	ω [s ⁻¹]
T3A	0	5.4	3	13.3	0.042	232
LH06	var.	9.0	0.6	11	0.0044	26.5
N3-60-4	var.	8.5	0.4	10.8	0.15	924

Table 1: *Inlet conditions.*

were selected as a result of grid independence studies, with particular emphasis placed on accurate near-wall discretization. In order to capture the laminar and transitional boundary layers correctly, the grid had to have a closest to wall y^+ value smaller than 1.

Detailed information on the flow conditions for those test cases is given in Table 1, together with inlet parameters used in the calculations (i.e. inlet velocity, turbulent intensity). The boundary condition for γ at a wall was zero normal flux while at the inlet γ was equal to 1. It is also important to note that the transition onset location proved very sensitive to the advection scheme used for the turbulence and transition model equations. For this reason all equations were solved with a bounded second order upwind scheme. Mass conservation was enforced via the SIMPLE pressure-correction algorithm.

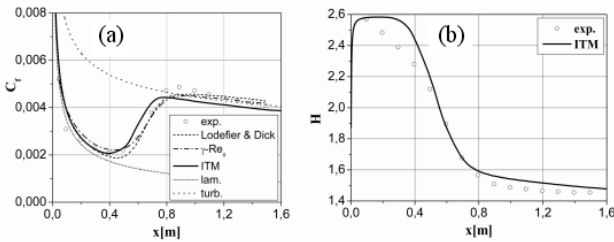


Figure 3: *Evolution of skin-friction (a) and shape factor (b) for the T3A Test Case.*

Fig. 3 shows distributions of local skin friction coefficient C_f obtained with the use of the proposed model for T3A. These results were compared with the experimental data and numerical results obtained by Lodefier & Dick [4] as well as with the results obtained with original Menter's [3] ($\gamma-Re_{\theta t}$) model. One may notice a very good agreement between numerical and experimental results both for the transition onset location and for the extent of the transition region.

The slope of C_f curve (Fig. 3a) in the transition area is a bit too steep, what results in shorter transition region in comparison with Lodefier & Dick and $\gamma-Re_{\theta t}$ results. This conclusion is confirmed by the analysis of shape factor distribution H (Fig. 3b), which in the range ($x = 0.1 - 0.45$) attains somewhat higher values in comparison to the experimental results, that indicates too small value of the laminar-turbulent transition length.

Fig. 4 shows the calculated and measured pressure coefficient C_p and the shape factor H along the plate for LH06 Test Case. The main flow over the flat plate is accelerated up to $x = 0.3$ m and then diffused by the adverse pressure gradient. Looking on C_p and H distributions, the separation point is identified at 0.39 m. It is seen that numerical results for shape factor follows closely the experimental data up to the maximum value defining the end of transition at $x = 0.45$ m. Only in the recovery region after the reattachment ($x = 0.47$ m)

the shape factor is slightly overpredicted. A qualitative comparison of the experimental and computed mean absolute velocity field is given in Fig. 5. One can observe that simulation reproduced the size of separation region properly.

It could be concluded, that the formulations for the transition onset and transition length proposed in the paper, appear to be sufficiently precise and enable accurate prediction of boundary layer development for flat plate configurations.

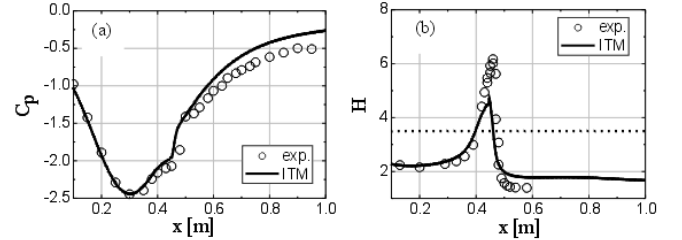


Figure 4: *Evolution of pressure coefficient (a) and shape factor (b) for LH06 Test Case.*

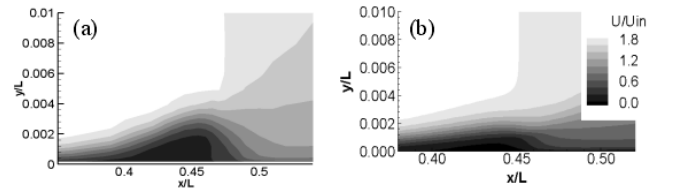


Figure 5: *Plot of normalized velocity for LH06 Test Case, experiment (a), simulation (b).*

4 Wake induced cascade test cases

Flow unsteadiness strongly affects the time dependent location of the laminar-turbulent transition region on the blade surface. The proper description of the unsteady flow is therefore very demanding for transition modelling.

Further tests of the ITM model described in detail in [4] were carried out for N3-60 Test Case. The shape of the profile is embedded on Fig. 6. The preliminary steady calculations were performed with inlet flow conditions given in Table 1. During unsteady calculations the self-similar wake profiles, which were defined based on the experimental data were used and prescribed at the inlet to the computational domain. The analysis of the response of the boundary layer to the passing wake is based on two key parameters i.e. intermittency and shape factor. Intermittency controls the production of turbulent kinetic energy in the turbulence model and the shape factor characterizes the state of the boundary layer i.e. whether it is laminar, transitional, turbulent or separated. Fig. 6 presents the comparison of numerical results obtained with ITM with experimental data for suction side of the blade. The data are given in the conventional time-space diagrams showing how boundary layer parameters vary with surface distance on abscissa and with time on the ordinate axis. The two dashed lines show the location of the wake based on local boundary edge velocity, where the first one represents the maximum periodic velocity path, while the

second indicates the location of periodic velocity perturbation minimum. The additional dotted line indicates the area of transitional and turbulent wedge induced by the wake defined based on the ITM results. It should be noticed that the intermittency γ_{eff} for numerical results was presented using different scaling than for the experiment. The scale from 0 to 2 was used in order to show the action of γ_{sep} on the boundary layer reattachment.

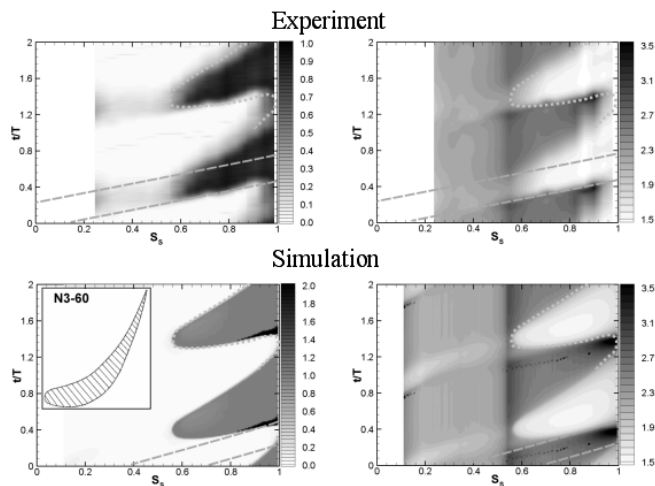


Figure 6: Time-space diagrams of intermittency - left column and shape factor - right column for N3-60_04.

The start of the transition under the wake was found to be almost identical with the experimental data. There are only some differences in the extent of the turbulent wedge and in the transition in between the wakes. One can notice that experimental shape factor reveals the trailing edge separation. ITM model detects the separation and also activates the separation induced transition, what is confirmed by the elevated level of intermittency to value $\gamma_{eff} = 2$, what is seen as a narrow black strip in front of turbulent wedge (left-down plot in Fig. 6).

5 Conclusions

The paper presents the results of tests and validations of $\gamma-Re_\theta$ model, which was extended by in-house correlations on onset location and transition length. The correlations developed were based on ERCOFTAC Data Base and were further validated using experimental data of Lou and Hourmouziadis [6] and of turbine blade profile N3-60_04 [7].

The tests proved that the formula for the transition onset and transition length proposed in the paper appear to be sufficiently precise and enable accurate prediction of boundary layer development for steady inflow conditions. The validation shows also that the model is able to reproduce the periodical evolution of the boundary layer under the influence of impinging wakes. The universal character of correlations proposed in the paper needs further tests and evaluation, however authors believe that the method proposed may serve as a useful tool for modeling both steady and unsteady $l-t$ transition on turbomachinery blading.

Acknowledgements

The research was supported by the Polish State Committee for Scientific Research BS-01-103-301/2004/P as well as research grant No. PBZ-MEiN-4/2/2006.

References

- [1] Suzen, Y.B., Huang, P.G., 2000. Modeling of flow transition using an intermittency transport equation. *J. Fluids Eng.* 122, 273-284.
- [2] Lodefier K., Dick E., 2006, Modelling of Unsteady Transition in Low-Pressure Turbine Blade Flows with Two Dynamic Intermittency Equations, *Flow, Turbulence and Combustion*, 76(2); pp.103-132.
- [3] Menter F.R., Langtry R.B., Likki S.R., Suzen Y.B., Huang P.G., Völker S., 2006, A correlation - based transition model using local variables P.I - Model formation, *ASME, J. of Turbomachinery* vol. 128, pp. 413-422.
- [4] Piotrowski W., Elsner W., Drobniak S., 2008, Transition Prediction On Turbine Blade Profile With Intermittency Transport Equation, *ASME paper GT2008-50796, ASME TURBO EXPO, Berlin* [5] <http://cfd.me.umist.ac.uk/ercoftac/>.
- [6] Lou W., Hourmouziadis, J., 2000, Separation Bubbles Under Steady and Periodic-Unsteady Main Flow Conditions, *Trans. ASME J. of Turbomachinery*, Vol. 122, pp. 634-643.
- [7] Zarzycki R., Elsner W., 2005, "The effect of wake parameters on the transitional boundary layer on turbine blade", *IMEchE Part A, J. Power and Energy*, vol.219, pp. 471-480.
- [8] Medic G. and Durbin P.A., 2002, "Toward improved prediction of heat transfer on turbine blades", *ASME J. of Turbomachinery*, vol. 124, pp. 187-192.

CALIBRATING THE $\gamma-Re_\theta$ TRANSITION MODEL

Paul Malan¹, Keerati Suluksna², Ekachai Juntasaro³

¹ *CD-adapco, Lebanon, USA.*

² *Suranaree University of Technology, Thailand.*

³ *King Mongkut's University of Technology North Bangkok, Thailand.*

Abstract

The $\gamma-Re_\theta$ transition model is the first correlation-based model designed for unstructured, parallel computational fluid dynamics (CFD) codes. Two out of the three correlations required to complete the model have not yet been published by the originators of the model. This paper presents plausible forms for the missing correlation functions and describes a procedure for calibrating the model.

1 Introduction

The $\gamma-Re_\theta$ model proposed by Menter, Langtry and co-workers [1-6] is a correlation-based approach to transition modeling that was designed specifically for unstructured CFD codes. Two key strengths of the model are: (1) it largely avoids the use of non-local quantities by employing two additional transport equations and using a strain-rate Reynolds number to trigger transition; and (2) it is designed to work with the SST $k-\omega$ turbulence model [7-8], which is well-validated and has wide acceptance in the aerospace and other industries.

Since two out of the three correlations required for the $\gamma-Re_\theta$ model were not openly published, early adopters of the model have been forced to develop their own correlations, with varying results [9-14].

This paper summarizes the key findings from our systematic efforts to synthesize the two missing correlations. The calibration procedure, described in detail herein, was used to create a complete version of the $\gamma-Re_\theta$ model [14] that has been demonstrated to replicate many of the excellent validation results shown in Refs. 1-6.

2 Model Implementation

The $\gamma-Re_\theta$ model has been implemented in STAR-CCM+ [15] a fully unstructured, cell-based finite volume code developed with a client-server architecture using object-oriented methods in C++ and Java. A second-order upwind scheme is used for all transport equations, including those of the SST $k-\omega$ turbulence model and the $\gamma-Re_\theta$ transition model.

Due to space limitations, the full formulation of the turbulence and transition models, reported in Ref. 14, has not been repeated herein. It is noted, however, that the SST $k-\omega$ turbulence model is enhanced in several ways. First, the wall boundary condition for ω is specified within the wall cell, rather than at the boundary as suggested by Menter [7], to facilitate the implementation of wall functions when they are needed. Second, in accordance with later recommendations [8], the strain rate tensor modulus is used in the production term rather than the vorticity as in the original model formulation

[7]. Third, dilatation dissipation in compressible flow is accounted for using the formulation outlined by Wilcox [16]. Fourth, the realizability constraint of Durbin [17] is used rather than the less-restrictive bound on the production favored by Menter [7]. Finally, the suggestions of Spalart and Rumsey [18] are incorporated to optionally suppress freestream turbulence decay through source terms.

To close the $\gamma-Re_\theta$ transition model, correlations for three variables are required: (1) $Re_{\theta t}$, the transition onset momentum thickness Reynolds number; (2) $Re_{\theta c}$, the critical momentum thickness Reynolds number; and (3) F_{length} , a parameter governing the transition length.

The forms and calibration of these correlations are discussed in the following two sections.

3 Correlation for $Re_{\theta t}$

The correlation for $Re_{\theta t}$, first presented by Menter et al. [1] as an update of the correlation of Abu-Ghannam and Shaw [19], was subsequently revised by Langtry [6]. This formula is as follows for the case of zero pressure gradient:

$$Re_{\theta t} = \begin{cases} 1173.51 - 589.428Tu + \frac{0.2196}{Tu^2} & ; Tu \leq 1.3 \\ 331.5 [Tu - 0.5658]^{-0.671} & ; Tu > 1.3 \end{cases} \quad (1)$$

In Eq. (1), Tu is the turbulence intensity computed from the turbulent kinetic energy, k , and the local velocity magnitude, U , using the formula

$$Tu \equiv \max(0.027, 100\sqrt{2/3k}/U) \quad (2)$$

The minimum limit of 0.027 on Tu corresponds to the low-turbulence transition measurements reported by Wells [20].

All three $Re_{\theta t}$ correlations are compared in Fig. 1 for the case of zero pressure gradient. Langtry's version is presently adopted since it is the most up-to-date, even though it does not necessarily exhibit the best fit to the experimental data cited in Refs. 1 and 6 for $Tu < 1\%$.

$Re_{\theta t}$ is evaluated in the freestream, and the source term in the equation for the transported transition onset momentum thickness Reynolds number, $\widetilde{Re}_{\theta t}$, is constructed such that $\widetilde{Re}_{\theta t} = Re_{\theta t}$ in the freestream. This requirement implies that the model is semi-local, rather than local, giving rise to two noteworthy complications that are not addressed in Refs. 1-6. First, one must define what the freestream is and where it is located. Second, the evaluation of the source term of the transport equation for $\widetilde{Re}_{\theta t}$ requires a mechanism by which the cells inside the boundary layer can reference the value of $Re_{\theta t}$ in the freestream. Our implementation addresses

the first issue only loosely by allowing the user to specify the location of the freestream in terms of a user-defined iso-surface. One simple definition of the iso-value might be a specified value of the distance from the cell centroid to the nearest wall. For complex flows, the sensitivity of the calculations to this choice ought to be tested. The second issue is addressed by using a KD tree algorithm to store the location of the mesh faces that most closely correspond to the freestream definition. The flow variables of interest are then interpolated from the cell values straddling the face. To reduce the communication costs when running in parallel, a policy for updating the KD tree every n iterations is optionally employed.

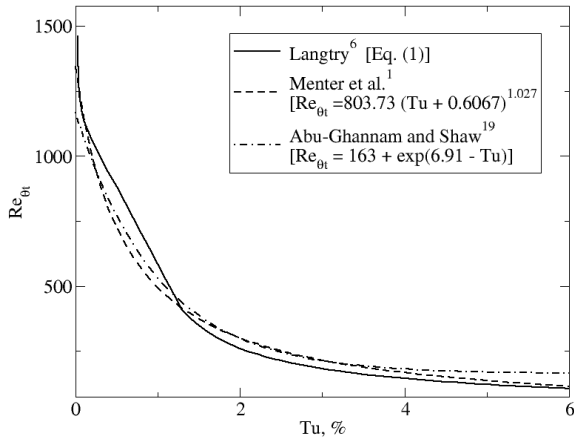


Figure 1: Comparison of Re_{θ_t} correlations.

4 Proposed Forms for Re_{θ_c} and F_{length}

Suluksna et al. [12,13] used both physical intuition and numerical experiments to propose plausible forms for the Re_{θ_c} and F_{length} correlations as functions of the transported transition momentum thickness Reynolds number, $\widetilde{Re}_{\theta_t}$. First, they reasoned that, in the freestream, $\widetilde{Re}_{\theta_t} = Re_{\theta_t}$ by design. Clearly, $Re_{\theta_c} \leq Re_{\theta_t}$, since Re_{θ_c} is the momentum thickness Reynolds number at which the intermittency first starts to grow, and Re_{θ_t} is the momentum thickness Reynolds number where the skin friction starts to increase. The simplest possible form is, therefore, the linear relationship:

$$Re_{\theta_c} = a\widetilde{Re}_{\theta_t} + b \quad (3)$$

where $0 < a \leq 1$.

To obtain a viable form for F_{length} , Suluksna et al. [12] devised the following numerical experiment: (1) Assume that $Re_{\theta_c} = Re_{\theta_c}$; (2) Use Eq. 1 to provide a value for Re_{θ_t} (considered constant for the entire flow) as a function of the leading edge freestream turbulence intensity; and (3) Manually adjust F_{length} (considered constant for the entire flow) to obtain a reasonable fit to the available flat plate skin friction data.

From this exercise, an inverse relationship between F_{length} and $\widetilde{Re}_{\theta_t}$ immediately becomes clear. This relationship is logarithmic, with large values of $\widetilde{Re}_{\theta_t}$ corresponding to very small values of F_{length} , and vice versa. A relationship of the form:

$$F_{length} = \exp\left(A - B\widetilde{Re}_{\theta_t}\right) + C \quad (4)$$

apparently satisfies these criteria.

Tu	Reference (Case)	Length scale?
0.1	Blair [29]	Yes
0.18	Schubauer & Klebanoff [26] (TSK)	No
0.7	Feirereisen & Acharya [27]	No
0.94	Roach & Brierley [22,23] (T3AM)	Yes
1.1	Kuan & Wang [24]	Yes
1.2	Blair [29]	Yes
1.25	Abu-Ghannam & Shaw [19]	No
1.3	Dhawan & Narasimha [28]	No
2.7	Blair [29]	Yes
3.4	Roach & Brierley [22,23] (T3A)	Yes
6.0	Roach & Brierley [22,23] (T3B)	Yes

Table 1: Flat Plate Transition Data.

The challenge remains to calibrate the coefficients of these proposed correlations using available data. Since Re_{θ_c} and F_{length} are assumed to be functions of $\widetilde{Re}_{\theta_t}$ alone, they can be calibrated using flat plate data, leaving pressure gradient effects to be accounted for in the Re_{θ_t} correlation.

5 Survey of Flat Plate Transition Data

Clearly the first challenge in finding the coefficients of the proposed correlations is to obtain suitable reference data. As Singer [21] points out, "transitional-flow data have often presented the research community with paradoxes and apparent inconsistencies. Most of the time, the problem is not a glaring mistake, but a surprisingly strong influence by some flow quantity" A decision thus needs to be made as to which data to include or weight more in the calibration. Table 1 summarizes available data, the left-most column indicating leading edge turbulence intensities and the right-most column indicating the availability of sufficient length-scale data to model the free-stream turbulence adequately. In the absence of length-scale data, one has two options: (1) estimate the leading edge turbulent Reynolds number (the parameter that governs the turbulence decay); or (2) suppress the decay using source terms, while using a sufficiently low turbulent Reynolds number to avoid contaminating the data through artificially elevated levels of turbulent diffusion.

The most often-referenced (and presumably reliable) transition data sets are those of Roach and Brierley [22] in the ERCOFTAC database [23]. Dick [25] prefers the data set of Kuan and Wang [24] over T3AM for two reasons: 1) T3AM does not contain data downstream of transition; and 2) the higher turbulence intensities characterize it more definitively as bypass transition. On the other hand, Kuan and Wang's data do not exhibit meaningful free-stream decay, so that the specification of the proper inflow boundary conditions is difficult.

The data of Schubauer and Klebanoff [26] are often assumed to represent natural transition even though the experiment appears to contain finite acoustical disturbances and freestream length scale information is not available. Other data sets that do not have comprehensive freestream scale information include Feirereisen and Acharya [27], Dhawan and Narasimha [28] and Abu-Ghannam and Shaw [19]. Finally, the data of Blair [29] has potential due to the wide range of turbulence intensities covered, but these data are difficult to digitize from the printed paper due to the low resolution of the plots.

Case	U_{in} [m/s]	k_{in} [J/kg]	ω_{in} [1/s]
T3B	9.40	0.8964	573.2
T3A	5.40	0.1386	712.2
T3AM	19.8	0.0780	680.4
TSK	50.1	0.0827	5134

Table 2: *Inflow Boundary Conditions.*

6 Calibration Procedure

The data sets selected for the present calibration are the Roach and Brierley [22] cases T3B, T3A and T3AM from the ERCOFTAC database [23] corresponding to moderately high- to low-turbulence intensity bypass transition, and the Schubauer and Klebanoff [26] case TSK, using skin friction data digitized from Langtry [6].

A Cartesian mesh containing 194 streamwise x 250 cross-stream cells was used for the calibration. The near-wall cell height of 1.5×10^{-5} m ensured that the wall-adjacent cell centroid height typically ranged between 0.1 and 0.5 viscous units. The domain of height 0.8 m extended from 0.15 m upstream of the plate to 2 m downstream. This domain size and mesh resolution resulted from sensitivity studies in which the domain extent, the wall-adjacent cell height, the cell count and the clustering were varied until mesh-independent results were achieved for all four cases. The leading edge radius of the flat plate was not modeled to avoid any possibility of transition occurring due to laminar-bubble separation.

The fluid density was taken to be 1.2 kg/m^3 and viscosity 1.8×10^{-5} Pas. A specified constant velocity inlet was used together with a specified constant static pressure at outlet. Slip walls were used on the top boundary and the lower boundary upstream of the plate. Inflow boundary conditions are reported in Table 2. For cases T3AM, T3A and T3B, the inflow turbulence values were adjusted to obtain a close match to the freestream decay data. Freestream turbulence decay profiles are not available for case TSK, so the inflow boundary conditions were chosen to match the leading edge values quoted by Langtry [6]. Schubauer and Klebanoff [26] report an inflow velocity of 24.4 m/s, different to that used by Langtry. However, this discrepancy affects only the bulk Reynolds number; it does not change the transition onset Reynolds number. An alternative approach of disabling the freestream decay for case TSK was investigated, thus fixing the freestream turbulence intensity and turbulent viscosity. This moves the transition onset slightly upstream, but whereas it might be considered an equally valid approach, it was not pursued.

As noted by Menter et al. [5], the Re_{θ_c} and F_{length} functions are strong functions of each other. This interdependence requires tedious iteration to obtain optimal fits to both curves. The basic approach to tuning the coefficients is as follows:

1. Assume plausible initial values of the coefficients a and b for the Re_{θ_c} curve of Eq. (3) (say $a=0.8$, $b=0$) and specify constant values for F_{length} based on the preliminary numerical experiment described above in Section 4.
2. Run the lower freestream turbulence cases TSK and T3AM and adjust the specified constant value of F_{length} to best match the skin friction data. Adjust the coefficients a and b to ensure that the specified F_{length} value is smaller for case TSK than

T3AM. The minimum value of F_{length} (typically $0.3 < F_{length} < 0.7$) is determined by the TSK case, the specific value being chosen to strike a balance between too short a transition length and the recovery of the fully turbulent skin friction downstream of transition.

3. Run cases T3A and T3B, adjusting constant values of F_{length} to obtain acceptable agreement with the experiment data.
4. Perform a regression curve fit for F_{length} as a function of $\widetilde{Re}_{\theta_t}$ for the cases T3A, T3AM and TSK. To do this, estimate representative values of $\widetilde{Re}_{\theta_t}$ at transition for each case. Respective values of 105, 190, 520 and 900 were used for T3B, T3A, T3AM and TSK in the present work.
5. Use the fitted curve for F_{length} together with the assumed linear relation for Re_{θ_c} and re-run all cases.
6. Iteratively adjust the coefficients of the correlations to obtain optimal agreement with the experimental data. The following notes are helpful when tuning the coefficients:
 - Adjusting the coefficients a and b in a manner that increases Re_{θ_c} will result in an earlier transition onset. (This is apparent from the model equations, since increasing Re_{θ_c} increases F_{onset} , the parameter that governs where intermittency first starts to increase in the boundary layer.)
 - For the TSK case, one can assume that $C \sim F_{length}$.
 - The proposed function for F_{length} decreases monotonically. This fact influences the slope of the Re_{θ_c} curve. If the value of a is too large, transition will occur too late for the T3AM case even assuming $F_{length} = C$.
 - Once the Re_{θ_c} curve has been established, the coefficients A and B of the F_{length} curve can be adjusted to match the T3A and T3AM data.
 - The solution is relatively insensitive to the exact value of F_{length} for the small values $\widetilde{Re}_{\theta_t}$, (i.e., high turbulence intensities) occurring in the T3B case. Therefore, the curve fit for F_{length} can largely proceed independently of case T3B.
7. As a final step, determine the limiting value of Re_{θ_c} that will yield a transition location of $Re_x = 4.9 \times 10^{-6}$ for nominal freestream turbulence intensities of 0.027%, in accordance with the data of Wells [20]. A value of $Re_{\theta_c} = 950$ was obtained in the present study.

The final calibrated correlations are

$$Re_{\theta_c} = \min[\min(0.615\widetilde{Re}_{\theta_t} + 61.5, \widetilde{Re}_{\theta_t}), 950] \quad (5)$$

$$F_{length} = \min\left[\exp(7.168 - 0.01173\widetilde{Re}_{\theta_t}) + 0.5, 300\right], \quad (6)$$

and are shown in Fig. 2.

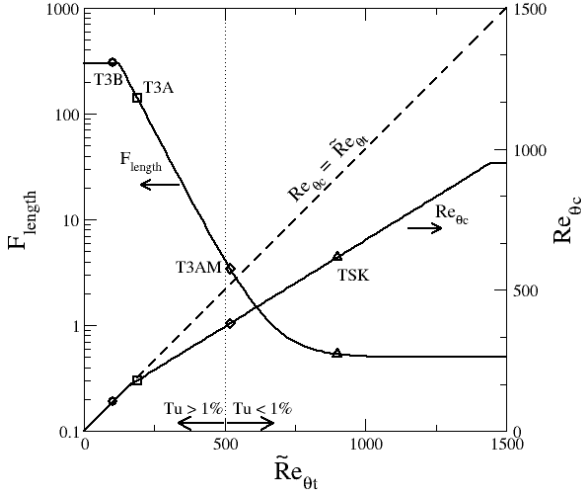


Figure 2: Final correlations for Re_{θ_c} and F_{length} .

Using the correlations of Eqs. (1), (5) and (6), the computed skin friction coefficient results of the TSK, T3AM, T3A, and T3B simulations are shown in Fig. 3. The skin friction coefficient results closely match the experimental data, and are comparable to those presented by Langtry [6]. The largest discrepancy is the failure to predict the trough in skin friction coefficient for case T3B (high freestream turbulence intensity). Langtry attributes this failure to the high values of turbulent viscosity ($\mu_t \sim 100\mu$) required to obtain the correct freestream turbulence decay.

Our numerical experiments indicate that even though Re_{θ_c} and F_{length} are assumed to be constant for $Tu < 0.027\%$, the transition onset Reynolds number continues to increase as Tu is further reduced. This contradicts the "quiet" transition data of Wells [20], which suggest that Re_{θ_t} ought to asymptote to a fixed value near the limit of vanishing freestream acoustic disturbances. Dick [25] questions the validity of any RANS-based transition model in this regime because it cannot be expected to properly represent the physics of the boundary layer instability. Furthermore, arbitrarily small turbulence intensities can give rise to numerical issues because turbulent kinetic energy is assumed to be positive-definite in most two-equation turbulence model implementations. Therefore, $Tu = 0.027\%$ seems to be a reasonable lower bound on the model's range of applicability.

7 Extension to Non-Zero Pressure Gradients

The three correlations given by Eqs. (1), (5) and (6) comprise a complete model calibration for zero-pressure gradient boundary layers. It might seem that the most logical way to extend them to non-zero pressure-gradient situations would be to use the Re_{θ_t} correlations that have been sensitized to streamwise acceleration. However, in Refs. 13 and 14, the predictions of the non-zero pressure-gradient cases T3C1-T3C5 of Roach & Brierley [22,23] are shown to be degraded by using these extended correlations. (Another disadvantage of using an extended correlation for Re_{θ_t} is that an iterative solution is required to evaluate it.)

The T3C result seems counter-intuitive and warrants further investigation. One possible hypothesis is offered by Suluksna et al. [13] They point out that the Re_{θ_t} correlations are designed to replace the correlation of Abu-Ghannam and Shaw [19], and were partly obtained by a curve fit to Abu-Ghannam and Shaw's correlation for

adverse pressure gradients. However, the Abu-Ghannam and Shaw correlation is based on an average of the turbulence intensities at the leading edge and the transition location, motivated by the desire to incorporate the effects of flow history. On the other hand, in the current model, the pressure gradient effects are to some degree implicitly accounted for by expressing Re_{θ_t} as a function of local freestream turbulence intensity. This is because the pressure gradient itself affects the local turbulence intensity; adverse pressure gradients tend to promote turbulence whereas favorable pressure gradients suppress it. Therefore, by omitting the streamwise pressure gradient from the correlation, one avoids an error due to double accounting.

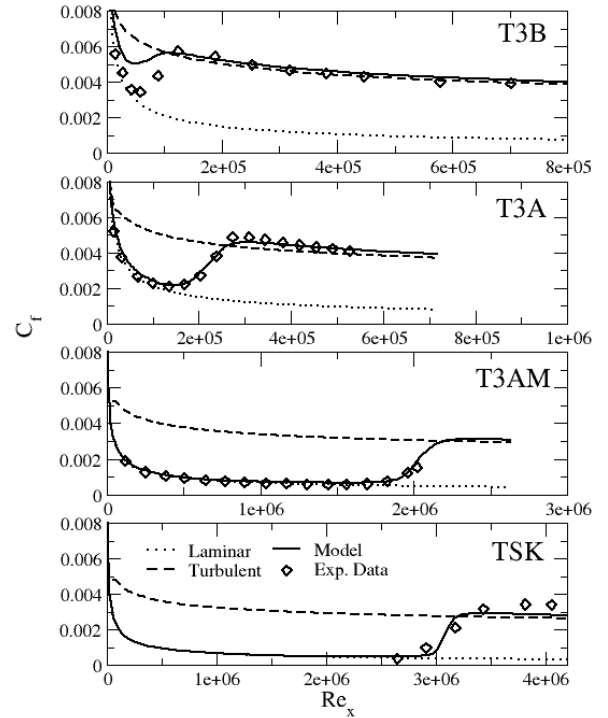


Figure 3: Skin friction coefficient for zero-pressure-gradient flat plate.

8 Conclusions

Plausible forms for the two correlations needed to complete the γ - Re transition model have been presented together with a procedure for calibrating them. This procedure can be used to tailor the correlations to fit additional data or to account for the effect of small differences in the implementation of the turbulence and transition models that might affect the calibration.

Clearly, the interdependence of the three correlation functions makes it unlikely that there is a unique calibration for the candidate data sets. For any suitable Re_{θ_t} function, there is apparently a range of Re_{θ_c} and F_{length} functions that can be constructed to best match the calibration data. Modifying Re_{θ_t} adds yet one more degree of freedom. The choices made in the calibration process might influence characteristics of the model aside from its predictive capabilities. For instance, Suluksna et al. [13] suggest that using lower values of F_{length} improves convergence. Choosing to minimize F_{length} would probably result in a polynomial function for Re_{θ_c} that is tangential to $Re_{\theta_c} \leq Re_{\theta_t}$ for small values of Re_{θ_t} and asymptotically approaches a constant value for large

$\widetilde{Re}_{\theta t}$. Such fine tuning remains a topic for further investigation.

The correlation functions presented herein offer sufficient degrees of freedom to match the transition onset location and transition lengths for the four candidate data sets fairly precisely. Accommodating additional data sets might necessitate a least-squares approach that would compromise this precision. Consistent with the goals of this study, however, the present correlations applied to more complex, two-dimensional flows [14] yield comparable results to those of Langtry [6] for the cases investigated.

References

1. Menter, F.R., Langtry, R.B., Likki, S.R., Suzen, Y.B., Huang, P.G., and Völker, S., "A Correlation-Based Transition Model Using Local Variables Part 1 - Model Formulation," ASME GT2004-53452, Proceedings of the ASME Turbo Expo, Power for Land Sea and Air, June 14-17, 2004.
2. Menter, F.R., Langtry, R.B., Likki, S.R., Suzen, Y.B., Huang, P.G., and Völker, S., "A Correlation-Based Transition Model Using Local Variables Part 2 - Test Cases and Industrial Applications," ASME GT2004-53454, Proceedings of the ASME Turbo Expo, Power for Land Sea and Air, June 14-17, 2004.
3. Langtry, R.B. and Menter, F.R., "Transition Modeling for General CFD Applications in Aeronautics," AIAA Paper 2005-522, Reno, Nevada, 2005.
4. Menter, F.R., Langtry, R.B., Völker, S. and Huang, P.G., "Transition Modelling for General Purpose CFD Codes," ERCOFTAC Int. Symp. Engineering Turbulence Modelling and Measurements, ETMM6, 2005.
5. Menter, F.R., Langtry, R., and Völker, S., "Transition Modelling for General Purpose CFD Codes," Flow, Turbulence and Combustion, Vol. 77, pp. 277-303, 2006.
6. Langtry, R.B., "A Correlation-Based Transition Model Using Local Variables for Unstructured Parallelized CFD Codes," Dr.-Ing thesis, Institute of Thermal Turbomachinery and Machinery Laboratory, University of Stuttgart, 2006.
7. Menter, F. R., "Two-Equation Eddy Viscosity Models for Engineering Applications," AIAA Journal, Vol. 32, No. 8, pp. 1598-1605, 1994.
8. Vieser, W., Esch, T. and Menter, F.R., "Heat Transfer Predictions Using Advanced Two-Equation Turbulence Models," CFX Technical Memorandum CFX-VAL10/0602, ANSYS Inc., 2002.
9. Piotrowski, W., Elsner, W. and Drobnik, S., "Transition Prediction on Turbine Blade Profile with Intermittency Transport Equation," ASME GT2008-50796, Proceedings of the ASME Turbo Expo, Power for Land Sea and Air, June 9-13, 2008.
10. Krause, M., Behr, M. and Ballmann, J. "Modeling of Transition Effects in Hypersonic Intake Flows Using a Correlation-Based Intermittency Model," AIAA Paper 2008-2598, Dayton, OH, 2008.
11. Cheng, G., Nichols, R., Neroorkar, K.D. and Radhamony, P.G., "Validation and Assessment of Turbulence Transition Models," AIAA Paper 2009-1141, Orlando, FL, 2009.
12. Suluksna, K. and Juntasaro, E. "Assessment of Intermittency Transport Equations for Modeling Transition in Boundary Layers Subjected to Freestream Turbulence," Int. J. Heat and Fluid Flow, Vol. 29, No. 1, pp. 48-61, 2008.
13. Suluksna, K., Dechaumphai, P. and Juntasaro E., "Correlations for Modeling Transitional Boundary Layers Under Influences of Freestream Turbulence and Pressure Gradient," Int. J. Heat and Fluid Flow, Vol. 30, No. 1, pp. 66-75, 2009.
14. Malan, P., Suluksna, K. and Juntasaro, E., "Calibrating the -Re Transition Model for Commercial CFD," AIAA Paper 2009-1142, Orlando, FL, 2009.
15. STAR-CCM+ Software Package, Version 3.06, CD-adapco, Melville NY, Dec. 2008.
16. Wilcox, D.C., Turbulence Modeling for CFD, 2nd ed., DCW Industries, Inc., La Canada, California, 1988, Chap. 5.
17. Durbin, P., "On the k- Stagnation Point Anomaly," International Journal of Heat and Fluid Flow, Vol. 17, pp. 89-90, 1995.
18. Spalart, P.R. and Rumsey, C.L., "Effective Inflow Conditions for Turbulence Models in Aerodynamic Calculations," AIAA Journal, Vol. 45, No. 10, pp. 2544-2553, 2007.
19. Abu-Ghannam, B.J. and Shaw, R. "Natural Transition of Boundary Layers - The Effects of Turbulence, Pressure Gradient, and Flow History," J. Mech. Eng. Sci., Vol. 22, No. 5, pp. 213-228, 1980.
20. Wells, C. S. "Effects of Freestream Turbulence on Boundary-Layer Transition," AIAA Journal, Vol. 5, No. 1, pp. 172-174, 1967.
21. Singer, B., "Modeling the Transition Region," NASA CR-4492, 1993.
22. Roach, P.E. and Brierley D.H. "The influence of a turbulent free stream on zero pressure gradient transitional boundary layer development. Part 1: Test cases T3A and T3B," in Numerical Simulation of Unsteady Flows and Transition to Turbulence, O. Pironneau, et. al. eds. Cambridge University Press, 1990.
23. ERCOFTAC (European Research Community on Flow, Turbulence, Combustion) Nexus. [online database], URL: <http://ercoftac.mech.surrey.ac.uk/> [cited 15 Feb 2008].
24. Kuan, C.L. and Wang, T. "Investigation of the Intermittent Behavior of Transitional Boundary Layer Using a Conditional Averaging Technique," Experimental Thermal and Fluid Science, Vol. 3, pp. 157-173, 1990.
25. Dick, E. Private Communication, Feb. 2009.
26. Schubauer, G.B. and Klebanoff, P.S. "Contributions on the Mechanics of Boundary Layer Transition," NACA Technical Note 3489, 1955.
27. Feiereisen, W.J. and Acharaya, M. "Modeling of Transition and Surface Roughness Effects in Boundary-Layer Flows," AIAA Journal, Vol. 24, pp. 1642-1649.
28. Dhawan, S. and Narasimha, R. "Some Properties of Boundary Layer Flow During the Transition from Laminar to Turbulent Motion," J. Fluid Mech., Vol 3, pp. 418-436, 1958.
29. Blair, M.F. "Influence of Free-Stream Turbulence on Turbulent Boundary Layer Heat Transfer and Mean Profile Development, Part 1 - Experimental Data," J. Heat Transfer, Vol. 105, pp. 33-40, 1983.

OVERVIEW OF WAKE INDUCED TRANSITION MODELLING FOR AXIAL COMPRESSORS

Adam Beevers¹, Joao Teixeira¹, Roger Wells²

¹ School of Engineering, Cranfield University, UK.

² Siemens Industrial Turbomachinery, Lincoln, UK.

Introduction

Historically, transition models have been developed more specifically to predict the effects of heat transfer on a high pressure gas turbine blade, in order to more effectively manage the longevity of the blade. In the last decade, attention has been turned to low pressure turbine blades in order to reduce engine weight [Howell, 1999], and more recently, transition models are also used for transition prediction on compressor blading to reduce production costs and weight through the use of wake effects upon the transitional boundary layer to reduce the blade count [Ottavy et al, 2004]. However, the flow regime around an axial compressor blade is inherently different from that of an axial turbine blade. Transition models do not generally perform as well when employed for compressor simulations as they do when used in turbines.

Key to producing higher lift blading and reducing blade count, is the process of wake-induced transition. Wake impingement and subsequent laminar calmed regions reduce the establishment of a separation bubble on the suction surface and reduces loss. Suppression of laminar or transitional separation bubbles on high lift aerofoils is essential in this exercise.

RANS based transition models are reliant on considerable empiricism as denoted by the fact that they make use of only a few variables to describe the transition process. This fact ensures that most RANS based transition models work well for only a selected number of cases. Most importantly, unsteady flow phenomena such as transition due to wakes, the induced calming effect behind the wakes, the subsequent suppression of a separation bubble and the negative jet effect have yet to be modelled accurately.

The transition model, (γ - θ model) developed by Menter et al [Menter et al, 2004] has been somewhat successful in the prediction of steady state axial turbine and compressor flows [Menter et al, 2005]. The work described here attempts to demonstrate the current capabilities of the ANSYS-CFX commercial code to simulate the unsteady transitional boundary layer affected by impinging wakes, using the Menter γ - θ transition model. The 1.5 stage axial compressor rig at the University of Tasmania will be used as a test case.

Experimental Data

Experimental data from the compressor rig at the University of Tasmania in Hobart, Australia was used to assess the application of the γ - θ model to an unsteady axial compressor boundary layer. The machine is a 1.5 stage low speed axial compressor with an rpm \approx 500, traditionally used to understand the unsteady effects on the de-

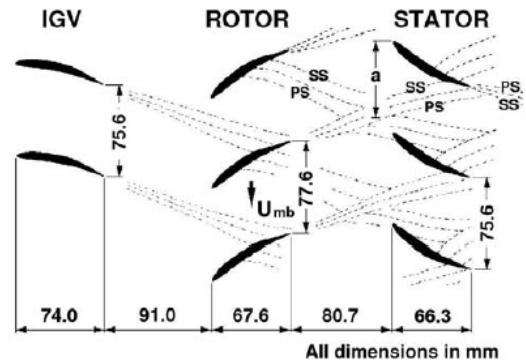


Figure 1: Cross section of University of Tasmania's low speed compressor at mid-span (Reproduced from Henderson et al 2006).

Loading	ϕ (V_a/U_{mb})	i°	Re_c	$Tu_s\%$
Medium	0.675	1.2	117,000	2.27

Table 1: Experimental conditions for the medium loading condition used for the analysis.

velopment of the flow on the stator at mid-span [Walker et al, 1999, Solomon & Walker, 2000, Henderson et al, 2005, Henderson 2006]. The layout is shown in Figure 1. Further details along with the data used for this work can be found in [Walker et al, 1999].

The data obtained was originally used to understand the effect of clocking on wake induced transition for three loading conditions. The experimental data used for comparison was for the medium loading, $a/S = 0$ clocking case (see Figure 1), where the IGV wake impinges on the leading edge of the stator blade. The machine operating conditions at the stator mid-span for the medium loading condition are shown in Table 1.

A quasi-2D slice at mid-span was used to approximate the stator geometry. The inlet was on the same plane at which the hot wire data was acquired. The O-grid contained 70 nodes with a maximum $y^+ < 1$, and 512 nodes distributed around the blade surface. 170 nodes were placed in the circumferential direction. The total size of the grid contained 232,200 nodes.

The experimental hot wire data at 55.7% chord upstream of the stator leading edge for the medium loading case is shown in Figure 2. The shaded-contour chart represents the time-varying data against rotor pitch. The data on the left of the figure represents the hot wire measurements at t^* for the normalised velocity (\bar{u}/u_s), random disturbance level (Tu) and the total disturbance

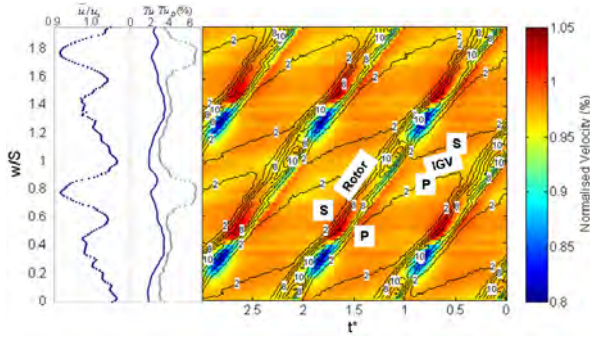


Figure 2: Normalised inflow velocity and turbulence at 55.7% chord axial distance upstream of stator leading edge. Shaded regions represent normalised velocity. Line contours represent turbulence intensity (%). Suction and pressure sides of the rotor and IGV wakes are labelled.

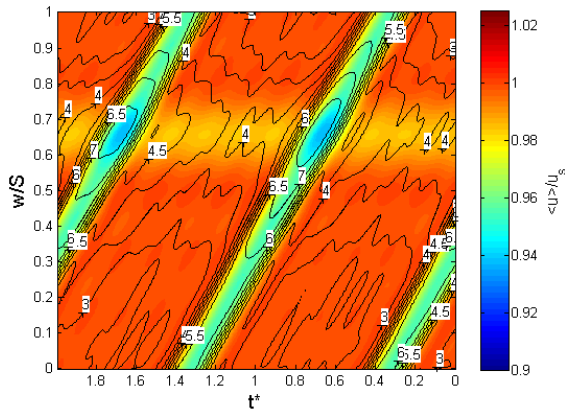


Figure 3: Normalised inflow velocity and turbulence the domain inlet. Shaded regions represent normalised velocity. Line contours represent turbulence intensity (%). Turbulence intensity contours are labelled.

level (Tu_D).

In the simulation, the IGV and rotor wakes were represented at the inlet by four separate Fourier series inputs. One for velocity and one for turbulence intensity, for both wakes. During the velocity defect in the wakes, the flow angle varied to create the negative jet effect.

Results

Figure 3 shows all the essential effects of the upstream wakes are present in the simulations. The IGV velocity defect is clearly visible as the band of horizontal lighter shading. The velocity deficit is reduced further when the IGV and rotor wakes meet. Within it, the maximum value of turbulence intensity rises to approximately 5.5%. Similar to experimental results, there is a reduction in the magnitude of the velocity defect just after the pressure surface side of the IGV wake within the rotor wake. Fluctuations of higher velocity seen in Figure 2 are observed either side of the rotor wake found at $w/S = 0$.

The experimental hot film data showing both the intermittency and the probability of relaxing flow for the medium loading case is shown in Figure 4. The probability of relaxing flow is a measure of the calming influence of the passing of turbulent spots in the flow. The figure shows the effect of the wakes on the development of

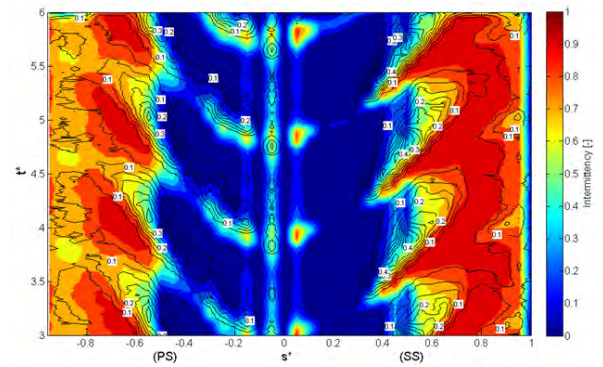


Figure 4: Experimental intermittency (shaded) and relaxing flow on blade surface for medium loading case.

the boundary layer on both the pressure (PS) and (SS) suction surfaces. Values of 1 represent a fully developed turbulent boundary layer and values of 0, a purely laminar boundary layer. On both surfaces, the effects of the impinging wakes are clearly visible. On the suction surface, the wakes are shown to bring the start of transition upstream to approximately $s^* = 0.25$. The transition process is complete by approximately $s^* = 0.5$. Between the wakes, the transition region occurs between approximately $s^* = 0.5$ and $s^* = 0.75$. The calmed region between the wakes can be seen as the lighter shading (values between 0.5-0.7) with the relaxing flow contours overlaid. The pressure surface shows that transition is only fully completed in the wake path.

A comparison of Figure 4 and Figure 5 finds similar patterns for the unsteady flow on the suction surface. In Figure 5, the local skin friction and transitional intermittency are shown. The effect of the wake is to cause the transition start point to move further upstream, thus reducing the local skin friction. Within the wake, transition is complete by approximately $s^* = 0.6$. The region of high skin friction between $s^* = 0.5$ & 0.7 indicates that a turbulent boundary layer is present. Separation occurs after $s^* = 0.8$ where the region of high turbulence meets the t^* axis. The regions of a potential separation bubble are shown by the darker shading $s^* \approx 0.5$. As transition occurs earlier in the wake path, the flow towards the trailing edge tends to separate further upstream, as shown by the lighter areas in the suction surface at $s^* > 0.8$. Between the wakes, separation occurs further downstream. However, the wake affects the boundary layer such that terminal separation only occurs a significant distance towards the trailing edge in comparison to separation in the wake path for at least $t^* = 0.2$ after the wake has passed. On the pressure surface, the same pattern as given by the measurements is not repeated by the CFD. This was the case for all of the variations of boundary conditions used in this study. In fact for all boundary condition variants, in contradiction to the experimental data, transition is still not complete at the trailing edge.

The stagnation pressure loss was compared with the profile loss given for a steady state simulation. The stagnation pressure loss coefficient (Y_p) is given by;

$$Y_p \approx \frac{2(\theta_{ss} + \theta_{ps}) u_{exit}^2}{p \cos \alpha_{exit} u_{inlet}^2} \quad (1)$$

The unsteady pressure loss, $Y_p = 6.68\%$ as compared to the steady state pressure loss of $Y_p = 6.52\%$, gives only a 2.3% increase in loss for the unsteady calculations. This may appear only a small amount at first, but

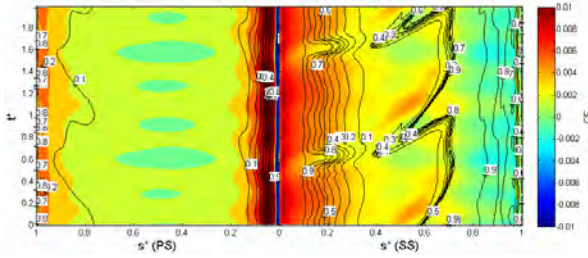


Figure 5: *Local skin friction (shading) and intermittency on the blade surface as predicted by the γ - θ model.*

this can be explained when considering the point of suction surface terminal separation between the steady state case. The steady state suction surface separation point is approximately $s^* = 0.76$, whereas for the unsteady simulation, the earliest separation occurs is approximately $s^* = 0.8$.

Conclusions

The simulations proved that the γ - θ model and the ANSYS-CFX code can simulate the main effects of unsteady wake-induced transition and its subsequent effects on the boundary layer. The model appeared to give a good qualitative comparison to the experimental data for the 2D medium loading cases. A calmed region was present in the results, which continued to suppress separation and transition for a period of wake passing. The use of multiple Fourier series to describe the flow worked well. However, more detailed information on wake structure and wake mixing behaviour is required. The negative jet created by the wake defect is essential in the prediction of wake-induced transition.

Whilst the γ - θ model gave a good prediction of the unsteady suction surface boundary layer, the simulations showed the streamwise position of the transition region on the pressure surface was poorly predicted. Experimental data shows that transition is complete within the wake path, and that $\gamma = 0.7$ toward the trailing edge between wakes. The simulations showed transition to not be complete at any stage on the pressure surface, and only a small variation in the completion of the transition region within the wake path. It is thought that this is due to the model not fully accounting for the effects of the impinging positive jet process on pressure surface.

From the work carried out, the following improvements are suggested; freestream length scale is required as it can significantly alter within the wake, which affects the rate of transition within the wake-induced path, the effect of pressure fluctuations within the wake-induced transition process [Wheeler et al. 2007].

Acknowledgements

The author would like to thank Greg Walker and Alan Henderson from the University of Tasmania for supplying and allowing the use of the experimental data. Financial support was kindly provided by Roger Wells from Siemens Industrial Turbomachinery (Lincoln, UK). Thanks also to Mark Savill and Joao Teixeira for their support and guidance during the project.

References

- Henderson, A., Walker, G., and Hughes, J. (2005). The influence of turbulence on wake dispersion and blade row interaction in an axial compressor. In ASME Turbo Expo 2005: Power for Land, Sea and Air, Reno-Tahoe, Nevada, USA. ASME. GT2005-68432.
- Henderson, A., Walker, G., and Hughes, J. (2006). Unsteady transition phenomena at a compressor blade leading edge. In Proceedings of GT2006, ASME Turbo Expo 2006: Power for Land, Sea and Air, GT2006-90641, Barcelona, Spain.
- Howell, R. (1999). Wake - Separation Bubble Interactions in Low Reynolds Number Turbomachinery. PhD thesis, Whittle Laboratory, Cambridge University Engineering Department.
- Menter, F., Langtry, R., Likki, S. R., Suzen, Y. B., Huang, P. G., and Völker, S. (2004a). A correlation-based transition model using local variables part 1 model formulation. In Proceedings of ASME Turbo Expo 2004, Power for Land Sea and Air, Vienna, Austria. GT2004-53452.
- Menter, F., Langtry, R., Volker, S., and Huang, P. (2005). Transition modelling for general purpose codes. In ERCOFTAC International Symposium on Engineering Turbulence Modelling and Measurements - ETMM6.
- Ottavy, X., Vilmin, S., Hodson, H., and Gallimore, S. (2004). The effects of wake-passing unsteadiness over a highly loaded compressor-like flat plate. ASME Journal of Turbomachinery, 126(1):13-23.
- Solomon, W. and Walker, G. (2000). Incidence effects on wake-induced transition on an axial compressor blade. Journal of Propulsion and Power, 16(3):397-405.
- Walker, G., Hughes, J., and Solomon, W. (1999). Periodic transition on an axial compressor stator: Incidence and clocking effects: Part 1 - experimental data. ASME Journal of Turbomachinery, 121:398-407.
- Wheeler, A., Miller, R., and Hodson, H. (2007a). The effect of wake induced structures on compressor boundary-layers. Journal of Turbomachinery, 129:705-712.

AN INTERMITTENCY TRANSPORT MODEL FOR WAKE-INDUCED TRANSITION

E. Dick¹, S. Kubacki²

¹ *Department of Flow, Heat and Combustion Mechanics, Ghent University, Belgium.*

² *Institute of Aeronautics and Applied Mechanics, Warsaw University of Technology, Poland.*

1 Introduction

A well accepted approach to describe transition is based on the concept of intermittency, as introduced by Narasimha [1]. The intermittency factor is the fraction of time that the flow is turbulent during the transition phase. It is zero in laminar flow and unity in fully turbulent flow. In most models, the calculated intermittency factor is a multiplier factor of the eddy viscosity from a turbulence model. In some models, the intermittency factor is described algebraically, often using the formula by Narasimha or a similar evolution law. Algebraic prescription is simple to apply for steady flows. It becomes more involved for unsteady flows. It is therefore much more common to describe intermittency by one or two transport equations. Examples of intermittency transport models are the models of Suzen and Huang [2], Vicedo et al. [3] and Menter et al. [4]. Also the model of Lodefier and Dick [5], improved by Kubacki et al. [6], that we discuss here, belongs to this class.

2 The intermittency model

The transition model uses an equation for free-stream intermittency ζ and one for near-wall intermittency γ , combined with the SST turbulence model. The near-wall factor γ represents the fraction of time during which near-wall velocity fluctuations, caused by the transition process, have a turbulent character. This intermittency factor tends to zero in the free stream. The free-stream factor ζ expresses the intermittent behaviour of the turbulent eddies, coming from the free stream, impacting onto the boundary layer. Near the wall, the eddies are dampened and the free-stream factor goes to zero. The free-stream factor is unity in the free stream. The turbulence weighting factor τ is the sum of the two factors and is the multiplication factor of the turbulent viscosity calculated by the turbulence model. Both intermittency factors are modelled by a convection-diffusion-source equation.

The reason for splitting the intermittency in two parts comes from the different time scales of the phenomena. In earlier work with the turbulence weighting factor by Steelant and Dick [7] and Lodefier et al. [8], this factor was described by a single convection-diffusion-source equation. This works well for steady flows. In unsteady flows, it becomes necessary to distinguish the impact phenomenon of the turbulence coming from the free stream on the pretransitional laminar boundary layer (free-stream factor) and the intermittency caused by the transition process in the interior of the boundary layer (near-wall intermittency factor). The propagation of the free-stream turbulence into the laminar boundary layer is mainly a diffusion process and is relatively slow. The

breakdown to turbulence of perturbation patterns inside the boundary layer may be a very rapid dynamic process. In steady flows, transition typically is rather gradual, certainly for transition in attached state. Wake-induced transition, however, typically is an extremely fast process.

Cho and Chung [9] investigated the intermittency at the interface of a turbulent jet and the surrounding laminar free stream. They developed a convection-diffusion equation to describe the intermittent submission of turbulent eddies coming from the jet disturbing the laminar free stream. Steelant and Dick [7] adapted this equation to describe the intermittency at the edge of a laminar boundary layer due to impacting free-stream turbulent eddies by extending it by a dissipation term. Steelant and Dick used the equation for conditionally averaged Navier-Stokes equations. The equation was modified somewhat and recalibrated by Pecnik et al. [10] for use with globally averaged Navier-Stokes equations. The final equation adopted by Lodefier and Dick [5] is

$$\frac{\partial(\rho\zeta)}{\partial t} + \frac{\partial(\rho U_i \zeta)}{\partial x_i} = -E_\zeta + \frac{\partial}{\partial x_i} \left[(\mu + \sigma_\zeta \mu_\zeta) \frac{\partial \zeta}{\partial x_i} \right], \quad (1)$$

$$E_\zeta = C_2 \mu_\zeta \frac{U}{U_\infty^2} \frac{\partial U}{\partial n} \frac{\partial \zeta}{\partial n}$$

The Prandtl number in the diffusion term is $\sigma_\zeta = 1.0$. The dissipation term E_ζ guarantees a zero normal variation of the free-stream factor near the wall. In combination with the wall boundary condition $\zeta = 0$, this leads to a zero free-stream factor throughout the major part of the boundary layer. The diffusion coefficient μ_ζ has been determined to create an inverse Klebanoff profile for the free-stream factor prior to transition:

$$\mu_\zeta = \mu C_1 T u^{-0.69} [-\ln(1 - \zeta)]^{-0.25(1-\zeta)} \quad (2)$$

The factors obtained in the calibration by Pecnik et al. [10] and used here are $C_1 = 3.5$, $C_2 = 15$.

The equation for near-wall intermittency is a convection-diffusion equation with a source term:

$$\frac{\partial(\rho\gamma)}{\partial t} + \frac{\partial(\rho U_i \gamma)}{\partial x_i} = P_\gamma + \frac{\partial}{\partial x_i} \left[(\mu + \sigma_\gamma \mu_t) \frac{\partial \gamma}{\partial x_i} \right] \quad (3)$$

$$P_\gamma = 2\beta_\gamma (1 - \gamma) \sqrt{-\ln(1 - \gamma)} \rho U_\gamma F_s \quad (4)$$

The Prandtl number in the diffusion term is $\sigma_\gamma = 1.0$. The role of the diffusion term is to allow a gradual variation of γ towards zero in the free stream. The boundary condition for γ at the wall is a zero normal derivative. The source term in the equation determines the transition onset location and the growth of the intermittency in the transition zone. The ingredients are a starting function F_s , a growth factor β_γ and a velocity scale U_γ .

Prior to transition, F_s is set to zero. The intermittency equation (3) then generates γ equal to zero. The source term (4) was made by Steelant and Dick [11] in such a way that for steady transition in an attached boundary layer, the Narashima law for intermittency is reproduced for $F_s = 1$, U_γ equal to the local velocity U and β_γ related to the spot growth rate with a correlation by Mayle [12].

For transition in separated state, the velocity scale U_γ is set to U_e , the velocity magnitude at the boundary layer edge. This modification was introduced by Lodefier and Dick [5], because the local velocity U inside a separation bubble is very low, so that the production term with local velocity becomes very small. The modification is essential for wake-induced transition because wake impact on a separation bubble causes an almost immediate breakdown of the free shear layer due to Kelvin-Helmholtz instability. This breakdown is a phenomenon at the edge of the boundary layer, which justifies the use of the edge velocity as velocity scale. With the modified term and the spot growth rate obtained from an empirical correlation by Mayle [12] for transition in separated state, the near-wall intermittency is forced to grow rapidly after wake impact. This corresponds to reality, as was shown by Lodefier and Dick [5].

3 Start and growth of transition

Transition in attached state is started with an empirical criterion by Mayle and Roberts [12] for steady bypass transition:

$$Re_\theta \geq Re_{\theta t} = 400 Tu^{-0.625} \quad (5)$$

Tu is the turbulence level in percent at the edge of the boundary layer. Re_θ is the Reynolds number based on momentum thickness θ , and edge velocity U_e . The starting function F_s in Eq. (4) is set to 1 as long as this criterion is satisfied. The same criterion is used for steady and unsteady transition. The argument for doing this is that the time scales of the unsteady mean flow are much larger than the time scales of the turbulence so that, with respect to modelling strategy, transition can be seen as a quasi-steady phenomenon.

The Abu-Ghannam and Shaw (AGS) correlation [13] is used together with the Mayle correlation for the prediction of the transition onset momentum thickness Reynolds number ($Re_{\theta t}$) for attached state transition. Both correlations are active together, so that the transition is initiated by whichever of the two criteria is satisfied first. The critical Reynolds number $Re_{\theta t}$ by the AGS-correlation is determined as a function of turbulence intensity Tu and the pressure gradient λ_θ :

$$Re_{\theta t} = 163 + \exp\left(f - \frac{f}{6.91} Tu\right) \quad (6)$$

where

$$f = \begin{cases} 6.91 + 12.75\lambda_\theta + 63.64\lambda_\theta^2 & \text{for } \lambda_\theta < 0 \\ 6.91 + 2.48\lambda_\theta - 12.28\lambda_\theta^2 & \text{for } \lambda_\theta \geq 0 \end{cases} \quad (7)$$

The pressure gradient parameter $\lambda_\theta = (\theta^2/\nu) dU/ds$ is determined at the edge of the boundary layer, where dU/ds is the acceleration along the streamwise direction.

The Mayle correlation (5) has been determined from experiments at free-stream turbulence levels higher than 1%. It is known that this criterion is less reliable for low free-stream turbulence levels, where it has the tendency

to generate too high values of $Re_{\theta t}$. The AGS-correlation has been determined taking into account experiments at very low levels of free-stream turbulence. This criterion is better suited for prediction of $Re_{\theta t}$ at low free-stream turbulence, both for natural transition and bypass transition. For wake-induced transition, typically, the Mayle criterion is active along the wake centre where turbulence intensities are high, while in between wakes the Abu-Ghannam and Shaw criterion is active.

A turbulent length scale correction is taken into account in the transition onset momentum thickness. The length scale correction proposed by Mayle [12] is used:

$$Tu = 1.93 Tu_e \sqrt[5]{\theta/L_t} \quad (8)$$

where Tu_e is the turbulence intensity and L_t is the turbulence length scale ($L_t = \sqrt{k}/0.09\omega$) at the edge of the boundary layer. The effective turbulence level (8) is implemented in both the Mayle and Abu-Ghannam and Shaw correlations.

For transition in separated state, other criteria are used [5, 6]. The criteria for transition in separated state and in attached state are used together. If one of the criteria is satisfied, F_s is set to one. So, for transition in separated state, a typical scenario is that after transition, the boundary layer reattaches and that then one of the criteria for attached transition takes over. If no criteria are satisfied anymore, F_s is set to zero and the flow is allowed to relaminarize. The production term in (4) then becomes zero and near-wall intermittency is convected out.

The procedure requires the definition of the free-stream turbulence intensity, Tu_e , and the calculation of the momentum thickness θ . So, the edge of the boundary layer has to be defined. This is done by determining the position on a normal to the wall where the magnitude of the rotation has decreased to 1% of its maximum value. For attached flow transition, the maximum value is at the wall. In separated flow regions, the maximum may be at some distance from the wall and there may be several local maxima. Then, the position is determined where the magnitude of the rotation has decreased to 1% of the value at the farthest maximum. The distance of the edge to the wall is defined as 130% of the distance of this position. The choice for the 1% criterion and the 30% distance augmentation is somewhat arbitrary, but the values are not critical [6]. It is essential that the edge position is far enough from the wall so that it senses a true free-stream turbulence intensity which is not influenced by turbulence produced in wall vicinity. As an approximation for a wall normal, a grid line is taken. When a starting criterion is satisfied, the starting function is activated on the wall normal from the wall to the edge of the boundary layer.

The growth parameter β_γ in the near-wall intermittency equation is related to the spot growth rate by $\beta_\gamma = \sqrt{\hat{g}\sigma} U_e/\nu$, where $\hat{g}\sigma$ is the nondimensional spot growth rate [5]. Empirical correlations by Mayle [12] express the parameters β_1 for growth in steady separated flow and β_2 for growth in steady attached flow:

$$\beta_1 = \sqrt{\frac{0.0000228}{Re_{\theta t}^{1.4}} \frac{U_e}{\nu}}, \quad \beta_2 = \sqrt{1.5 \cdot 10^{-11} Tu^{7/4} f_K \frac{U_e}{\nu}} \quad (9)$$

with

$$f_K = \begin{cases} 10^{-3227K^{0.5985}} & \text{for } K > 0 \\ (474Tu^{-2.9})^{(1-\exp(2 \cdot 10^6 K))} & \text{for } K < 0 \end{cases} \quad (10)$$

where

$$K = \frac{\nu}{U_e^2} \frac{dU_e}{dx} \quad (11)$$

with Tu the local free-stream turbulence intensity, U_e the local free-stream velocity, all defined at the boundary layer edge, K the local acceleration parameter and $Re_{\theta t}$ the momentum thickness Reynolds number at transition onset. Spot growth formulae for steady flow are also used for wake-induced transition. But, for wake-induced transition, the growth rate is always taken to be β_1 , so the value for separated flow, in the beginning of transition, even if the transition is in attached state [6]. Remark that β_1 is much higher than β_2 . Without this modification, as in the earlier version of the model [5], the start of wake-induced transition in attached boundary layer state has a large delay. The experimental observation is that transition starts almost immediately after the impact of the wake. It was found by Kubacki et al. [6] that the delay can be much reduced by replacing the growth factor β_2 for transition in attached state by the value β_1 for transition in separated state during the beginning of the transition process. This observation suggests similarity at the start of transition between wake-induced bypass transition in attached state and wake-induced transition in separated state. This similarity was indeed observed by Wu et al. [14] in DNS simulations of wake-induced bypass transition on flat plates. They showed that the impacting wakes cause instantaneously backward jets located near the top of the boundary layer. They associated these backward jets with a Kelvin-Helmholtz type inflectional instability that interacts with the free-stream eddies. This observation is a justification to use the growth rate for transition in separated state β_1 in the beginning of wake-induced transition in attached state. To model the more rapid growth of transition at the start of bypass transition, the β_γ parameter in the production term (4) is made dependent on the temporal gradient of the free-stream turbulent kinetic energy. The switch between fast (β_1) and quasi-steady (β_2) growth rates is realized by comparing the time scale based on the temporal gradient of the turbulent kinetic energy $T_{start} = k/(dk/dt)$ and the time scale determined by the turbulence model $T_{turb} = k/\varepsilon = 1/(\beta^*\omega)$. The β_γ term reads

$$\beta_\gamma = \begin{cases} \beta_1 & \text{for } T_{start} < T_{turb} \\ \beta_2 & \text{for } T_{start} > T_{turb} \end{cases} \quad (12)$$

The time scales T_{start} and T_{turb} are determined at the boundary layer edge.

The ω -equation of the SST model is unchanged for transition modelling. The time scale bound by Medic and Durbin [15] is introduced in the destruction term to improve behaviour in impact zones. The production term of the k -equation is slightly changed into

$$P_k = [\tau \mu_t + F_s(1 - \tau) 0.08\mu] S^2 \quad (13)$$

The destruction term of the k -equation is multiplied with the turbulence weighting factor τ . So, prior to transition, the turbulence model is active since τ is equal to ζ . The objective is to generate values of the turbulent quantities k and ω in the laminar boundary layer prior to transition that are small but non-zero. These small values are necessary to let start turbulent quantities at the beginning of transition. Also, the small molecular term, which is added to the production term in the k -equation, helps to let start the turbulent quantities, when the starting function is activated. The starting values are

obtained in a somewhat different way in the one-equation model version of Lodefier et al. [8] than in the later two-equation versions [5, 6]. Also in the one-equation version, the starting function F_s does not go immediately from zero to unity at onset of transition. However, the predictions for steady flow transition in attached state on flat plates are for the two-equation versions almost the same as with the one-equation version as shown on figure 5 of Lodefier et al. [8]. In principle, for steady cascade flows with transition in attached state, all versions of the model are equivalent.

4 Numerical code

The intermittency transport model is coupled with the FLUENT Navier-Stokes solver. Via User Defined Transport Equations (UDF) the two turbulence equations and the two intermittency equations are added to the Fluent solver. In FLUENT, the governing equations are discretised in space with the cell based finite volume scheme. The time integration is a second order backward scheme for convection, integrated with a dual time stepping technique. Pressure correction is used to satisfy the continuity equation. The method is second order in space and time.

5 Predictive qualities of the model

We illustrate the performance of the model for wake-induced transition in attached state in the cascade with the N3-60 profile, as measured by Zarzycki and Elsner [16]. The profile N3-60 is the stator vane of the high-pressure part of a steam turbine. Wakes are generated by a rotating bar system. The exit velocity is $U_1 = 30\text{m/s}$, which gives an exit Reynolds number of 6×10^5 . The free-stream turbulence intensity Tu is generated by a grid upstream of the bars. Data are available for $Tu = 0.4\%$ and $Tu = 3\%$, for flows without bars and for bar diameters 4mm and 6 mm. We use here the data for bar diameter 6 mm with inflow turbulence level $Tu = 3\%$. Results for wake-induced transition in separated state with an earlier version of the model can be found in [5]. For separated state transition, the newer version [6] and the older version [5] should be equivalent. Results for wake-induced transition for $Tu = 0.4\%$ and bar diameter 4 mm are given in [6].

First, the cascade was simulated for steady flow. At inlet to the computational domain, far from the cascade, a uniform flow was imposed. In the experiments, the oncoming flow is in the axial direction, but the inlet angle had to be set to 5° in order to get good comparison with the experimental time-averaged pressure distribution for bar diameter 6 mm. The difference in the inlet flow angle is due momentum from the bars and airflow leakage through the slots located upstream of the blade, where the moving bars system is mounted. For the unsteady flow calculations, the computational inlet section is taken downstream of the bars and the effect of the moving bars is superimposed on the flow distribution obtained from the steady calculation. The bar pitch has been increased to be equal to the blade pitch, but the bar velocity has been adjusted, so that the frequency of the impacting wakes is unchanged. Per pitch-wise traverse, 800 time steps are used. This high accuracy is chosen to guarantee accurate simulation of the unsteady movement of the wake. Self-similar profiles for velocity and turbulent kinetic energy are imposed at the inlet according to

$$\begin{aligned}
U &= U_\infty - (U_\infty - U_{center}) \exp \left[-(\ln 2) \left(\frac{y}{y_{1/2}} \right)^2 \right], \\
k &= k_\infty + (k_{center} - k_\infty) \exp \left[-(\ln 2) \left(\frac{y}{y_{1/2}} \right)^2 \right]
\end{aligned} \tag{14}$$

In these expressions, y is the distance perpendicular to the wake with $y = 0$ the centre of the wake and $y_{1/2}$ is the position where the defect of the velocity attains half of its maximum value. The parameters in the expressions have been fitted to experimental data for wakes of stationary bars. The specific dissipation at the inlet is imposed by

$$\omega = \omega_\infty + C_\mu^{1/4} \frac{\sqrt{k}}{l_{mix}}, \quad l_{mix} = 0.18y_{1/2} \tag{15}$$

The background dissipation ω_∞ has been used to adjust the wake evolution to the experimental one for moving bars.

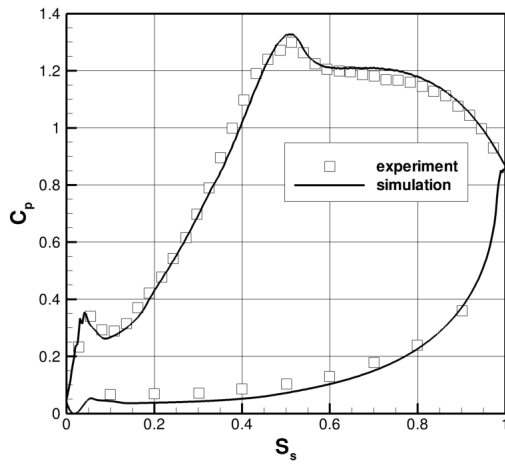


Figure 1: Pressure coefficient C_p distribution on the N3-60 profile. Time-averaged values for $d = 6$ mm and $Tu = 3\%$.

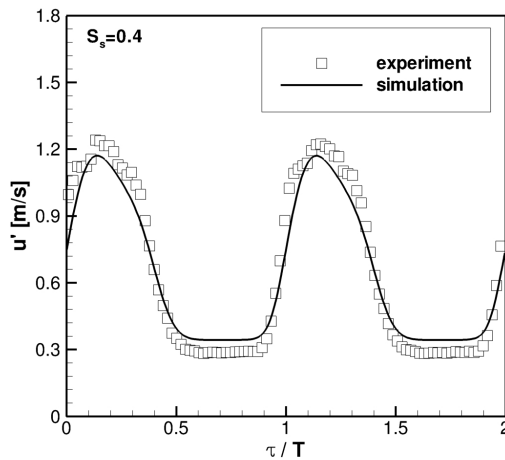


Figure 2: Time traces of fluctuating velocity component in streamwise direction at 10 mm from the suction surface of the blade at $S_s = 0.4$ for $d = 6$ mm and $Tu = 3\%$.

Figure 1 shows the comparison of the experimental and numerical time-averaged pressure coefficient C_p . Figure

2 shows the comparison between computed and measured profiles of the fluctuating velocity component parallel to the blade, $u' = \sqrt{2k/3}$, at distance 10 mm from the surface of the blade at relative position $S_s = 0.40$ on the suction surface, so well upstream of the transition area. The agreement between simulation and measurements is very good. Figures 1 and 2 demonstrate that the inflow conditions have been generated accurately [6].

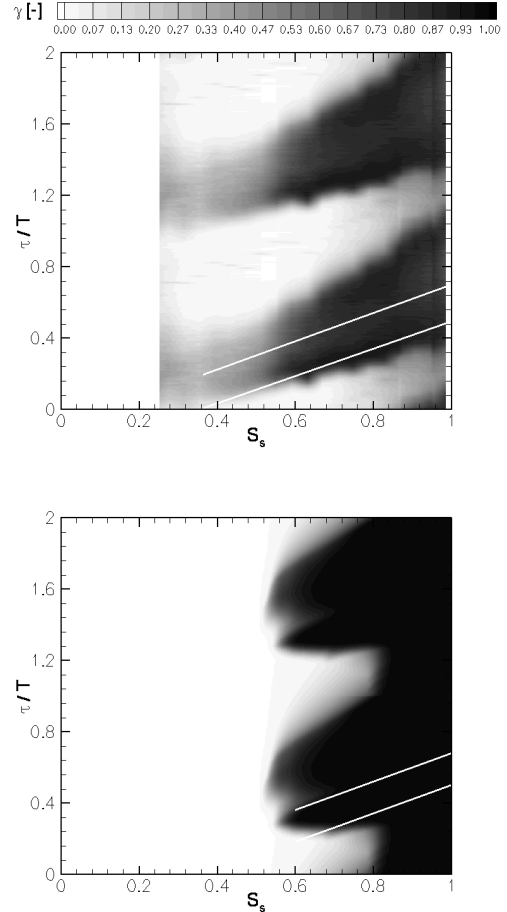


Figure 3: Space-time diagrams of near-wall intermittency. Top: experiment. Bottom: simulation.

Figure 3 shows the space-time distribution of the measured and computed intermittency. The intermittency is measured near the wall. The computational intermittency is the value at the wall. The two lines represent the maximum and minimum perturbation velocity at the edge of the boundary layer, so show the passing wake. The experimental data show that transition is initiated immediately after the wake impact and that the intermittency rapidly grows to unity. The activation position ($S_s \sim 0.55$ and $\tau/T \sim 0.3$) is correct in the simulation, but there is a slight delay in the growth of the intermittency at the front part of the transition. The relaminarization after the wake passage seems to be somewhat too late. Close to the trailing edge, there seems computationally no relaminarization, in contrast to the experiments. Remark that in the model nothing special is done to describe the relaminarization after wake passage and the calming effect associated with it (the enhanced resistance to transition). These effects should come spontaneously from the Navier-Stokes equations. We should also remark that an experimental intermittency is never exactly zero or exactly unity. The lowest and highest values are around 0.1 and 0.9. This should be taken into account in the comparison between experimental

and computational results. Another remark is that a numerical intermittency has as objective to bring the flow through transition or relaminarization and therefore, follows quite closely the evolution of the shape factor. Further, the intermittency has a profile across the boundary layer. Figure 3 shows only the wall value. So, one has to be careful in the comparison of physical and numerical intermittency and this comparison should be made together with the comparison of the shape factor, as we discuss hereafter.

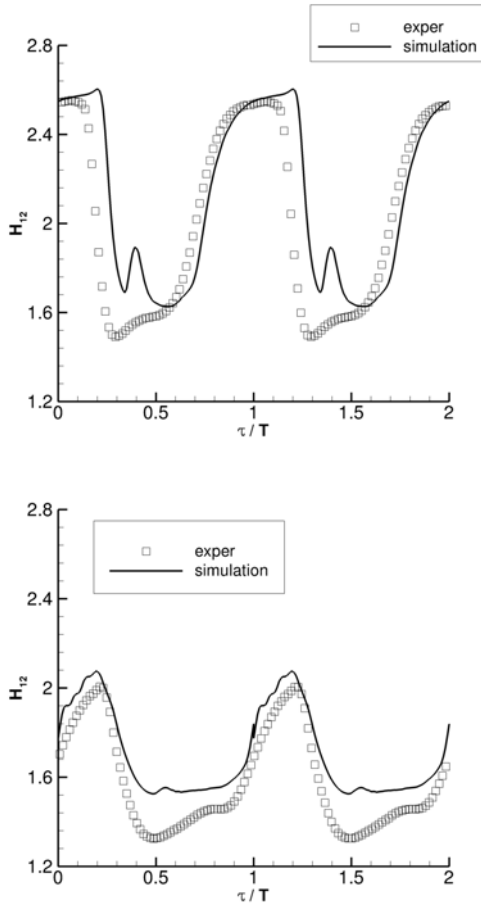


Figure 4: Time traces of shape factor at (top) $S_s = 0.65$, (bottom) $S_s = 0.85$.

Figure 4 shows experimental data and numerical results for the shape factor. The drop in shape factor coincides with the increase in intermittency. Good agreement is obtained between simulation and experiment under the wake impact. There is some delay in the start of transition at the first position ($S_s = 0.65$). The shape factor level near the trailing edge ($S_s = 0.85$) is somewhat too high under the wake impact ($\tau/T = 0.5 - 0.9$). An explanation for the delay at the front positions is that the RANS simulation does not contain the mechanism of velocity-pressure fluctuations that acts over a rather large distance between the impacting wake and the boundary layer [6]. Numerically, transition is only activated when the wake makes contact with the boundary layer edge. An explanation for the too low shape factor at the rear positions is the inability to reproduce in the 2D RANS simulation the interaction between the moving wakes generated by the rods and the wakes generated by the nearest blade [6]. As a consequence, the computed free-stream turbulence level is somewhat too low in the rear part of the blade. This reduces the growth rate β_γ , in Eq. (4) under the wake impact, so that the shape factor does not reach fully turbulent values near

the trailing edge (Fig. 4, bottom). The relaminarization in between the wakes is correctly predicted in time and the shape factor level is correct. Remember that relaminarization is purely a relaxation effect coming from the Navier-Stokes equations and that nothing specific is done in the transition model equations. Overall, the correspondence between calculation and experiment for shape factor (Fig. 4) is quite good and is much better than for intermittency (Fig. 3).

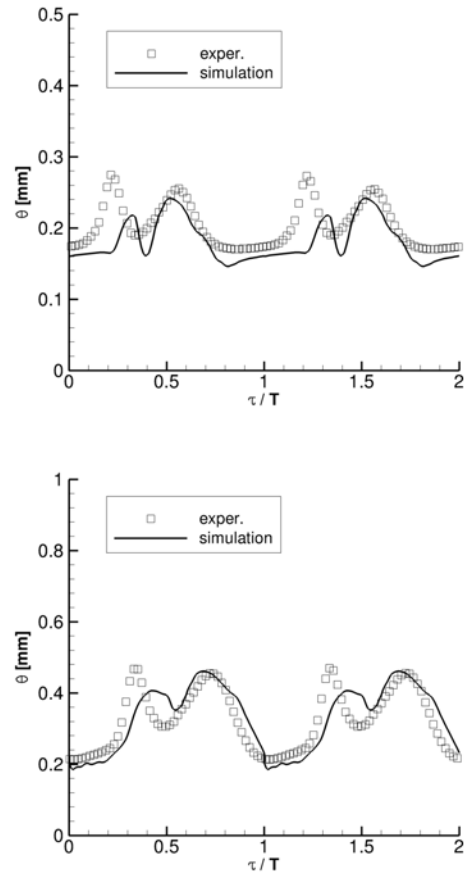


Figure 5: Time traces of momentum thickness at (top) $S_s = 0.65$, (bottom) $S_s = 0.85$.

The time traces of the momentum thickness are compared to the experiments in Figure 5. The thickening of the boundary layer under the beginning of the wake impact ($\tau/T \sim 0.2$ and $\tau/T \sim 0.3$) is simulated somewhat too late and too weak. The explanation might be the same as for the delay in the shape factor. The second peak in the wedge of the turbulent boundary layer ($\tau/T \sim 0.5$ and $\tau/T \sim 0.7$) is well reproduced. The appearance of two peaks comes from the acceleration followed by the deceleration due to the passing wake. The momentum thickness in between wakes is correctly predicted.

6 Conclusion

The capabilities of an intermittency transport model were presented for simulation of the wake-induced transition in attached state on the suction side of the N3-60 profile. Clearly, a prerequisite for accurate simulation is the generation of realistic inflow conditions. It was demonstrated that a fast intermittency growth rate should be applied in the initial stage of the wake impact in order to express the Kelvin-Helmholtz type instability

of the boundary layer. Further, the benefit was demonstrated of combining the Mayle correlation, suitable for high free-stream turbulence under the wakes, with the Abu-Ghannam and Shaw correlation, suitable for low free-stream turbulence in between wakes, and applying a length scale correction to both bypass starting criteria.

References

- [1] Narasimha R.: On the distribution of intermittency in the transition region of a boundary layer. *J. Aero. Sci.* 24, 711-712 (1957).
- [2] Suzen Y.B. and Huang P.G.: Numerical simulation of unsteady wake/blade interactions in low-pressure turbine flows using an intermittency transport equation. *J. of Turbomachinery* 127, 431-444 (2005).
- [3] Vicedo J., Vilmin S., Dawes W.N. and Savill A.M.: Intermittency transport modelling of separated flow transition. *J. of Turbomachinery* 126, 424-431 (2004).
- [4] Menter F.R., Langtry R., Likki S.R., Suzen Y.B., Huang P.G. and Völker S.: A correlation-based transition model using local variables. Part 1: model formulation, Part 2: test cases and industrial applications. *J. of Turbomachinery* 128, 413-434 (2006).
- [5] Lodefier K. and Dick E.: Modelling of unsteady transition in low-pressure turbine blade flows with two dynamic intermittency equations. *Flow, Turbulence and Combustion* 76, 103-132 (2006).
- [6] Kubacki S., Lodefier K., Zarzycki R., Elsner W. and Dick E.: Further development of a dynamic intermittency model for wake-induced transition. *Flow, Turbulence and Combustion*, to appear (2009).
- [7] Steelant J. and Dick E.: Modelling of laminar-turbulent transition for high free-stream turbulence. *J. Fluids Eng.* 123, 22-30 (2001).
- [8] Lodefier K., Merci B., De Langhe Ch. and Dick E.: Intermittency based RANS bypass transition modelling. *Progress in Computational Fluid Dynamics* 6, 68- 78 (2006).
- [9] Cho R. and Chung M. K.: A $k-\epsilon-\gamma$ equation turbulence model. *J. Fluid Mech.* 237, 301-322 (1992).
- [10] Pecnik R., Sanz W., Geher A., and Woisetschläger J.: Transition modelling using two different intermittency transport equations. *Flow, Turbulence and Combustion* 70, 299-323 (2003).
- [11] Steelant J. and Dick E.: Modelling of bypass transition with conditioned Navier-Stokes equations coupled to an intermittency transport equation. *Int. J. Num. Methods in Fluids* 23, 193-220 (1996).
- [12] Mayle R. E.: The role of laminar-turbulent transition in gas turbine engines. *J. of Turbomachinery* 113, 509-537 (1991).
- [13] Abu-Ghannam B.J. and Shaw R.: Natural transition of boundary layers - the effects of turbulence, pressure gradient, and flow history. *J. Mech. Eng. Science* 22, 213-228 (1980).
- [14] Wu X., Jacobs R.G., Hunt J.C.R. and Durbin P.A.: Simulation of boundary layer transition induced by periodically passing wakes. *J. Fluid Mech.* 398, 109-153 (1999).
- [15] Medic G. and Durbin P.A.: Toward improved prediction of heat transfer on turbine blades. *J. of Turbomachinery* 124, 187-192 (2002).
- [16] Zarzycki R. and Elsner W.: The effect of wake parameters on the transitional boundary layer on a turbine blade. *IMEchE Part A, J. Power and Energy* 219, 471-480 (2005).

PHYSICAL INTERPRETATION OF TRANSITION-SENSITIVE RANS MODELS EMPLOYING THE LAMINAR KINETIC ENERGY CONCEPT

Keith Walters

Mississippi State University, Department of Mechanical Engineering, USA.

Abstract

The laminar kinetic energy (LKE) concept has led to the recent development of RANS-based turbulence models intended to reproduce laminar, transitional and turbulent flows without the use of intermittency factors or empirical correlations. These models can be viewed as "physics-based" or "phenomenological", and have shown some promise for practical CFD computations of complex transitional flows. Several authors, including this one, have proposed different physical mechanisms and scaling laws for the production, transport, and destruction of laminar kinetic energy in the pretransitional boundary layer, as well as for the mechanisms governing the transition process itself. This paper examines the physical interpretation of LKE modeling by comparison with the Reynolds stress transport equations, and poses an argument for a new form of the terms governing pretransitional and transitional behavior in the models. A recently documented eddy-viscosity model incorporating these concepts is presented, and selected results are shown to highlight the performance of the model.

1 Introduction

Accurate and efficient numerical prediction of boundary layer transition is a daunting task. Since direct numerical simulations (DNS) and large-eddy simulations (LES) of complex flows are still beyond the reach of current and even next-generation compute systems, a number of "practical" approaches have been developed and adopted with some degree of success. With regard to computational fluid dynamics (CFD), "practical" often refers to the Reynolds-averaged Navier-Stokes (RANS) approach. Several RANS methods have been developed, including eddy-viscosity models that adopt modifications to allow prediction of transitional flows in addition to fully turbulent ones. These can be loosely classified as correlation-based models [1-3], physics-based (phenomenological) models [4-6], or hybrid approaches that incorporate aspects of both [7,8]. While none of these approaches has emerged as clearly superior, all have helped to enhance the CFD toolkit available to end users.

This paper focuses on the class of physics-based eddy-viscosity models first introduced by Walters and Leylek [6], which adopts the laminar kinetic energy concept proposed by Mayle and Schulz [9] to develop modified $k - \omega$ [6] and $k - \omega$ [10,11] models capable of predicting transition with some degree of accuracy, and requiring neither specialized user inputs nor calculation of non-local parameters. These models and subsequent modifications have been shown to perform reasonably well for a number of different transitional flow test cases [12-15].

Because the pretransitional boundary layer under a turbulent freestream is known to contain significant ve-

locity fluctuations - Klebanoff modes or "streaky structures" - the use of laminar kinetic energy is appealing. However, the dynamics of pretransitional fluctuation development is not completely understood, and the mechanisms responsible for breakdown of these fluctuations to classical turbulence even less so. As such, the details of the laminar kinetic energy approach vary considerably among different model forms. For example, the original model developed by Mayle and Schulz [9] proposed that pressure diffusion was responsible for kinetic energy transfer from the freestream to the boundary layer, while the model of Walters and Leylek [6] employed a more traditional mean strain production mechanism. Likewise, different models have relied upon different scaling arguments to inhibit turbulent production in the pretransitional region and to induce transition initiation. These arguments have been (and continue to be) based on phenomenological understanding.

The objective of this paper is to examine the transitional boundary layer in terms of the Reynolds transport equations, and to present a theory for the appropriate scaling arguments to be used in the model terms governing laminar kinetic energy growth and breakdown to turbulence. This theoretical argument has not been previously documented, but it forms the basis of a recently published LKE-based eddy-viscosity turbulence model [15]. Key aspects of that model are discussed and results are presented for two representative transitional flow test cases.

2 Reynolds Stress Equations in the Transitional Boundary Layer

Reynolds averaging of the equations of motion is no less valid in the pretransitional and transitional regions than in the fully turbulent region. The exact form of the Reynolds stress transport equation for incompressible flow is:

$$\begin{aligned} \frac{D}{Dt} \overline{u_i u_j} = & - \frac{(\overline{u_i u_k} S_{kj} + \overline{u_j u_k} S_{ki})}{\rho} \\ & + p \left(\frac{\partial u_i}{\partial x_j} + \frac{\partial u_j}{\partial x_i} \right) - 2\nu \frac{\partial u_i}{\partial x_k} \frac{\partial u_j}{\partial x_k} \\ & - \frac{\partial}{\partial x_k} \left[\overline{u_i u_j u_k} + (\overline{p u_i} \delta_{jk} + \overline{p u_j} \delta_{ik}) + \nu \frac{\partial \overline{u_i u_j}}{\partial x_k} \right] \end{aligned} \quad (1)$$

Uppercase denotes mean quantities, lowercase denotes fluctuating quantities, and the overbar denotes Reynolds averaging. All terms except convection, production, and viscous diffusion are unclosed. A number of models expressing these unclosed terms as functions of the mean flow and Reynolds stress tensor (and typically a scale-determining variable) have been developed for and successfully applied to fully turbulent flows. Experimental and numerical studies of the transitional boundary layer

clearly show that these "fully turbulent" model forms do not accurately represent the behavior in the pretransitional region. In theory, model forms for these terms could be developed that accurately describe transitional behavior.

The role of each term of Eq. (1) in fully turbulent flow is fairly well understood. Of particular interest are the production term, $-(\overline{u_i u_k} S_{kj} + \overline{u_j u_k} S_{ki})$, which transfers energy from the mean to the fluctuating flow, and the pressure strain term, $p \left(\frac{\partial u_i}{\partial x_j} + \frac{\partial u_j}{\partial x_i} \right)$, which serves to redistribute energy among the normal Reynolds stress components and modify the shear stress components. The effect of the pressure strain term is typically modeled as a "return to isotropy" in which high energy components transfer energy to lower energy components. Moreover, this term is expressed as the sum of a rapid part, which incorporates interactions between turbulent eddies and the mean velocity field, and a slow part that incorporates inter-eddy interactions.

In fully turbulent flow, the pathway leading to production of the Reynolds stress components can be summarized as: 1) transfer of energy from the mean flow to \overline{uu} via interaction of \overline{uv} with the mean strainrate; 2) transfer of energy from \overline{uu} to \overline{vv} and \overline{ww} due to the action of pressure strain; and 3) generation of \overline{uv} via interaction of \overline{vw} with the mean strainrate.

Large-eddy simulations presented by Voke and Yang [16] indicate that in the pretransitional region, step 2 does not occur. The effect of shear sheltering apparently acts to inhibit the normal, "turbulent" effect of the pressure strain term. Their results show evidence of a positive contribution of the pressure strain term to the \overline{uu} component very close to the wall, and this is presumably a wall reflection effect, which works to suppress rather than increase the wall-normal component \overline{vv} . This behavior is further evident in more recent DNS and LES simulations [17-19], all of which show that no peak in \overline{vv} or \overline{ww} occurs within the pretransitional region of the boundary layer. The Reynolds stress budgets are clearly dominated by the production and dissipation terms, with little action by the pressure strain except for near-wall reflection of the wall-normal fluctuations.

Assuming that the pressure strain terms are negligible leads to the following set of simplified equations in the pretransitional region:

$$\frac{D}{Dt} \overline{uu} \approx \overline{uv} \frac{\partial U}{\partial y} - \varepsilon_{11} + Transport \quad (2)$$

$$\frac{D}{Dt} \overline{uv} \approx \overline{vw} \frac{\partial U}{\partial y} - \varepsilon_{12} + Transport \quad (3)$$

$$\frac{D}{Dt} \overline{vv} \approx -\varepsilon_{22} + Transport \quad (4)$$

$$\frac{D}{Dt} \overline{ww} \approx -\varepsilon_{33} + Transport \quad (5)$$

A clear picture begins to emerge of the RANS-based description of fluctuation growth and transition. Freestream turbulence enters the boundary layer, either at the leading edge or through diffusive transport of low frequency modes farther downstream [19]. It is clearly only the wall-normal \overline{vv} component of this entrained turbulence that leads to the growth of Klebanoff modes, and in fact the dependence of pretransitional energy production on wall-normal freestream fluctuations is well established [16-24]. Significantly, the wall-normal and spanwise \overline{ww} Reynolds stress components do not exhibit appreciable growth in the pretransitional boundary layer.

In classical laminar boundary layer theory, the peak velocity gradient $\frac{\partial U}{\partial y}$ varies as $Re_x^{1/2}$. Given relatively small levels of dissipation, it is expected that the wall-normal Reynolds stress component \overline{vv} remains approximately constant in the streamwise direction. Further assuming negligible dissipation and diffusion of the shear stress \overline{uv} results in an approximate streamwise growth rate $\overline{uv} \sim Re_x^{1/2}$. Likewise the streamwise Reynolds stress component, in the absence of significant dissipation or diffusive transport, will exhibit a growth rate of $\overline{uu} \sim Re_x$. Such an approximately linear streamwise growth rate of pretransitional kinetic energy has been reported in previous experiments and simulations [cf. 25,26].

Finally, the transition process itself can be viewed as the "activation" of the pressure strain terms which tend to return the fluctuations toward isotropy, effectively leading to a rapid increase in the wall-normal and spanwise energy components. At the same time, the development of energetic three-dimensional fluctuations allows the development of the well known eddy scale range and energy cascade process characteristic of high-Re turbulence.

To summarize the above discussion, there seem to be several key physical mechanisms embodied in the RANS-based description of Reynolds stress dynamics for the transitional boundary layer. These include: 1) production of one-dimensional streamwise fluctuation energy in the pretransitional region by entrained freestream turbulence interacting with the mean strainrate; 2) no generation of three-dimensional (normal and spanwise) fluctuations in the pretransitional region, due to suppression of the pressure strain mechanism found in turbulent flow; 3) transition initiation due to an increase in magnitude of the pressure strain term, which can be viewed as a transfer of energy from the one-dimensional streamwise fluctuations to the three-dimensional fluctuations more indicative of fully turbulent flow.

3 Implications for LKE Modeling

The above picture of the transition process, as viewed from a RANS standpoint, can inform the development of transition-sensitive eddy-viscosity models. It is clear that what is typically referred to as laminar kinetic energy is simply the streamwise component of the Reynolds stress tensor, and that its production is due to stress-strain interactions. Likewise, the corresponding turbulent kinetic energy represents the energy contained in the three-dimensional fluctuations that have either been entrained from the freestream or generated through nonlinear interactions downstream of transition. The transition process itself is simply a transfer of energy from one to the other via the pressure strain terms. A remaining question for modeling purposes is "are there appropriate local dimensionless quantities that can be used to incorporate the above physics into eddy-viscosity models in a relatively simple fashion, and if so what are they?"

DNS simulations [17,19] have shown that the magnitude of the streamwise fluctuations in the pretransitional region is independent of the freestream forcing spectrum, but dependent on the freestream turbulence intensity. This is consistent with the view that freestream turbulence is entrained into the boundary layer and interacts with the mean flow through the production term. It is proposed here that the suppression of the pressure strain effect is due to the presence of short molecular diffusion time scales within the pretransitional region, relative to

the characteristic time scale of the rapid pressure strain terms. Potential fluctuations associated with energy redistribution are therefore quickly dissipated. The role of shear sheltering in this scenario is to reduce the effective wall-normal length scale of the entrained $\overline{v'v'}$ stress component, reducing the diffusion time scale and stabilizing the mechanisms responsible for intercomponent energy transfer.

In the pretransitional region, entrained turbulent fluctuations do not couple strongly with the freestream velocity gradient [19], instead acting as perturbations on the mean (approximately laminar) velocity profile. Locally, then, turbulent streamwise fluctuations can be expected to scale as:

$$u \sim l_v \frac{\partial U}{\partial y} \quad (6)$$

where l_v is a fluctuation length scale in the wall-normal direction. Alternatively,

$$l_v \sim u/\Omega \sim \sqrt{k_T}/\Omega \quad (7)$$

where Ω is the local mean vorticity magnitude. An estimate for the molecular diffusion time scale may therefore be constructed as:

$$\tau_d \sim l_v^2/\nu \sim \frac{k_T}{\nu\Omega^2} \quad (8)$$

The time scale associated with the rapid pressure strain mechanisms is taken to be proportional to the inverse of the vorticity magnitude:

$$\tau_r \sim 1/\Omega \quad (9)$$

The ratio of molecular diffusion to rapid pressure strain time scales may therefore be expressed as:

$$\frac{\tau_d}{\tau_r} \sim \frac{k_T}{\nu\Omega} \quad (10)$$

For the theory proposed here, Eq. (10) is the relevant local dimensionless quantity governing shear sheltering and transition initiation. When the ratio in Eq. (10) is small, pressure strain is suppressed and one-component fluctuations (i.e. laminar kinetic energy) are generated. When the ratio reaches a critical value, the rapid pressure strain term quickly increases in magnitude to generate three-dimensional turbulent fluctuations, and transition begins.

4 LKE Based Eddy-Viscosity Model

The three-equation eddy viscosity model presented in Walters and Cokljat [15] is based on the physical description of transition presented above. Key aspects of the model are given here. Readers are referred to [15] for the full set of model equations.

The model incorporates transport equations for turbulent kinetic energy k_T , laminar kinetic energy k_L , and specific dissipation rate ω :

$$\begin{aligned} \frac{Dk_T}{Dt} &= P_{k_T} + R_{BP} + R_{NAT} - \omega k_T - D_T \\ &+ \frac{\partial}{\partial x_j} \left[\left(\nu + \frac{\alpha_T}{\sigma_k} \right) \frac{\partial k_T}{\partial x_j} \right] \end{aligned} \quad (11)$$

$$\frac{Dk_L}{Dt} = P_{k_L} - R_{BP} - R_{NAT} - D_L + \frac{\partial}{\partial x_j} \left[\nu \frac{\partial k_L}{\partial x_j} \right] \quad (12)$$

$$\begin{aligned} \frac{D\omega}{Dt} &= C_{\omega 1} \frac{\omega}{k_T} + \left(\frac{C_{\omega R}}{f_W} - 1 \right) \frac{\omega}{k_T} (R_{BP} + R_{NAT}) - C_{\omega 2} \omega^2 \\ &+ C_{\omega 3} f_{\omega} \alpha_T f_W^2 \frac{\sqrt{k_T}}{y^3} + \frac{\partial}{\partial x_j} \left[\left(\nu + \frac{\alpha_T}{\sigma_{\omega}} \right) \frac{\partial \omega}{\partial x_j} \right] \end{aligned} \quad (13)$$

Per the above discussion, the laminar kinetic energy represents the one-component streamwise fluctuations that arise in the pretransitional region, while the turbulent kinetic energy represents the three-dimensional fluctuations indicative of fully turbulent flow. The shear sheltering effect that inhibits transfer of energy from streamwise to wall-normal (and spanwise) components is manifested through a damping function f_{SS} in the turbulent production term:

$$P_{k_T} = \nu_{T,s} S^2 \quad (14)$$

$$\nu_{T,s} = f_{\nu} f_{INT} C_{\mu} \sqrt{k_{T,s}} \lambda_{eff} \quad (15)$$

$$k_{T,s} = f_{SS} f_W k_T \quad (16)$$

$$f_{SS} = \exp \left[- \left(\frac{C_{SS} \nu \Omega}{k_T} \right)^2 \right] \quad (17)$$

The initiation of bypass transition is included through the term R_{BP} , which may be viewed as an analog to the pressure strain term that transfers energy from the streamwise to the other components of the Reynolds stress tensor. This term is also a function of the time-scale ratio expressed in Eq. (10), with transition initiating at a critical value $C_{BP,crit}$:

$$R_{BP} = C_R \beta_{BP} k_L \omega / f_W \quad (18)$$

$$\beta_{BP} = 1 - \exp \left(- \frac{\phi_{BP}}{A_{BP}} \right) \quad (19)$$

$$\phi_{BP} = \text{MAX} \left[\left(\frac{k_T}{\nu\Omega} - C_{BP,crit} \right), 0 \right] \quad (20)$$

5 Test Case Results

The eddy-viscosity model presented above has been applied to a number of test cases and has been shown to provide reasonably accurate transition prediction, relative to fully turbulent model forms and to previous incarnations of the laminar kinetic energy based model [6,10-11]. Selected results are presented below. Further details are available in [15].

Results from the zero pressure gradient T3 test cases of the ERCOFTAC database [28] are shown in Figures 1-5. Figures 1-3 show the wall distribution of skin friction coefficient. The fully laminar and fully turbulent distributions are shown in the plot for reference purposes. The new eddy viscosity model [15] shows good agreement with experimental data for all three values of the freestream turbulence intensity (FSTI), with the transition location moving upstream as FSTI is increased.

Figure 4 shows the predicted behavior of boundary layer mean velocity profiles upstream, during, and downstream of transition for the test case with 3% FSTI, at locations corresponding to $Re_x = 1 \times 10^5$, 2×10^5 , and 4×10^5 , respectively. Figure 5 is similar to Figure 4, but shows profiles of the total fluctuating kinetic energy ($k_L + k_T$) in different regions of the boundary layer. Agreement between experiments and computations is again quite good.

A considerably more complex test case is found in the S809 airfoil, which has been specifically designed for wind turbines operating under a varying range of freestream conditions. These include angle of attack, which can have a significant impact on the boundary layer behavior. Simulations were performed corresponding to experiments with a freestream Mach number of 0.15, Reynolds number based on chord length of 2×10^6 , and angle of attack varying from 0° to 15° [29].

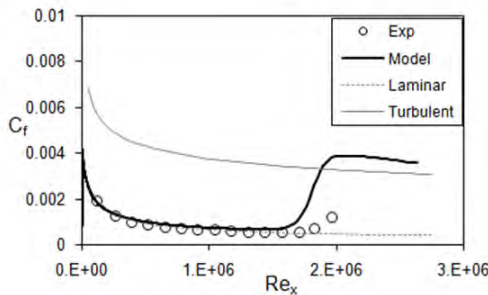


Figure 1: Streamwise distribution of skin friction coefficient for zero pressure boundary layer case T3A- (FSTI = 0.8%).

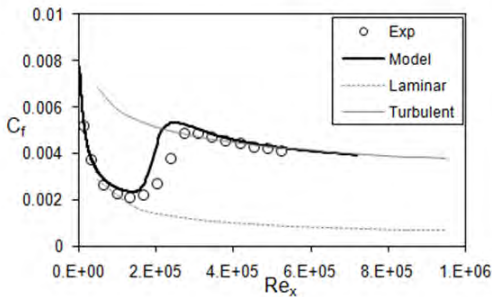


Figure 2: Streamwise distribution of skin friction coefficient for zero pressure boundary layer case T3A (FSTI = 3%).

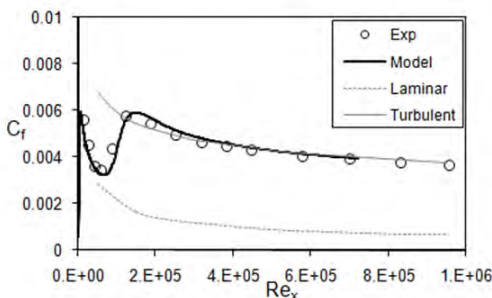


Figure 3: Streamwise distribution of skin friction coefficient for zero pressure boundary layer case T3B (FSTI = 6%).

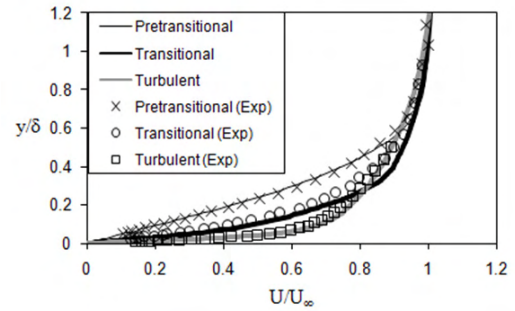


Figure 4: Mean velocity profiles in three regions of the boundary layer, comparison between experimental data [28] and LKE based eddy-viscosity model.

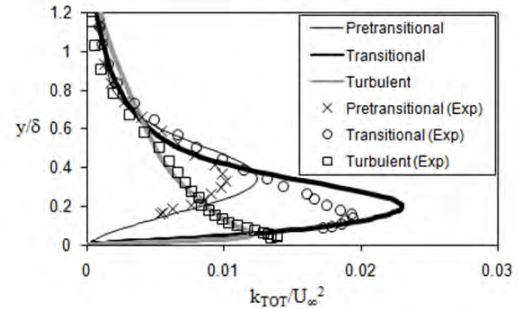


Figure 5: Boundary layer profiles of total fluctuating kinetic energy in three regions of the boundary layer, comparison between experimental data [28] and LKE based eddy-viscosity model.

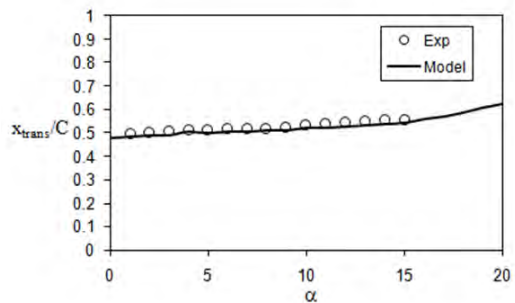


Figure 6: Transition location as a fraction of airfoil chord length versus angle of attack, on the pressure surface of the S809 airfoil.

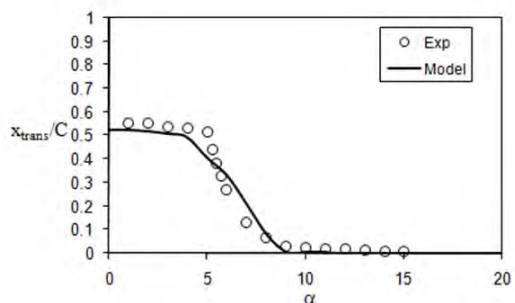


Figure 7: Transition location as a fraction of airfoil chord length versus angle of attack, on the suction surface of the S809 airfoil.

Figures 6 and 7 show the predicted versus measured transition location on both the pressure and suction surfaces, as a function of angle of attack α . On the pressure surface, the transition location moves slowly and

steadily downstream as α is increased, but remains close to one-half chord for all α up to 15° . More interesting behavior is observed on the suction surface, with transition initially at approximately one-half chord, but moving rapidly upstream towards the leading edge over the range $5^\circ < \alpha < 9^\circ$, and remaining there as α continues to increase. The LKE based model is able to reproduce this behavior, and overall shows good agreement with the measured data.

6 Conclusion

The physics of turbulence suppression in the pretransitional boundary layer and subsequent transition to turbulence has been examined from a strictly RANS-based perspective, with the goal of providing insight for transitional eddy-viscosity model development using the laminar kinetic energy (LKE) concept. It is proposed that the key feature of the pretransitional region is the inhibition of the pressure strain terms, which in fully turbulent boundary layers tend to generate strong wall-normal (as well as spanwise) fluctuations and sustain the turbulence production pathway. Likewise, transition itself is viewed as the "activation" of these pressure strain terms. In terms of LKE modeling, transition is represented as a transfer of energy from the single component streamwise fluctuations (laminar kinetic energy) to strongly three-dimensional fluctuations (turbulent kinetic energy) by the pressure strain. A new scaling theory has also been proposed in which the relevant dimensionless quantity governing these processes is a time-scale ratio, represented in the model as $k_T/\nu\Omega$. Results obtained with a recently documented model incorporating this time-scale ratio show good agreement with experimental data for the test cases presented.

References

[1] Suzen, Y.B., and Huang, P.G., 2000, "Modeling of Flow Transition Using an Intermittency Transport Equation," ASME Journal of Fluids Engineering, 122, 273-284.

[2] Steelant, J., and Dick, E., 2001, "Modeling of Laminar-Turbulent Transition for High Freestream Turbulence," ASME Journal of Fluids Engineering, 123, 22-30.

[3] Menter, F.R., Langtry, R.B., Likki, S.R., Suzen, Y.B., Huang, P.G., and Volker, S., 2006, "A Correlation-Based Transition Model Using Local Variables - Part I: Model Formulation," ASME Journal of Turbomachinery, 128, 413-422.

[4] Edwards, J.R., Roy, C.J., Blottner, F.G., and Hassan, H.G., 2001, "Development of a One-Equation Transition/Turbulence Model," AIAA Journal, 39, 1691-1698.

[5] Wang, C. and Perot, B., 2002, "Prediction of Turbulent Transition in Boundary Layers Using the Turbulent Potential Model," Journal of Turbulence, 3.

[6] Walters, D.K. and Leylek, J.H., 2004, "A New Model for Boundary Layer Transition Using a Single-Point RANS Approach," ASME Journal of Turbomachinery, 126, 193-202.

[7] Lardeau, S., Leschziner, M., and Li, N., 2004, "Modelling Bypass Transition With Low-Reynolds-Number Non-Linear Eddy-Viscosity Closure," Flow, Turbulence, and Combustion, 73, 49-76.

[8] Lardeau, S., and Leschziner, M., 2006, "Unsteady RANS Modeling of Wake-Induced Transition in Linear LP-Turbine Cascades," AIAA Journal, 44, 1845-1865.

[9] Mayle, R.E. and Schulz, A., 1997, "The Path to Predicting Bypass Transition," ASME Journal of Turbomachinery, 119, 405-411.

[10] Holloway, D.S., Walters, D.K. and Leylek, J.H., 2004, "Prediction of Unsteady, Separated Boundary Layer Over a Blunt Body for Laminar, Turbulent, and Transitional Flow," International Journal for Numerical Methods in Fluids, 45, 1291-1315.

[11] Walters, D.K. and Leylek, J.H., 2005, "A CFD Study of Wake-Induced Transition on a Compressor-Like Flat Plate," ASME Journal of Turbomachinery, 127, 52-63.

[12] Cutrone, L., De Palma, P., Pascazio, G., Napolitano, M., 2007, "An Evaluation of Bypass Transition Models for Turbomachinery Flows," International Journal of Heat and Fluid Flow, 28, 161-177.

[13] Cutrone, L., De Palma, P., Pascazio, G., Napolitano, M., 2008, "Predicting Transition in Two- and Three-Dimensional Separated Flows," International Journal of Heat and Fluid Flow, 29, 504-526.

[14] Vlahostergios, Z., Yakinthos, K., Goulas, A., "Separation-Induced Boundary Layer Transition: Modeling With a Non-Linear Eddy-Viscosity Model Coupled with the Laminar Kinetic Energy Equation," International Journal of Heat and Fluid Flow, In Press (available online).

[15] Walters, D.K. and Cokljat, D., 2008, "A Three-Equation Eddy-Viscosity Model for Reynolds-Averaged Navier-Stokes Simulations of Transitional Flow," ASME Journal of Fluids Engineering, 130, 121401.

[16] Voke, P.R. and Yang, Z., 1995, "Numerical Study of Bypass Transition," Physics of Fluids, 7, 2256-2264.

[17] Jacobs, R.G. and Durbin, P.A., 2001, "Simulations of Bypass Transition," Journal of Fluid Mechanics, 428, 185-212.

[18] Brandt, L., Schlatter, P. and Henningson, D.S., 2004, "Transition in Boundary Layers Subject to Free-Stream Turbulence," Journal of Fluid Mechanics, 517, 167-198.

[19] Zaki, T.A. and Durbin, P.A., 2005, "Mode Interaction and the Bypass Route to Transition. Journal of Fluid Mechanics, 531, 85-111.

[20] Andersson, P., Brandt, L., Bottaro, A. and Henningson, D.S., 2001, "On the Breakdown of Boundary Layer Streaks," Journal of Fluid Mechanics, 428, 29-60.

[21] Brandt, L., Schlatter, P. and Henningson, D.S., 2004, "Transition in Boundary Layers Subject to Free-Stream Turbulence," Journal of Fluid Mechanics, 517, 167-198.

[22] Lardeau, S., Li, N. and Leschziner, M.A., 2007, "Large Eddy Simulation of Transitional Boundary Layers at High Free-Stream Turbulence Intensity and Implications for RANS Modeling," ASME Journal of Turbomachinery, 129, 311-317.

[23] Volino, R.J. and Simon, T.W., 1997, "Boundary Layer Transition Under High Free-Stream Turbulence and Strong Acceleration Conditions: Part 2 – Turbulent Transport Results," ASME Journal of Heat Transfer, 119, 427-432.

[24] Leib, S.J., Wundrow, D.W. and Goldstein, M.E., 1999, "Effect of Free-Stream Turbulence and Other Vortical Disturbances on a Laminar Boundary Layer," Journal of Fluid Mechanics, 380, 169-203.

[25] Matsubara, M. and Alfredsson, P.H., 2001, "Disturbance Growth in Boundary Layers Subjected to Free-Stream Turbulence," Journal of Fluid Mechanics, 430, 149-168.

[26] Andersson, P., Berggren, M. and Henningson, D.S., 1999, "Optimal Disturbances and Bypass Transition in Boundary Layers," Physics of Fluids, 11, 134-150.

[27] Gibson, M.M. and Launder, B.E., 1978, "Ground Effects on Pressure Fluctuations in the Atmospheric Boundary Layer," Journal of Fluid Mechanics, 86, 491-511.

[28] Roach, P.E. and Brierly, D.H., 1990, "The Influence of a Turbulent Freestream on Zero Pressure Gradient Transitional Boundary Layer Development, Part I: Test Cases T3A and T3B. ERCOFTAC Workshop: Numerical Simulation of Unsteady Flows and Transition to Turbulence, Lausanne, Switzerland, pp. 319-347, Cambridge University Press.

[29] Somers, D.M., 1997, "Design and Experimental Results for the S809 Airfoil," NREL/SR-440-6918, January 1997.

MODELLING BYPASS AND SEPARATION-INDUCED TRANSITION BY REFERENCE TO PRE-TRANSITIONAL FLUCTUATION ENERGY

Sylvain Lardeau, Atabak Fadai-Ghotbi, Michael Leschziner

Imperial College London, Department of Aeronautics, UK.

Abstract

The article reports the main elements of an approach to modelling bypass and separation-provoked transition by combining a conventional (here, non-linear) eddy-viscosity model with transition-specific modifications, which take into account the non-turbulent fluctuations upstream of the transition region on the transition process itself. The performance of the combined model is illustrated by reference to four flows, two attached and two separated, all subjected to moderate-to-high free-stream turbulence. Other applications, involving passing wakes, are reported elsewhere, in some of the reference listed.

1 Introduction

Transition is a feature of virtually all practical flows around immersed solid bodies. Of these, external aerodynamic and turbomachinery flows are exceptional, in so far as the transition process is usually of major importance to the primary operational characteristics of the body – say, a blade, a wing, a fin, or a streamlined fuselage. Transition may be natural or of the bypass type, and it may occur in the boundary layer or following laminar separation. Correspondingly, the fundamental flow physics at play vary greatly, and this poses a major challenge to any modelling approach, especially one that is rooted in the RANS framework.

The focus of the work reported here is on turbomachine blades. Although the blade geometry and flow conditions differ greatly in different parts of a typical engine – e.g. there are major differences between HP compressor and LP turbine blades – common characteristics include a relatively low Reynolds number (based on chord) and the usually highly turbulent passage flow bordering the evolving blade-surface boundary layer. In such circumstances, a major proportion of the boundary layer is laminar or transitional, and transition tends to be of the bypass type. Alternatively, in highly loaded blades, transition may occur following laminar separation. In the most complex of circumstances, transition is highly unsteady, due to passing wakes, involving periodic boundary-layer transition, separation, post-separation transition, calming and even relaminarisation.

Over the past few years, DNS or high-resolution LES have been used with increasing frequency to examine flow stability, natural boundary-layer transition and transition following laminar separation. The most challenging DNS/LES studies, undertaken within the past 3-5 years, have focused on boundary-layer transition on realistic blade geometries and the (sensitive) receptivity of boundary layers to the spectral properties of freestream perturbations (Zaki & Durbin, 2005, Liu et al. 2008). The principal aim of all such simulations has been to promote insight into the fundamental mechanisms involved

in the transition process. In contrast, the extremely high cost and complexity of simulations preclude their use for quantifying the effects of transition in a practical setting. This can currently only be done by use of RANS methods in combination with transition models.

Although the most advanced, anisotropy-resolving RANS models for fully turbulent flows are very sophisticated, transition models are, on the whole, rather more basic, relying on correlations, limiters, ad-hoc corrections and concepts which are only weakly rooted in rational physical principles. This applies even to the most elaborate models that utilise intermittency-transport equations. To a large degree, this weakness is due to the inescapable fact that transition is characterised by a narrow spectral range of scales with physical behaviour that is incompatible with the statistical concepts underpinning RANS. An additional challenge (which is actually linked to the narrow range of scales) is that transition is much more sensitive than fully turbulent flows to boundary conditions, especially the spectral characteristics and perturbations in the approached free stream. This suggests that any serious modelling of transition \bar{U} - unless purely phenomenological or based on correlations – must be non-local.

One specific phenomenon that is observed in transitional boundary layers subjected to free-stream turbulence is that transition is preceded by non-turbulent fluctuations that are highly anisotropic, being dominated by the streamwise component and having an intensity that can reach r.m.s. values of order 150% of that in the post-transitional, turbulent state. These fluctuations are observed in both experiments and simulations. Simulations by Lardeau et al. (2007) have examined the energy budgets in this regime and suggest that the fluctuations arise in a layer removed from the wall, develop slowly by weak shear-strain/shear-stress interactions (in a statistical sense) and eventually lead to a rapid rise in wall friction, conventionally taken to signify transition. This phenomenon can be expected to play an important role in the transition process, but has not been accounted for in transition modelling, except in the framework proposed by the present authors. This paper summarises the current status of efforts designed to account for the interaction between pre-transitional fluctuations and the transition process. It focuses specifically on the modelling of bypass transition in laminar boundary layers under the influence of high free-stream turbulence (FST), and transition in a separation bubble, again for high FST.

2 Pre-transitional phenomena in bypass transition

Mechanisms by which free-stream perturbations can induce transition in a laminar, attached, boundary layer

are now fairly well understood. A recent series of stability analyses (Liu et al. 2008, Zaki & Durbin 2005, Brandt et al. 2004) have reproduced the main features of bypass transition using only a few continuous Orr-Sommerfeld (OS) modes. Indeed, continuous and discrete OS modes compete against (or complement) each other in most routes to transition. Once the Klebanoff modes (elongated streaks) or Tollmien-Schlichting (TS) waves are amplified, they are receptivity sites for higher free-stream turbulence frequencies. How any of these mechanisms can be incorporated into a statistical model is unclear. A proposal by Johnson & Ercan (1999) involves a frequency dependence within a boundary-layer-integral model.

One of the main findings of previous studies is that the streaks (Klebanoff modes) are associated with streamwise-velocity perturbations only, implying a vanishing shear stress $\langle uv \rangle$ in the pre-transitional region. In contrast, Lardeau et al. (2007) have found that the shear stress is not zero, well before the wall shear stress rises abruptly, thus leading to a slow build-up of (quasi-)turbulence activity and eventually transition. In classical turbulence models, the onset of transition is entirely reliant on a high rate of production $\langle uv \rangle \frac{\partial U}{\partial y}$, and this is conditional on an elevation of the shear stress, without which the boundary layer remains laminar. Hence, any physically credible approach to modelling transition must include a model component that accounts for the effects of pre-transitional fluctuations on the production-induced turbulence amplification.

Mayle & Schulz (1997) derived a transport equation for the so-called laminar fluctuation energy, based on the assumption that the only term which could overcome the dissipation in the transitional region is by amplification associated with pressure fluctuations. However, the budgets presented by Lardeau et al (2004) contradict this concept, showing that the pressure-velocity correlation is insignificant. Thus, while Mayle & Schulz's model of the generation term procures the requisite build-up of fluctuation energy, the underlying concept does not appear to be correct.

3 Laminar separation

On highly-loaded LP turbine blades of modern engines, the Reynolds number is very low, and the pressure gradient is strong enough to induce separation in the laminar region. The separated shear layer then usually becomes turbulent and reattaches quickly, usually upstream of the trailing edge. The separation bubble formed as a consequence alters the effective shape of the blade, thus degrading the blade's performance and increasing losses. The process by which a separated shear layer undergoes transition to turbulence is very different from that of a boundary layer: the inflection point in the velocity profile prior to separation renders it unstable to 2D perturbations, and the growth of the perturbations is primarily dictated by stability constraints. On the other hand, just as is the case in attached flows, the transition process is substantially altered when free-stream turbulence is introduced (Wissink & Rodi, 2006). Thus, transition occurs earlier and the bubble length reduces as the FST intensity increases. The need for a turbulence model to accommodate both forms of transition clearly constitutes a major challenge, because the response of the pre-transitional fluctuations to pressure gradient is unknown.

4 Modelling of laminar kinetic energy

4.1 Basic approach

Mayle & Schulz (1997), and subsequently Lardeau et al. (2004) and Walters and Leylek (2004), proposed the use of a transport equation for the energy of the non-turbulent fluctuations k_l . The original derivation of this equation follows the same route as that used to derive the turbulence-energy equation. However, the closure is different. First, based on measurement and simulation, it is found that, in the pre-transitional region, the streamwise fluctuations strongly dominate over fluctuations in other directions, hence implying a close-to-zero shear stress, and consequently a very low production of turbulence energy, P_k . The transport equation for the laminar fluctuations can then be written, in a general form, as:

$$\frac{Dk_l}{Dt} = P_l - \nabla \cdot \mathbf{T}_1 - \varepsilon_l - R \quad (1)$$

where P_l is the production term and depends on the type of transition considered (bypass or separated-induced), the energy flux \mathbf{T}_1 is assumed to be purely viscous, i.e.: $\mathbf{T}_1 = \nu \nabla k_l$, while the dissipation rate is approximated in a manner analogous to that for turbulent flows, namely on dimensional grounds with the turbulence energy and wall-normal distance as the relevant scales, i.e.: $\varepsilon_l = 2\nu k_l / y^2$, where y is the distance from the wall. The right-most term R represents the transfer of laminar kinetic energy to its turbulent counterpart, and this should thus appear as a source term in the transport equation for k , with an opposite sign.

4.2 Bypass transition

Mayle & Schulz proposed an approximation of the source term P_l in Eq. 1, based on the assumption that shear production is zero. The pre-transitional fluctuations are then held to be induced by the "work" of pressure forces through the term $\langle u \partial p / \partial x \rangle$, which is equivalent, subject to several assumptions, to $\langle u \partial U / \partial t \rangle$, where u are local fluctuations and U are free-stream fluctuations. However, as noted already, Lardeau et al. (2007) have shown, using budgets extracted from large-eddy simulation of transition in laminar boundary layer, that pre-transitional fluctuations are associated with classical turbulence/shear production, although the ratio of shear stress to fluctuation energy is much lower than the turbulent-flow value 0.3, and this production occurs in the upper part of the boundary layer. In other words, the behaviour is very different to that in a canonical turbulent boundary layer.

Mayle & Schulz proposed the following closure:

$$P_l = C_\omega \frac{U_\infty^2}{\nu} \sqrt{k \cdot k_\infty} \cdot \exp^{-y^+ / C^+} \quad (2)$$

where C_ω relates to the effective free-stream frequency (Jonás et al. 2000) and U_∞ and k_∞ relates to free-stream quantities. This closure may equally be regarded as a specific model of the production $\langle uv \partial U / \partial y \rangle$ using the viscous length scale ν / U_∞ .

One element in the coupling of Eq. 1 with the turbulence model is the transfer term R . This transfer is supposed to be proportional to the laminar-fluctuation energy:

$$R = C_2 f_2 \frac{\varepsilon}{k} k_l \quad (3)$$

This works well in separation-induced transition (see section), but not in bypass transition. Hence, in the

latter transition mode, coupling between k_l and k is established via the proposal $k_t = (1-\gamma)k_l + \gamma k$ ($0 < \gamma < 1$) in the production P_l and in the eddy-viscosity

$$\nu_t = f_\mu c_\mu \frac{k(\gamma k_t)}{\varepsilon} \quad (4)$$

In the above, γ is used to damp the tendency of the turbulence model to induce premature transition by an excessive and too rapid a build-up of turbulence production. Although γ is essentially viewed here as a limiter, rather than a physically meaningful quantity, the current model form makes use of the Sintermittency parameter $\tilde{\gamma}$, originally introduced by Dhawan and Narasimha (1958), which is modified here to take into account the variation of intermittency in the wall-normal direction:

$$\gamma = 1 - f_\omega(26) \left[-(x - x_b)^2 \hat{n}\sigma \frac{U_\infty}{\nu^2} \right] \quad (5)$$

f_ω is a damping function given by $f_\omega(A) = \exp[-(\sqrt{k_l y/\nu})^2/A]$, x_b is the transition onset which is determined from the correlation (Abu-Ghannam and Shaw, 1980):

$$Re_{\theta_b} = (120 + 150Tu^{-2/3}) \coth[4(0.3 - K \times 10^5)] \quad (6)$$

$\hat{n}\sigma$ relates to the propagation rate of turbulent spots in laminar boundary layer (Steelant and Dick, 1996):

$$\hat{n}\sigma = \left[1.25E^{-11} \times Tu^{7/4} \right] 10^{-3227K^{0.5985}} \quad (7)$$

with Tu being the local free-stream velocity and $K = (\nu/U_\infty^2)(dU_\infty/dx)$ being the local acceleration parameter.

4.3 Separation-induced transition

The physical mechanisms involved in the transition process in separated shear layer are very different from those guiding the above modelling practices. In particular, the instability mechanism involved are different \tilde{U} -K-H waves rather than streaks associated with viscous processes – and the effect of free-stream turbulence is to enhance the instability mechanism in the shear layer, rather than completely bypassing them (e.g. Wissink and Rodi's (2006) arguments on the influence of free-stream disturbances on a separated shear layer). The problem of modelling separation-induced transition is thus very different from that of modelling bypass transition: in the later, transition tends to be triggered too early, due to the imbalance of production vs. dissipation, while in the former, the presence of an inflexion point in the velocity profile triggers transition, leading to instability.

In the model adopted here, the production term in a free-shear layer is compatible with the turbulent-flow form:

$$P_l = 2\nu_l S_{ij} S_{ij} \quad (8)$$

with $S_{ij} = \frac{1}{2} \left(\frac{\partial U_i}{\partial x_j} + \frac{\partial U_j}{\partial x_i} \right)$. The pre-transitional viscosity ν_l is defined as a function of a length scale l_m and a time scale u_l pertinent to the flow physics,

$$\nu_l = C_1 u_l l_m \quad (9)$$

The relevant velocity scale u_l in a separated shear flows is the phase velocity of the most amplified perturbation, here taken as the square root of the laminar energy $u_l =$

$\sqrt{k_l}$. A relevant length-scale in separated (free shear) flows is the vorticity thickness,

$$l_m = \delta_\omega = \frac{U_1 - U_2}{2} \max \left[\left(\frac{\partial U}{\partial y} \right)^{-1} \right]_y \quad (10)$$

The total fluctuating energy is then defined by $k_{tot} = k + k_l$. An analogy to the intermittency parameter define in Section can be computed from the ratio between turbulent and the pre-transitional fluctuation energy,

$$\gamma = \frac{k}{k_{tot}} = 1 - \frac{k_l}{k_{tot}} \quad (11)$$

This energy is then transferred to the turbulence field by using the source/sink term R (Walters & Leylek, 2004). The transfer rate is assumed to be proportional to the laminar energy, Eq. 3, where $C_2 = 0.3$ is obtained from calibration on different test cases, and f_2 is a damping function defined in a similar as f_ω (eq. 5):

$$f_2 = 1 - \exp^{-\psi/C_3} \quad (12)$$

with $\psi = \max \left(\frac{y\sqrt{k}}{\nu} - C_4; 0 \right)$, with $C_4 = 10$. This damping function controls, in effect, the location at which transition sets in and ends. In particular, if $\psi = 0$ then $f_2 = 0$ and no transfer from laminar fluctuation energy to turbulence kinetic energy takes place.

5 Validation examples

	Re_L	Tu	Pressure Gradient
T3A	$5.76 \cdot 10^5$	3 %	Zero
T3B	$10.03 \cdot 10^5$	6 %	Zero
WR	$6 \cdot 10^4$	5 %	Adverse
T106C	$5 \cdot 10^4$	4%	Blade geometry

Table 1: *Nomenclature and flow characteristics.*

Four statistically-steady flows are considered in the present article; these are summarised in Table 1. The first two are boundary layers developing in zero pressure gradient along a flat plate with sharp leading edge. These two cases were examined experimentally by Roach and Brierley (1992). The third case (WR) is a separated flat-plate boundary layer, subjected to adverse pressure gradient. Both experimental and DNS data are available for this case; here, we use the DNS data of Wissink and Rodi (2006). The fourth is a turbine blade (Fig. 1), and this is included to illustrate the performance of the model for strongly separated flow over a realistic, highly-curved configuration at moderate Reynolds number and high free-stream turbulence intensity. Experimental data for this flow have been obtained by Himmel and Hodson (2008) within the EU TaTMO project. Application of the model to unsteady bypass transition, involving passing wakes, is reported in Lardeau and Leschziner (2006).

Geometries T3A and T3B were computed with a numerical grid containing 120x120 nodes, while a grid of 120x180 was used for the WR case. These meshes were chosen on the basis of careful grid-independence studies, with particular emphasis placed on the location at which transition sets in. For the blade geometry (Fig. 1, a 12-block grid was constructed, the block closest to

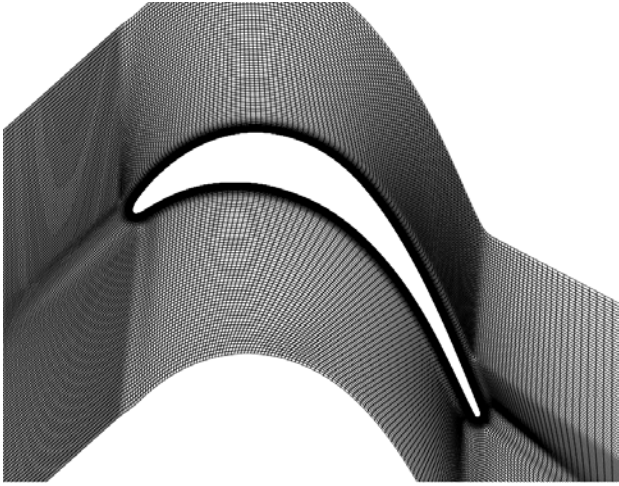


Figure 1: Geometry and grid for the T106C test case.

the blade having an O-type topology and comprising close-to-orthogonal sets of grid lines. The total number of cells was 48,000, again chosen following a grid-independence study. All calculations were performed using a multi-block version of the general, fully-collocated, non-orthogonal finite-volume scheme STREAM (Lien et al., 1996). Convection of all transported properties was approximated by the second-order UMIST-TVD scheme (Lien & Leschziner, 1994). Mass conservation was enforced via the SIMPLE pressure-correction algorithm, which yields the correct pressure field by an iterative sequence that, effectively, nullifies the mass residuals in all computational cells.

The principal formulation for the turbulence model employed herein is the quadratic model of Abe et al. (2002). This adopts a four-part representation of the effects of strain, vorticity and wall proximity on the anisotropy tensor. An important feature of this model is that it returns the correct wall-asymptotic variation of all Reynolds stresses. However, the modification proposed below have also been tested using a more conventional $k-\omega$ model (Pacciani et al., 2009). Details about the performance of Abe et al.'s model for turbomachine-blade flows can also be found in Lardeau et al. (2004).

Selected results are shown in Figs. 2-4. In what follows, “AJL” identifies the basic Abe et al model, while “LKE” identifies the combination of this model with the transition-related modifications.

Fig. 2 shows the streamwise variation of the skin-friction coefficient and the wall-normal maximum of the total fluctuation energy for the T3A and T3B cases, using both the AJL and LKE models, in comparison with the experimental results by Roach and Brierley (1992). In the case of T3A, there is a substantial build-up of non-turbulent fluctuation energy well ahead of the onset of transition, and this is reproduced well by the modified model. In the case T3B, where the free-stream turbulence is high, the basic AJL model returns very early transition, together with a corresponding early rise in turbulence energy. Although the AJL and LKE models predict very similar energy levels upstream of $Re_x < 10^5$, the nature of this energy is very different: the modified model returns a high level of laminar fluctuation energy, together with low pre-transitional C_f values, while the AJL model predicts an early rise in the turbulence energy leading to premature transition. One point that has rarely been addressed before in relation to the T3B case is the peak in k_{max} prior to transition (Fig. 2b).

This peak, also reproduced well by the modified model, is mostly due to a significant level of laminar-fluctuation energy coinciding with a high level of turbulence energy just after transition is initiated.

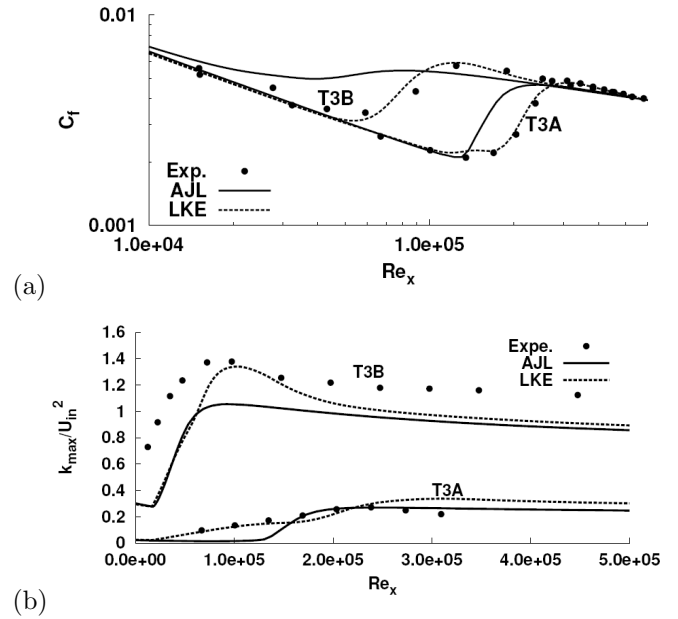


Figure 2: (a) Skin friction coefficient and (b) streamwise variation of the maximum (in wall-normal direction) fluctuation energy in the boundary layer for the AJL and the LKE model, compared with experimental results (Roach and Brierley, 1992), for case T3A and T3B.

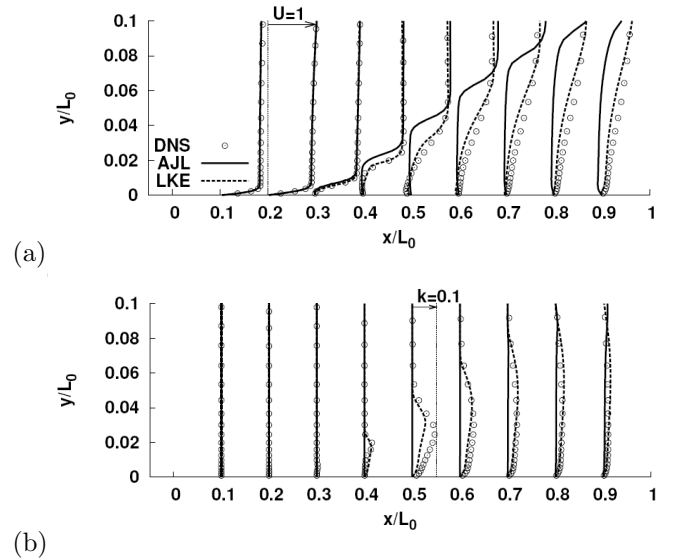


Figure 3: (a) Streamwise velocity and (b) fluctuation-energy at different streamwise position along the flat plate, for the AJL and the LKE model, compared with DNS data (Wissink and Rodi, 2006).

Profiles of mean velocity and fluctuation energy for the separated WR case are shown on Fig. 3. The baseline model predicts the laminar separation at the correct position, but fails to reproduce the transition in the separated shear layer, resulting in a massively too long recirculation bubble, with transition starting much too late. The LKE model, on the other hand, reproduces the

correct evolution of the transition process upon separation and is therefore able to predict correctly both the velocity and the fluctuation-intensity fields.

the maximum fluctuation energy is closer to the blade suction side. Nevertheless, the predicted behaviour may be regarded as realistic and broadly satisfactory.

Acknowledgements

The research reported in this paper was undertaken within the European Commission research projects TATMo (contract No. AST5-CT-2006-030939, www.tatmo.eu) and UTAT (contract No. G4RD-CT-2001-00628).

References

- Abe K., Jang Y.-J. and Leschziner M. (2002) An investigation of wall-anisotropy expressions and length-scale for non-linear eddy-viscosity models. *Int. J. Heat Fluid Flow* **28**(2):181–198.
- Abu-Ghannam B. and Shaw R. (1980) Natural transition of boundary layers—the effect of turbulence, pressure gradient and flow history. *J. Mech. Eng. Sci.* **22**(5):213–228.
- Brandt L., Schlatter P. and Henningson D. (2004), Transition in boundary layers subject to free-stream turbulence. *J. Fluid Mech.* **517**:167–198.
- Dhawan S. and Narasimha R. (1958) Some properties of boundary layer during the transition from laminar to turbulent flow motion. *J. Fluid Mech.* **3**:418–436.
- Johnson M.W. and Ercan A.H.(1999) A physical model for bypass transition. *Int. J. Heat and Fluid Flow* **20**:95–104.
- Lardeau S., Leschziner M. and Li N. (2004) Modelling bypass transition with low-Reynolds-number non-linear eddy-viscosity closure. *Flow, Turbul. Combust.* **73**:49–76.
- Lardeau S. and Leschziner M. (2006) Unsteady RANS modeling of wake- induced transition in linear LP-turbine cascades. *AIAA J.*, **44**(8):1845–1865.
- Lardeau S., Li N. and Leschziner, M. (2007) Large eddy simulation of transitional boundary layers at high free-Stream turbulence intensity and implications for RANS modeling. *J. Turbomach.* **129**:311–317.
- Lien F., Chen W. and Leschziner M. (1996) A multiblock implementation of a non-orthogonal collocated finite volume algorithm for complex turbulent flows. *Int. J. Numer. Methods Fluids* **23**:567–588.
- Lien F. and Leschziner M. (1994) A general non-orthogonal collocated finite volume algorithm for turbulent flow at all speeds incorporating second-moment turbulence-transport closure, Part 1: Computational implementation. *Comput. Meth. Appl. Mech. Eng.* **114**:123–148.
- Liu Y., Zaki T.A. and Durbin P. A.(2008) Boundary-layer transition by interaction of discrete and continuous modes. *J. Fluid Mech.* **604**:199–233.
- Mayle R. and Schulz A. (1997) The path to predicting bypass transition. *J. Turbomach.* **119**:405–411.
- Roach P.E. and Brierley D.H. (1992) The influence of a turbulent free-stream on transitional boundary layer development, in *Numerical Simulation of Unsteady Flows and Transition to Turbulence*, O. Pironneau, W. Rodi, I.L. Ryhming, A.M. Savill and T.V. Truong (eds.):319–347.
- Pacciani R., Marconcini, M., Fadai-Ghotbi A., Lardeau S. and Leschziner, M.A. (2009) Calculations of high-lift cascades in low pressure turbine conditions using a three-equation model. *ASME Turbo Expo 2009, GT 2009*.
- Steelant J. and Dick E. (1996) Modelling of bypass transition with conditioned Navier-Stokes equations coupled to an intermittency transport equation. *Int. J. Numer. Methods Fluids* **23**:193–220.
- Wissink J.G. and Rodi W. (2006) Direct numerical simulations of transitional flows in turbomachinery. *J. Turbomach.* **128**:668–678.
- Walters D.K. and Leylek J.H. (2004) A new model for boundary-layer transition using a single-point RANS approach. *J. Fluids. Eng.* **26**:193–202.
- Zaki T.A. and Durbin P. A. (2005) Mode interaction and the bypass route to transition. *J. Fluid Mech.* **531**:85–111.

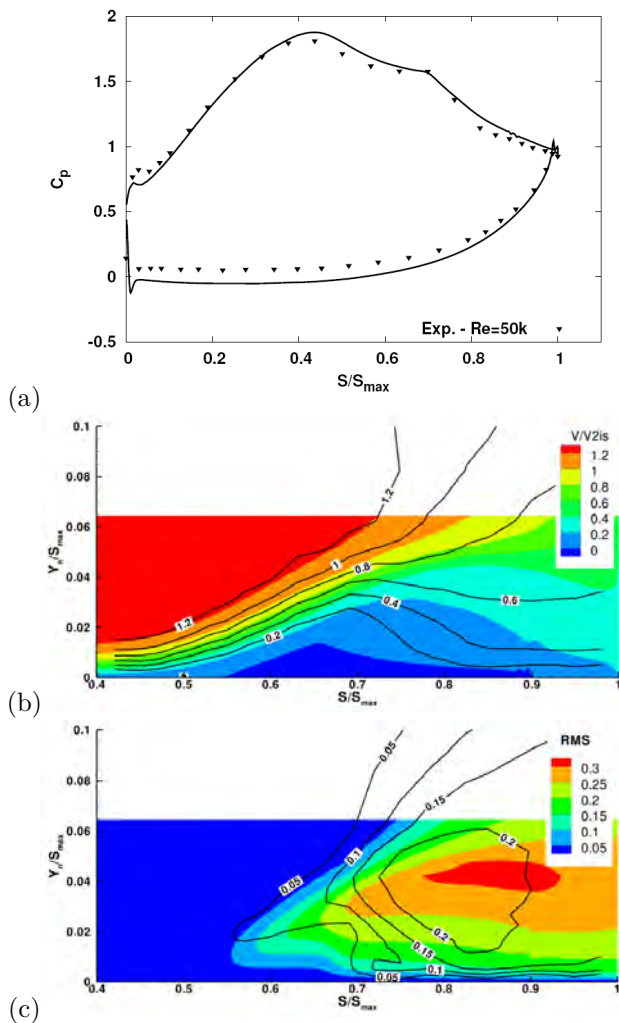


Figure 4: *T106C* cascade blade, $Re=50,000$; (a) Pressure coefficient, (b) wall-tangent velocity field and (c) RMS velocity, along the suction surface of the blade (local coordinate system based on S/S_{max}): distance from the leading edge divided by suction surface length. Experimental results are shown with lines and the same scale has been used for both experiments and simulations. V_{2is} corresponds to the isentropic (tangential) velocity.

Fig. 4 provides comparisons between predictions with the LKE model and experimental results for the lowest Reynolds number examined ($Re = 50,000$ based on inflow conditions). No results with the baseline model are included, as it was impossible to obtain a converged field, due to a serious delay in the transition process and the presence of K-H-type instability in the highly separated, non-reattaching shear layer. The pressure coefficient on the suction side is seen to match closely that obtained in the wind tunnel, signifying the correct resolution of the separation bubble. Comparisons between hot-wire measured and computed streamwise (tangential) velocity and RMS fluctuations are presented in Fig. 4b and c. Despite the close agreement in respect of C_p , some discrepancies arise in relation to the flow field: the thickness of the separation bubble is larger in the experiment, with a more abrupt end, the predicted growth of kinetic energy (Fig. 4c) is slower than in the experiment, and the location of

e^N - WHY IT WORKS; WHEN IT DOESN'T; WHAT'S NEXT?

Chris Atkin

School of Engineering and Mathematical Sciences, City University London, UK.

1 Introduction

The increasing attention being paid to the impact of aviation upon climate change has prompted a renewed interest on both sides of the Atlantic in Laminar Flow Control (LFC) Technology. One of the most common claims about the tools used in LFC design, particularly the e^N method of Van Ingen [1], are that they are too simplistic in their modelling of the physics. LFC design tools are here discussed with reference to the author's experiences in the UK aircraft industry and in government service over the past 15 years, most of them directed in some way in the development and exercising of methods for laminar flow design.

2 Parallel-flow stability theory and e^N

Although by no means a general description of the laminar-turbulent transition phenomenon, for an LFC wing the conceptual model of the transition process is as outlined in Figure 1 below.

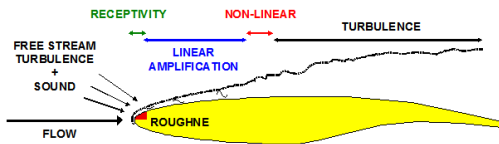


Figure 1: *Schematic of natural boundary layer transition on a wing section.*

Perturbations are introduced into laminar boundary layer flows through the phenomenon of receptivity and are then convected and amplified, over an extensive region of the wing, in a manner which can be described by linear mathematics to an acceptable degree of accuracy. A significant distance downstream of the region where receptivity is important, the perturbations have grown to amplitudes where non-linear interactions between large-amplitude perturbations eventually lead to turbulence. It is an important simplification of the transition process that these three phases can be separated geographically on the aircraft wing.

A plan view of a swept wing section, illustrating the main types of disturbances considered in the linear-amplification region, is given in Figure 2. The origin of all streamlines at the attachment line of the wing means that instability or contamination of the attachment line flow will affect the entire wing, so we note that this problem needs to be managed - usually by some kind of device which strips the contaminated flow from the attachment line. Remaining instabilities on the attachment line may require active control. However we focus on the management of crossflow (CF) and Tollmien-Schlichting (TS) instabilities as the major task in the aerodynamic design

of a laminar flow wing at cruise. Note that CF instabilities usually precede TS instabilities as shown in the figure but, depending upon the pressure distribution, there may be an extensive overlap region.

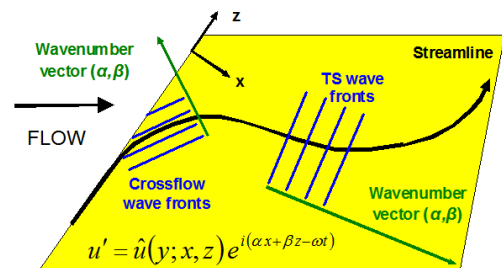


Figure 2: *Schematic showing crossflow (CF) and Tollmien-Schlichting (TS) instabilities.*

Both types of instability follow the receptivity, linear amplification, non-linear breakdown route, as illustrated in Figure 3 and Figure 4 respectively, but display different characteristics at each phase.

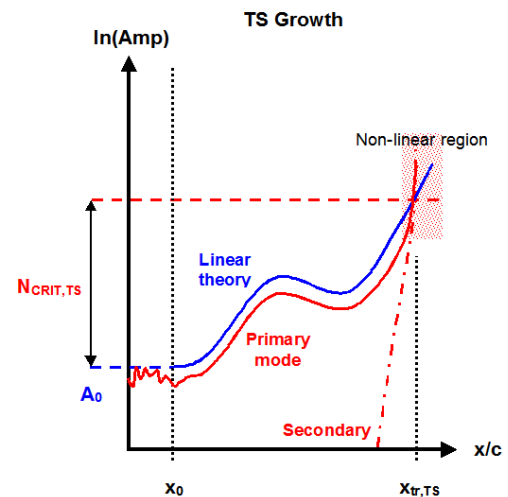


Figure 3: *Schematic of TS instability growth.*

During the receptivity phase, disturbances are constantly introduced into the boundary layer. Upstream of the neutral point we hypothesize some sort of equilibrium between disturbance introduction and decay as the disturbances are convected downstream. As the neutral point is passed the disturbances start to be amplified: receptivity physics rapidly becomes of secondary importance to convective amplification which can be captured by linear theory, as shown by the blue lines on Figures 3 and 4.

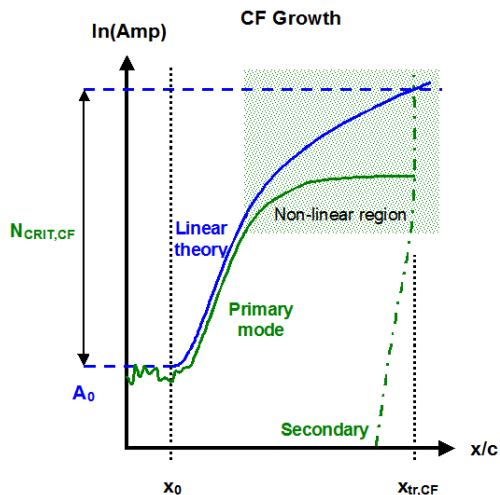


Figure 4: Schematic of CF instability growth.

Finite-amplitude effects immediately following the receptivity phase, such as transient growth and even bypass transition, are usually neglected in LFC design because the receptivity process is supposedly managed, by suitable choice of manufacturing tolerances, so as to restrict the perturbations to infinitesimal amplitudes: that, at least, is the intention but our modelling of receptivity phenomena may not be able to verify that this is true in practice. More will be said on this topic later. The normal modes are amplified independently by the boundary layer, growing by many orders of magnitude until non-linear effects become significant, indicated by the shaded regions in the figures above, and harmonic modes begin to be forced.

By integrating the gradient of the blue lines the separation of the amplitudes typical of receptivity and non-linearity/breakdown can be estimated. This separation, measured logarithmically, is termed an N -factor. As shown in the figures there is a finite interval between the onset of non-linear behaviour and the recognition that the flow is 'fully' turbulent. The simplicity of the mathematics allows the linear stability equations to be solved even in these regions, even though the physics is a good deal more complex. This leads to accusations that the use of N -factors is irrational and inappropriate. Nevertheless there is a simple pragmatism into which the N -factor approach fits neatly. Although the physics of receptivity and breakdown have little in common, the latter is usually dictated by the former since it is usually the receptivity phase which determines which type of perturbations will dominate the transition process. Both phenomena are therefore sensitive to parameters which drive the receptivity process, and these parameters are not varied enormously during a design exercise: the manufacturing standard of the model or aircraft, and the environment in which it is tested or flown. At present there is little knowledge of exactly how receptivity and breakdown respond to changes in Mach number, Reynolds number, angles of incidence and sweep, and wing shape. Conversely these are all variables which have a major impact upon the amplification of the normal modes, unlike the manufacturing standard and test/flight environment. Quite simply the blue lines on Figures 3 and 4 are (theoretically) capable of capturing the response to all the design variables available to the cruise design team. The amplitudes of the end points, as described, tend to be a fixed distance apart as far as the designer is concerned. Hence tracking the blue line between known $\Delta \ln(Amp)$ is a useful way of estimating the spatial separation of

the receptivity and breakdown regions and, therefore, the 'position of transition'. Clearly care is then required when there are indeed changes to manufacturing standard and test/flight environment! Crouch [2] gives a good overview of the N -factor techniques which may be used under these circumstances and also techniques for managing local growth modifiers (steps, gaps, etc) which may not be resolved at a preliminary design stage.

3 N -factor correlations

Clearly the above technique relies upon some reliable measure of the separation $\Delta \ln(Amp)$ between disturbance amplitudes at each end of the blue N -factor curve. This are usually obtained from a representative experiment (or set of experiments) where the location of breakdown is accurately measured. Sufficient supporting information (surface pressures, geometric lines, sweep angles, etc) is also gathered to allow linear stability theory to be applied to determine the position of the neutral point: this then yields the spatial separation of the receptivity and breakdown phases which, following the calculation of the rest of the blue N -factor curves in Figure 3 and Figure 4, leads to the separation in amplitudes - this is termed the critical N -factor.

From the discussion above it follows that the critical N -factor is a function (ultimately) of the receptivity physics: which modes are introduced at what amplitudes. For example it is normal to separate CF and TS modes, and indeed hybrid CF/TS cases, when defining critical N -factors in the manner shown in Figure 5 taken from Ref. 3. This figure also illustrates the scatter present in most similar correlations. In principle the critical N -factors should, for each data point, be corrected for the particular receptivity condition applicable to that point. In Figure 5, aside from the differences between the two wind tunnel models and campaigns, the data points simply encompass different span-wise stations on a given model and different onset flow conditions (Mach and Reynolds numbers, incidence) and at different suction levels (Hybrid Laminar Flow Control). While it is understood that the variation in tunnel conditions will be accompanied by changes to the acoustic and vortical signature of the free stream, the scatter is still appreciable.

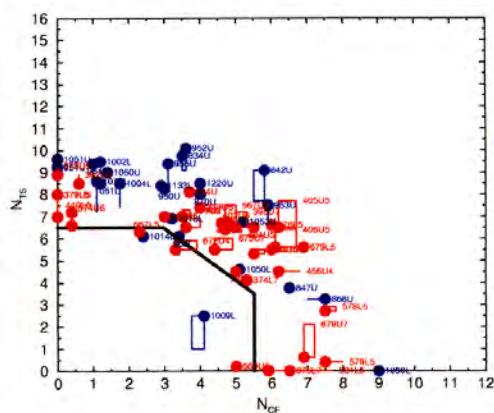


Figure 5: Comparison between incompressible N -factor pairs obtained from the ELFIN II HLF tunnel tests and the ELFIN I HLF tunnel tests³.

Such correlations were carried out in the absence of any useful information and understanding as to how the initial disturbance characteristics and amplitudes might

vary from data point to data point. Even today, although our understanding and modelling of receptivity has developed, it would be extremely difficult to include receptivity 'compensation' to reduce critical N -factor scatter. The result of such uncertainties is the black line drawn on Figure 5 which marks out the 'safe' N -factors for laminar flow design. While this provides a robust tool set for the designer it tantalisingly offers between 50% and 80% additional N -factor margin for some combinations of surface and flow conditions. The problems with the e^N method are not always associated with low critical N -factors: it is the randomly high values which underline what might be achieved with better understanding and modelling.

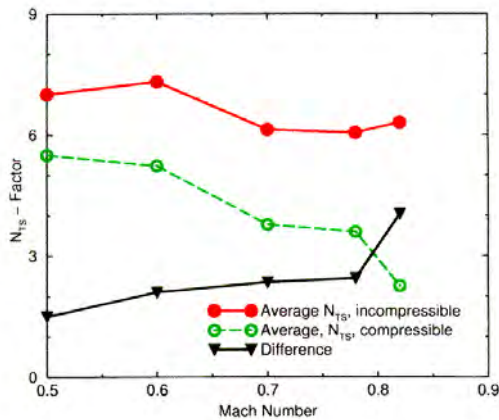


Figure 6: Difference between compressible and incompressible N_{TS} -factors with increasing Mach number. ELFIN II HLF tunnel tests3.

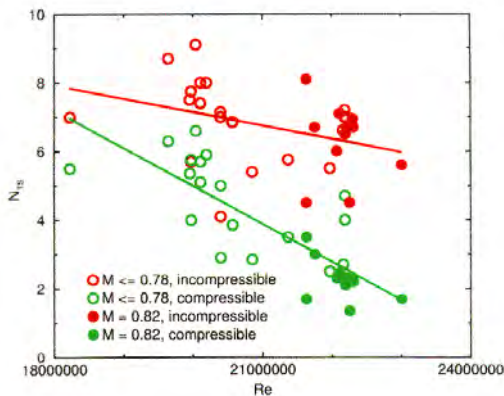


Figure 7: Comparison of compressible and incompressible N_{TS} -factors with increasing Reynolds number. ELFIN II HLF tunnel tests [3].

There are some other unsatisfactory aspects to the use of N -factor correlations which are chosen on the basis of robustness. Figure 6 and Figure 7, taken from Ref. 3, illustrate the more consistent performance - i.e. the reduced sensitivity of critical N -factor to Mach and Reynolds numbers - of incompressible stability analysis. While the adoption of incompressible N -factors effectively reduces the scatter, it also removes any scope for exploiting in design the stabilising effect of compressibility offered by theory. The most likely explanation of the

trends shown in Figure 6 and Figure 7 is that the receptivity physics is indeed sensitive to Mach and Reynolds numbers here. Unfortunately the analysis tools are not available to correct the critical N -factors obtained from the tunnel measurements.

4 Emerging techniques

Classical e^N methods have been supplemented in recent years by linear and non-linear PSE [4]. UK developments have been carried out at Imperial College. Linear PSE and equivalent methods (such as a correctly-scaled multiple-scales approach) incorporate non-parallel and curvature effects. The former, although important for reconciling stability theory with detailed flowfield measurements [5], is not usually significant in N -factor calculations. The latter can be but this has yet to be verified experimentally. The difficulty is that surface curvature is significant only in the vicinity of the wing leading edge, while experiments in which transition occurs in the mid-chord region are unlikely to be dominated by modes which have been influenced by curvature. Not many research programmes have been courageous enough to demonstrate transition near the leading edge and thus to capture the effect of curvature on calculated critical N -factors. Figures 8 and 9 illustrate the point.

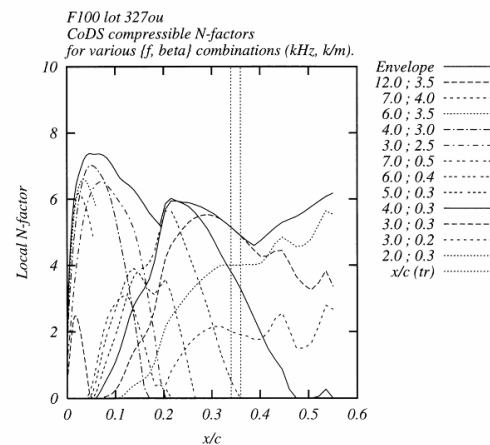


Figure 8: N -factors obtained from classical linear stability analysis for ELFIN I F100 case 327ou.

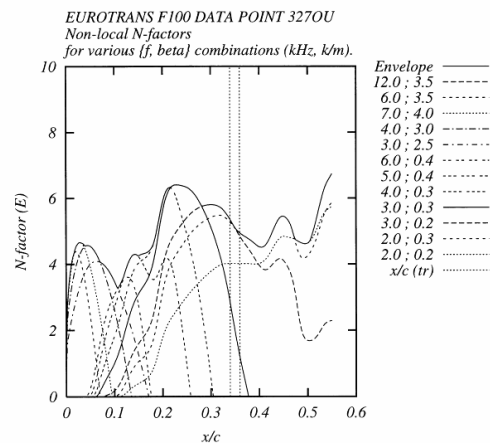


Figure 9: N -factors obtained from linear PSE analysis showing the reduction in crossflow amplification near the leading edge. ELFIN I F100 case 327ou.

The large N -factor hump ($N \sim 7$) at around 5% chord in Figure 9 is reduced to $N < 5$ in Figure 9, calculated using linear PSE. However the modes contributing to this hump have no bearing upon transition, so the correlated critical N -factor is largely unchanged. Nevertheless studies on the aircraft-level impact of HLFC, where suction is used to limit leading edge N -factors, have shown a 25% reduction in the required mass flow rates predicted by linear PSE compared to a standard e^N method. This is because, for the control problem, the amplification of modes in the leading edge region (where the flow curvature is greatest) is a significant factor.

Figure 9 also provides a good introduction to the subject of non-linear PSE. It can be seen that transition occurs at 35% chord where all modes are found to be linearly stable. Of course, just prior to this the modal amplitudes are quite high and it can easily be shown [6], using non-linear PSE, that modes of sufficient amplitude will interact causing the rapid growth of higher harmonics which leads to transition. Non-linear PSE adds a semi-quantitative tool for tackling situations like this: semi-quantitative because the important initial amplitudes required to initialise the non-linear analysis have to be assigned arbitrarily in the absence of a functioning receptivity model.

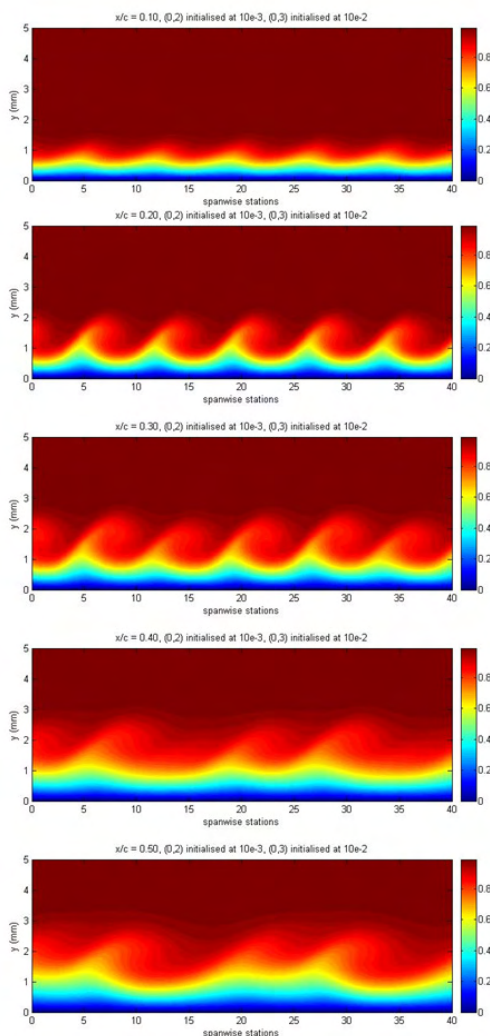


Figure 10: *Saric NLF(2)-0415 experiment (sweep 45° , $Re = 2.4$ million, $\alpha = -4^\circ$). Interacting crossflow vortex arrays (span-wise spacing $\beta = 8\text{mm} \ \& \ 12\text{mm}$). Contours of stream-wise velocity at 10%, 20%, 30%, 40% and 50% chord. Initialisation $A_{8\text{mm}} = 10^{-2}$, $A_{12\text{mm}} = 10^{-3}$.*

Non-linear PSE has also been used extensively at QinetiQ [6,7] to explore the applicability of Saric's Distributed Roughness technique [8,9], providing rewarding animations of the development of crossflow vortices on swept wings in the presence of span-wise arrays of roughness elements. Figure 10, obtained using non-linear PSE, illustrates the interactions between two arrays of stationary crossflow vortices, spaced at 8mm and 12mm, over the surface of a swept wing exhibiting a favourable pressure gradient. The 12mm mode is the one predicted to dominate by linear theory but, when the 8mm mode is forced to be ten times greater in amplitude than the 12mm mode, simulating the addition of discrete roughness elements, the non-linear development of the 12mm mode is disrupted and the vortical structure, after strong initial growth, appears to decay.

The exact conditions under which these vortical patterns become susceptible to secondary instability, and therefore whether these forcing amplitudes are plausible, are the subject of ongoing research at Imperial College. Yet this example illustrates the role of non-linear PSE in current LFC research: the method has been used to develop an understanding of the conditions required for crossflow vortices to interact; yet further and higher-order analysis is required to interpret the implications of these non-linear mechanisms for the control of transition.

5 Receptivity modelling

Although receptivity is an active area of research, the author believes that there is a lack of practical tools to help with the management of surface roughness and environmental forcing. As described earlier, linear stability theory is predicated upon the assumption that finite-amplitude effects immediately following the receptivity phase, such as transient growth and even bypass transition, can be neglected. The e^N technique assumes a uniformity of receptivity physics which may be representative in some idealised conditions but is unlikely to be accurate for real aerodynamic surfaces and environments. This is the most likely explanation of the scatter commonly found in N -factor correlations.

Non-linear methods have illustrated how finite-amplitude disturbances can introduce mean flow distortion and periodic streaks which persist downstream and modify the stability properties of the boundary layer. The character of the free stream environment will select between stationary or travelling crossflow disturbances as the dominant transition mechanism on a swept wing: surface imperfections will excite the former while vortical structures in the free stream will excite the latter. Tunnel and flight testing of swept wings may therefore reveal entirely different breakdown mechanisms. The challenge is the need for quantitative guidance on the magnitudes of the forcing mechanisms and the relationship between the spectra of the forcing sources and the properties of the naturally-amplified normal modes, if indeed there is one.

Surface roughness and waviness are topics where there is still ambiguity over whether these are receptivity sources or growth modifiers which act throughout the boundary layer. These are important questions because surface tolerance is expensive to achieve on a production aircraft: if a roughness or waviness criterion can be applied locally, for example just in the vicinity of the neutral point, rather than over the entire laminar flow surface, then this will impact significantly on the cost to design, manufacture and maintain the surface.

6 Where next

The e^N method broadly captures the influence of pressure gradient, Reynolds number, Mach number and wing sweep: these are the key parameters available to the wing designer. It has been in use for many years for LFC research, and is even now beginning to be used alongside Navier-Stokes methods for the modelling of transition in CFD [10]. Irrespective of the arguments about physical modelling, however, the method suffers in practice because the critical N -factors in use tend to be rather conservative. This is in response to large amounts of scatter in correlation plots. Hybrid laminar flow designs tend to suffer by having both conservative N -factor distributions and large safety margins applied to the suction system specification.

Unfortunately the economics of laminar flow design mean that a conservative approach is going to yield little benefit. In today's world of bio-fuels and carbon-fibre airframes, if the most promising aerodynamic technology can only contribute a few percent to aircraft performance then it will indeed be left on the shelf. There needs to be a real effort to extend our knowledge of receptivity and late-stage transition. The end product, for industrial use, is likely to be additional corrections to critical N -factors to account for non-linear and other finite-amplitude effects, rather than a complete replacement for the e^N method involving more complex and time-consuming analysis.

Acknowledgments

The author would like to acknowledge the collaboration with and input from Dr Geza Schrauf of Airbus SAS, Dr Shahid Mughal of Imperial College, Dr Malcolm Arthur of QinetiQ Ltd and Mr Rob Sunderland of EADS Innovation Works, as well as the past support of the United Kingdom Government, through the Civil Aerospace Research and Development (CARAD) programme and the Ministry of Defence Research Programme. Much of the understanding gleaned on this topic has been through participation in the laminar flow projects funded by the European Commission 3rd, 4th, 5th and 6th Framework Programmes.

References

- [1] Van Ingen J. e^N Method for Transition Prediction: Historical Review of Work at TU Delft. AIAA paper 2008-3830, 38th AIAA Fluid Dynamics Conference, Seattle, 23-26 June 2008.
- [2] Crouch J D. Modeling Transition Physics for Laminar Flow Control. AIAA paper 2008-3832, 38th AIAA Fluid Dynamics Conference, Seattle, 23-26 June 2008.
- [3] Atkin C J, Schrauf G S. Progress in linear stability methods for design applications. Proceedings of ECCOMAS 2000, Barcelona, 11-14 September 2000.
- [4] Herbert, T., Parabolized stability equations, AGARD R 793.4, 1994.
- [5] Gaster M. On the effect of boundary layer growth on flow stability, J. Fluid Mech. Vol. 66, 1974.
- [6] Atkin C J, Mughal M S. Parametric Studies on the Application of Distributed Roughness Elements for Laminar Flow Control. AIAA paper 2005-5263, 35th AIAA Fluid Dynamics Conference, Toronto, 6-9 June 2005.
- [7] Atkin C J, Sunderland R, Mughal M S. Parametric PSE Studies on Distributed Roughness Laminar Flow Control. AIAA paper 2006-3694, 36th AIAA Fluid Dynamics Conference, San Francisco, June 5-8 2006.
- [8] White E B, Saric W S. Application of Variable Leading-Edge Roughness for Transition Control on Swept Wings. AIAA paper 2000-0283, Reno, January 2000.

[9] Saric W S, Reed H L. Toward Practical Laminar Flow Control - Remaining Challenges. AIAA paper 2004-2311, Portland, June 2004.

[10] Arthur M T, Atkin C J. Transition modelling for viscous flow prediction. AIAA paper 2006-3-52, 36th AIAA Fluid Dynamics Conference, San Francisco, June 5-8 2006.

COMPARISON BETWEEN THE WALL ROUGHNESS EFFECT AND THE FREE STREAM TURBULENCE IMPACT AND THEIR JOINT ACTION ON BOUNDARY LAYER DEVELOPMENT

Pavel Jonas, Oton Mazur, Vaclav Uruba

Institute of Thermodynamics v.v.i. AS CR, Prague, Czech Republic.

Abstract

In the paper, the consequences of the individual action and joint action of a sand roughness of the plate surface and homogeneous close to isotropy free stream turbulence on the zero pressure gradient boundary layer development are considered.

1 Introduction

The effects of the roughness elements distributed over a wall (WR) and of the free stream turbulence (FST) on laminar turbulent boundary layer transition are known long ago. In general each of them accelerate the boundary layer development into turbulent boundary layer in comparison with a boundary layer on a smooth surface under a non-turbulent flow and otherwise equal conditions. Understanding of these effects is of practical importance for prediction of flows in many environmental and technical areas. Numerous investigations were published (reviews e.g. [1-5]) on the individual effects of the roughness or free stream turbulence on wall shear flow but the knowledge on the joint action of these effects is very poor [6,7] even though they may be important under many circumstances.

The disturbance of a laminar boundary layer by a surface with sand-roughness had not evoked a big attention in past. Kendall [8] gave only three older references and mentioned that the flow is merely displaced outward from the plane on which the roughness grains were adhered. Some data on the effect of 2D or singular 3D roughness are described in [9-11]. The starting point of the surface roughness effect analysis is usually Nikuradse's investigations of flows in pipes of various roughnesses. Particularly turbulent boundary layer is considered.

We shall handle a boundary layer on a flat plate generally with a rough surface under a zero pressure gradient turbulent flow. Many geometrical forms of the surface roughness are possible but here the surface covered with sand paper, the K -type roughness, will be discussed only (e.g. [1 and 9-11]). The maximum height of the roughness grains has been introduced as the representative length (height) s . The effect of the wall roughness on a boundary layer determine: the Reynolds number Re_s formed with the length s and the external flow mean velocity U_e , the ratio of the length s to the viscous length scale δ_ν (the roughness Reynolds number s^+) and the ratio of the boundary layer thickness δ to the roughness height s

$$Re_s = \frac{sU_e}{\nu}; \quad s^+ = \frac{s}{\delta_\nu}; \quad \delta_\nu = \frac{\nu}{u_\tau}; \quad \frac{\delta}{s} \quad (1)$$

ν and u_τ are viscosity and friction velocity.

The effect of surface roughness appears only after exceeding a critical roughness height s_1 , giving $Re_s > 120$. Then the critical Reynolds number $(Re_1)_{crit}$ decreases below the value about 950 valid for the smooth plate e.g. [4]. Customary presented analyses (e.g. [3-5, 11 and 12]) of the roughness effect relate to turbulent boundary layer or channel. They can be briefly summarized as follows. The flow is developing as on a hydraulically smooth surface if the roughness grains are nest in the viscous sub-layer $s^+ < 5$ and the surface behaves as completely rough with grains overhanging the buffer-layer $s^+ > 70$. Further increase of roughness grains does not cause additional qualitative changes of the flow. Transitional roughness region ranges between the above mentioned extreme cases

$$5 \leq s^+ \leq 70 \quad (2)$$

The effect of roughness on the mean flow appears namely in the inner layer in vertical shift of the velocity profile zero level below the level of the roughness peaks (inside the layer of roughness grains), in decreasing the viscous length scale δ_ν and in a downward shift of the log-law. Roughness does not affect the velocity profiles in the overlap and outer regions. Schultz and Flack [3] published a comprehensive analysis of the problem with many interesting references.

The effect of the free stream turbulence (FST) level Iu on the location of transition onset is known as very important and has been investigated long ago, since Dryden, Schubauer and Skramstad in forties e.g. [13]. Later the effect of the turbulence length scale on the start of boundary layer by-pass transition was also proved e.g. [14]. The transition from laminar to turbulent flow structure depends on the specific type of flow and on the type of the acting disturbances that influence the process. Higher level of external flow disturbances $Iu_e > (0.6 \div 1.0)$ percent causes "by-pass transition" with a mechanism converting outer flow turbulence into boundary layer eigen oscillations e.g. Morkovin [15, 16]. According to Greg et al. [17], the stability of boundary layer flow remains the same as in the case of the low external disturbances. But now, the external disturbances continuously penetrating into the layer amplify the production of turbulent spots and thus accelerate the onset of transition and shorten the length of the transition region.

The turbulent boundary layer perturbed by outer flow turbulence is an example of a complex flow. The fundamental difference between a canonical turbulent boundary layer on a smooth wall in non-turbulent stream and the boundary layer under equal conditions except for the external turbulence comes from the fact that the turbulent outer stream is three dimensional, rotational and variable in time and space. Therefore both molecular and

turbulent diffusions are passing through the interface between the layer and the surrounding turbulent flow. The reasons for the existence of the Corsint's super-layer disappear e.g. [18-21]. Owing to this the fluid particles from the interior of the layer driven by the large scale motions penetrate deeper into the surrounding turbulent external flow and on the contrary, the outer flow particles-turbulent eddies are entrained into the layer nearer to the wall. Turbulent diffusion across the layer amplifies. This has an impact on the increase of the friction velocity. The external turbulence is indistinguishable from the turbulence generating inside the layer provided that the external flow velocity fluctuations are not too large in comparison with the friction velocity. Thus the external turbulence does not affect the universal features of the mean flow in the inner region. The FST effect appears namely in the thickening the layer, altering the velocity defect law in the outer layer and decreasing the viscous length scale e.g. [18-21].

The aim of the paper is to compare consequences of the individual action and the joint action of the sandpaper roughness on the flat plate surface and grid turbulence in external flow on the development of the zero pressure gradient boundary layer. It seemed useful to follow up the experiments conducted in the framework of investigations for the COST/ERCOFTAC Test Case T3A+ e.g. [22].

2 Experimental facility and measurement technique

In the primary configuration, the flat plate boundary layer, is investigated experimentally on an aerodynamically smooth plate (2.75m long and 0.9m wide) in the close circuit wind tunnel IT AS CR, Prague (0.5x0.9)m². The leading edge is very thin (2mm) and its shape was designed after Kosorygin et al. [23]. Covering the primary plate with the sandpaper (grits 80) on a thin plywood plate (7mm thick) modifies the wall roughness. The rough plate leading edge has an elliptic shape ($a \times b = 60 \times 20 \text{ mm}^2$), which covers the primary leading edge. The maximum height of grains on the sandpaper, the representative roughness length, is

$$s(\text{grits } 80) = 0.343 \pm 0.009\text{mm}. \quad (3)$$

The orthogonal clockwise coordinates system $[x, y, z]$ is introduced with the coordinate x in the streamwise direction and the plane $z = 0$ identical with the plane of vertical symmetry. The $x = 0$ is in the leading edge plane and the plane $y = 0$ is the zero level i.e. the plane where the mean flow velocity equals zero $U(0) = 0$. The zero level lies on the aerodynamically smooth surface. In case of a rough surface the velocity zero level is between the roughness grains bottoms plane and the grains tops plane. Hence an auxiliary coordinate y' is useful with $y' = 0$ in the grains tops plane.

Free stream turbulence (FST) is either natural (indicated as No GT) or produced by means of square mesh (M) plane grids/screens with cylindrical rods (d). Grid placed in the plane $x = x_{GT}$ generates homogeneous and close to isotropy turbulence. The intensity and the dissipation length parameter [27] characterize the fundamental features of the grid turbulence

$$Iu = \sqrt{\overline{(u^2)}} / U_e; \quad L = -\overline{(u^2)}^{3/2} / U_e \frac{\partial \overline{(u^2)}}{\partial x} \quad (4)$$

Grid	$d[\text{mm}]/M[\text{mm}]$	$-x_{GT}[\text{m}]$	$Iu(0)$	$Le(0)$ [mm]
No GT			0.003	~ 10
GT1	3/20	0.454	0.030	5.9
GT4	6/20	0.738	0.030	16.2
GT5	10/35	1.2107	0.030	33.4
GT8A	1.65/5.75	0.787	0.010	5.7
GT8B	1.65/5.75	0.194	0.030	3.8
GT8C	1.65/5.75	0.125	0.050	2.2

Table 1: *Main characteristics of free stream turbulence downstream individual grid generators.*

where U_e and u are the mean velocity of external flow and the longitudinal component of velocity fluctuations. Subscript e attached to any quantity denotes value valid in the plane $x = 0$. Main characteristics of FST in the course of experiments are shown in Table 1.

More details of experimental facility and free stream turbulence structure are presented in [14].

The essence of this investigations are measurements of mean velocity profiles $U(x, y, 0)$ in the plane $z = 0$. So it was possible prefer the pressure measurements to CTA method (well proved in past [14]) with regard to the surface roughness and the breakability of hot-wire probes. Measurements were carried out by means of the couple of the flattened Pitot probe (0.18 x 2.95mm²) and round nosed static pressure probe (dia = 0.18mm). The space between probes was 55mm in y direction. The pressure difference - dynamic pressure q [Pa] was measured by means of the pressure transducer BARATRON (special order on high accuracy, max 1kPa; $\pm 0.02\%$ of reading above 20Pa). The pressure transducer Druck DPI 145 (max 100kPa; $\pm 0.005\%$ FS) was used for measurement of the absolute static pressure P [Pa] and the barometric pressure B [Pa]. Pitot-static tube (dia = 6mm) connected with the pressure transducer OMEGA Techn. Ltd., (max 1.2 kPa; $\pm 0.25\%$ FS) was used for measurement of the representative pressure q_r (the location of the probe nose: $x = 0.23\text{m}$, $y = 0.13\text{m}$ and $z = 0.36\text{m}$) and thermometer Pt100 connected to the Data Acquisition/Switch Unit HP 34970A was applied for the flow temperature t [°C] measurement. The vertical feed of the probe was controlled by the PC.

Output signals proportional to the mean values of P , B and t were read by means of the unit HP 34970A just after the start of measurement in any point $[x, y, 0]$ and each time recorded. Afterwards representative pressure q_r [Pa] and the local dynamic pressure $q(x, y)$ [Pa] were simultaneously measured and 30 seconds sampled (10kHz, 16 bit) and recorded in a personal computer.

3 Error estimates and evaluation methods

Estimates of upper limits of relative measurement errors derived from the accuracy of applied devices and with the regard to the scatter of repeated observations are following

$$\begin{aligned} \frac{\Delta q_r}{q_r} &\leq \pm 0.02atU_r \cong 5\text{m/s}; \\ \frac{\Delta q}{q} &\leq \pm 0.02atU(x, y) \geq 0.6\text{m/s}; \\ \Delta P &\approx \pm 5 \text{ Pa} \end{aligned} \quad (5)$$

The representative velocity U_r was held in average on 5m/s in the course of all measurements presented here. The mean velocity error was less then 1 percent during

measurements more than 1mm from the surface, closer to the surface the error approached 3 percent.

Estimates of relative probable errors of the displacement thickness δ_1 and the momentum one δ_2 , the shape factor H_{12} and the wall friction τ_w follow essentially from the performed error analysis in the case of a smooth surface. In fact a dead travel of the probe traversing unit and the shift of zero level in the case with rough surface introduce some additional errors.

At the beginning of the evaluation, the correction was done to avoid errors caused by small and slow variations of the external flow velocity U_e in course of the measurement and the effect of wall proximity on measurement by means of a flattened Pitot tube was rectified after the procedure proposed by MacMillan e.g. [25]. Wall shear stress $\tau_w(x)$ [Pa] was evaluated from mean velocity profiles $U(x, y)$ either from the slope interpolated very near the surface or from the interpolation of log-law. The first procedure is generally applicable from the onset of boundary layer up to the termination of laminar/turbulent transition. It requires a high accuracy determination of the Pitot probe displacements from the starting position $y' = 0$ with the probe nose in contact with the surface. The observed distance from the wall y' of the probe nose was measured with an accurate cathetometer (reading of 0.01mm). Unfortunately the dead travel of the traversing unit and elastic deflection of the probe nose were sources of uncertainty in ideal touch with the wall. For that reason the interpolation of velocity very near the surface must determine the effective position of wall y'_0 as well as the velocity derivative $(\partial U / \partial y)_w$.

$$U(y) = a + b y' = b(y' - y'_0) = b y; \quad (6)$$

$$0.15\text{mm} < y' \leq 1.0\text{mm}$$

The magnitude of y'_0 is stepwise searching so as reach the best fit of (6). Then the wall friction $\tau_w(x)$, friction velocity u_τ and friction coefficient C_f are computed from formulas

$$\tau_w = \mu \left(\frac{\partial U}{\partial y} \right)_w = \mu b; \quad (7)$$

$$u_\tau = \sqrt{\frac{\tau_w}{\rho}}; \quad C_f = \frac{\tau_w}{q_e}.$$

This procedure works very satisfactory in laminar layers and in boundary layers that are not far from the transition start. The estimated error of calculated τ_w is less than 4 percent. The error estimate increases with thickening of the viscous sublayer.

The log-law interpolation can be applied for the evaluation of y'_0 , u_τ and the function of roughness Δu^+ (in case with rough surface) in the overlap (logarithmic) layer of a fully developed turbulent boundary layer. It is customary to write the log-law in the form

$$u^+ = \frac{U}{u_\tau} = \frac{1}{\kappa} \ln(y^+) + B - \Delta u^+(s^+); \quad (8)$$

$$y^+ = \frac{y u_\tau}{\nu}; \quad y = y' - y'_0. \quad (9)$$

where $\kappa = 0.41$ and $B = 5$ are the von Kármán constant and the smooth wall log-law intercept. The evaluation of the three unknowns is executed by means of the equation (8) rearranged in the form

$$\frac{\bar{U}}{\bar{U}_e} = a \ln \left(\frac{(y' - y'_0) \bar{U}_e}{\nu} \right) + b \quad (10)$$

The task is: to interpolate this regression function in the region of the log-law validity (in the 1st approximation: $\sim 30 < y^+ < \sim 750$) and to determine unknowns so

as the correlation coefficient became maximum (canonical definition of r^2) and simultaneously the following requirements are to be met: the relation $\min u^+ \leq y^+$ and at least several points of measurement have to approach the Clauser approximation

$$\frac{U_e - U(y)}{u_\tau} = -\frac{1}{\kappa} \ln \left(\frac{y}{\delta} \right) + 2.5 \quad (11)$$

outward the log-region and little further. Subsequently the remaining unknowns u_τ and Δu^+ are determined

$$\frac{u_\tau}{\bar{U}_e} = \kappa a; \quad \Delta u^+ = \frac{1}{\kappa} \ln \left(\frac{u_\tau}{\bar{U}_e} \right) + B - \frac{1}{\kappa} \frac{b}{a}. \quad (12)$$

It was possible to apply both procedures (6) and (10) occasionally. The differences in estimates of unknowns were less than 10 percent.

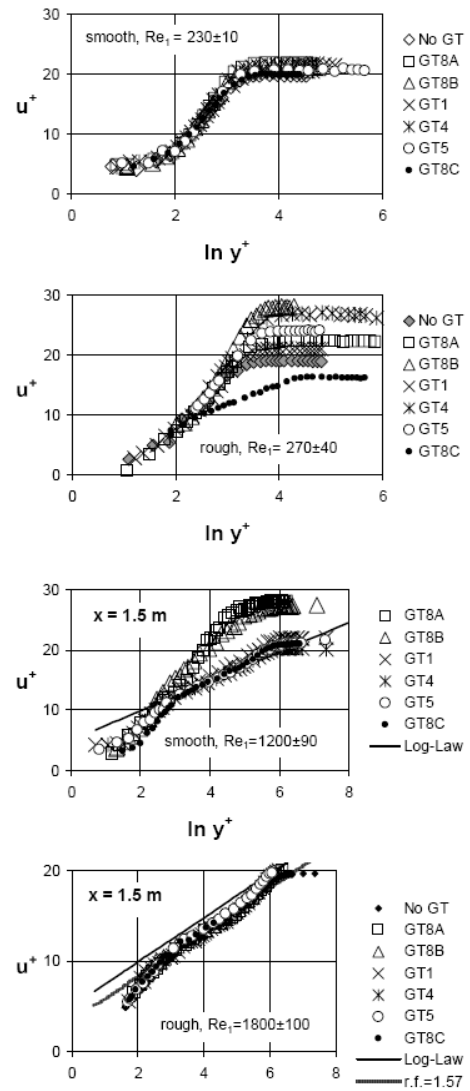


Figure 1: Comparison between mean velocity profiles on smooth and rough surface at $x = 0.05$ and 1.5m .

4 Results

A series of semi-logarithmic plot of velocity profiles shown in Figure 1 illustrates differences between boundary layers on hydraulically smooth flat plate and boundary layers on flat plate with transitional roughness of

the surface at otherwise same boundary conditions. The profiles acquired very near the leading edge, $x = 0.05\text{m}$ and those acquired at the downstream end of the investigated region, $x = 1.5\text{m}$ are demonstrated. The laminar profiles, very close to the Blasius solution are near the onset of boundary layer on aerodynamically smooth wall. The surface roughness induces a malformation of laminar shape of profiles and FST intensity accelerates this progress. Profiles measured in the section $x = 1.5\text{m}$ are of transitional kind on smooth plate provided that the level of FST is not high enough. Surface roughness accelerates the transition to turbulent state and the velocity profiles follow the log-law (8).

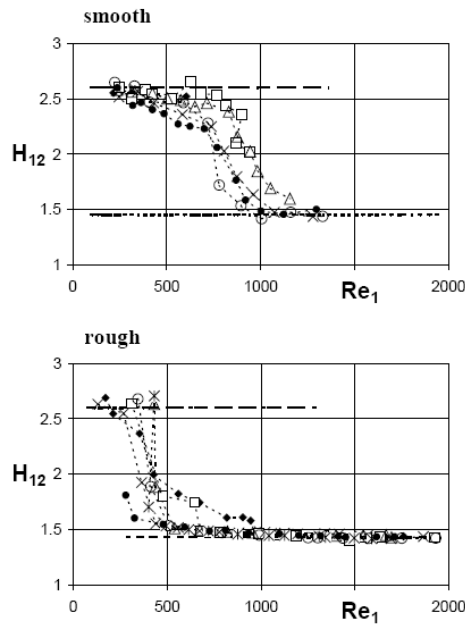


Figure 2: Comparison of the shape factor distribution (meaning of the symbols see figure 1).

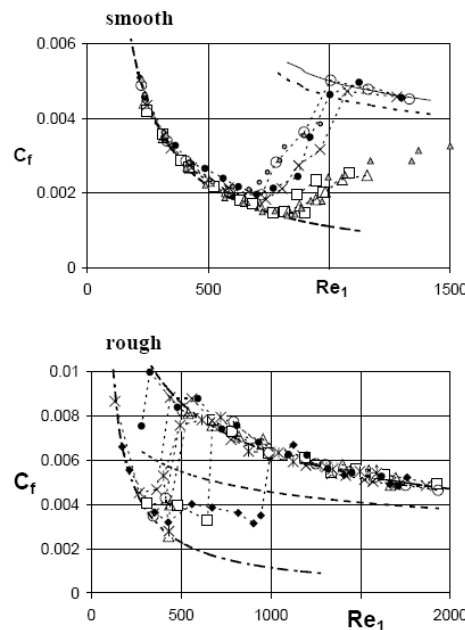


Figure 3: Comparison of the skin friction coefficient distributions (symbols as in figure 2).

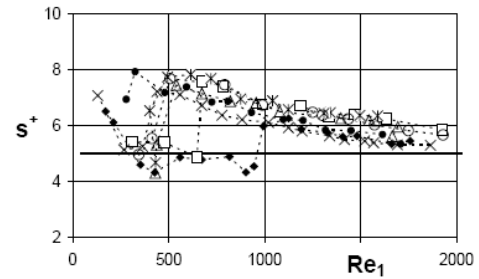


Figure 4: Surface roughness parameter (symbols as in figure 1).

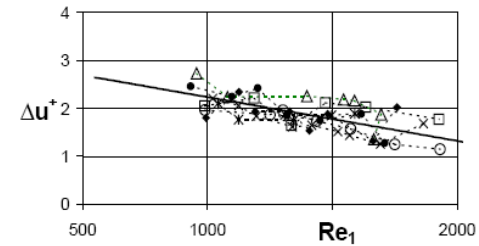


Figure 5: Roughness function Δu^+ (symbols as in figure 1).

Analysing the mean velocity profiles, the displacement thickness Reynolds number $Re_1 = \delta_1 U_e / \nu$, the distributions of the shape factor H_{12} (Figure 2), the skin-friction coefficient C_f (Figure 3), the surface roughness parameter s^+ (Figure 4), the roughness function Δu^+ (Figure 5) and the mean velocity zero level y'_0 were evaluated.

The distributions shown in Figures 2 and 3 clearly confirm the dominant effect of surface roughness on the transition process but simultaneously demonstrate the contribution of FST to the acceleration of transition process. The distributions shown in Figures 1 to 3 indicate that there is necessarily a boundary layer evolution from quasi laminar state to turbulence even though the surface is considerably rough.

A more detailed analysis proves that the effect of FST scales on boundary layer on rough surface is similar to that effect known from investigations of boundary layers on smooth surfaces e.g. [14]. In Figures 2 and 3, the distributions of characteristics H_{12} and C_f valid in boundary layers on a smooth plate are drawn by dashed lines (Blasius solution) and by dotted line (Ludwig and Tillmann empirical formulae) e.g. [4]. Full line represents the course of the interpolation of results received in external turbulence with 3% intensity at the leading edge regardless the length parameter.

The evaluated distributions of the surface roughness parameter s^+ are shown in Figure 4. The values of s^+ stay near the lower bound of the transitional roughness region (2) and they are continuously decreasing with the increasing distance x from the leading edge after completing the transition.

The roughness function Δu^+ derived from the log-law interpolation (8) moderately decreases with the increasing Reynolds number Re_1 (see Figure 5). Standard deviations of the individual estimates of Δu^+ are about 0.3. Preliminary analysis indicates that this function decreases with the increasing distance x at $U_e = \text{const}$, Δu^+ constant with increasing velocity at $x = \text{const}$. and the roughness function increases with the turbulence intensity Iu_e .

The velocity zero level y'_0 (6), (8) was derived simultaneously with the log-law interpolations. Technically speaking the value of y'_0 does not depend on the distance x and on the intensity Iu_e . Its average value is of $(0.12 \pm 0.05)\text{mm}$. Then the zero level ($U = 0$) is below the top plane of the highest roughness elements $s = (0.34 \pm 0.01)\text{mm}$ of about 34 percent of the dimension of largest roughness grains.

5 Conclusions

The surface roughness, though near the lower bound of transitional roughness region, affects the boundary layer development more dramatically than the free stream turbulence. The FST accelerates the evolution of a boundary layer on rough surface to turbulent flow structure. The intensity as well the length scale of FST play an important role in the process.

The surface roughness significantly shortens the transitional region but the existence and the length of this region could not be neglected even if the FST intensity is remarkable increased.

The evaluations of the wall friction, the roughness function and the shift of mean velocity zero level from the mean velocity measurements are quite a task if not enough points were taken in the region of the wall-low (7) validity. The derived procedure works but the error estimates are not quite satisfactory. A method of direct measuring the wall friction on generally rough surface is needed.

Acknowledgements

This work was supported by the Grant Agency of the Academy of Sciences of the Czech Republic (project IAA 200760614).

References

[1] Jimenez J. (2004), Turbulent flows over rough walls. Annual Rev. Fluid Mech. 36, 173-196.
 [2] Jonas P. (2008), Mean velocity profiles in a boundary layer under the joint action of surface roughness and external turbulent flow. Applied and Computational Mechanics 2, 273-284.
 [3] Schultz M.P. and Flack K.A. (2007), The rough wall turbulent boundary layer from the hydraulically smooth to the fully rough regime. J. Fluid Mech., 580, 384-405.
 [4] Schlichting H. and Gersten K. (2000), Boundary-Layer Theory. Springer, Berlin.
 [5] Rotta J. C. (1962), Turbulent boundary layer in incompressible flow. In: Progress in Aeronautical Sciences (A. Ferri, D. Kuchemann & L. H. G. Sterne eds.) Pergamon Press, Oxford, 1-220.
 [6] Gibbins J.C. and Al-Shukri S.M. (1996), Characterisation of sandpaper roughness under a turbulent incompressible boundary layer. Aeronaut. J., June/July, 1996, Paper No. 2157, 235-239.
 [7] Gibbins J.C. and Al-Shukri S.M. (1997), Effect of sandpaper roughness and stream turbulence on the laminar layer and its transition. Aeronaut. J., January, 1997, Paper No. 2197, 17-24.
 [8] Kendall J. M. (1990), The effect of small-scale roughness on the mean flow profile of a laminar boundary layer. In Instability and transition (ed. Hussaini & Voigt), Springer, Berlin 1990, pp. 296-302.
 [9] Lachmann G.V. (Ed.) (1961), Boundary Layer and Flow Control. Pergamon Press, Oxford. [10] White E.B. and Ergin F.G. (2003), Receptivity and transient growth of roughness-induced disturbances. AIAA Paper 2003-4243.
 [11] Leonardi S., Orlandi P. and Antonia R.A. (2007), Properties of d- and k-type roughness in a turbulent channel flow. Phys. Fluids 19, 125101.
 [12] Pope S. B. (2000), Turbulent flows. Cambridge University Press, Cambridge.

[13] Schubauer G.B. and Skramstad H.K. (1948), Laminar boundary layer oscillations and transition on a flat plate. NACA Rept. 909.
 [14] Jonas P., Mazur O. and Uruba V. (2000), On the receptivity of the by-pass transition to the length scale of the outer stream turbulence. Eur. J. Mech. B - Fluids 19, 707-722.
 [15] Morkovin M.V. (1969), On the many faces of transition. In: Viscous Drag Reduction, (ed. C.S. Wells), Plenum, New York, pp. 1-31.
 [16] Morkovin M.V. (1993), Bypass transition research: issues and philosophy. Instabilities and Turbulence. In: Engineering Flows (D. Ashpis, T. Gatski & R. Hirsh, eds.) Kluwer, Amsterdam, 3-30.
 [17] Grek G.R., Kozlov V.V. and Ramazanov M.P. (1991), Boundary layer stability investigation at increased outer stream turbulence level. Sibir. Phys.-Tech. J., 6, 106, pp. 117-125. (in Russian).
 [18] Hancock P.E. (1980), The effect of free stream turbulence on turbulent boundary layer. PhD. -Thesis, Imperial College, University of London.
 [19] Hancock P.E. and Bradshaw P. (1989), Turbulence structure of a boundary layer beneath a turbulent free stream. J. Fluid Mech., 205, 45-76.
 [20] Huffman G.D., Zimmerman D.R. and Bennet W.A. (1972), The effect of free stream turbulence level on turbulent boundary layer behaviour. AGARD Proc. of Meeting on Boundary Layer Effects in Turbomachines. Vol. AG164, 91-115.
 [21] Jonas P. (1992), On turbulent boundary layer perturbed by outer flow turbulence. Energetika Nr. 3 (ISSN 0235-7208), Vilnius, Latvia, 69-80.
 [22] Savill A.M. (1995), COST-ERCOFTAC transition SIG COST action workshop IT AS CR Prague. ERCOFTAC Bulletin No. 25, 36-37.
 [23] Kosorygin V. S., Levchenko V. Ja. and Polyakov N. F. (1982), On problem of the origin of waves in a laminar boundary layer. Preprints ITPM, No. 12-82, ITPM SO AN SSSR, Novosibirsk (in Russian).
 [24] Hancock P.E. and Bradshaw P. (1983), The effect of free stream turbulence on turbulent boundary layers. Trans. ASME, J. of Fluid Engng., 105, 287-289.
 [25] Tropea C., Yarin A. L. and Foss J. F. (Eds.) (2007), Springer Handbook of Experimental Fluid mechanics. Springer-Verlag Berlin.

BYPASS TRANSITION INDUCED BY ROUGHNESS ELEMENTS: PREDICTION USING A MODEL BASED ON KLEBANOFF MODES AMPLIFICATION

Olivier Vermeersch & Daniel Arnal

ONERA, Aerodynamics and Energetics Department, France.

1 Introduction

Many experiments have demonstrated that roughness imperfections could have a deep impact on the laminar-turbulent transition process. Many surface imperfections (such as rivets, insects ...) are unavoidable. So it is necessary to estimate their effects on the stability of the boundary layer. Roughness elements have a dual-influence on the flow. First, they modify the mean flow and so modify its stability properties. Secondly, they can introduce small perturbations inside the boundary layer : they act on the receptivity process which is a key stage for stability studies. The influence of the roughness elements on the mean flow used to be taken into account with a Reynolds number Re_{kk} based on the height of the roughness and the value of the velocity at this height without roughness. It has been shown that two-dimensional surface imperfections can be analysed with the linear stability theory : for increasing roughness height, the transition moves upstream : physically, two-dimensional defects strongly amplify the unstable TS waves [3]. Nonetheless, Reshotko highlights the fact that attempts to find a TS explanation for three-dimensional roughness, both discrete and distributed, have failed [11]. For isolated roughness element, Von Doenhoff and Braslow [6] showed that transition occurred when the R_{kk} reached a threshold : this value depending on the ratio between the diameter and the height of the roughness. Acarlar and Smith [1] have shown that an isolated roughness element induced a horseshoe vortex whose legs consisted in two counter-rotating stationary vortices. Optimal perturbation theory [9, 2, 13] has pointed out that the most amplified perturbations inside both incompressible and compressible boundary layer were also created by stationary streamwise vortices. It is the "Lift-up effect" introduced by Landahl : a vortex superimposed to the boundary layer shear pushes up low speed particles from the wall to the top of the boundary layer, and pulls down high speed particles towards the wall leading to a spanwise alternation of backward and streamwise jet streaky structures called the Klebanoff modes [8]. Klebanoff modes can undergo a 'transient growth' process meaning that the amplitude of the streaks can be heavily amplified. If the energy of the Klebanoff modes significantly raises, an early laminar turbulent transition can be triggered : this is the so-called Bypass, a term introduced by Morkovin [10], meaning that the natural transition process, driven by the TS waves, has been short-circuited. Transient growth is an attractive mechanism to consider with respect to roughness induced transition [11].

As a matter of fact, Fransson and *al.* [7] have observed a transient amplification of the longitudinal velocity fluctuation behind an array of roughness elements.

The streamwise velocity fluctuation clearly showed a transient amplification for the fundamental mode corresponding to the roughness array periodicity. Fransson also noted that the streaks induced by the roughness were suboptimal ones. This may be due to the fact that vortices don't match with the ones predicted by optimal perturbations and are closer to the wall. White and *al.* [15, 16], performed many experiments of roughness induced transient growth. They found out that the higher harmonics $\lambda_0/3$ and $\lambda_0/4$ have transient amplification just aft the element and that the amplification of the fundamental spanwise wavenumber perturbation started downstream. A striking characteristic is that Fransson obtained a positive u' -fluctuation in the centerline of the roughness whereas White has a negative one. The discrepancy has been explained by Tumin and Reshotko [12] : using bi-orthogonal decomposition, they showed that behind a hump, there was a deficit velocity region, called 'wake region', surrounded by the legs of the horseshoe vortex : if the magnitude of the vortices is high enough the wake region may be filled in and cancelled by the wash motion induced by the vortices and the sign of the u' -fluctuation may be switched over. We can think that the larger the roughness is, the more extended the wake region would be. So, the topology of the flow behind a roughness defect is not only linked to the height but also depends on the diameter (or in the same way on the shape) of the roughness element.

This short paper aims at presenting a model to compute the transient amplification of Klebanoff modes behind 3D roughness elements and predict the early roughness induced transition location.

2 Equation of the model

If the amplitude of the streaks is too high, their influence on the mean flow cannot be neglected. A natural approach consists in applying the boundary layer turbulent equations to describe the laminar zone, even though the fully turbulent state has not been reached yet. Instantaneous quantities are split into a mean part and a fluctuating one :

$$Q = \tilde{Q} + q' \quad (1)$$

In order to make the equation dimensionless, typical length and velocity scales are introduced. We know that subcritical roughness induced streaky streamwise elongated structures : therefore, a typical scale of the geometry L (for instance the length of the flat plate or the chord of the wing) is used to normalize the streamwise coordinate. In the wall normal direction, a typical boundary layer thickness $\delta = L/\sqrt{Re_L}$ is applied to characterize the diffusion process. The continuity equation, satisfied by the Klebanoff modes implies that if u' is in order of

$U_0, v' = O(U_0/\sqrt{Re_L})$. These scales were introduced by Prandtl to study laminar boundary layers. These assumptions for two-dimensional incompressible boundary layers lead to the following system of equations :

$$\tilde{U}_x + \tilde{V}_y = 0 \quad (2a)$$

$$\tilde{U}\tilde{U}_x + \tilde{V}\tilde{V}_y = U_e U_{e_x} + \nu \tilde{U}_{yy} + \overline{u'u'_x} + \overline{u'v'_y} \quad (2b)$$

$$u'_t + (\tilde{U}u')_x + \tilde{V}u'_y + v'\tilde{U}_y = \nu (u'_{yy} + u'_{zz}) \quad (2c)$$

The terms $\overline{u'u'_x}$ and $\overline{u'v'_y}$ describe the influence of the streaks on the mean flow. The Klebanoff modes consist in u' -fluctuations and verify the equation (2c). In order to close the system (2) in the laminar region, the wall normal velocity has to be modelled.

This aims at expressing the "Lift-up" effect in accordance with the fact that a wall normal velocity perturbation in a shear flow brings about the emergence and the amplification of streamwise velocity fluctuations. Owing to the Prandtl scales, all dimensionless equations are parabolic in nature. So if the wall normal velocity is modelled, u' can be computed by an upward numerical scheme using the values of the mean flow at the previous station. So the averaged equation (2b) can be solved taking into account the terms which describe the influence of the streaks on the mean flow. The key stage now, is to model the wall normal velocity disturbance induced by the roughness element.

3 Wall normal velocity fluctuation modelling

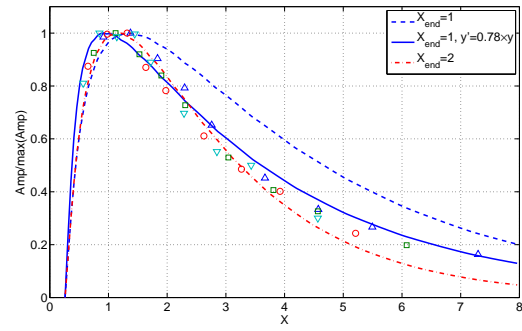
In order to model the wall normal velocity fluctuation induced by roughness elements, we use the experimental results of Fransson [7].

Fransson experiment

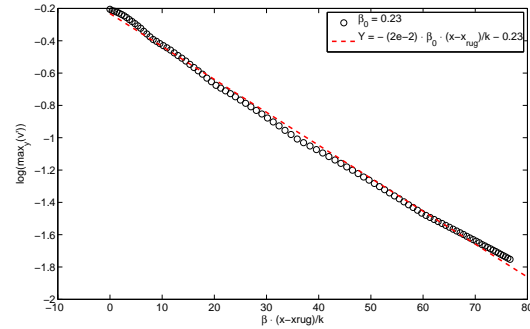
Fransson and *al.* performed streaks hot wire measurements behind an array of cylinders. The cylinders were located at $x_0 = 40$ [mm] from the leading edge, had a diameter of $d = 2$ [mm] and were $\lambda_0 = 8$ [mm] spaced out. They were $k = 780$ [μm] tall such as at $U_\infty = 7$ [m/s] the Reynolds number based on the roughness height is $Re_{kk} = 285$ *ie.* below the transition threshold of Von Doenhoff and Braslow criterion. Experiments were performed at four different free stream velocities $U_\infty = 5, 6, 7$ and 8 [m/s] in order to regulate the amplitude of the streaks changing the ratio k/δ which varied between 2.24 and 2.84. Hot wire measurements have clearly shown that the streamwise velocity fluctuation inside the boundary layer underwent a transient amplification as illustrated by the symbols of the figure 1(a). In this figure, Fransson and *al.* have used a non dimensional X coordinate, given by the relationship (3), and found out a universal streaks behaviour. The relation implies that at $X = 1$, the spanwise wavenumber matches with the optimal one $\beta = \beta_{opt} = 0.45$ [2, 9].

$$X = \left(\frac{\beta^*}{\beta_{opt}} \right)^2 \cdot \nu \cdot \frac{1}{U_{inf}} \cdot x \quad (3)$$

Besides, power spectral density (PSD) showed that the dominating wavelength was dictated by the roughness array periodicity in the far wake region. Fransson and *al.* have computed the optimal disturbance which corresponded with the most amplified streak at $X_f = 1$; the



(a) Evolution of the Streaks amplitude. Comparison between experimental data (symbols) and Optimal Perturbation Theory (curves).



(b) Amplitude evolution of v' function of β_0

Figure 1: Calibration on the Fransson experiment.

corresponding curve is the dashed line on figure 1(a). They explained the difference between experiment and optimal perturbation theory (OPT) by the fact that the cylinders induced sub-optimal initial disturbances closer to the wall. Fransson and *al.* computed an artificial initial perturbation by compressing the wall normal coordinate y by a factor c : for $c = 0.78$, *ie.* an initial disturbance closer to the wall, the numerical result is in good agreement with the measurements (solid line on figure 1(a)). Here we propose another approach : we have calculated the initial disturbance which maximises the amplitude of induced streaks at the station $X_f = 2$. This also provides good agreement with experimental data as illustrated by the dash-dotted line on figure 1(a). The evolution of the corresponding wall normal velocity fluctuation is presented on figure 1(b) : v' -fluctuation amplitude is decaying exponentially in the streamwise direction.

v' profile

To model the wall normal fluctuating velocity profile, we used the function () proposed by Biau [4, 5]. This function is continuously increasing from the wall to the boundary layer edge, and may not match with the wall normal velocity fluctuation profile really induced by roughness elements. Nonetheless, the goal is to impose a v' fluctuation able to create a lift-up effect and to lead

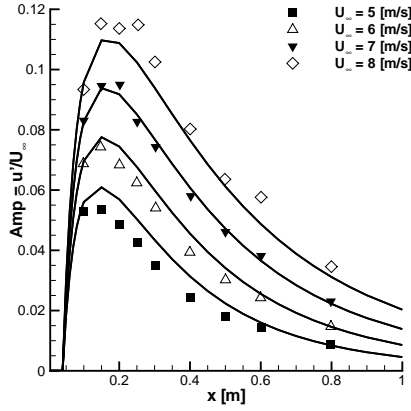


Figure 2: Comparison between Fransson measurements and model.

to the formation of Klebanoff modes.

$$g(y) = \begin{cases} \frac{y^2 e^{-\alpha \cdot y}}{\max_y |y^2 e^{-\alpha \cdot y}|} & \text{if } y \leq \delta_{99} \\ \text{cst} & \text{if } y > \delta_{99} \\ g(y=0) = 0 & \text{(No slip condition)} \end{cases}$$

$$\Rightarrow \begin{cases} \left(\frac{\partial g}{\partial y} \right)_{y=0} = 0 & \text{(Continuity equation)} \\ \alpha = \frac{2}{\delta_{99}} \Rightarrow \left(\frac{\partial g}{\partial y} \right)_{y=\delta_{99}} = 0 & \text{(Derivability at } y = \delta_{99} \text{)} \end{cases}$$

In agreement with *OPT* we choose an exponential formulation for v' :

$$v' = A_1 \cdot (k/\delta_0) \cdot U_e \cdot e^{\left(-A_2 \cdot \beta_0 \cdot \frac{x-x_{r,u,g}}{k}\right)} \cdot g(y) \quad (4)$$

The constant A_2 is given by the slope of the v' evolution on figure 1(b) : $A_2 = 2 \cdot 10^{-3}$. The exponential formulation is function of β_0 : physically, this means that for high spanwise wavenumber, *ie.* $\lambda_z \ll 1$, which corresponds to tightened vortices, the longitudinal dissipation will be higher. In the contrary, extended vortices will tend to propagate further downstream inside the boundary layer. The constant A_1 is chosen such as the numerical amplitude of the streak matches with the measurement at $U_\infty = 7$ [m/s]. We consider that the amplitude depends on the relative height of the roughness compared to the boundary layer thickness. The numerical results obtained solving the system (2) and using the relationship (4) for v' are plotted and compared to Fransson's results in figure 2 for the different free stream velocities. The four cases considered here are all below the critical Reynolds number based on the height of the roughness element (for $U_\infty = 8$ [m/s], $Re_{kk} = 340$). Therefore, the amplitude of the induced streaks is not sufficient to trigger transition. In the next part, we are going to introduce a criterion based on the streaks evolution in order to compute the laminar turbulent transition location.

4 Bypass transition Criterion

Determination of the location of the transition onset is important to determine the boundary layer properties.

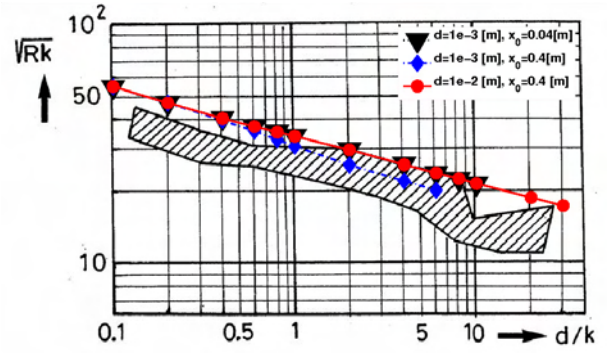


Figure 3: Comparison with Von Doenhoff and Braslow.

Indeed, it determines the streamwise length of the region where the boundary layer remains laminar and fixes the starting point of turbulent area which develops downstream. The computation of the transition location is usually based on a criterion *ie.* a quantity resulting from the calculation of the laminar boundary layer is compared to a threshold value. In the present simulation we use the following expression :

$$\max_{\forall y} \left| \frac{-\rho \cdot \overline{u'v'}}{\mu \frac{\partial U}{\partial y}} \right| = C \quad (5)$$

From a physical point of view, this relationship expresses the fact that transition occurs only when the ratio between the driving term of streak formation $\overline{u'v'}$ and the dissipative one $\partial U / \partial y$ reaches a certain value. This criterion has been calibrated and successfully applied to predict Bypass transition for boundary layers subjected to significant free stream turbulence (*FST*) level [5, 14]. Even though the receptivity process induced by surface defaults is different from the *FST* one, we keep the same transition threshold $C = 0.65$.

For isolated roughness element, the spanwise wavenumber β seems to be dictated by the diameter (thickness). As a matter of fact, Fransson has shown that even though the dominated wavelength corresponded to the distance between the cylinder λ_0 up to $x = 70$ [mm], upstream in the near wake region, higher harmonics presented energy peaks. In the same way, White and *al.* [15, 16] measured transient amplification of $\lambda_0/3$ (which corresponds to the diameter) and $\lambda_0/4$ harmonics just aft the element and before the amplification of the fundamental. This means that for isolated or in the near wake region of an array of roughness elements, the spanwise wavenumber is dictated by the diameter $\beta_0 = (2\pi/d) \cdot \delta_0$.

Van Doenhoff and Braslow criterion

For isolated 3D roughness element of height k , it has been assumed for many years that the relevant parameter is a characteristic Reynolds number based on the roughness height : Re_{kk} . It is often assumed that the value of Re_{kk} for which transition is triggered depends on the ratio d/k . The corresponding critical Reynolds numbers are plotted on figure 3 and scale with $(d/k)^{-\frac{2}{5}}$. We applied our model to transition induced by isolated 3D roughness element. In figure 4, we have plotted the numerical evolution of the streaks amplitude 4(a) and the corresponding value of the criterion, 4(b), $\overline{u'v'}/(\nu dU/dy)$. In the computation, the roughness element has a diameter of 5 [mm] and is placed at $x_0 = 0.2$ [m] from the leading edge. The upstream velocity is fixed to $U_\infty = 10$ [m/s] and the height of the roughness is progressively raised

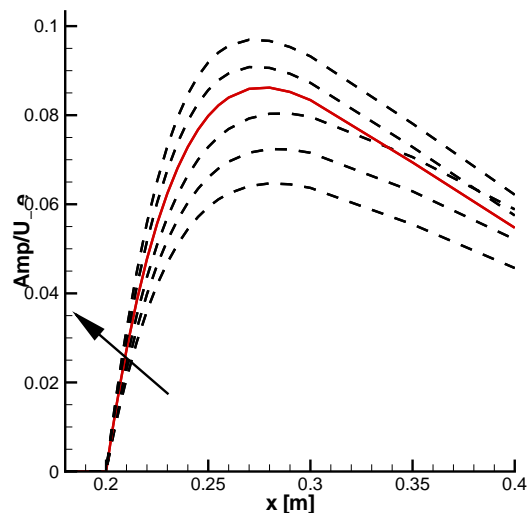
until triggering transition. Bypass transition occurs for $k = 1.15$ [mm], such as $d/k = 4.34$ and $Re_{kk} \approx 500$: this is in close agreement with the value of Von Doenhoff and Braslow. Moreover, we performed three additional simulations, with roughness elements of 1 and 10 [mm] placed at $x_0 = 0.04$ and 0.4 [m] from the leading edge. This time the height is fixed and the upstream velocity is progressively increased so that streaks reached a sufficient amplitude to trigger transition. The results are reported with the Von Doenhoff and Braslow criterion on figure . The agreement is good, in particular the evolution $Re_{kk, crit} \propto \left(\frac{d}{k}\right)^{-2/5}$ is uncovered.

5 Conclusion

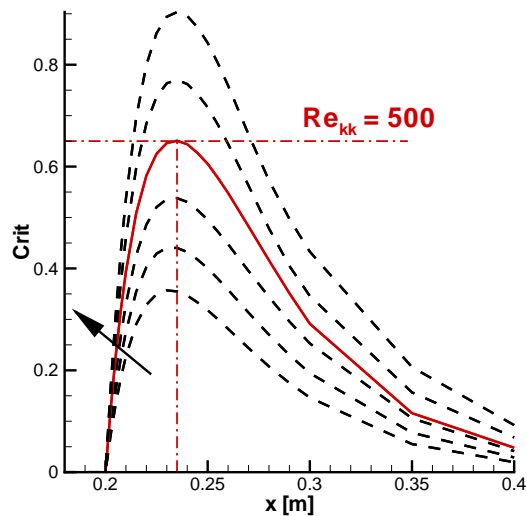
The model proposed here has been calibrated and compared with Fransson's experimental data. It has then be coupled with a Bypass transition criterion and provides numerical results in close agreement with the Von Doenhoff and Braslow's critical Reynolds number. Therefore, transient amplification of Klebanoff modes appeared as a convenient explanation for the early transition due to 3D roughness elements.

References

- [1] M.S. Acarlar and C.R. Smith. A study of hairpin vortices in a laminar boundary layer: part 1, hairpin vortices generated by a hemisphere protuberance. *J. Fluid Mech.*, 1987.
- [2] P. Andersson, M. Berggren, and D.S. Henningson. Optimal disturbances and bypass transition in boundary layers. *Phys. Fluids*, 1999.
- [3] D. Arnal, J. Perraud, and A. Seraudie. Attachment line and surface imperfection problems. Lectures Series 'Advances in Laminar-Turbulent Transition Modelling', VKI, 2008.
- [4] D. Biau. Etude des structures longitudinales dans la couche limite laminaire et de leur lien avec la transition. PhD thesis, Ecole Nationale Supérieure de l'Aéronautique et de l'Espace ENSAE, 2006.
- [5] D. Biau, D. Arnal, and O. Vermeersch. A transition prediction model for boundary layers subjected to free-stream turbulence. *Aerospace Science and Technology*, 2006.
- [6] A.E. Von Doenhoff and A.L. Braslow. Effect of distributed surface roughness on laminar flow. *Boundary Layer Control*, vol. II, Pergamon, Lachmann (ed.), 1961.
- [7] J.H.M Fransson, L. Brandt, A. Talamelli, and C. Cossu. Experimental and theoretical investigation of the nonmodal growth of steady streaks in a flat plate boundary layer. *Phys. Fluids*, 2004.
- [8] P.S. Klebanoff. Effect of free-stream turbulence on a laminar boundary layer. *Bulletin of the American Physical Society*, 1971.
- [9] P. Luchini. Reynolds-number-independent instability of the boundary layer over a flat surface : optimal perturbation. *J. Fluid Mech.*, 2000.
- [10] H.J. Obremski, M.V. Morkovin, and M.T. Landahl. A portfolio of stability characteristics of incompressible boundary layers. *AGARDograph*, 1969.
- [11] E. Reshotko. Roughness-induced transition. Transient growth in 3-D and supersonic flow. Lectures Series 'Advances in Laminar-Turbulent Transition Modelling', VKI, 2008.
- [12] A. Tumin and E. Reshotko. Receptivity of a boundary-layer flow to a three-dimensional hump at finite Reynolds numbers. *Phys. Fluids*, 2005.
- [13] A. Tumin and E. Reshotko. Spatial theory of optimal disturbances in boundary layer. *Phys. Fluids*, 2001.
- [14] O. Vermeersch and D. Arnal. Bypass transition prediction using a model based on transient growth theory. *AIAA Conference*, San Antonio, 22-25 June 2009, 2009.
- [15] E.B White. Transient growth of stationary disturbances in a flat plate boundary layer. *Phys. Fluids*, 2002.
- [16] E.B White, J.M Rice, and F.G Ergin. Receptivity of stationary transient disturbances to surface roughness. *Phys. Fluids*, 2002.



(a) Streak amplitude.



(b) Transition criterion

Figure 4: Transition criterion evolution in function of the roughness height k . The arrow indicates increasing k from 1mm to 1.3mm with a 0.05mm step. $U_\infty = 10$ m/s, $d = 5$ mm, $x_{rug} = 0.2$ m.



Technology Awareness: 2nd Industrial Seminar

'Microfluidics & Microheat'

11th November 2009

Philips Applied Technologies,
Eindhoven, The Netherlands.

ERCOFTAC, world community in applied fluid mechanics, is proud to announce a seminar on 'Microfluidics and Microheat' as part of the **ERCOFTAC Technology Awareness Industrial Seminar Series**.

The development of microscale systems has been growing rapidly, making many engineering applications possible. It is now commonly accepted that miniaturization associated to micro-technologies will give birth in the near future to new objects which will affect industrial practice and our daily life in many aspects. There is no end to the field of application, from basic mixing, to compact heat exchanger, chip cooling in electronic devices, micro-reactors, biological systems and beyond. This field represents one of the best arenas for innovation and the emergence of green technologies, without incurring a large capital cost, as demonstrated by lab-on-chip technologies.

The aim of the seminar is to deliver a set of presentations that captures much of the aforementioned in the field of microfluidics and microheat, with emphasis on technologies that are amenable to early industrial R&D cycle. Therefore, the talks will indicate present level of research with a speculative view on what the future holds, with practicability borne in mind. At the end of the day, the delegates are offered a tour of the facilities.

Invited Speakers

- Baelmans, T. *Univ. of Kuleuven, Belgium.*
- Baroud, C. *Ecole Polytechnique, France.*
- Celata, G.P. *ENEA, Italy.*
- den Toonder, J. *Philips Applied Technologies, The Netherlands.*
- Frijns, A. *TU Eindhoven, The Netherlands.*
- Tardu, S. *Université J. Fourier Grenoble, France.*

Proposed Schedule

- 8:45 *Registration and coffee*
- 9:15 'Micro-mixing systems'
Prof. Sedat Tardu
- 10:00 'Optically controlled droplet microfluidics'
Prof. Charles Baroud
- 10:45 *Refreshments*
- 11:05 'Microfluidics for lab-on-chip applications'
Prof. Jaap den Toonder
- 11:50 'Fluid flow and heat transfer in single and two-phase flow'
Prof. Gian Piero Celata
- 12:35 *Lunch*
- 13:40 'Micro-channel applications for heat sinks and compact heat exchangers'
Prof. Tine Baelmans
- 14:25 'Evaporative cooling of electronic devices'
Dr. Arjan Frijns
- 15:10 *Refreshments*
- 15:30 Brief Q&A
- 15:50 Tour of facilities
- 16:30 *Seminar closes*

Registration and fees

- €170 *ERCOFTAC members*
- €260 *Non-ERCOFTAC members*

- ★ This fee includes: seminar registration, seminar material, refreshments, lunch and a tour of the facilities. Please note that accommodation is not included in this fee. Places are limited, so please contact Dr. Richard Seoud at the earliest opportunity to reserve a place:

Dr. Richard E. Seoud
ERCOFTAC Industry Engagement Officer
Tel: +44 208 543 9343
Email: richard.seoud-ieo@ercoftac.org

ERCOFTAC Special Interest Groups

1. Large Eddy Simulation

Geurts, B.J.
University of Twente, Holland.
Tel: +31 53 489 4125
Fax: +
b.j.geurts@math.utwente.nl

4. Turbulence in Compressible Flows

Comte, P.
University of Poitiers, France.
Tel: +33 5 49 36 60 11
Fax: +33 5 49 36 60 01
Pierre.comte@tea.univ-poitiers.fr

5. Environmental CFD

Morvan, H.
University of Nottingham, England.
Tel: +44 115 846 6374
Fax: +44 115 951 3898
herve.morvan@nottingham.ac.uk

10. Transition Modelling

Dick, E.,
University of Gent, Belgium.
Tel: +32 9 264 3301
Fax: +32 9 264 3586
erik.dick@ugent.be

12. Dispersed Turbulent Two Phase Flows

Sommerfeld, M.
Martin-Luther University, Germany.
Tel: +49 3461 462 879
Fax: +49 3461 462 878
martin.sommerfeld@iw.uni-halle.de

14. Stably Stratified and Rotating Flows

Redondo, J.M.
UPC, Spain.
Tel: +34 93 401 7984
Fax: +34 93 401 6090
Redondo@fa.upc.es

15. Turbulence Modelling

Jakirlic, S.
Darmstadt University of Technology,
Germany.
Tel: +49 6151 16 3554
Fax: +49 6151 16 4754
s.jakirlic@sla.tu-darmstadt.de

20. Drag Reduction and Flow Control

Choi, K-S.
University of Nottingham, England.
Tel: +44 115 9513 792
Fax: +44 115 9513 800
kwing-so-choi@nottingham.ac.uk

24. Variable Density Turbulent Flows

Anselmet, F.
IMST, France.
Tel: +33 4 91 505 439
Fax: +33 4 91 081 637
fabian.anselmet@irphe.univ-mrs.fr

28. Reactive Flows

Tomboulides, A.
Aristotle University of Thessaloniki,
Greece.
Tel: +30 2310 991 306
Fax: +30 2310 991 304
ananiast@enman.auth.gr

32. Particle Image Velocimetry

Stanislas, M.
Ecole Centrale de Lille, France.
Tel: +33 3 20 337 170
Fax: +33 3 20 337 169
stanislas@ec-lille.fr

33. Transition Mechanisms, Prediction and Control

Hanifi, A.
FOI, Sweden.
Tel: +46 8 5550 4334
Fax: +46 8 5550 3481
ardeshir.hanifi@foi.se

34. Design Optimisation

Giannakoglou, K.
NTUA, Greece.
Tel: +30 210 772 1636
Fax: +30 210 772 3789
kgianna@central.ntua.gr

35. Multipoint Turbulence Structure and Modelling

Cambon, C.
ECL Ecully, France.
Tel: +33 4 72 186 161
Fax: +33 4 78 647 145
claude.cambon@ec-lyon.fr

36. Swirling Flows

Braza, M.
IMFT, France.
Tel: +33 5 61 285 839
Fax: +33 5 61 285 899
braza@imft.fr

37. Bio-Fluid Mechanics

Van Steenhoven, A.A.
Eindhoven University of Technology,
Holland.
Tel: +31 40 2472 722
Fax: +31 40 2433 445
a.a.v.steenhoven@wtb.tue.nl

38. Microfluids and Micro Heat Transfer

Tardu, S.
Laboratoire des Ecoulements
Géophysiques et Industriels,
France.
sedat.tardu@hmg.inpg.fr

39. Aeroacoustics

Juvé, D.
Ecole Centrale de Lyon, France.
Tel: +33 4 72 186 429
Fax: +33 4 78 331 140
denyse.juve@ec-lyon.fr

40. Smoothed Particle Hydrodynamics

Violeau, D.
EDF, France.
Tel: +33 1 30 87 78 31
Fax:
damien.violeau@edf.fr

41. Fluid Structure Interaction

Longatte, E.
EDF, France.
Tel: +33 1 30 87 80 87
Fax: +33 1 30 87 77 27
elisabeth.longatte@edf.fr

42. Synthetic Models in Turbulence

Nicolleau, F.
University of Sheffield, England.
Tel: +44 114 22 27867
Fax: +44 114 22 27890
f.nicolleau@sheffield.ac.uk

43. Fibre Suspension Flows

Hämäläinen, J.
University of Kuopio, Finland.
Tel: +358 17 162279
Fax: +358 17 162585
jari.hamalainen@uku.fi

101. Quality and Trust in Industrial CFD

Hutton, A.G.
Airbus UK, England.
Tel: +44 117 936 7519
Fax:
anthony.hutton@airbus.com

102. ERCOFTAC Database Interests Group

Laurence, D.
UMIST, England.
Tel: +44 161 200 3704
Fax: +44 161 200 3723
dominique.laurence@manchester.ac.uk

ERCOFTAC Pilot Centres

Alpe – Danube – Adria

Reichl, C.
Austrian Institute of Technology,
Giefinggasse 2,
A-1210 Wien,
Austria.
Tel: +43 1 50550 6605
Fax: +43 1 50550 6439
christoph.reichl@arsenal.ac.at

Belgium

Geuzaine, P.
Cenaero,
CFD Multi-physics Group,
Rue des Frères Wright 29,
B-6041 Gosselies,
Belgium.
Tel: +32 71 919 334
philippe.geuzaine@cenaero.be

Czech Republic

Bodnar, T.
Institute of Thermomechanics AS CR,
5 Dolejskova,
CZ-18200 Praha 8,
Czech Republic.
Tel: +420 224 357 548
Fax: +420 224 920 677
bodnar@marian.fsik.cvut.cz

France – Henri Bénard

Cambon, C.
Ecole Centrale de Lyon.
LMFA,
B.P. 163,
F-69131 Ecully Cedex,
France.
Tel: +33 4 72 18 6161
Fax: +33 4 78 64 7145
claude.cambon@ec-lyon.fr

France South

Braza, M.
IMF Toulouse,
CNRS UMR – 5502,
Allée du Prof. Camille Soula 1,
F-31400 Toulouse Cedex,
France.
Tel: +33 5 61 28 5839
Fax: +33 5 61 28 5899
marianna.braza@imft.fr

France West

Bonnet, J-P.
Université de Poitiers,
Centre d'Etudes Aérodyn. et Thermiques,
43 Route de l'Aérodrome,
F-86036 Poitiers Cedex,
France.
Tel: +33 5 49 36 60 31
Fax: +33 5 49 45 60 01
jean-paul.bonnet@univ-poitiers.fr

Germany North

Gauger, N.
German Aerospace Center – DLR,
Institute of Aerodynamics,
Lilienthalplatz 7,
D-38108 Braunschweig,
Germany.
Tel: +49 531 295 3339
Fax: +49 531 295 2914
nicolas.gauger@dlr.de

Germany South

von Terzi, D.
Inst. Thermische Strömungsmaschinen,
Universität Karlsruhe (TH),
Kaiserstr. 12 (Geb. 10.91, Zi. 201)
D-76131 Karlsruhe,
Germany.
Tel: +49 721 608 6829
vonterzi@its.uni-karlsruhe.de

Germany West

Schröder, W.
RWTH – Aachen,
Institute of Aerodynamics,
D-52062 Aachen,
Germany.
Tel: +49 241 809 5410
Fax: +49 241 809 2257
ek@aia.rwth-aachen.de

Greece

Papailiou, K.D.
National Tech. University of Athens,
Laboratory of Thermal Turbomachines,
9 Iroon Polytechniou,
P.O. Box 64069,
Gr-15710 Athens, Greece.
Tel: +30 210 772 1634
Fax: +30 210 772 1658
kpapail@lts.ntua.gr

Iberian East

Onate, E.
Universitat Politecnica de Catalunya,
Edificio C-1, Campus Norte,
Gran Capitan s/n,
E-08034 Barcelona,
Spain.
Tel: +34 93 401 6035
Fax: +34 93 401 6517
onate@cimne.upc.es

Iberian West

Theofilis, V.
Universidad Politécnica de Madrid,
Plaza Cardenal Cisneros 3,
E-28040 Madrid,
Spain.
Tel: +34 91 336 3291
Fax: +34 91 336 6371
vassilis@torroja.dmt.upm.es

Italy

Martelli, F.
University of Florence,
Department of Energy,
Via Santa Marta 3,
I-50139 Firenze,
Italy.
Tel: +39 055 479 6237
Fax: +39 055 479 6342
francesco.martelli@unifi.it

Nordic

Wallin, S.
Swedish Defence Research Agency FOI,
Computational Physics,
S-16490 Stockholm,
Sweden.
Tel: +46 8 5550 3184
Fax: +46 8 5550 3062
stefan.wallin@foi.se

Poland

Drobnik, S.
Technical University of Czestochowa,
Thermal Machinery Institute,
Al. A. Krajowej 21,
PL-42200 Czestochowa,
Poland.
Tel: +48 34 325 0507
Fax: +48 34 325 0555
drobnik@imc.pcz.czyst.pl

Switzerland

Rudolf von Rohr, P.
ETH Zürich,
Institute of Process Engineering,
Sonneggstrasse 3, ML H 19,
CH-8092 Zürich,
Switzerland.
Tel: +41 44 632 2488
Fax: +41 44 632 1325
vonrohr@ipe.mavt.ethz.ch

Netherlands

Ooms, G.
J.M. Burgerscentrum,
Research School for Fluid Mechanics,
Mekelweg 2,
NL-2628 CD Delft,
Netherlands.
Tel: +31 15 278 1176
Fax: +31 15 278 2979
g.ooms@wbmt.tudelft.nl

United Kingdom

Barton, I.
BAE Systems,
ATC – Sowerby, FPC 267,
P.O. Box 5,
Bristol BS34 7QW,
England.
Tel: +44 117 302 8251
Fax: +44 117 302 8007
iain.barton@baesystems.com



Best Practice Guidelines for Computational Fluid Dynamics of Dispersed Multi-Phase Flows

Editors

Martin Sommerfeld, Berend van Wachem
&
René Oliemans

The simultaneous presence of several different phases in external or internal flows such as gas, liquid and solid is found in daily life, environment and numerous industrial processes. These types of flows are termed multiphase flows, which may exist in different forms depending on the phase distribution. Examples are gas-liquid transportation, crude oil recovery, circulating fluidized beds, sediment transport in rivers, pollutant transport in the atmosphere, cloud formation, fuel injection in engines, bubble column reactors and spray driers for food processing, to name only a few. As a result of the interaction between the different phases such flows are rather complicated and very difficult to describe theoretically. For the design and optimisation of such multiphase systems a detailed understanding of the interfacial transport phenomena is essential. For single-phase flows Computational Fluid Dynamics (CFD) has already a long history and it is nowadays standard in the development of air-planes and cars using different commercially available CFD-tools.

Due to the complex physics involved in multiphase flow the application of CFD in this area is rather young. These guidelines give a survey of the different methods being used for the numerical calculation of turbulent dispersed multiphase flows. The Best Practice Guideline (BPG) on Computational Dispersed Multiphase Flows is a follow-up of the previous ERCOFTAC BPG for Industrial CFD and should be used in combination with it. The potential users are researchers and engineers involved in projects requiring CFD of (wall-bounded) turbulent dispersed multiphase flows with bubbles, drops or particles.

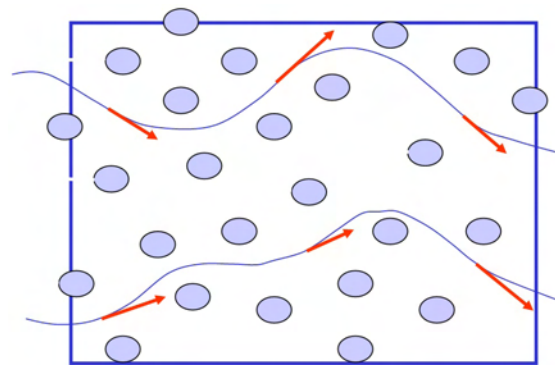


Table of Contents

1. Introduction
2. Fundamentals
3. Forces acting on particles, droplets and bubbles
4. Computational multiphase fluid dynamics of dispersed flows
5. Specific phenomena and modelling approaches
6. Sources of errors
7. Industrial examples for multiphase flows
8. Checklist of 'Best Practice Advice'
9. Suggestions for future developments

* * *

Copies of the Best Practice Guidelines can be acquired electronically from the website:

www.ercoftac.org

Or from:

Ms. Anne Laurent,
ADO-ERCOFTAC,
Ave. Franklin Roosevelt 5,
B-1050 Brussels, Belgium.

The price per copy is €90, €45 and €30 for ERCOFTAC industry, academic-and student members, respectively; and €180 for non-members.